Bulletin 42

(Part 1 of 5 Parts)

THE SHOCK AND VIBRATION BULLETIN

Part 1
Invited Papers, Specifications, Mechanical Impedance, Transportation and Packaging

JANUARY 1972

A Publication of
THE SHOCK AND VIBRATION INFORMATION CENTER
Naval Research Laboratory, Washington, D.C.

Office of
The Director of Defense
Research and Engineering

SYMPOSIUM MANAGEMENT

THE SHOCK AND VIBRATION INFORMATION CENTER

William W. Mutch, Director
Henry C. Pusey, Coordinator
Rudolph H. Volin, Coordinator
Edward H. Schell, Coordinator

Bulletin Production

Graphic Arts Branch, Technical Information Division,
Naval Research Laboratory

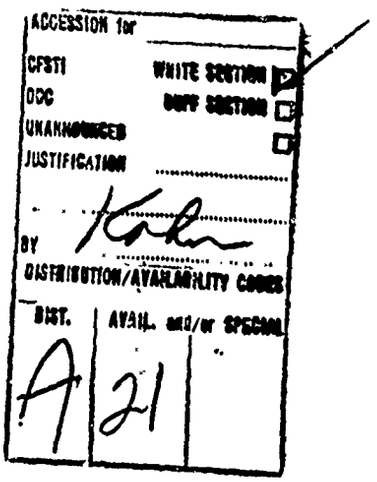

$ 40. for the set
Copies from SVIC

Bulletin 42
(Part 1 of 5 Parts)

THE SHOCK AND VIBRATION BULLETIN

JANUARY 1972

A Publication of
THE SHOCK AND VIBRATION
INFORMATION CENTER
Naval Research Laboratory, Washington, D.C.

The 42nd Symposium on Shock and Vibration was held at the U.S. Naval Station, Key West, Florida, on 2-4 November 1971. The U.S. Navy was host.

Office of
The Director of Defense
Research and Engineering

CONTENTS

PAPERS APPEARING IN PART 1

Invited Papers

Specifications

Measurement and Application of Mechanical Impedance

Transportation and Packaging

PAPERS APPEARING IN PART 2

Ground Motion

Dynamic Analysis

PAPERS APPEARING IN PART 3

Test Control

Test Facilities and Techniques

PAPERS APPEARING IN PART 4

Isolation and Damping

Structural Analysis

Ship's Problems

INVITED PAPERS

"SMALL SHIPS - HIGH PERFORMANCE"

RADM HARRY C. MASON
COMMANDER, NAVAL SHIP ENGINEERING CENTER
HYATTSVILLE, MARYLAND

The Navy is now into its first large scale Fleet renewal program since World War II. And we are proceeding very carefully, because we realize that decisions made today will affect the Navy for many years to come. Our goal is to create a Navy which will meet the demands of the next generation of Americans, as well as lower the age of our ships.

In planning this new Navy, we look, of course, to the future, where we see the Navy retaining responsibility for covering large areas of the world's surface. We see also that this mission will have to be accomplished with fewer numbers of men and ships. Our goal, therefore, is a tightly organized, efficient force equipped with superior weapons. As Admiral Zumwalt, our Chief of Naval Operations, put it, "a lean, mean force."

Covering large expanses of ocean with a smaller fleet means that our new Navy must be highly flexible and highly mobile. We must be able to quickly assemble units to present a concentrated force, and to rapidly disperse ships in smaller groups to support friendly nations anywhere in the world. To achieve this mission with reasonable investments, we intend to supplement our conventional ships with small, High Performance ships.

We call these craft "High Performance" because they can achieve much higher speeds than other ships and maintain these speeds in rough seas. Included in this high performance category are hydrofoils, air cushion vehicles and surface effect ships.

First, let's consider hydrofoils -- ships that can rise out of the water and skim along on wing-like appendages.

The oft-made analogy between hydrofoils and airplanes is relatively accurate: when hydrofoil ships "fly," the foils function in much the same manner as wings; and the ship itself is weight critical. Also like planes, hydrofoils have cockpit-type control stations, light weight aluminum structures and gas turbine engines.

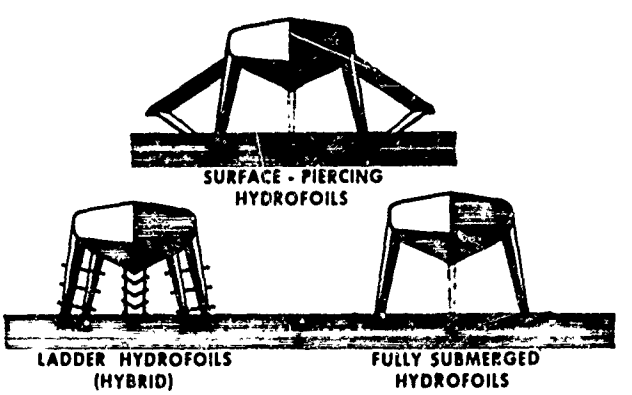

Fig. 1 - Three types of hydrofoils

There are three types of hydrofoils as shown in Fig. 1 -- surface piercing, fully submerged and hybrids. The Navy has opted for the submerged foil system because it produces far superior rough weather performance and requires less propulsion power.

In 1957, SEA LEGS, a Chris Craft cabin cruiser fitted with fully submerged foils proved that a hydrofoil could operate with a fully automatic control and stabilization system. Verification

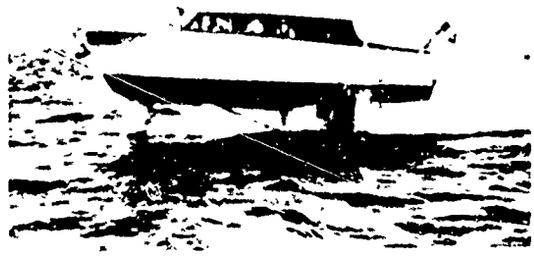

Fig. 2 - SEA LEGS

of this system was an important step because the submerged hydrofoil concept depends upon automatic control systems to sense the motions caused by waves and create forces to oppose them, thus allowing stable flight in the ocean. The height at which the ship "flies" above the waves is determined by the strut length. During the design process, NAVSEC engineers consider the probable distribution of wave heights to be encountered and design an appropriate strut length so the vehicle can fly without hull impact or foil broaching.

Today, the U.S. Navy is the recognized leader in submerged foil, ocean-going hydrofoils. And, although several hundred hydrofoil ferries ranging from 15-150 tons are now in successful commercial operation throughout the world, use of larger vessels in the open sea is currently limited to military applications where the cost of additional performance is justified by tactical necessity.

To give you an idea of where we presently stand, I'd like to quickly acquaint you with the Navy hydrofoils developed to date.

The very first U.S. Navy hydrofoil, the HIGH POINT (PCH-1), became operational in 1963. HIGH POINT's

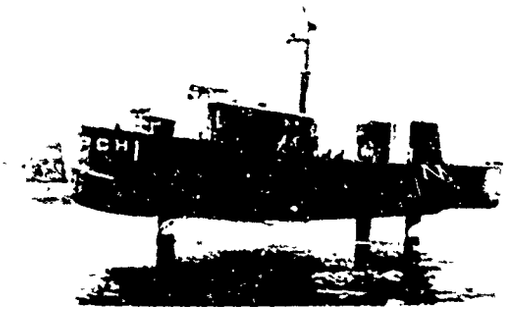

Fig. 3 - HIGH POINT

120-ton, 116-foot hull is powered by 2 3100HP Rolls Royce Proteus gas turbines. Her maximum foil-borne speed is in excess of 40 knots, an impressive increase over hullborne ships.

The PLAINVIEW (AGEH-1) at 320 tons is the largest hydrofoil in the world. She has had all the aches of

Fig. 4 - PLAINVIEW

a developmental program -- a development in which size is one of the technological problems.

But it is really the Patrol Gunboat Hydrofoil (PGH) program which has demonstrated the hydrofoil's ability to operate in high seas and its suitability for the 50-knot Navy. During service in Vietnam, 2 hydrofoil gunboats proved they can operate in seas above their designed sea state; that gas turbine-water-jet propulsion is rugged and reliable; that the electronic/hydraulic control system is dependable and that a minimum of shore support is required. All of which adds up to the fact that hydrofoils can provide a fast, reliable, all weather combat system.

These two 60-ton gunboats are the FLAGSTAFF and the TUCUMCARI (PGH-1 and #2), both with fully retractable foils. The FLAGSTAFF foils are arranged in typical airplane fashion (2 forward, 1 aft) with most of the lift provided by the forward foils. The TUCUMCARI was the first hydrofoil with waterjet propulsion. Powered by a 3300HP Rolls Royce gas turbine engine, water is sucked through rear foil struts up into the pump and jets out at 100 tons per minute.

Fig. 5 - FLAGSTAFF

Fig. 6 - TUCUMCARI

Last winter, highly successful 152mm gun trials were conducted aboard the FLAGSTAFF. These tests verified our prediction that the ship could "take" a recoil load equal to the 60-ton displacement of the craft. More simply, it proved that the 60-ton ship could stay foilborne when the recoil force of

the gun equalled the weight of the ship. (Pounds mass equal to pounds force.)

The hydrofoil's ability to operate at high speeds in a high sea state is its main selling point. The reason the hydrofoil can maintain high speeds in the flying mode is because the ship's hull is above the water's wave action and resistance is greatly reduced, resulting in a fast, stable ride. Because the hydrofoil's hull is clear of the seaway, it loses very little speed in higher sea states. For example, sea state 5 (10' waves) would reduce speed about 12% while small destroyers would have their speed cut in half.

Now, let's consider air cushion vehicles and surface effect ships which are less maneuverable but more adaptable. The concept behind these craft can be traced back to the early 18th century (Swedenborg in 1716), but they are the newest in terms of development. Generically air cushion and surface effect ships are the same, in that they both operate above a surface supported primarily by a self-generated, contained cushion of air.

The distinctions between the two can be seen in Fig. 7. The term Air Cushion Vehicle has come to mean a craft with a flexible seal system extending completely around the periphery of the ship. The flexible skirt not only contains the supporting air cushion but allows the craft to be amphibious, its most important characteristic. In contrast, the Surface Effect Ship generally has rigid surface piercing sidewalls,

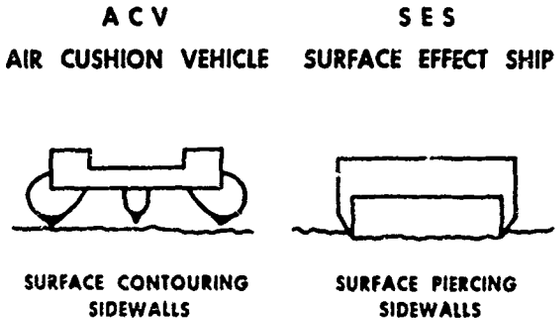

Fig. 7 - ACV SES

with a flexible skirt at the bow and stern only. This configuration is not amphibious, but should have greater potential for higher speeds and efficiency in larger sizes. Either configuration can have air propulsion or water propulsion but, of course, the air cushion vehicle requires air propulsion to maintain its amphibious capability. Because water thrusters have higher efficiency than air propellers, SES will probably have either a water jet or a supercavitating propeller.

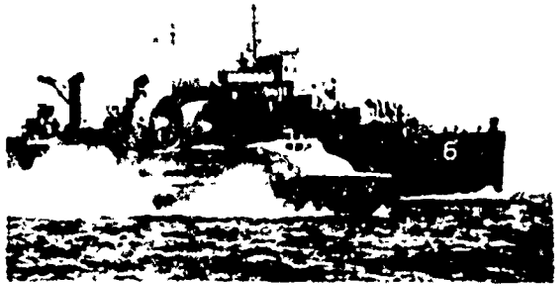

Fig. 8 - SKMR-1

Early U.S. Navy efforts in this field are usually identified with the 30-ton test craft designated SKMR-1 shown in Fig. 8. Built in 1963, it remains to this day the most capable ACV designed, built and operated in this country. Supported by her air cushion, the ACV can travel easily from land, where she can go over any obstacle no higher than her 4 foot skirt height, through the surf to being completely waterborne. This capability offers great potential for intermodal transport situations. It can eliminate the need for off-loading and transfer of cargo at the shoreline.

The British, who call them hovercraft, have produced a number of successful air cushion designs, both large and small. One 177-ton British ACV commercially operated as a ferry can carry 254 passengers and 30 cars. But we now feel we are catching up. While English development has been largely commercially oriented, the U.S. has pursued primarily military applications.

The Navy is interested in air cushion craft both because of their amphibious capability and because of their high speed potential, particularly in rough water. This interest has fostered a Navy program to develop several configurations of amphibious assault landing craft, initially 4 150-ton ACVs of two different designs. Shown in Fig. 9, the Bell design features, for the first time on a large craft, "bow thrusters" which can be trained in any horizontal direction to improve low speed manuevering and control. This Aerojet design incorporates trainable air propellers and a new type of lift system (see Fig. 10). The

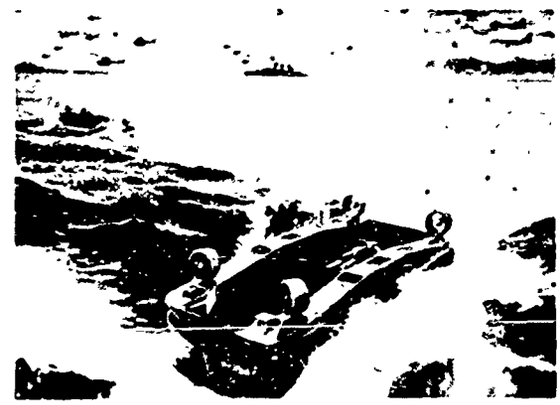

Fig. 9 - Bell design

Fig. 10 - Aerojet design

ultimate output of this program of 4 ships is the technology from which NAVSEC can design the operational machines.

Another program just getting underway, the Arctic Surface Effects Vehicle Program, has as its goal the development of ACVs for Arctic oper-

ations. The amphibious capability is attractive here because the craft must travel over a variety of surfaces -- water, ice and land -- and over obstacles.

Newest of the high performance ships in terms of development is the Surface Effect Ship. It was 1967 when the Joint Surface Effect Ships Program Office (JSESPO) was established with a charter to develop large (about 4000 tons), fast (80-100 knots in smooth water) surface effect ships. The "Joint" in JSESPO's title referred to the fact that initially the program was supported cooperatively by the Commerce Department and the Navy. It has recently become exclusively a Navy program under a NAVMAT Program Manager.

As the first major step toward realizing their goal, the program has just completed the construction of the two 100-ton, 80-knot test craft shown in these Figures (11 & 12). One of the

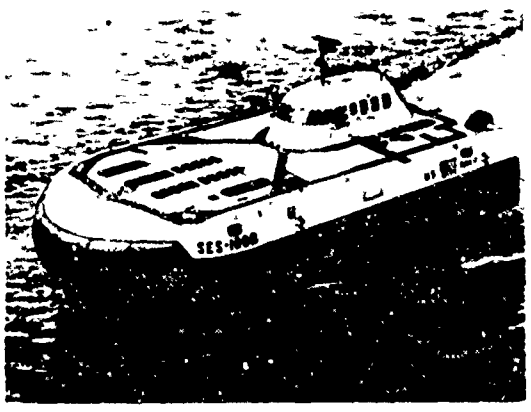

Fig. 11 - Waterjet propulsion

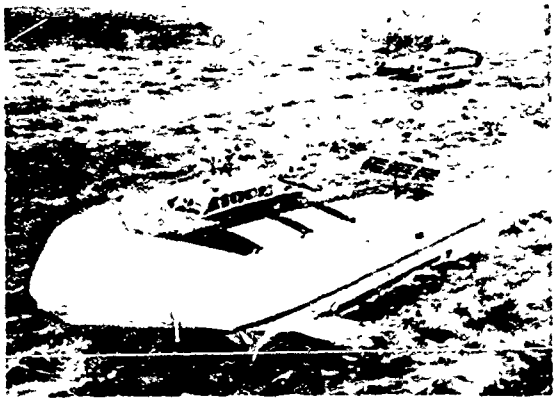

Fig. 12 - Supercavitating propeller

major differences between them is in the propulsion system -- one is powered by waterjet (Aerojet) and the other with a new type of supercavitating propeller (Bell). Both crafts are presently being outfitted and undergoing systems check-out, and are expected to be operating within a few months. We certainly hope these ships demonstrate the potential indicated by the lengthy analytical work and model testing on which they are based.

This then is where we stand at present in the high performance field -- at the state-of-the-art, so to speak. We have utilized existing knowledge to its fullest extent and require breakthroughs before significant advances can be made.

For example, consider the cavitation problem. When a hydrofoil is flying through the water, cavitation -- the boiling of water due to local low pressure regions -- occurs. This cavitation can erode metal surfaces as though a strong acid were applied. Fig. 13 shows cavitation

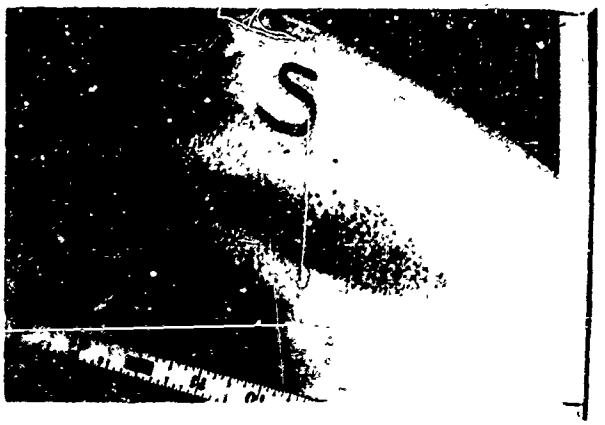

Fig. 13 - Cavitation damage

damage which had occurred on the HIGH POINT's aft propeller after 15 hours of use under full power conditions. The cavitation barrier occurs at about 50 knots. Until we break through this cavitation barrier, we are limited to speeds below 50 knots.

There is an answer to the dilemma, and that is to learn to operate in the supercavitating regime. This solution is a dramatic indication of the technological problems involved. Fig. 14 shows the two foils. If the subcavitating foil is pushed too fast the effects of cavitation occur directly on the foil, causing severe damage and loss of control. The cavity on the supercavitating foil doesn't collapse until it's well aft of the foil and, therefore, prevents the detrimental erosive effects from taking place. But the supercavitating foil also has its drawbacks in that it doesn't provide as much lift as the subcavitating foil, and the drag factor is increased. Maintaining a stable cavity in the variable angle of attack environment induced by the seaway is a difficult control problem. To sum up it's a long way from being reduced to practical engineering and experimental facilities are minimal.

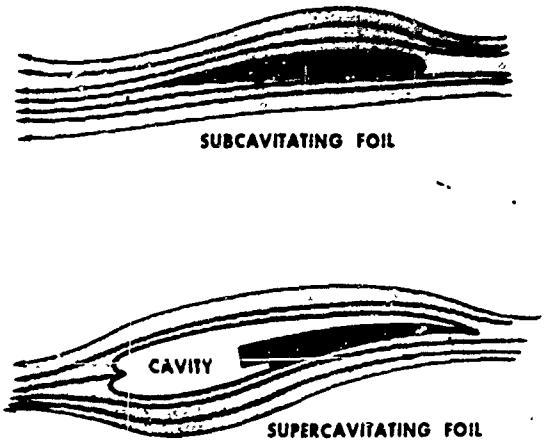

Fig. 14 - Cavitating foils

Another unique problem of a military hydrofoil is the interfacing of weapons systems with the vehicle. The motion of a hydrofoil is more like the vibration of an aircraft than the rolling, pitching motion of a conventional ship. This requires the development of new stabilization devices to adapt the weapons to this unique motion.

Also peculiar to hydrofoils is the problem of noise interference with the proper operation of the autopilot's sonic height sensor. Sensors presently in use have been found to give erroneous readings when they receive not only their own signals, but the noise of certain types of aircraft, helicopters, and the firing of automatic weapons. These erroneous readings have caused foil broaching.

Common to all high performance craft is the need for light weight.

While it has been found that riveted aluminum structures have very low weight, the working of the hull over time can cause loose rivets. These loose connections will result in the re-radiation of electromagnetic energy, interfering with the proper operation of electronic countermeasures and fire control systems.

All of these interface problems point to the possibility of concurrent weapons and platform development where feasible in order to obtain the optimal warfare system.

As you can see, few engineering situations have clear-cut solutions. Our job at NAVSEC is to study the various alternatives and make the necessary tradeoffs to achieve the BEST, cost-conscious operational capability.

In addition to state-of-the-art restrictions in the high performance field, we are also nearing the limits of R&D technology to place aboard these craft. For example, all high performance ships are weight critical.

Range is limited due to conflicting requirements for light weight and fuel payload. We need longer range propulsion systems; that is, propulsion systems with higher overall efficiencies because fuel and payload are tradeable.

We don't have a suitable menu of weapons and sensors for these ships. As designers, we of the engineering community examine various systems possibilities and try to bring the right system on board. But the plain fact is, what we need for high performance ships doesn't exist. We need systems which are light, compact, potent in the naval warfare environment and suitable for maintenance at sea. We should be thinking aircraft technology--but application of that technology to a rugged marine environment.

In discussing weapons systems, it becomes apparent that the physical parameters of some foreign weapons systems are better than ours. Their weapons require lower manning and produce "more bang per pound." Plus, their weapons have more R&D behind them.

We are in the early phases of the PHM (Patrol Hydrofoil Missile) which has both surveillance and attack capabilities. Basically the requirement is for patrol boats which can exhibit high speed and outstanding performance in a high sea environment. The Navy's existing hydrofoils have demonstrated that hydrofoils can satisfy these requirements. However, we have had a bit of trauma in our initial studies for we wind up with a choice of foreign-made weapons for these ships because, by virtue of being smaller and lighter with comparable firepower, they are more attractive. Foreign designers have made some concessions, such as barrel life of the guns, but the important point is that foreign weapons are closer to what we needed than anything the U.S. has produced.

Lest I've placed too much emphasis on these small ships and their fascinating problems. The Navy has many missions and many types of ships to accomplish these missions. We need a balance of capability -- submerged, in the air and on the surface. We have a deficiency in the kinds of ships I've been discussing today -- small, low cost, high performance ships -- ships capable of patrolling and controlling large

portions of the ocean with effective weapons delivery or transport capability. The technology of materials and power packages now permits us to consider high performance with reasonable pay loads and the technology of today's weaponry apparently permits us to give the small package a massive destruct power.

However, even though the technology of the combat suit apparently exists, it has not yet been reduced to engineering practice -- and our job as ship designers and developers -- to design and build operational ships -- is complicated by these gaps.

Thus, for this special class of craft, for these new ships of the Navy, we all have to shift our thinking and remember that for these applications we are space and weight constrained. We do need the maximum of automation. It does require a new dimension in Navy thinking and a new dimension in technical support by industry -- but the rewards are a new dimension in naval capability -- which we surely need to be the strongest Navy in the world.

SPECIFICATIONS

SURVEY OF VIBRATION TEST PROCEDURES IN USE BY THE AIR FORCE

Wayne B. Yarcho
Air Force Flight Dynamics Laboratory
Wright-Patterson Air Force Base, Ohio

A survey has been conducted of specifications and standards containing vibration test procedures in use by the Air Force, to assess progress toward the establishment and maintenance of uniform procurement guidelines. A representative sample of hardware specifications selected from the DOD Specification Index was examined to establish the direction and extent of use of vibration tests offered in the various test specifications and standards. A number of documents presenting vibration test methods were reviewed to determine what procedures are available for application to hardware items. Conclusions relative to the current status of vibration testing methods are presented.

INTRODUCTION

The effect of the vibration environment on the operational performance of military vehicles and equipment has been recognized as a problem for many years. However, prior to the early 1940's, little standardization existed in regard to requirements and test procedures. Test philosophies and techniques varied among civilian manufacturers and government and commercial testing laboratories, for the hardware items for which they were responsible.

After the start of World War II, an urgent demand for new, reliable, air and ground vehicles and equipment brought out the need for standard testing procedures in the field of vibration. To satisfy this requirement for uniform procurement guidelines, AF Specification 41065 was published on 7 December 1945, containing what were apparently the first standard Air Force vibration test procedures. Revisions to the original specification were published at intervals during the next few years, as testing practice developed.

In August 1950, Specification 41065 was converted to MIL-E-5272, with additional vibration tests included. At about the same time, other documents presenting vibration and other environmental tests began to appear, including MIL-T-5422 (BuAer) for Naval aircraft electronic equipment, MIL-E-4970 for Air Force ground support equipment and MIL-STD-202 for electronic and electrical component parts. By 1962, 1/ test specifications and standards were in existence, as indicated in Figure 1, and the number of "standard" environmental tests had increased to the point that some attempt to restandardize the general testing area was deemed necessary.

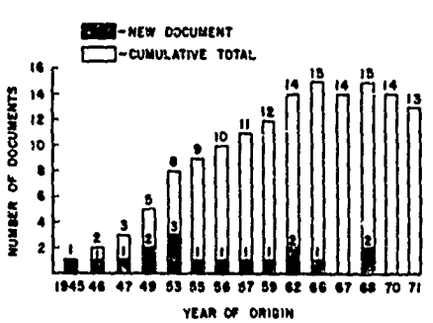

Figure 1. Total of Vibration Test Documents 1945 - 1971

Accordingly, in June 1962 MIL-STD-810 was issued, in an effort to combine at least the major test aspects of specifications into one document and standardize vibration and other environmental test procedures to reduce confusion. The "B" revision of the standard, dated 15 June 1967, Notice 1 dated 28 October 1969, and Notice 2 dated 29 September 1969 are currently in effect. Some of the older documents such as MIL-E-5272 and MIL-T-5422, have been reclassified as "limited" (not to be used for development and new procurement) in an effort to gradually phase them out. The current survey was undertaken to assess the progress toward this objective by determining the extent to which MIL-STD-810 is called out in hardware procurement specifications.

SURVEY PROCEDURE

The DOD Specifications and Standards Index contains approximately 43,000 document titles used in military procurement. Many, but not all, of these documents contain descriptions of quality assurance tests to be used to determine acceptability of the item concerned. The vibration tests specified are usually selected from the procedures described in test specifications or standards of the type discussed above. These relatively few test specifications and standards are identifiable by title from the Index, but no such indication is provided as to which hardware specifications contain vibration tests. This necessitated review of many documents to obtain this information. Because of the number of hardware specifications involved, a detailed review was not considered feasible. Instead, an examination was made of a representative sample of the documents listed in the DOD index, selected from those Federal Stock Classes (FSC) pertaining to Air Force materiel. Approximately 6,000 hardware specifications were chosen for review.

REVIEW OF HARDWARE SPECIFICATIONS

A total of 5,917 detailed hardware or equipment specifications was selected at random from 14 FSC groups pertaining to Air Force materiel. 1,381 or approximately 23% of these contained vibration test descriptions.

In most specifications, when a vibration test was described, reference was also made to the test specification from which it came. In other cases, the origin of the tests was not identified. Sometimes the origin could be determined from the test details, but generally, the modifications of the parameters of a standard test made identification of origin impossible.

Of the hardware specifications found to contain vibration tests, 69% pertained to electrical or electronic equipment (generators, motors, radio sets, capacitors, tubes, relays, resistors, fuses, etc.), and the remaining documents described instruments (17%), aircraft accessories (5.0%), engines (2%), and miscellaneous items (camera lenses, fire extinguishers, etc. (7%), as shown in Figure 2. These results are believed to be generally indicative of the types of Air Force equipment which require vibration testing. Although a survey in greater depth (of the entire specification index, for example) might result in minor alterations of the percentages of hardware items requiring vibration tests, it is believed that the overall result would be similar.

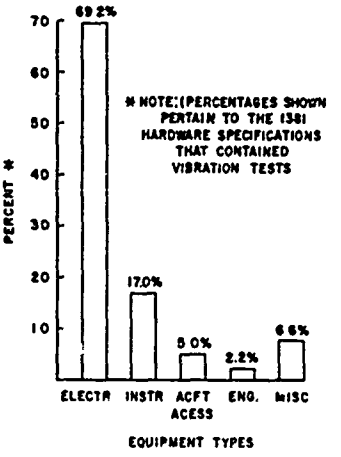

Figure 2. Types of Equipment Most Often Subjected to Vibration Test

REVIEW OF TEST SPECIFICATIONS AND STANDARDS

In addition to the review of the hardware specifications, a number of test specifications and standards as listed in Table 1 were compared to determine the number and type of vibration tests presented therein.

Table 1

Test Specifications and Standards

Number	Title	Date of Origin	Last Revision
MIL-E-5272 (formerly 41065)	Environmental Testing of Aeronautical and Associated Equipment	12/7/45	1/20/60
MIL-E-5009	Turbojet and Turbofan Aircraft Engines	6/14/46	11/13/67
MIL-T-945	Test Equipment for Electronic Equipment	7/2/47	4/11/68
MIL-E-5400	Airborne Electronic Equipment	12/1/49	5/24/68
MIL-T-5422	Environmental Testing for Airborne Electronic Equipment	12/1/49	11/15/61
MIL-STD-202	Test Methods for Electronic and Electrical Component Parts	1/29/53	4/14/69
MIL-STD-167	Mechanical Vibrations of Shipboard Equipment	1/29/53	4/14/69
MIL-C-172	Vibration for Aircraft Electronic Equipment Cases	12/15/53	12/8/58
MIL-T-7743	Store Suspension Equipment Testing	12/5/56	3/22/62
MIL-T-4807	Ground Electronic Equipment Vibration and Shock Tests		10/7/58
MIL-STD-750	Test Methods for Semi-Conductor Devices	1/19/62	8/26/68
MIL-STD-810	Environmental Test Methods	6/14/62	6/15/67
MIL-STD-1311	Test Methods for Electron Tubes	4/19/68	7/10/69
MIL-STD-883	Test Methods for Microelectronics	5/1/68	5/1/58

All of the above-listed test specifications present various types of vibration test descriptions as illustrated in Figure 3 or contain references to tests in other specifications in Table 1, such as MIL-STD-202, MIL-E-5272, etc. To show the type and number of vibration test procedures involved, these documents are again tabulated by title in Table 2.

Table 2

Types of Test Procedures in Test Specifications and Standards

Spec. No.	Resonance	Cycling	Endurance Steady	Endurance Cycling	Random Vib.	Temp. Vib.	Weight Allow Vib.	Total Vib. Tests
MIL-E-5272	4	4	1	1	0	1	1	12
MIL-E-5009	1	0	0	0	0	0	0	1
MIL-T-945	1	2	0	0	0	0	0	3
MIL-E-5400	0	4	0	0	0	0	0	4
MIL-T-5422	2	0	0	0	0	1	0	3
MIL-STD-202	1	5	0	0	1	0	0	7
MIL-STD-167	1	1	0	0	0	0	0	2
MIL-C-172	2	0	0	0	0	2	0	4
MIL-T-7743	0	0	1	0	0	0	0	1
MIL-T-4807	0	1	0	0	0	0	0	1
MIL-STD-750	0	1	1	0	0	0	0	2
MIL-STD-810	14	6	0	0	2	1	14	37
MIL-STD-1311	0	2	3	1	0	0	0	6
MIL-STD-883	0	1	1	0	0	0	0	2
TOTAL	26	27	7	2	3	5	15	85

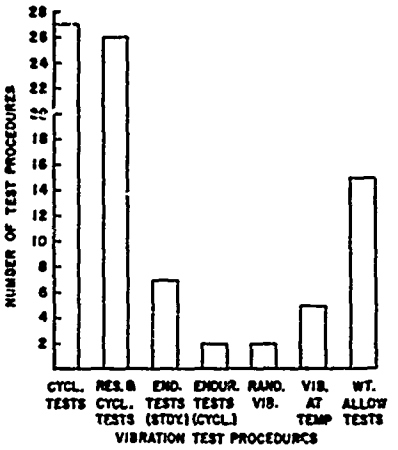

Figure 3. Content of Vibration Test Documents

APPLICATION

The application of the vibration test procedures described in the test specifications and standards listed in Table 2 depends upon (1) the type of hardware or equipment, e.g., a mechanical or electrical device, (2) the type of vehicle in which the equipment is mounted (missiles, airplanes, helicopters, etc.), and (3) the location of the equipment in the vehicle (engine-mounted or mounted on vehicle structure). Also, special procedures are applied which depend upon whether the equipment is attached directly to the structure (hard mounted) or mounted on isolators. Furthermore, the selection of test procedures depends upon the type of possible malfunction which is under investigation, such as a possible fatigue failure or a possible instrument error due to vibration.

A very common test procedure indicated in Table 2 is a resonance search followed by resonance dwell testing. This test is normally intended to investigate possible fatigue damage in equipment which is to be installed in airplanes and helicopters. The resonant dwell may be followed by cycling tests to check for equipment malfunction or for internal resonances which are difficult to detect. In other cases, only cycling testing is required, especially for equipment in a vehicle with a short service life such as an air launched missile. Table 3 shows a range of test parameters for typical cycling type tests and for a variety of equipment locations. Resonance dwell and cycling tests are conducted with sinusoidal type excitation.

Table 3

Cycling Test Parameters

For Equip. Mtd. On	Double Ampl. (Inches)	Accel. (G's)	Freq. (Hz)	Total Vib. Time (Hrs)
Recip. & Gas Turb. Eng.	.036-.10	1-20	5-500	9
Turbo-Jet Eng.	.036-.10	1-20	5-2000	9
Aircraft Struct. on Mounts	.010	2	5-500	9
Helicop. Struct. on Mounts	.036-.10	2-5	5-500	9
Helicop. Struct., No Mounts	.10	2	5-500	9
Air-Launched Missiles Captive Phase	.036-.10	1-10	5-500	6
Air-Launched Missiles	.036-.10	1-10	5-2000	1.5
Grnd-Launched Missiles	.06-.20	1-50	5-2000	1.5
Grnd. Supt. Vehicles	.06-.10	1-50	5-2000	9

An additional type of test with sinusoidal excitation is the endurance test, also listed in Table 2. This type of test is a fatigue test, and it is generally of longer duration than the previously indicated resonance or cycling test. Table 4 indicates parameters associated with some types of endurance tests. MIL-STD-810B does not specifically call out endurance tests as such, but other specifications such as MIL-E-5272C, do recommend this type of testing.

Table 4

Endurance Test Parameters

Equip. Type	Double Ampl. (Inches)	Accel. (G's)	Freq. Range (Hz)	Total Test Time (Hours)
Microelect.	.06	20	20-60	96
Store Susp.	.03	10	50	300
Eng.-Mtd. (on turbo-jet or turbo-fan)	.01-.05	20	15-250	36

Only two of the specifications, MIL-STD-810B and MIL-STD-202, recommend random vibration testing. Table 5 indicates typical parameters for random vibration tests. When wide-band random vibration tests are conducted, no resonance search or cycling is required.

Table 5

Random Vibration Test Parameters

Equip. Type	Power Spectral Density	Overall RMS "G"	Total Time
All equipment attached	.02	5.2	Three minutes to eight
to structure of air	.04	7.3	hours in one or three
vehicles and missiles	.06	9.0	directions as specified
powered by high thrust	.10	11.6	in detail specification.
jets and rocket engines	.20	16.4	
	.30	20.0	
	.40	23.1	
	.60	28.4	
	1.00	36.6	
	1.50	44.8	

In addition to the above test procedures, some of the test specifications listed in Table 2 provide for combined environment type testing and make special allowances for the weight of the item being tested. Vibration tests under conditions of high temperature are conducted to investigate possible malfunction of equipment exposed to sources of heat such as electronic gear operating in closed compartments, on engines, or near rocket exhausts. Provision is made for vibration testing of heavy items by test procedures which specify a progressive reduction in vibratory acceleration when the weight of the test item exceeds 50 lbs., decreasing ultimately to a minimum of 50% of the test curve.

Of the 14 general requirements documents reviewed, five, as indicated in Table 6, were found to contain the majority (74%) of the vibration tests described, which consisted of cycling, combined cycling-resonance, steady state, and random excitation.

Table 6

Test Specifications Most Often Referenced

MIL-STD-202	Test Methods for Electronic and Electrical Component Parts
MIL-E-5400	Airborne Electronic Equipment
MIL-T-5422	Aircraft Electronic Equipment Environmental Testing
MIL-STD-810	Environmental Test Methods
MIL-E-5272	Environmental Testing of Aeronautical and Associated Equipment

Figure 4 shows these test specifications or standards from which vibration test procedures were most frequently referenced and the percent of all hardware specifications that called them out. Test procedures in the above five test specifications most frequently specified are given in Table 7 below:

Table 7

Test Procedures Most Often Referenced

MIL-E-5272	Meth. V (cycl.) and XII (Resonance and cycling)
MIL-STD-202	Meth 201A and 204B, Cond. A (cycling)
MIL-STD-810	Meth. 514, Proc. I, Curve B (resonance and cycling)
MIL-E-5400	Sim. to Meth. XII, MIL-E-5272
MIL-T-5422	Sim. to Meth. XII, MIL-E-5272

DISCUSSION

MIL-STD-810 is the most detailed of the General Test Specifications, has been recently revised, and contains most vibration tests presented in any of the other documents. In addition, MIL-STD-810 is the only test specification of those in this study to describe a gunfire test (Notice 2 (USAF), 29 September 1969) and one of two (the other is MIL-STD-202) to present random vibration test procedures. It is however, referenced much less often than MIL-E-5272 which presents vibration tests formulated for the air vehicles and equipment of 15 to 20 years ago. The reason for this infrequent reference to an updated, improved specification apparently lies in the regulations concerning automatic review of specifications at five-year intervals. During these reviews, if test requirements have not changed, the test document reference may be left unchanged even though it is in the "limited" category.

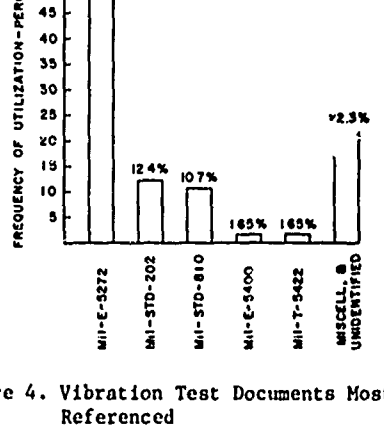

Figure 4. Vibration Test Documents Most Often Referenced

MIL-E-5272 is the test specification referenced as a source of vibration test procedures in about 51% of the hardware specifications. MIL-STD-202 is referenced in about 12% of the specs, MIL-STD-810 in 11%, MIL-E-5400 and MIL-T-5422, about 2% each. Approximately 22% of the vibration tests are described in detail but not identified as to origin.

No positive indication has been obtained recently in regard to the adequacy of the vibration tests currently presented. The fact that many of the hardware specifications reviewed had not been updated for the last 15 to 20 years might be a cause of many of the current vibration problems. A review of outstanding test procedures and comparison with what is available in MIL-STD-810B is apparently needed.

Method 514.1 "Vibration", the section of MIL-STD-810 pertaining to vibration test procedures, presents a wide variety of test methods

and is the most complete and up-to-date of the test specifications (or standards) reviewed. However, in an effort to avoid repetition of certain descriptive material common to a number of test procedures, the tabular and graphical data have been highly condensed, to what some believe is a confusing extent. Detachment of vibration tests to form a separate vibration test standard might be an answer, although this suggestion has not met with acceptance in the past.

Also, results of recent vibration surveys have not yet influenced test specifications and standards. For example, according to data presented by Bolds and Ach (1), the test level specified in the Helicopter Vibration Test Curve "M" in MIL-STD-810B is inadequate as to frequency range. Inadequate design and testing of helicopter equipment to realistic levels of vibration in the 5 to 10 Hz range and the absence of requirements in the 500 to 3,000 Hz range may possibly account for many current field equipment failures. In addition to sinusoidal vibration testing of equipment mounted in helicopters, there also exists a need for random vibration testing in the 300 to 3,000 Hz frequency range (1).

CONCLUSIONS

1. Although MIL-STD-810 contains most vibration test procedures presented in MIL-E-5272, plus a number of additional tests, and has been available for use since 1962, only 11 percent of hardware specifications containing vibration test requirements reference MIL-STD-810A or 810B.

2. Over 50 percent of the hardware specifications reviewed referenced the original requirements of MIL-E-5272. These requirements are based on 1950-55 technology. It appears that hardware specifications should be revised to reflect the latest Vibration Technology.

3. It would appear the most serious deficiencies of some specifications are the limited frequency ranges and the limited use of random vibration testing requirements.

4. No index exists of hardware specifications containing vibration test requirements. A survey of hardware specifications to identify those that contain vibration tests is needed to permit compilation of an index which would be of assistance in determining requirements for development of new and improved vibration tests.

REFERENCES

(1) Phyllis G. Bolds and John T. Ach, "Inflight Vibration and Noise Study of Three Helicopters," The Shock and Vibration Bulletin, December 1970.

SPECIFICATIONS

A Panel Session

Moderator: Henry C. Pusey, Shock and Vibration Information Center
Co-Moderator: Clyde Phillips, 6585 Test Group, Holloman AFB

Panelists: Dave Earls, AFFDL, Wright-Patterson AFB
Robert E. Wilkus, ASD, Wright-Patterson AFB
A. R. Paladino, Naval Ship Systems Command
D. M. Lund, Naval Ship Engineering Center
David Askin, U. S. Army Frankford Arsenal
O. A. Biamonte, U. S. Army Electronics Command

OPENING REMARKS BY THE PANEL

Mr. Earls: I am going to talk about the effectiveness in specifications and standards from the standpoint of environmental failures that are occurring in service. I want to tell you about a few environmental failures that occur in operational aircraft. We conduct an array of tests using all these specifications and standards, and we assume that after 2 to 5 years these aircraft are going to be operating satisfactorily. What is the effectiveness after 2 to 5 years? We had a contractor make a study of this. It was a two year field failure investigation of 175 aircraft scattered mostly in Vietnam with some on U. S. coasts. They made a detailed analysis of the equipments that were failing and tried to pin-point the environment that caused the failure. They studied the failure analysis reports and other documentation and made a good engineering analysis of a selected group of these equipments that they thought were failing environmentally. It turned out that from the selected group 52 percent were failing environmentally. Twenty-one percent of the failures over the two year period were because of temperature, 14 percent were from vibration and 10 percent from moisture. The rest were from related environments such as sand and dust, salt spray, altitude and shock. The 52 percent of equipments that failed for environmental reasons represents 12,000 failures per year, which is quite a goof-up. What is this costing us? Fifty-five percent of all environmental failures are from temperature, and they cost us four and one-half million dollars a year in one operational aircraft weapons system. Moisture accounts for 1 1/2 million and vibration 1.4 million. Temperature, moisture and vibration are therefore tremendous problems in operational aircraft. Out of these selected equipments, these environments cost 8.3 million dollars per year. We then estimated what it costs for the whole operational system. About 20 to 40 percent of the failures that we are having in operational aircraft are environmental, and they are costing us around 16 million a year. Equipments in this particular airplane were qualified to MIL-E-5272 and MIL-E-5400. I think it is significant that 53 percent of the field failures from vibration also occurred in the qualification tests. This means that when they ran the test they got failures, but in many cases did not correct them. To solve this problem we must provide good failure criteria. We are putting failure criteria in MIL-STD-810 which we hope will be directed toward correcting this. People are not really correcting the failures, they are not retesting equipment and they are not getting fixes into operational systems. I have mentioned some environments other than vibration but I think most of us are environmental people in general anyway. Present tests do not consider the frozen moisture situation on an airplane taking off in the tropics and going to altitude. The equipment freezes and will not work at altitude, but when it is checked out back on the ground, it is alright. We have to start from scratch on this problem. Many failures occur from forced air cooling and we expect to put a test for this into the standards. Some of our new aircraft systems in the Air Force already have these types of tests. We are working right now on a new temperature-altitude-humidity test which we want to put in MIL-STD-810. If we can take care of some of these temperature, humidity and vibration problems, we will eliminate a lot of the field failures. I think random vibration may be one of the answers. With our old test methods using sinusoidal dwells, one cannot really find the resonances and the ones you do find are not the significant ones. I think we need

to test all the resonances using random vibration. We really need a functional test and an endurance test. People talk about how high the test levels are. As far as I am concerned they should be functioning at that level. We should even have a higher level for endurance because there is a lot of fatigue in this equipment. Equipment is breaking and falling apart in service. In general, standards should be flexible. You have to have an environmental engineer or somebody who can apply engineering judgement to a standard like MIL-STD-810. You cannot expect to apply it across the board without somebody putting in a little knowledge. You have to have some flexibility and adaptability. We expect to put more flexibility into MIL-STD-810 if we can. I also feel that these specifications and standards must be developed for combat environment. Think of the maintenance and man hours, 100,000 per year, just on the thirty equipments in this operational system I was talking about. I think anything we can do to improve these specifications and standards to make them really work certainly justifies some expense, considering the cost of failures in service.

Mr. Wilkus: It is pretty hard to apply a standard; they are really only guides. They might be used as guides to industry as to what levels they must develop equipment. Over the years people have asked for the vibration environment of airplanes. It is like asking how deep the ocean is, because the vibration varies throughout the airplane. At Wright field, we have an Aeronautical Systems Division in which we have Systems Project Offices or managers. The managers of these systems have systems engineering groups which support all systems. I am in an airplane directorate which is structures-oriented. I am in the Structures Division and have the Dynamics Branch involving vibration and acoustics. There is also the Avionics Directorate. There are a lot of people involved in the procurement of equipment and a lot of different attitudes. We have ours. The avionics people may well apply a specification or standard that they know. We in dynamics, treating environmental vibration as structural vibration, provide our own input to the requirements and carry it up to the test specifications. On a major system we are going to define the environment, either by measurement or prediction. We are asking people to be reasonable. By reasonable I mean they must do it our way. If a reasonable environment is 2 g, then that is what it is. It may be 15 g like Mahaffy's prediction on the B58. In the aircraft industry they negotiate the test requirements. In the case of the B58 MIL-E-5272 was in the contract documents, but this did not mean anything. We knew from some B52 experience, that in the back end of the B58 we could expect at least 15 g. This was how the Mahaffy study came about. It was a B58 contractor's specification, an estimate and prediction of what the environments were and a derivation of the test specifications that was reasonable. This is what we adhere to in the Aeronautical Systems Division. We will argue about what is reasonable, but define what the environment is and then proceed with the test. There are a good many people who are arguing that the specifications are too high, and they are spending more time arguing than testing. This is where a real problem exists. Our prime function is to prepare aircraft specifications, but we do get out and do some testing. We do not know what we are doing unless we know something about the environment. We probably put more instrumentation in the RF-4C than has ever been put in any airplane. We are utilizing this experience. We found that in the RF-4C no one even considered the vibrations in the outer wing where levels were so high the wing was stalling. A compass transmitter was failing. We found that the transmitter was tested at 10 g, but it was on a rigid block. It is never installed in the airplane this way. Nothing was measured during the test. There was a requirement on accuracy but that was measured a couple of days later. These are just a few of our problems which may be enough to generate a little discussion.

Mr. Paladino: The standard that I am going to talk about is MIL-STD-167. This standard covers the requirements for naval equipment including machinery both for internally and externally excited vibrations. There are five types of test in this standard. Many people are not familiar with the five types. Type 1 is on environmental testing which includes testing for equipment to go on all types of Navy ships. Type 2 is on internally-excited vibration, which is better known as balance requirements. Type 3 is for torsional vibration which is usually associated with gas turbines or high speed equipment. Type 4 is for longitudinal vibration which includes shaft and propulsion systems. Type 5 is lateral excitation associated with the shafting systems of ships, which are the lateral bending modes. I will address myself primarily to Type 1, because this really offers the most controversy. A researcher in ship dynamics wants to understand all the delicate forces that may act on the ship, externally or internally, as well as understanding the structural response to such forces and the vibratory energy transfer of the structure.

The ultimate concern is to bring the vibration to an acceptable level by having low input forces if possible, and to provide design criteria for shipboard equipment so that it can endure its dynamic environment. Shipboard equipment must be designed to enable the Navy to fulfill its mission under any adverse environmental condition. The philosophy in arriving at vibration standards is a realistic approach that vibration of shipboard structures cannot be prevented but only minimized. Vibration is generated by shaft and machinery imbalance, variable blade frequency due to nonuniform weights, sea waves, wind, weapon firings and maneuvers. Equipment mounted on the hull experiences the ships greater vibration level amplitudes by some magnification factor which should be kept as small as possible. It is necessary to consider certain functional threshold levels for equipment such as maximum levels tolerable to have the equipment operational, levels at which the equipment is not operational but functional so that checks may be made, and levels at which equipment is neither operable nor functional, but does not sustain structural damage or become a missile. Restrictions may also exist whereby ships may have to reduce speed in heavy seas to minimize sliding or shipping green water. The area of ship dynamics is rather complex and includes mechanical, hydrodynamical and operational generation of vibration. Response includes all kinds of vibration patterns and mode couplings which are different at various ship locations due to structural configuration. Measurements at certain locations may lead to erroneous conclusions or at best to results which cannot be generalized. Basically, the vibration amplitudes to which shipboard equipment should be submitted before installation on ships are given in MIL-STD-167. The philosophy in arriving at this standard is a realistic approach that vibration of a ships' hull and structure is considered inevitable. We must accept this. The standards are kept uniform for all shipboard equipment. No differentiation is made for either type of ship or location on the ship with one exception, namely mast-mounted equipment, even though there may be areas on the ship which may be vibrated at lower amplitude levels than other areas, for example stern versus midship. It must be mentioned that most vibration standards for equipment testing for ships, even in foreign navies or foreign commercial ships, consider MIL-STD-167 as a guide. The navies of NATO nations use it as a mandatory requirement. In fact there is no departure from this standard. MIL-STD-167 was last revised in 1969. So far it has proven quite adequate in all cases where equipment has been actually tested in accordance with its requirements. There are many cases of failure due to vibration, but not one instance is recorded where equipment failed after it passed this test requirement. When designing equipment for shipboard use it is best to avoid a natural frequency which will coincide with the natural frequency of a ship's hull. Such a design is possible for a selected ship and a particular mode of vibration. The use of one type of equipment on different ship classes makes the objective unattainable. As a taxpayer, gentlemen, logistics is an important thing, to have one piece of equipment on many types of ships. As such the provision of this standard to show that equipment is properly functioning even at a natural frequency falling within the testing range is considered mandatory and shall not be by-passed. Finally, considering the response of ships in calm and rough seas, can we successfully design shipboard equipment to assure the proper functioning during adverse conditions? MIL-STD-167 provides the procedures for testing the adequacy of equipment to assure that properly tested equipment is placed on board ship. The frequency range substitution in the revision of this vibration standard has been taken down to 4 Hz and up to 50 Hz. Adequate design of equipment for frequencies below 4 Hz should not cause any difficulties when realistic calculation procedures are applied. Selection of the location on the ship for the installation of sensitive equipment must be considered from an early design stage. However, this equipment must also be submitted to MIL-STD-167 testing.

Mr. Lund: I would like to cover two basic points in my introductory remarks. First, for our non-Navy friends, I would like to give you a rough notion of just how the Navy specifies shock requirements. The basic Navy shock test specification is MIL-S-901C. This specification provides procedures for shock testing on the Navy's light weight and medium weight shock machines and also on the floating shock platform. The specification does not require shock testing of anything. It applies only if it's involved by some other specification. The MIL-S-901C test procedures are very generalized with the intent that once an item passes the test, it should be suitable for installation on virtually any ship and in almost any location in this ship. In this respect it is somewhat similar in philosophy to the vibration specifications that Mr. Paladino was addressing a moment ago. Next step up the ladder is the equivalent specification usually referred to as the MIL specification which may invoke MIL-S-901C. It may say that you shall test all valves or all turbogenerators to MIL-S-901C, and that might be all it says. Hopefully, the MIL specifications will support MIL-S-901C by giving information, such as what the operating

conditions of the equipment shall be during the test. Which test fixture shall be used in the shock test? What are the acceptance and rejection criteria? The MIL specifications essentially support MIL-S-901C, but do not supersede it. Finally, we have the shipbuilding specifications; these are specifications that the ship builder is required to observe when he is building his ships. First the ship building specification indicates which shipboard systems requires shock protection and which do not. For those systems which require protection MIL-S-901C is directly involved, provided that the item in question is shock testable, which usually means that it weighs less than 60,000 lbs. If the item is not shock testable, a dynamic shock analysis procedure is invoked. I will not go into detail on that procedure except to indicate that this provides an analytical equivalent of the shock test. It gives the Navy an indication of the shock resistance of the equipment. That, in a nut shell, is how the Navy specifies shock requirements.

The second type is one that I am sure that we will hear more from tonight, but I will try to stir things up a little bit. MIL-S-901C states how to shock test something, what procedure to use, but it does not tell you how many g's you are going to see. I get a number of phone calls every year from people who ask "How many g's am I going to see?" For the benefit of those people, I would like to offer a few remarks to kick off what I expect to be a long discussion of this matter. The first thing that I tell a man is that I do not know. I try to convince them that the Navy cannot tell him how many g's he will see, because it depends on the dynamics of your requirement and upon the dynamics of the test fixture that you select. You can see from 5 g to 250 g, but I cannot tell you that until I know exactly what your equipment looks like. If you are still pressing it we will suggest you take a quick cut at dynamic analysis of the equipment. The Navy dynamic analysis requirements are intended to address the same shock environment that we are trying to address by the shock test requirements. The dynamic analysis should, of course, include the test fixture and you will get some notion of how many g's you will be seeing during the shock test. I also find it is often necessary to point out that despite the fact that you have heard that 10,000 g's were recorded during the last shock test of some equipment, you have no need to worry about this. This is high frequency garbage that has practically no damage potential. Just confine your worries to the frequency range of interest, usually the first one or two modes. Furthermore, even if I could tell you how many g's you are going to see on this test, that will not tell you if you are going to pass the test. We have seen all sorts of equipment pass the test because it is still functionally operable, yet it is quite a bit bent up. If you had used the yield as your failure criterion, you would have failed the test and would have doubled the weight of the thing for nothing. I suggest that you consult and carefully observe all the guidance given in MIL-S-901C. There is really a lot of good information there. This information should suffice to get 95 percent of you folks through the shock test with virtually no problems at all. Finally, just to conclude with a word of reassurance, I point out that we have found that the majority of off-the-shelf items that are shock tested to Navy requirements pass these tests. There might be some minor modifications required, but not the kind of thing that requires a full redesign. We end up stiffening this part or that part and adding a lock washer here or there. It looks pretty terrible when that hammer comes down but, from simple observation of the shock test results, it really is not quite that bad.

Mr. Askin: It is a pleasure to be here to talk about specifications and standards because I have been in this field for many years. One of the things that struck me from Wayne Yarcho's talk is that MIL-STD-810B, which originated as an Air Force specification, is only being used 11 percent of the time by the Air Force. I know, since the middle 60's, the rule in the Army had been to really try to use MIL-STD-810B. I venture to say that we are using it for at least 50 percent of all our current new procurement specifications. We are having troubles with it, but I am convinced that it is the best specification that exists to date. The biggest trouble with MIL-STD-810B is in its misuse. Many people that write specifications do not really understand it; they do not have the faintest idea of how to write or to even distinguish between environmental criteria and environmental test methods or procedures. Many people confuse the limits of the environment with a test specification. They will spell that out as a test requirement. So I think the big problem is in really educating specification writers and writers of procurement documents on how to use MIL-STD-810B. There is a current revision of MIL-STD-810B now going on in the three services and industry. They have a big job on their hands in that there is a lot of difference of opinion on the application of this particular test specification. I think we do have a basic document that is worthwhile, and if its attacked diligently by the three services and industry in the present effort, we will end up with a much more usable document than we

now have. One of the things that we are now trying to do is to issue along with the new standard a separate document on how to use the MIL Standard. I think this will really help a lot. One of the big problems is to update the various procedures as we learn more about the actual environment. If you know what the true environment is, that is the environment you are going to use in your test laboratory and forget about MIL-STD-810B. You can always get a waiver on it if you can prove you know what the true environment is. We, at my particular installation, have attempted to get the true environment on a fire control mounted in tanks and helicopters because we felt that we have been overtesting a lot of the equipment, especially the equipment meeting the existing MIL-STD-810B. We made measurements on the mounting pads where our fire control equipment was to be installed and found in most cases, it was considerably lower than the curves that are now in MIL-STD-810B. Another area in particular with which I find fault is the resonance dwell test. Many people spell out a resonance dwell test on equipment for which we never find a resonance. Even if there was one, it would be very hard to find it. Then, if you do find it, the specification says dwell for one half hour at each resonant frequency and that is one sure way to kill almost any piece of equipment. It is not realistic because in the field you very seldom will find a resonance that occurs at a discrete frequency. We talked to the Air Force about this and we are proposing that maybe in some cases we ought to try a sweep around a resonance point instead of the resonance dwells. One other mistake that has been made is to use the same limits for vibration or shock testing an item in all three directions. Very often you know the equipment is going to be installed in one orientation in which it will get its worst shock or vibration. To indiscriminately require a standard test in all three directions at the same limits very often invokes a much more severe test than you need. If the designer or the specification writer will get together with the environmental people before they set up their test program, they will have a much more intelligent application of MIL-STD-810B.

Mr. Biamonte: Documentation formulating the basic requirements for factors both for the natural and induced stresses common to all DoD military equipment is not available. We do have a document, MIL-STD-210 which deals with climatic environments that are common to Army, Navy and Air Force and Marines. There is no equivalent document covering the induced environments for the Department of Defense. Very obviously the reason that we do not have such a thing is that nobody has defined what the environments are. The reason for this is that there is an infinite number of variables regarding the induced environments. These are man-made environments, those which occur as the result of design of an end item such as an aircraft, a space vehicle, a ship or a ground vehicle. To try to define this is difficult although there is no doubt that with regard to a specific application we can measure it and find the environments. However, our basic specifications are designed to buy material for all applications. Therefore we need a generalized specification. Such a specification does not exist. The specifications that do exist call for tests based on past experience. There is a difference between the requirements or criteria, and the test. We do have a three-section and a four-section to all military specifications. The three-section calls out requirements, the four-section calls parallel or equivalent tests to prove out a particular requirement. I dare say that industry does not care about the three-section. They look at the four-section and design to meet a test. This may or may not be the equivalent of a real environment. With MIL-STD-810 we tried to arrive at a common denominator for the Army, Navy and Air Force for all applications. It is quite an impossible task, but we ended up in 1967 with a document that tried to do these things. There are many things wrong with MIL-STD-810, but my recommendation is to eliminate all documents which call out tests rather than criteria. Refer to MIL-STD-810 for any test that is in a four-section of a specification. That is the only way you are ever going to achieve any degree of standardization. Again remember the document is not perfect but new people can help make it perfect by its utilization. I realize the importance of the degree of standardization that is required. In many cases there are occasions whereby in a specification, the end use environment is far more rugged than, for example, the transportation environment and I find in reviewing MIL-STD-810 there are duplications of testing. If the environments in which an end item is used are far more rugged than the handling and transportation environments, let us not test for handling and transportation. There has been some reference to various procedures in MIL-STD-810. I think, if I hear right, we might end up with several procedures for vibration. I do not understand why we should have more than two or three. Vibration is vibration. Why we need 13 or 14 procedures is beyond me. The Army is concerned, believe it or not, with aircraft and marine design. We have more helicopters than the Air Force and I am beginning to think we

have more barges and ships than the Navy. Therefore, it is high time that we end up with a single test document for all these particular areas.

DISCUSSION

Mr. Panaro (IBM, Owego): We do environmental analysis and testing on avionics equipment, space equipment and shipboard equipment. Presently, we are involved in shipboard equipment, specifically submarine equipment. I feel that some of the specifications we have designed to were realistic. Why design for unrealistic specifications if the environments are much less than the criteria spells out? That was the point. As far as MIL-STD-167 is concerned, we are working to it. I do not think the specifications for shipboard equipment are that unrealistic. I do not think the shock specifications are unrealistic. I do think that the specifications for avionics equipment are definitely unrealistic. I have gotten some information from China Lake telling me that power spectral density levels not exceeding 0.04 g^2/Hz were observed in actual flight conditions and they are testing in specifications to 0.12 g^2/Hz, from 20 to 2,000 cycles. To me that is completely unrealistic.

Mr. Paladino: We get many statements that the standards or specifications are unrealistic, but gentlemen, we have human lives involved. In particular, submarine type requirements, we have about 100 American boys on those ships. We have lost two of our ships now in peace time and it is a sadness to all of us that we lost them. We in the Navy have decided that we shall not lose a third one in peace time. If the skipper or a man on the control station calls for a command, and a piece of equipment does not respond immediately, that submarine and 100 human lives may be lost. We cannot play this kind of game. MIL-STD-167 is not unrealistic. Please do not look at it and go to the Modal Basin or one of these Navy laboratories and get a specific report. These data are taken under highly controlled situations. Everything is at a controlled speed. The maneuvers are not there. It is humanly impossible to set up in one document, for a situation with a ship underway, what the environment is going to be under shock or vibration. So what do we do? We pick a set of frequencies and amplitudes. Sure, you can argue that the amplitude is too high, but gentlemen all it is trying to do is ferret out a resonance frequency. It is not the standard that kills equipment. The standard requires a maximum of 1.2 g at 25 Hz. Our failures are not occurring at 33 Hz or at 25 Hz. They are occurring at 8 or 9 Hz; this is about 0.2 or 0.3 g. Now, if you people who are designers tell me that this is an unrealistic specification and say that our equipment cannot survive 0.2 or 0.3 g, I will not send my son on a submarine.

Mr. Turkheimer (Wyle Laboratories): I think you have a very valid point when it comes to the survivability and the reliability of the equipment that your contractors are building and the test laboratories are testing. I think there is a need for it. However, sometimes when you get down to the point of actually performing a test, you wonder how realistic the specifications are. We should know what goes on upstairs and what is really realistic. This is one of the problems that I foresee as we come up with more sophisticated pieces of equipment.

Mr. Wilkus: I can recall a previous experience on Snark. Now this was at the time when they had Snark infested waters down here. There were some measurements the contractor had made. The frequencies were limited to 500 Hz; actually they were limited in shake capability to something like 500 Hz. The instrumentation was indicating higher frequencies. They were measuring something like 40 g which seemed impossible. The reaction of course is to start arguing about this. Actually you should just start taking a real look at the equipment. It was guidance equipment and there were many problems with it. The program was shut down and we set up a program to go on a stand to fire the missile. The question now was to get this stuff able to meet the firing in natural environment. It was tested to 40 g below 500 Hz. A little vibration testing will do a lot of good even at 500 Hz. You are principally ruggedizing the equipment. This was done, and the first Snark that was fired after people really took this to heart and tested it and corrected difficulties in the equipment went down range 6,000 miles the first time and hit the target. It can be done.

Mr. Johnson (Hughes Aircraft): My question is on MIL-STD-167. Much of the equipment we build is relatively large. In almost every case these will be installed on surface craft as opposed to the submarine. Am I correct in assuming the primary reason for going to 50 Hz was to include submarine gear? Some of the other surface vehicles such as hydrofoils and others do have a much

higher frequency. Do the old figures of 33 Hz and 25 Hz cut-off still apply to the larger vehicles that could carry the heavier gear?

Mr. Paladino: The 50 Hz was added for hydrofoils and the 33 Hz is primarily for submersibles. The other two brackets are for surface ships. The carriers usually fall in the first bracket. The new version has included an instruction on mass-mounted equipment, which is what you are working on. The mass does act as a cantilever to a soft structure which is the hull which has low frequencies. They took this into account.

Mr. Johnson: Is there some simple way that we can find out in advance what frequency range would be applicable for a particular piece of gear, since they are generally designed for a particular class of ship. In other words is there a class listing of ships we could get?

Mr. Paladino: My suggestion is that when solicited for a contract for equipment, you ask the people what class of ship this is to go on. If they do not know the answer our office, Nav Ships 037, is available and we will direct you to the proper Type desk which will give you the answer you want.

Mr. Mains (Washington University): I think it is possible to bring a slightly different angle to this discussion which may be helpful to both sides. When I hear speakers on the platform say they cannot answer your question because they are not a reliability type or because they are an analyst and do not know about design, or perhaps they are a designer and do not know about testing, this reveals to me the fact that one of our principal troubles is suffering from tunnel vision. We see too much of our own little speciality and do not take the trouble to learn enough about the other guy's problem. Now about two years ago a manufacturer called me and said that he had been asked to submit a bid on the below-decks missile handling equipment for a batch of destroyers. The prime contractor said the equipment had to take 50 g; what does this mean? Well, of course, it does not mean anything. It simply means that the prime contractor is misinterpreting the whole business. So it takes about 6 or 8 months of cycling back and forth through the system to get to a point where there is sufficient understanding between the designer or manufacturer and the guy who has a contract for ships to get to the point where the designer can begin to make a reasonable proposal that will eventually allow him to design the stuff properly. I think that this is one of the big troubles. It does not really matter a great deal whether the specification says one number or another number, somebody somewhere in the operation has got to understand materials and components and tests and environments enough to be sure that the equipment when it gets designed will function properly. This is what we are really after. Whether the specification is right or wrong is not important and whether the contract is right or wrong is not important. The thing that is important is that the equipment function properly when it is installed and in service. I think we make too much of trying to be explicit about everything. We can say, for example, that the equipment has to go on board a destroyer so the upper limit of frequency is going to be about 25 Hz. So, if I design equipment that is resonant under 25 Hz, it is going to flunk the vibration test. So I know that the floor of the frequency is going to be somewhere in the 25 to 30 cycle range so I have a shock requirement. If the shock requirement is 60 inches per second, that says that you will have 1 g of equivalent static load for each cycle per second of frequency. You have to give the designer some number to work with to get this stuff sized so that the analyst can begin to do something with the analysis and so that the test men can begin to do something with the test equipment. Somewhere you have to begin. This means making some kind of generalization about the conditions and the equipment which will allow you to get started in the direction that gives you a chance of finishing properly. All I can say is that it works if you go at it right. Then, when you get to the shock test, you relax and everything passes and there is no problem. When you get to the vibration test you might have a nut or a bolt to fix here and there, but this is minor and does not give you any trouble. When you are all through, the stuff functions properly on board ship, which is what you are after. So I would argue for trying to stand back a little bit and look at a somewhat wider view than is portrayed in much of what I hear at these sessions.

Mr. Kilroy (Naval Ordnance Station, Louisville): Somebody has introduced cast iron into MIL-STD-167 and I am having a hard time getting enough shovels to pick up the cast iron pieces. Do you know why it was introduced into that standard?

Mr. Paladino: This is a type 3; it has been in since the beginning. Type 3 was not changed. I think you better read the old version. We have had very little trouble with Type 3. This is on torsional vibrations. The major

changes were made to Type 1, ballast in Type 2 and longitudinal stresses in Type 4. We also added mass-mounted equipment.

Mr. Kilroy: I still have a problem which I will take up with you later. In MIL-S-901, was there a change so that we can have the report form included in the specification. We now have to send fifty cents to buy the forms. We cannot do reports, because we cannot get the forms sometimes.

Mr. Lund: That is a very easy question. MIL-S-901 is currently under revision and will be coming out soon. We have a parting date of January and all your wishes will be fulfilled.

Mr. Spång (Institutet för Miljöteknik, Sweden): This question concerns the adoption of international standards. When you are considering probable new revisions of MIL-STD-810 and MIL-STD-202 for component testing, do you consider the adoption of test methods given in IEC publication 68, which are the agreed international standards for environmental testing procedures? You would perhaps say that those testing procedures are not suitable for your purposes, but in fact many of those procedures are very much based on military procedures used in different countries and on military procedures used in the USA. You have had a very good participation in this international work and you still have, both in the mechanical area and in the climatic area. Therefore I would like to note that I think it would be worthwhile to find out your aims for the future regarding the adoption of international standards in this field.

Mr. Earls: I have had no personal experience with the document you are talking about. I have had some with NATO documents which were based on MIL-STD-810. We are not considering the IEC standard as far as coming up with a MIL-STD-810 is concerned. Most of our input for MIL-STD-810 comes from the services and industry in the U.S. We have not taken anything from an international standard, so far.

Mr. Spång: Actually, the shock test in MIL-STD-810 is almost identical to the international IEC publication shock test. I do not know which way it has come about. I have some idea by asking some people in this country. There is a lot of discussion at the moment on humidity tests where the Americans are asking IEC and the ISO to adopt the U.S. humidity test in MIL-STD-202 for component testing. I think if you have no intention at all in this country to care about international standards, it could be rather difficult for the international bodies to find reasons for adopting American standards as international standards. Then you do not base your standards on international standards? This is to me a little bit surprising.

Mr. Askin: The IEC standardization work is not directly related to the MIL-STD-810 effort. We have been concerned primarily with standardizing within the U. S., and that is a big enough job in itself. We have not yet standardized even within these three services. I sat in on a few of the climactic standardization efforts in IEC TC 50, and the U. S. did not have a unified stand on the procedures, especially the one on humidity that is still being thrashed out. There is a basic disagreement between the American approach to humidity testing and the British. I know that we in the MIL-STD-810 coordination effort have not considered international standardization, and I think rightly so. We first have to solve our own standardization problem.

Mr. Paladino: The U. S. is cooperating with both the IEC and the ISO. In fact, in this country the American National Standards Institute has working groups, to one of which I belong, and they tie in to the IEC. If we do not have complete agreement in this country between industry and the DoD community, in no way can we make a united stand to an international group. Many times the data that is involved in the DoD requirements is not for open publication, which makes it extremely difficult. We do participate in international groups. We do have members who go over to all the meetings.

Mr. Root: I was chairman of the S2W60 working group which corresponds with group TC 50. Charles Fridinger is now the chairman. We are presently working with this IEC 68 document, attempting to come up with our own U. S. standard on sine testing. The consensus of the committee at this time is there are some weaknesses in IEC 68 but parts of it will be incorporated into the standard along with documents in use in the U. S. We are not overlooking this document, but we do not think at this time that it is a complete answer.

Mr. Spång: It is encouraging to know that somebody here really knows something about IEC publication 68 at least. Of course there are weak points in publication 68; there are weak points in MIL-STD-810 and in MIL-STD-202. Especially as an individual you will always find weak points because you have your own opinion on how this standard should look. But, in fact an international standard is worked out as a kind of a cooperation between different countries,

and all the countries have their possibilities to change the standard if they can press their arguments hard enough. In many cases this publication 68 is actually based on American practice. It might also be based in a certain degree on English practices, especially this humidity test. I happen to be in the working group which produced the original humidity test and I am not completely happy with that test. Actually, if you look at the other climatic test, the new dry heat test, you will find that it better suits your purposes. That is a test for heated test specimens and a test for specimens which are connected to an artificial cooling system. There is also this method on random vibration testing which is in the voting procedure. At the moment as far as I know, there is no existing random vibration standard. This means that you will not have the same difficulties of adopting an international standard. At least you should look at this before you start working on your own standard; that is the whole purpose of international standardization.

Mr. Pusey: Part of the purpose of this session is to solve our family problems as far as specifications is concerned. Do you have this same problem in Sweden?

Mr. Spång: Yes, we have. I think the problems are very similar, although we are fewer people. The loudness is about the same but the number of participants are fewer. We might not be able to create a panel of this size. We would only be about 4 or 5 people on the panel and we might get about 60 in the room, but the problems are the same.

Mr. Biamonte: Back in 1940-41 we got involved in a great World War, and most of our forward equipment we found deteriorated because of humidity. Humidity was an extreme problem. The Department of the Army at that time expended an extreme amount of money, manpower, and material to run a program for about four years evaluating humidity, humidity effects and humidity test procedures. If you remember, the Air Force was a part of the Department of the Army in those days. We have been gathering data for 30 years to come up with a test procedure. In MIL-STD-810, we have five test procedures. Why should we have five testing procedures? I can understand a steady-state humidity procedure. I can understand a cycling procedure, but I cannot understand why should we have five of them. Now if in 30 years we cannot standardize within DoD, how can we standardize with other countries? It is a difficult problem and possibly the only solution is a dictatorship which will say this is the way it will be done and will be done no other way. Perhaps if we standardize for one procedure right or wrong, we will find out whether we are right or wrong and correct it. Believe me, we are all concerned with the IEC and with the international standards, but it is not an easy problem. We have nine commands within the Army and I cannot get standardization. It is not an easy problem, but we are not ignoring the international standards. It took so many years up until now and it is going to take another 10 or 15 years before we get one standard.

Mr. Paladino: I am not a humidity man but I know that humidity is different on land vehicles than on ships. It is different on an airplane than on a tank in the Sahara Desert. It is not that easy. No one on this earth can design a piece of equipment which will survive the Army, Air Force, Navy and Marine Corp environments. So you primarily fix your own standards and design a specific piece of equipment for them. In the Navy we are concerned with ships and therefore all equipment will be designed to survive ship environments. Air Force and Army would do the same. The interplay comes in for example if the Army has transported some equipment to a war zone and they use the ship as a common carrier. Then we have to be careful. I do not say that you make them design Army equipment for the ship environment. We had one case in particular where the Air Force was transporting jet engines to an island and they shipped them on a Navy ship as cargo. When they got to the zone and were checked out they fell apart. A little investigation showed that the ship vibration Brinelled the bearings in the engine. We should always package them in mitigating capsules and we will have no more casualties. It is fine to have one document, but I think you are going to have to have families in that document for each service environment.

Mr. Dreher (Air Force Flight Dynamics Laboratory): Will Mr. Earls say something about the new plans for MIL-STD-810?

Mr. Earls: There is talk about two documents. The second document is called the limits document. It is more of a requirements document on what the actual environment is and what the test limits should be. The test methods document of MIL-STD-810 is just test methods; this is how you go about it. But in the second document there is a rationale behind it. Further, as Wayne Yarcho pointed out there are around 5,000 specifications. We were asked to review thirty, or forty of them and we are not going to bring all of theminto line with MIL-STD-810.

It is the idea to eliminate as many of these others as we can and, I think we can eliminate some of them. We will put in MIL-STD-810 what these other specifications have where possible so that it can be used in their place.

Mr. Askin: Just to amplify a little on what Mr. Earls has said, we have to keep separate the environmental criteria and the test procedures. This is really a very difficult task that a standardization group has taken upon itself. The effort to standardize MIL-STD-810B for all three services and to eliminate thereby a lot of the superfluous older standards that exist is one of the main tasks that this committee will have. One of the big problems is to try to incorporate the Navy, Army and Air Force standards that are current. Wherever they are common we must try to reduce the number of procedures. Right now the standard does not really represent all of these services adequately.

Mr. Forkois (Naval Research Laboratory): I agree with Mr. Biamonte to a certain extent. For example, shipboard equipment that has been passed to MIL-STD-167 and MIL-STD-901C is pretty rugged. The Navy does not require a transportation test on top of these tests. They do require some protection for storage against humidity and they have packaging for accidents against marring or dents in the equipment. I feel that a lot of equipment that I have tested to Navy Specifications would certainly satisfy truck or railroad transportation. A lot of the equipment would satisfy aircraft transportation. They may be a little heavy but, if you put them on isolators they certainly would meet the requirement for higher vibration. So to this extent I agree with Mr. Biamonte, that in many cases we have specifications which can embrace other specifications. I think that it is silly to retest to this extent. Perhaps these committees would do well to consider the possibility of eliminating some tests on the basis that one test actually embraces the requirements of another environment.

Mr. Johnson (US Army Electronic Proving Ground): We have a basic statement that the Mil-Spec be written to require the manufacturer to use a specific design method. That is why we look at procedures 9 and 11 in MIL-STD-810 as design methods, not as a finished product to meet a service environments. That is why we do not like to test with that procedure. I would like some comment on that.

Mr. Askin: You do not use MIL-STD-810 to design to. It is not intended for that purpose. MIL-STD-810 is a test document. The design requirements should be spelled out in Section 3 of your specifications. That is where they should tell you what environment you will see. MIL-STD-810 is there for the purpose of telling you how to run a test. You have to know what design limits you have from other documents.

Mr. Biamonte: I believe Mr. Johnson has a very valid question. The design requirements for the procedures 9 and 11 in a specification say that you shall meet rough handling in transportation environments without defining what they are. That is what is in Section 3 of the document and that is what he is complaining about. However, we do not have a definition of these environments. So what industry does through trial and error is to design something that meets the rough environment of procedures 9 and 11. Procedure 11 is nothing more than a simulation of the environment which loose cargo would see in a vehicle. For an item being driven as a part of a vehicle it is procedure 9. What these environments are is very difficult to determine. Some 20 years ago some work was done in this area and it has been shown that vibration excitation with extreme amplitudes of about 30 to 40 g and frequencies over a range up to about 2000 Hz are excited on the individual item as loose cargo. With respect to procedure 9, we ask that the item be designed to withstand repetitive shock impulses of about 10 g. This is all the data that is available. However, to put this as a design requirement might create a situation where a specification is not important. A specification is very important, maybe not from the technical point of view, but certainly from the administrative and contractual point of view. A specification is a legal document; it is important. We do not know what the environment is. We therefore say, and rightly so, industry has no alternative but to design to an actual test.

Mr. Johnson: The particular part of the procedure I was referring to was necessarily the second part, which is what you were referring to. I am referring to the first part, which is the 10 to 55 part.

Mr. Biamonte: Somebody back in 1965 decided to print MIL-STD-810 as a coordinated document. The Army Electronics Command had a test where we ask that the item be adapted to a plate which represented a vehicular adapter. The first part of this test was a survey and it was based strictly on development specifications. We asked the contractor to survey the equipment from 10 to 55 Hz at 0.03 inches amplitudes to make sure that the vibration amplitudes did not exceed a particular value. In past

experience, we found that if it did, the equipment would fall apart when subjected to the second part of the procedure. This was a diagnostic test. It was one merely to look at it. It did not have any criteria for acceptance or rejection. However, when it got inserted into MIL-STD-810, somebody decided that this was a test and applied a criterion to it. We never, if I can help it, hold anybody to the line. If the item does not fall apart in procedure one, we go right to procedure two and run the test, and use only procedure two as a criterion. I am sorry that has created a problem, but it is in MIL-STD-810, and you are perfectly right; it is a bad test.

Mr. Johnson: In MIL-STD-810 there is a procedure eight which is for ground equipment. That goes into detail as to what type of equipment for what type of vehicle. Procedure eight seems to be a single service environment for the particular selection of equipment. Procedure 10 seems to be a field service environment for loose cargo or transportation. That is what we want referenced in the specifications, instead of procedures 9 and 11.

Mr. Biamonte: I think Mr. Forkois brought it up very well before. Procedure eight is an item in MIL-STD-810 which calls out a specific environment, it talks about a wheeled vehicle, a tracked vehicle or some other kind of vehicle. There are three different curves in procedure eight. Procedure 10 is what a particular group within the Army called the Transportation environment or common carrier test, which I do not want to go into right now because that might take all night. However, what has been happening with our equipment is that when we call out procedures 9 and 11, a particular testing group would incorporate, regardless of our specifications, a common carrier test on the equipment. This is where we run into a lot of trouble, because a common carrier test calls for resonance dwells. I dare say that there is not a single piece of ground equipment that I cannot make fail when subjected to the common carrier test of MIL-STD-810. I do not care who designed it; I could fail it. This is mainly because there is no procedure within MIL-STD-810 that tells you how to find the resonances and what resonances you shall dwell on.

Mr. Mains: There are only, as far as I know, three ways that a design requirement can be specified. You may specify a design procedure which is to be followed to produce the given piece of equipment. You may specify a performance to be achieved within a given defined environment, or you may specify a test procedure which is to evaluate the equipment once it has been designed. Now if we concede that everybodys heart is in the right place and what we really want is for this equipment to work in the field, then we must specify a performance within an environment. To specify design procedures or to specify a test begs the question. Right now, we are in the anomolous position of having to try to satisfy all three things simultaneously, but knowing that the final criterion of acceptance will be the test. It seems to me we ought to get off the fence and stop mugwumping. Either call for performance within an environment and shut up about tests and design procedures, or frankly admit we do not know how to define the environment and the performance and specify the test. Shut up about the other things; set up a design procedure for them to follow and make everybody clear regardless of what happens with the test or performance in the final environment. You cannot be all things to all people at once; it will not work. From the standpoint of the manufacturers I have lived with, they would prefer and I would prefer to have a requirement for performance within the defined environment. We can do this. But we know that as far as the Navy is concerned, we have to pass that barge test. So we fix the design to pass the barge test and if necessary, we dress up the other things to fulfill the requirements. This is not tne way it should be.

Mr. Pusey: I think you made a very good point. The question of whether you design to a test or whether you design for the environment is a very important thing. Unfortunately, there are no ways to prove sometimes whether you have designed to the environment, unless you create a test which may be perhaps conservative, and run it.

Mr. Lund: I think the barge test, although you can criticize it, is about the best alternative we have. We have given design methods a hard try. We found that, if given the opportunity to choose between satisfying the Navy's dynamic analysis requirement or the barge test, most vendors really jump to the barge test. It seems to be the preferred route. One reason for this I think is the difficulty we had in applying failure criteria. If we specify design methods, we are forced to specify failure criteria to go along with it. If we design to yield and if in our analysis we predict stress above yield, that must be rejected simply because we cannot constantly predict what is going to happen to the equipment once it starts yielding. However, many manufacturers

have gotten a bit smart with the shock testing business, including the barge testing business. They have found that you need not design up to yield in order to pass the barge test; you can get away with much less in many cases. This requires a lot of engineering judgement, of course, and it is possible to make mistakes, but we find that they are seldom made. There are not many equipments that fail the barge test and, when they do, no one is particularly surprised as to why they did. So I think the straight testing procedure does have certain advantages over the straight design procedure. What we try to do here is mix these two procedures by offering some guidance as to how to pass the test. We leave the rest up to the good engineering judgement of the contractor.

Mr. Mains: This is something I think needs to be said. Mr. Forkois, if you wanted to make a piece of equipment pass a shock test you could do so, and nobody watching over your shoulder could tell the difference between your wanting to make it pass or make it not pass. When I have produced three inches of IBM output of analysis, I can make that analysis say everything is good or everything is bad, and nobody in the world can determine which I was trying to do. So the real reason why the test is such an important thing in the Navy end of things is that it is the one criterion that is not rigged and cannot be rigged as long as you play it square. I do not know how many know the name, H. F. Moore, but 30 years ago he was the grand old man of materials testing. I remember a class under him in which he gave out a batch of fatigue data and the assignment was to take the stuff home and come back with an argument that showed this was a good material for the specified application. We brought it back the next day he said take it home again and prove to me it is not the right material for the specified application. We brought that back. He had illustrated the point, that given the same set of data, you can prove both sides of the question depending on how you present the argument. This, I think, is a point we should all keep in mind. We can slant the analysis or slant the test or slant the test data interpretation any old way we want to. As of now we depend on the barge test or the hammer test to be an impartial kind of thing if you like, adjudicated by people who are not trying to make it go one way or another. So we can all play it square and come out in the right place in the end, we hope.

Mr. Nankey (General Electric Company): I think there is a very important feature of the shock and vibration design and test problem that has not been brought up tonight. It is rather incredible that we have discussed shock and vibration testing and design requirements for some three hours now, and no one has brought up the very important subject of the impedance relationship between the driven system and driving system. I know that there are some people who are doing some research along this line. I am doing a little myself. We find that it is central to the problem of obtaining proper test and design procedures. We heard the argument earlier that test specifications were entirely adequate or maybe not stringent enough. We also heard counter arguments suggesting that perhaps test specifications are too stringent. Both are right if you do not experience a certain kind of frequency blindness that fails to separate high impedance products from low input impedance areas. I think a great deal of this would be cleared up if we were to recognize that when we are dealing with shock and vibration and environmental problems, we have a situation in which the driving point impedance of products can vary over perhaps two or three decades. At some frequencies we have nearly infinite impedance reflected back to the driving system. Other frequency domains have nearly zero impedance reflected to the driving system. I would like to hear some comments from the panel on this particular aspect of the shock and vibration problem.

Mr. Earls: I have very little information on the impedance situation. We have had some limited investigations. I realize that on a shaker you use an infinite impedance input which is not the same as on the airplane. I do not think we have gone far enough yet.

Mr. Paladino: In the Department of Navy the impedance type measurements are primarily used in acoustic work. We have not used it in the mechanical vibration test.

Mr. Biamonte: I do not think I can contribute anything with regard to impedance measurements. We have not been doing it in the Laboratory. I think the impedance type work, where we are looking at signature shock effects and so forth, should be limited to the investigation leading up to a specific type test. I do not see how we could apply it to final test specifications.

Mr. Ludwig (Pratt & Whitney Aircraft): There are people working on impedance. We saw a whole session on mechanical impedance in the Shock and Vibration Symposium here. There is a writing group, S2W58, working on such specifications. I think I will leave it to them to make the specifications. Impedance is

a very useful tool if used in the right place; it can evaluate development hardware and it can tell you a lot about it.

Mr. Dreher: It sounds to me as if everybody is trying to say that maybe we should get rid of specifications. We have to admit that our business, getting equipment qualified, is a very tricky business. It is not something that some equipment project engineer can handle. It sounds to me as if most of the specifications are called out by equipment project engineers. Let us assume that a radar engineer develops a specification. In addition to having to be an expert in radar and electronics, he also has to be an expert in environment. Let us face it, all people that I have talked to in that situation tell me they wish they had someone to help them out. We should take specifications off the public market. Only an environment group should handle them. Every development agency should have an environmental engineering group, engineers who know what an environment is all about. Equipment project engineers should get everything signed off by this group. The only organization that I have come across that really does this is one aircraft company. This came to pass simply because of the forcefulness of the man in charge of the dynamics group. He is the kind of man that does not let anybody do anything without his knowing about it. He has caused all the project engineers in his company to come through his office. I think that is what all of you are trying to say, that we need this control.

Mr. Paladino: What the gentleman said sounds very good but, for example, consider a system like an aircraft carrier. It has the aircraft, land type vehicles, radar operating equipment, missile systems, and so forth. I cannot walk on the water. That is why we have what we call Type desks. They are specialists in particular systems. DoD is highly concerned about having an environmental desk, but the thing is to staff it with competent engineers.

Mr. Biamonte: I would like to commend the gentleman who suggested getting rid of specifications. I would like to get rid of specifications, also. I do not know how many industry people we have here, but is there anybody here from industry that is willing to sell to the government on a warranty.

Mr. Dreher: You missed my point. I do not want to get rid of them; I just want to take them out of the public domain.

Mr. Wilkus: I can remember Dr. Rogers back in the old dynamics group at Wright Field. He came up with a simple specification for noise. He did not put a number on it. He had letters ABC and there were numbers that associated with these letters, but it depended on the application. I appreciate what Dr. Dreher had to say, but I do not know whether we are going to get that many environmental engineers. In my opinion what we need is some better guidance on testing. Engineers have to be taught. We have problems such as: What is a resonance? I do not know even whether we can agree on what a sine wave is. Sometimes, it comes to that. There is a proposal to come out with a document to define procedures. I think that is what we are lacking. For example, if we improve the equipment in aircraft there is a man back here worrying about the levels. Now he may be trapped in that, but there is an alternative of location. A lot of people do not know that and they do not ask the question: Can it be relocated? It is amazing how much work is done on things like damping materials and when we look at vibration in a piece of equipment, we find out that it is resonant and magnifies the vibration quite a great deal. I would have encouraged that it be worked on some more. But maybe these things need to be proven and a little bit more solid information put out.

Mr. Askin: I would like to agree with Dr. Dreher and Dr. Mains. I think there are two basic problems. One is the age old problem of communications. There is not enough intelligent communication between the designer, the tester and the environmentalist. The second is the parochial view taken by the designer. He thinks he knows everything. He does not want to come to an environmental engineer to get any help. I think these environmental engineers have to become more aware of the problems of the designer. It has got to be a joint effort. All of this means more research to find out the actual environment that we have to design for and test for. We have to educate top level people in the government to fund more of this research. Industry also should do more research when they are designing something new. If they came to the government and pointed out what information they have and how valid it is, they can jointly reach an agreement on what specifications ought to be used. It is basically a matter of better communications.

Mr. Lund: Starting about the mid 1950's the Navy got quite serious about the shock problem due to installation of very shock-sensitive systems on ships, such as electronic systems and delicate weapons systems. At

that time we also had a development of the nuclear weapons threat, and this had led to a rapid rate of change in shock requirements. This is one thing you folks put up with quite admirably. This goes for the contractors and the Navy. If it is any comfort to you, I think we have about stabilized the situation. I really doubt that we will see major quantum jumps of the sort you have seen in the last 10 or 15 years in the shock business. Judging from the response tonight, the shock troops do not seem to be in very deep trouble. I do not think we will get you back into trouble again, at least for some time to come.

Mr. Phillips: I have reached a conclusion that we should not do away with all the specifications. This is a method of communicating and it should be considered just as that. It is a method that hopefully will get better as we use the specifications and can interpret them better. I also reaffirm my conviction that one of the most important paragraphs in MIL-STD-810 is in the original version as one of the paragraphs in the beginning. It was an introductory remark that this standard should be used only if you did not have something better. If you knew the operating environment better than stated in the standard, then you should definitely use the operating environment. In other words it is to be used as a guide. This paragraph should certainly be in the next version and underlined. This would clear up a lot of the problems. Look at the final product and the final environment and get there the best way you can. If you can use the standards use them, but if you have something better by all means use that.

SOME ADMINISTRATIVE FACTORS WHICH INFLUENCE TECHNICAL APPROACHES TO SHIP SHOCK HARDENING

Donald M. Lund
Naval Ship Engineering Center
Hyattsville, Maryland

This paper briefly examines the technical side of a few administratively-oriented factors which are of importance to the Navy's ship shock hardening effort. It is illustrated that these factors will increasingly influence the selection of technical approaches to ship hardening.

BACKGROUND

The general objective of the Navy shock hardening effort is to fully optimize the shock resistant qualities of Navy ships. All factors which must be accounted for in order to optimize these qualities cannot be meaningfully discussed in a brief paper of this sort, but a review of basic considerations is needed to establish a context for subsequent discussion. For purpose of this review, all factors which influence the optimization of ship hardness have been loosely separated into four categories; each category is defined and discussed in the following paragraphs:

1. Threat Factors. Potential shock threats are posed by any sizable weapon, nuclear or conventional, self or enemy-delivered, which can detonate underwater in the vicinity of the ship (primarily, influence mines/torpedoes, near miss conventional bombs or missiles, and far-miss nuclear weapons). Threat considerations are strongly mission-oriented, and include:

(a) Likelihood of exposure to enemy-delivered underwater explosions, in an absolute sense and relative to likelihood of exposure to other types of enemy-delivered weapons effects.

(b) Requirements to intentionally encounter the shock environment in connection with mission roles (sweeping and destruction of mines, for instance).

(c) Benefits associated with capability to withstand close-in self-delivery of weapons which induce shock (primarily, ASW weapons).

2. Vulnerability Factors. These factors express the vulnerability of ships to shock, either in absolute terms or relative to other weapon effects. When considered in conjunction with threat, need for shock hardening of various ship systems can be determined and compared with need for hardening against other weapons effects. Such an analysis permits development of a total hardening approach which affords logically balanced (thus, optimum) resistance against all weapons effects.

3. Shock Hardening State-of-the-Art Factors. These factors essentially serve to determine which specific technical approaches could be employed -- either now, or possibly later after further research and development -- to reduce the vulnerability of ships to shock. Technical confidence levels are generally associated with all alternatives in this category; these confidence levels can vary in accordance with shock severity, type of shipboard system under consideration, and a number of other variables. Given a detailed ship design baseline, knowledge of the state-of-the-art, and a basis for shock hardening which has been optimized from a threat/vulnerability standpoint, one may select technically optimized approaches to hardening of the ship in question. By definition, this process yields maximum shock hardening effectiveness. Were it not for the influence of administrative factors (as defined below), all Navy RDT&E programming in the shock area and all shipbuilding specification shock requirements would reflect a single and outwardly desirable goal -- to fully optimize the shock resistant qualities of Navy ships through development and application of technically optimized hardening procedures.

4. Administrative Factors. For purposes of this paper, these are defined as factors which influence administration of the Navy shock hardening effort but which are not based upon shock threats, vulnerability to shock, or

shock technology. The most noticeable effect of these factors is one which all of us have probably regarded with varying degrees of discomfort from time to time; they serve to modify technically optimized approaches to ship hardening in response to outside influences of questionable character, such as schedules, contracting regulations, availability of funds, and the like.

Most members of the technical community which supports the Navy shock hardening effort are naturally well informed concerning vulnerability and state-of-the-art factors which influence ship hardening optimization. Some threat factors are given less publicity within this community due to security restrictions, but technically-oriented information in this area is nonetheless available where needed.

Relative to the factors mentioned above, administrative factors are not so widely understood or appreciated by many members of the technical community -- despite the strong influence which these factors exert upon ship shock hardening technical progress and the structure of technical tasks performed in support of this effort. This phenomenom is of course easily rationalized; some members of the technical community are simply not very interested in administrative affairs, others who might be interested may find no easy or sympathetic lines of communication open to all levels of the administrative community, and some administratively-oriented topics are rather sophisticated in their own right and thus are not easily interpreted by persons lacking background in this area.

There is little question that the above situation merely reflects the natural order of things -- an order strengthened, perhaps, by purposeful organizational divisions which have been erected in part to protect technologists from administrators and vice-versa. Nonetheless, there is equally little question that the shock hardening effort will progress with maximum efficiency if all of its participating supporters can recognize and thus account as necessary for all of the major factors (including administrative factors) which influence achievement of basic hardening objectives.

Against this background, some administrative factors which the writer believes are most influential in determining selection of technical approaches to ship hardening are briefly discussed in the following section of this paper. The intent of the following discussion is definitely not to make the technical community expert in the field of administrative affairs (it will not), but rather to convey a basic but perhaps improved understanding of how and why certain administrative factors influence selection of technical approaches to ship hardening.

DISCUSSION

Since the Navy and supporting contractors are engaged in a great variety of efforts which involve selection of technical approaches to ship hardening, it would be appropriate at the onset of this discussion to clarify which of these selection processes are being referred to. Generally, this discussion is keyed to issues directly applicable to shipbuilding per se, and the technical approaches in question here are generally those which are invoked as requirements in shipbuilding specifications. This approach was selected for several reasons. First, shock hardened ships represent, in one way or another, the end product of all of our efforts. Second, it appears certain that the vast majority of technical manhours being expended in support of the ship shock hardening effort are, in fact, being spent in direct response to shipbuilding specification requirements. Finally, it is in this area that administrative influences are most pronounced; ship acquisition managers, who are not card-carrying members of the Navy Shock Program, are responsible for implementing ship hardening requirements.

The fact that this discussion is largely keyed to shipbuilding is not considered particularly limiting. Selection of shock-oriented applied research goals, for instance, is strongly influenced by the knowledge that most RDT&E accomplishments must eventually be reflected in shipbuilding specifications in order to benefit the Fleets.

Emphasis will be given in this discussion to only three basic administrative factors: Procurement policies, cost considerations, and scheduling considerations. This choice of discussion topics simply reflects the principal functions of the ship acquisition manager's job--to acquire ships within the constraints imposed by procurement policies, scheduling constraints, and fiscal limitations.

Navy procurement policies will be considered first. Some fundamental points:

1. A body of law has evolved over the years which is applicable to government procurements. This body of law is reflected in the context of DOD policies in the Armed Services Procurement Regulations (ASPR). Navy procurement policies, in turn, essentially establish how the Navy shall go about procuring goods and services within the framework of ASPR.

2. One of the first steps which the Navy takes when planning a ship procurement (or any other procurement) is to select from available alternatives the procurement procedures which are best suited, legally and otherwise, to the acquisition in question. Selection of procurement procedures is normally accomplished well in advance of the selection of shock requirements for the ship in question; early selection of procurement procedures is absolutely necessary to give direction to the acquisition process.

3. Central to the process of selecting procurement procedures is selection of contract type. Two general categories of contract types are worthy of brief attention here:

(a) Fixed Price Contracts. Under any type of fixed price contract, the contractor must assume at least some responsibility (hence, risk) for performance in accordance with contract provisions at a previously agreed upon price. In order to remain competitive and maximize profits in an atmosphere of fixed price contracting, the contractor must constantly strive to devise more efficient ways of doing business and must carefully control his costs. The principle prerequisite to fixed price contracting is that the nature and extent of contract effort must be sufficiently well defined to permit realistic advance estimation of contract cost.

(b) Cost Reimbursement Contracts. If cost of contract performance cannot be realistically estimated in advance -- as is often the case with research-oriented or research-dependent efforts -- the government generally assumes the bulk of cost risk through issuance of some type of cost reimbursement contract. Such contracts commonly provide for payment of costs borne by the contractor, plus profit (fee). Contracts of this type are generally more difficult to administer than fixed price contracts, and provide the contractor with little real incentive to hold down costs.

4. Owing to the above considerations, ASPR and derived Navy policies require application of fixed price contracting procedures whenever feasible. When a new design ship class is being procured, some work under cost reimbursement contracts may be required for the purpose of more fully developing new concepts applicable to the ship in question; output from these contracts serves to definitize ship design and performance requirements to the point where subsequent design and construction efforts may be accomplished under some type of fixed price contract. Despite this potential opportunity to address some shipbuilding requirements under cost reimbursement contracts, it remains that procurement policies strongly encourage development of shipbuilding specification requirements which can be applied directly under fixed price contracts, and discourage the specification of requirements which can only be addressed under some type of cost reimbursement arrangement.

The first two points cited above suggest the general relationship (or pecking order) between shock requirements and procurement policies. We find that the laws of physics and the "laws of procurement" possess capability to exert a similar overall influence upon how we harden ships, since in their own way they both ordain what can or cannot be done -- and neither will yield readily to a desire on our part to do otherwise. The second two points suggest that procurement policies will, in fact, exercise their prerogatives -- they will influence the selection of technical approaches to ship hardening. This influence, which largely reflects the firmly established need to implement shock requirements within the framework of fixed price contracting constraints, may often be evidenced in ways which tend to counter technical considerations. Examination of only three issues which have a bearing upon the technical quality of Navy shock requirements should be sufficient to illustrate this point:

1. State-of-the-art. From a purely technical standpoint, the best approach to ship hardening is the latest approach -- the one which incorporates all new technical findings. From a procurement policy standpoint, the best approach is the way we did it last time, because industry's experience with the previous requirement serves to establish a good basis for advance estimation of the cost of fixed price contract performance. Some measure of shock requirement "newness" is of course acceptable. However, it is to be expected that those who are in contention for the contract (hereafter referred to as "bidders") will compensate for their lack of experience with new shock requirements by factoring some "worst case" assumptions into their contract bids. Cost to the Government will thus likely be driven in an upward direction for reasons solely associated with the newness of the requirement, an undesirable effect. Of course, bidders may declare any major alteration of shock requirements to be unbiddable on a fixed price basis if they cannot estimate its cost implications with reasonable confidence. As suggested by previous discussion, such a happening will more often force alteration of the shock requirement than alteration of procurement procedures.

2. Complexity. The researcher rightfully observes that shock is a complex dynamic phenomenon which cannot be rationally addressed by simple rules such as "design everything to withstand 60 G's". Consequently, as we learn more and more about shock and all its vagaries, proposed technical solutions to shock problems tend to become more complex. Procurement policies will favor that easily priced out "60 G" requirement, however. If any shock requirement is very complex, the bidder may realize that he simply hasn't time (within the period allotted for bid formulation) to fully evaluate the impact of the requirement upon costs. His options in this case include development of conservative (protective) cost estimates, requesting more time to formulate a bid, or refusing to bid. None of these options are administratively pleasing.

3. Influence of installation variables. Inasmuch as equipment shock response can be dependent upon installation variables such as type of ship, location aboard ship, nature of supporting structure, and location of adjacent

major masses, it would be technically desirable to express shock requirements in terms of these installation variables. In that way, resultant equipment designs would better and perhaps more economically reflect actual needs associated with a specific shock environment. (As is, Navy shock requirements are often predicated upon somewhat conservative assumptions in order to address the general case.) The procurement adminstrator would likely view the improved technical approach with skepticism, however. He would probably point out that the contract bidders will not know, at the time of bidding, exactly how or exactly where most shock resistant equipments will be installed. (The successful bidder may not even have this information at the time he must place orders for the equipment, in fact). Therefore, the bidders will understandably make conservative assumptions when estimating costs, which leads us right back to where we were when the Navy was predicating requirements on the basis of conservative assumptions. Or beyond where we were before; estimates of contract performance cost may be somewhat higher than would have been the case if the original requirement had been invoked, owing to the newness and added complexity of the requirement.

The impact of fixed price contracting constraints upon selection of technical approaches to ship hardening is reasonably evident from the previous discussion. Basically, we find that this particular administrative factor will always serve to promote simple, straightforward technical approaches to shock hardening. It tends strongly to limit important shock design parameters to those which can be determined in advance of detailed ship design (during the bidding period), and serves to resist rapid change of technical approaches.

It should be noted that the above administrative influences do not flow only from the Navy side of the house. Shipbuilders and their attendant sub-contractors obviously view fixed price bidding issues from a frame of reference difference than the Navy's, but this really makes little difference. When faced with lack of firsthand experience with a new or very complex shock requirement, the bidder is immediately faced with some difficult decisions: Assume the worst case (protect company profits by reducing cost risk), or bid less conservatively in the interest of being the lowest bidder? Tell the Navy I can't bid the job on a fixed price basis (perhaps conveying the impression that I'm not as technically astute as my competitors), or give it a try? No one likes to be faced with decisions of this sort. The fact that Navy and industrial procurement administrators will arrive at similar conclusions (for perhaps different reasons) concerning the administrative worthiness of shock requirements is not surprising; the governing procurement policies are intended to protect the free enterprise system (including its industrial participants) as well as the Navy's own interests.

One other aspect of Navy procurement policies should be considered in this discussion -- the issue of competition. We all enjoy the benefits of free and active industrial competition, which tends to keep prices down while promoting quality and improvement of goods and services. Navy procurement policies reflect our own feelings in this respect; they insist that competition for Navy's business be encouraged to the maximum extent practical.

The influence of procurement policies applicable to the competition issue is twofold. First, these regulations tend to discourage implementation of technical approaches which are so technically specialized that only a few (or worse, only one or two) bidders can realistically compete for the contract in question. Thus, they effectively favor reasonably straightforward technical approaches, and favor approaches which do not demand possession of specialized facilities. The second influence of policies in this area is slightly more subtle; they inveigh against many types of highly tailored contract requirements, even though the requirements in question could be satisfied by many different contractors. Take for example a previously discussed hypothetical shock requirement, which was expressed in terms of a particular shock environment defined by type of ship, location aboard ship, nature of supporting structure, and location of adjacent major masses. Any contractor who satisfies this requirement during the course of a given shipbuilding program will possess a decided competitive advantage in a follow-ship program or in the event that some other shipbuilding program finds need for the same equipment type to be installed in a corresponding shock environment. Conversely, this contractor may find himself somewhat outside of the sphere of real competition if his previous shock qualification cannot be extended to the next potential application. In either case, desirable competitive advantages are mitigated by the nature of the speciallized shock requirement.

Again, the Navy is not the only party interested in the issues discussed above. One can count upon an expression of righteous indignation from any well established Navy supplier who suddenly finds himself effectively excluded from active competition by a difficult shock requirement. The usual private industry response to a highly tailored shock requirement of the type exampled in the previous paragraph is equally understandable: "But, how can I shock-qualify my equipment so that the shock qualification will be applicable to a variety of shipboard installation requirements?" In either case, the naval supplier is simply seeking an opportunity to effectively compete for Navy business, an objective which is fundamentally coincident with the intent of the

Navy's own procurement policies.

It is interesting to note that the impact of the competition issue upon selection of technical approaches to shock hardening reinforces the impact of fixed price contracting constraints. The former administrative factor, like the latter, serves to encourage implementation of shock requirements which are technically straightforward, and discourages highly tailored "case basis" hardening approaches.

This discussion now turns to the subject of cost considerations. Little need be said concerning the basic impact of cost factors upon selection of technical approaches to ship hardening; we all know that Defense Department dollars are in critically short supply, and that cost factors will always strongly favor the least expensive hardening approach. It may be instructive, however, to examine how certain shock hardening parameters and hardening approaches can influence cost (and vice-versa).

First, consider hardness level -- the level of shock severity which is to be addressed and effectively defeated through implementation of ship hardening requirements. Figures 1, 2, and 3 illustrate how the major direct contributors to hardening cost might be generally expected to vary with hardness level. Requirements that ships be capable of resisting sea motions and shipboard vibration largely serve as functional substitutes for shock requirements until we arrive at a shock severity level where shock loads can exceed these other environmental loadings. In order to achieve adequate resistance to shock severities above this "inherent protection level", we must invoke shock design and shock test requirements on a very broad scale. Figures 1 and 2 reflect this consideration. Once invoked, shock design and shock test costs can be expected to increase only slightly with increasing shock severity. Important shock testing costs which do not vary significantly with shock test level are costs associated with shipment of equipment to and from test facilities, installation of the test item on the shock testing device, labor costs associated with running the test, and post-test teardown and inspection. In the area of design, cost associated with initial shock design checkout of proposed designs does not vary significantly with hardening level. The modest increase of shock testing and shock design costs with increasing hardening level is largely attributable to the fact that more and more equipment areas become critical from a shock standpoint as hardness level increases, which implies increasing requirements for redesign and retesting. Design costs will eventually increase rapidly at the point where it becomes necessary to design a significant amount of shock resistance into basic ship structure -- hull plating/framing, decks, bulkheads, and the like. Ship construction costs solely related to shock will begin to increase at a more rapid rate than test or design costs as increasing level of protection overtakes the individual inherent shock resistance levels of various types of shipboard equipments and foundations. Principal costs in this area are associated with the "beefing up" of structural members, which adds labor and materials cost. These costs will begin to rise sharply at the point where protection levels begin to surpass the level of inherent hardness associated with the hull and other basic ship structure.

Figure 4, which represents a composite of costs shown in Figures 1, 2 and 3, illustrates how cost considerations are likely to influence selection of hardness levels. If hardening payoff is low, "hardening" within region "A" of Figure 4 will likely be the most attractive choice. If payoff is medium to high, hardening to some level within region "B" is indicated.

In connection with the above, we might also consider how cost considerations influence the potential for alteration of hardness levels from those currently specified to some other value. Figure 4 reflects steady state conditions, i.e., conditions which exist after the hardness level in question has been invoked for a long period of time. Figure 5 illustrates the effect of sudden alteration of hardening level from point "A" (an assumed long-established level) to any other level. We find that decrease of protection level results (as expected) in a cost reduction, but costs do not drop immediately to steady state levels due to the influence of design standardization. Increase of protection level will first reduce or completely wipe out the applicability of previously conducted shock tests and previous shock design analyses -- an important factor. Significant increase of protection levels would lead to at least partial obsolescence of currently available shock testing devices, and would naturally imply requirements for shock hardening modification of many currently acceptable shipboard equipments. Therefore, cost considerations tend to keep hardening levels constant, and particularly inveigh against even a modest increase of well established hardening levels.

In the previous paragraph, reference was made to a most important shock program resource: The large reservoir of equipment designs which have been previously approved for installation on shock resistant ships on the basis of satisfaction of still-current shock test requirements. Present Navy shock test procedures are rather generalized in the sense that a conservative shock environment is usually represented during the shock test, rather than a specific environment associated with a specific ship and shipboard mounting arrangement/location. This approach permits broad application of "shock test extension" policies, which permit acceptance of previously shock tested and approved

Figure 1

Shock Testing Cost vs. Hardening Level

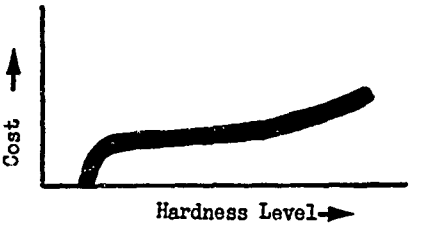

Figure 2

Shock Design Cost vs. Hardening Level

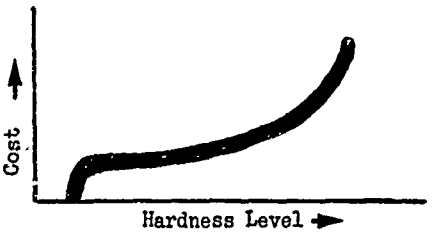

Figure 3

Added Labor and Material Cost vs. Hardness Level

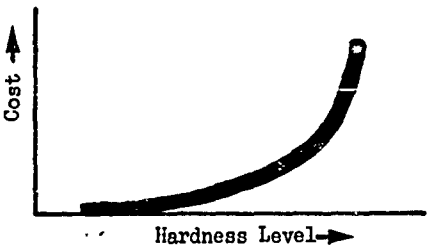

Figure 4

Composite Hardening Cost vs. Hardness Level

(Steady State)

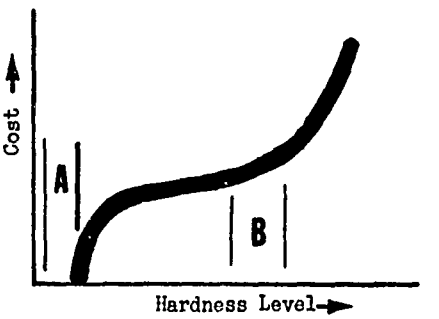

Figure 5

Composite Hardening Cost vs. Hardness Level

(Transient)

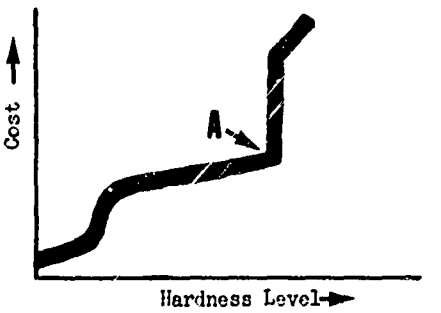

equipments for subsequent installation in various locations on almost any type of ship. Furthermore, these policies permit acceptance of untested equipments if they can be shown to possess a degree of shock resistance equal to or better than that of a similarly-designed equipment which has already satisfied the shock test requirement.

It is clear that continuing growth of our reservoir of previously shock tested and approved equipments is playing a very major role in reducing ship hardening costs. The majority of shock hardened equipments being installed aboard combatant ships are now being accepted on the basis of shock test extension, and the trend could no doubt continue until, at some not-too-distant date, nearly all equipments will be accepted on this basis. It is equally clear that the cost conscious Navy administrator will instinctively resist adoption of technical approaches which could lessen the potential for shock test extensions, i.e., approaches involving increase of hardening level or tailoring of shock test requirements to reflect specific shock environments in specific ships.

Similar considerations apply to our other onboard shock program resources. It would be quite undesirable, from a cost standpoint, to adopt new technical approaches which would significantly reduce the potential for utilization of presently available shock test facilities, shock design resources (computer programs, able personnel, etc.) and related industrial capabilities/facilities. These resources have not been easily won; any technical rationale which leads to their dismissal must therefore be extremely compelling.

Before closing this portion of the discussion, it might be worthwhile to briefly summarize all principal cost considerations which would normally be given administrative attention during the development of shock specifications. These are as follows:

1. Direct labor and material costs. Includes only those costs directly and immediately associated with satisfying the requirement, such as shock design costs, shock testing costs, cost for "beefing up", and the like.

2. Indirect labor and material costs. If satisfaction of the requirement entails addition of weight, it is possible that the ship will have to grow (increase in length, beam, or both) in order to accomodate the weight increase. (Weight which is added low in the ship may serve only to decrease requirements for ballast, but weight added high in the ship can be penalizing). Shock requirements which entail added space requirements can also exert a direct effect upon ship growth in some cases. Ship growth, of course, implies added cost; more hull and structure, longer piping and cabling runs, and so forth. The Navy's preference for directly hardening equipment, as opposed to mounting non-hardened equipment upon shock-mitigated decks or shock-mitigated platforms, is partly predicated upon consideration of costs in this category; truly effective shock mitigation systems are relatively inefficient from the standpoint of space and weight added.

3. Administrative costs. These are costs associated with administration of the shock requirement. If the requirement is simple and straightforward, these costs will normally be very low. Costs in this category can become fairly significant, however, if the shock requirement entails application of stringent quality control measures or leads for other reasons to the flow of a large amount of information between the Navy and the contractor.

4. Costs related to reliability. Because shock requirements have a generally "ruggedizing" effect upon equipment design, a shock hardened equipment is generally a more reliable equipment. Nonetheless, reliability issues will be considered when alternate approaches to shock hardening are being evaluated -- particularly when the shock hardening process will involve addition of any sort of moving parts or addition of materials which are subject to gradual deterioration.

5. Maintenance costs. Anything added to an installation for shock purposes will likely require some form of periodic maintenance during the life of the ship; for instance, the added items may require painting, lubrication, or may wear out or deteriorate. Related maintenance costs can become quite significant when considered over the 30 year lifetime of a class of ships, so careful attention will be given to this potential source of shock cost. The previously discussed question of direct hardening vs. shock mitigation also serves as a good example of how maintenance considerations can influence technical approaches to ship hardening. The essential question is usually simple: Will the cost to develop, manufacture, provide space for, install, and <u>maintain</u> shock mitigating devices and associated structure on a given number of ships exceed, or be less than, the cost to develop a directly hardened design?

6. Maintainability-related costs. As the name implies, costs in this category reflect the impact of shock requirements upon ability to maintain shipboard equipments and structures. To date, the maintainability issue has been raised seriously only with respect to foundation shock requirements ("bulky shock resistant foundations restricting access to surfaces which must be painted and to equipment which must be maintained"). The writer is firmly convinced that shock requirements need not (inherently) cause such problems, but the issue is nonetheless sensitive and

and will be given close attention during review of proposed shock specifications.

7. Operating costs. Any shock requirement which causes addition of ship weight also causes increased fuel consumption. Some sort of penalty (possibly a cost penalty) will also be borne if shock requirements cause any shipboard operation to become more difficult or time consuming.

Shock hardening costs in many of the above categories are currently very low or near-zero, and costs in all categories of significance are dropping sharply in response to the shipbuilding industry's rapid adaption to presently-specified shock requirements and due to increased shock test extension opportunities. Needless to say, the administrative community has a strong interest in preserving present cost-reduction trends and in holding costs down in areas where shock requirements currently exert little cost impact.

It can be seen that discussion of cost considerations amounts to the central theme of this paper. Procurement policies were found to be predicated in many ways upon cost considerations, and the immediately preceding discussion illustrated a number of relationships between cost and selection of shock hardening approaches. The following discussion of scheduling considerations will again illustrate the predominance of the cost factor. These scheduling considerations are discussed separately only for convenience; in effect, scheduling considerations are strictly cost-oriented administrative factors for all practical purposes.

Assume for a moment that a shipbuilder is bidding on a contract to build a class of combatant Navy ships for which no shock requirement has been invoked. During the bidding period, the shipbuilder will develop schedules which define when various shipbuilding events (design, procurement, and production events) would be performed during the term of the contract. This schedule will reflect the shipbuilder's lowest cost, most efficient way of building non-hardened ships. Now, assume that the Navy changes its mind at the last moment and imposes a shock requirement upon the ships in question. The shipbuilder, in response to this change, will likely alter his formerly-optimum schedule of events at least slightly to account for the impact of shock requirements upon design, procurement, production, and other shipbuilding activities.

The extent to which such otherwise-optimum shipbuilding event schedules must be altered to permit satisfaction of the shock requirement has a direct and significant bearing upon hardening cost, and provides a direct measure of the compatibility between the shock requirement and the shipbuilding process in general. Selection of technical approaches to ship hardening is strongly keyed to the goal of maximizing compatibility in this area, in the interest of keeping hardening costs low.

Specifically, these scheduling considerations influence selection of technical approaches to hardening in two principal ways. First, and in direct reflection of the fact that "time is money", they strongly favor the least time-consuming approach. This influence is strongest, of course, if there is any possibility that introduction of the shock requirement will cause stretch-out of time between major shipbuilding events or cause overall lengthening of the ship design and construction period. Naturally, this scheduling factor fundamentally influences the question of how precise a technical approach shall be taken. This, in turn, influences the degree of shock design conservation associated with any hardening approach, since we must necessarily adopt a conservative approach in cases where time does not permit development of technically precise solutions.

The second principal influence of scheduling considerations involves sequence of shipbuilding events. Sequence of shipbuilding events can vary to some extent, depending primarily upon which sequence of events best suits the individual shipbuilder and secondarily upon other factors such as ship size. Therefore, it is undesirable to key general shock requirements to any assumed sequence of shipbuilding events, unless it is implicit that the sequence in question would always be followed. Many examples could be given of how shipbuilding event sequence and the variability of same influence shock hardening approaches. Perhaps most important, we find that consideration of these factors is partially responsible for the Navy's "piecemeal" approach to the shock hardening of ships. A systems approach to achievement of shock resistance may be preferable from a purely technical standpoint, but the success of such an approach is dependent upon "everything coming together at once" -- implying an assumed sequence of events which could easily disturb the usual routine of shipbuilding events. The piecemeal hardening approach, which allows shipboard equipments and other items to be "shock qualified" on an individual basis and with minimum regard for the design of supporting decks and other "system" characteristics, is thus highly attractive from the standpoint of scheduling considerations.

Having considered the primary influences of some administrative factors upon selection of ship hardening approaches, it seems appropriate to briefly reconsider the basic objective of the Navy ship hardening effort: To fully optimize the shock resistant qualities of Navy ships. What is really being sought here is maximum shock hardening cost-effectiveness; no other parameter can adequately define "what's optimum" in a meaningful way. It directly follows that administrative factors (cost factors,

essentially) and effectiveness factors must be given equal consideration as we go about the business of optimizing the shock resistant qualities of Navy ships.

CONCLUDING REMARKS AND RECOMMENDATIONS

We might first consider some trends which have an important bearing upon the subject of this paper. The need for improved ship shock resistance took a sharp swing upward during the 1950's, in response to a marked increase in the inherent shock sensitivity of many new shipboard systems (primarily, new and sophisticated electronics and weapons suites) and due to development of nuclear weapon threats (which added a new dimension to the shock problem). This situation led to Navy sponsorship of a considerable amount of shock-oriented RDT&E, which was understandably directed almost entirely at effectiveness-related goals. Recent full scale ship shock tests attest to the success of these efforts; we now have the technical capability to deliver almost any reasonable amount of ship shock resistance.

The administrative influence did not lay dormant while the events described above were taking place, however. Owing at least in part to DOD's recent difficulties with cost overruns and associated contractor claims, considerably increased attention is now being given to DOD procurement policies -- and to the requirements which we attach to things being procured. Attention to cost considerations has also greatly increased, for reasons we all know about.

The overall influence of administrative factors is thus seen to be rapidly increasing at a time when the requirement for further upgrading of ship hardness characteristics is declining. The implications of these trends are clear, and some of you may have already felt their impact. Those technical personnel who to date may have seen no real need to seriously account for the administrative side of the shock hardening effort might reconsider their position in the light of present trends; things are changing.

So much for trends; what might we do about them? Above and elsewhere in this paper, it has been suggested that the technical community can contribute significantly to the ship hardening effort by "accounting for" or "considering" administrative factors which are becoming increasingly important to the ship hardening effort. These are nice words, but they lead to an obvious question: Exactly how might the technical community "account" for needs in this area? The following paragraphs summarize some possibilities.

If necessary, learn more about administrative factors. This paper provides about as much shock-oriented insight into procurement policies and basic cost considerations as might normally be needed (in the writer's opinion) by technical personnel who are not required for other job-related reasons to be knowledgeable in these fields. Note, however, that this paper does not tell all that could be told concerning shipbuilding event sequences, shipboard maintenance requirements/problems, and other specific cost-related matters. The general importance of these factors relative to the selection of ship hardening approaches has already been stressed; the reader may judge for himself whether or not further study in such areas might prove beneficial.

Improve efficiency at the technical/administrative interface. A more deliberate effort could be made to address administrative factors in technical proposals and in technical reports which will receive administrative attention. A possible criterion for determining how much administratively-oriented information might be included in such documents: Provide all readily available information in this area which might be unknown to the cognizant administrator. The writer of the technical proposal or technical report may understandably be in a poor position to furnish explicit information in this area. However, his superior acquaintance with the technical concepts/practices in question and his usually intimate acquaintance with private industry's technical capabilities and limitations may easily place him in the best position to ascertain the basic administrative implications of his proposal or recommendations. Some example "administrative implications" which could often be addressed (with a minimum of homework) at the technical level are: Whether or not implementation might force alteration of shipbuilding event sequences. Extent to which private industry is prepared to respond to the technical requirements. What sort of shipboard maintenance might be required. Whether or not added weight will result. (An example administrative implication could be cited for every such factor mentioned in this paper).

Structure technical tasks to yield information of administrative interest. Naturally, it cannot be expected that meaningful administratively inclined information of the sort referred to above will be initially available in all cases -- particularly when basic technical concepts, rather than technical practices, are the subject of the technical proposal or report. However, it is generally possible to structure follow-on developmental efforts in a manner which will permit early identification of important administrative implications.

Finally (and inevitably): Directly address administrative factors at the technical level; take a head-on approach to solution of problems related to procurement policies, costs, and schedules. Opportunities to promote further optimization of ship hardness qualities

are perhaps nowhere more numerous than in this area. A few of many technical objectives which directly reflect administratively-oriented needs: Develop ways of expanding the scope and applicability of shock test extension policies. More fully develop a basis for extension of dynamic analysis qualifications. Develop short-cut methods for optimized design of shock resistant foundations. Pursue investigation of maintenance-free shock mitigating devices. Further standardize shock design/shock testing procedures. Develop additional shock test and shock design guidance material. (This list could go on and on. The general theme should be clear, however).

We've seen, by example in this paper and elsewhere, that administrative influences can run counter at times to rapid technical progress and other technical interests. Hopefully, it has also been conveyed that the administrative influence must be accounted for in a constructive fashion at the technical level if we are to realize fully optimized ship shock resistance. The question of how our technical resources might best be directed at administratively-oriented needs is at once difficult and important. Think about it.

MEASUREMENT AND APPLICATION OF MECHANICAL IMPEDANCE

FORCE TRANSDUCER CALIBRATIONS RELATED TO MECHANICAL IMPEDANCE MEASUREMENTS

E. F. Ludwig
Assistant Project Engineer
N. D. Taylor
Senior Engineer

Pratt & Whitney Aircraft
Florida Research & Development Center
West Palm Beach, Florida

(U) Mechanical impedance measurements have become a popular time and cost-saving, nondestructive industrial test tool. To obtain these measurements, only small, nondestructive dynamic forces are required at the test item. A common problem in measuring any parameter is the suitability of the transducers and associated instrumentation required. In studying mechanical impedance parameters, cognizance of the base strain amplitude and sensitivity linearity of the force transducer is particularly important. Special emphasis is given to these two topics and to a survey of several time and cost-saving, mechanical impedance test programs.

INTRODUCTION

The Pratt & Whitney Aircraft Florida Research & Development Center has used mechanical impedance measurements extensively in the past few years on jet and rocket engine development programs. Much state-of-the-art experience has been acquired in impedance testing techniques.* These techniques save time and cost in nondestructive industrial testing. To obtain these measurements, only small, nondestructive dynamic forces are required at the test item. These small forces measured by force transducers, allow the test engineer to use portable exciters, which can be maneuvered into almost any test location. Some transducer characteristics are not defined clearly in specifications. Base strain sensitivity and amplitude linearity are discussed in this paper.

To evaluate base-strain sensitivity, the force transducer is attached to a simple, fixed-free beam. The structural characteristics of this beam, such as spring rate, effective mass, damping, strain, and natural frequency will be presented analytically. The force transducer base-strain sensitivity test procedure and data obtained from the described test beam will be discussed. The beam calculations will be compared with impedance and strain test data taken during the force transducer base-strain test program. A math model of the test beam's bending modes also will be presented and compared with impedance test data.

The force transducer calibration test data described in this paper illustrates the need for standard procedure to describe amplitude linearity and sensitivity deviation. A proposed procedure is defined and discussed. The paper concludes with a description of several impedance test programs that yielded considerable savings at Pratt & Whitney Aircraft's Florida Research & Development Center.

*The author E. F. Ludwig, is presently a member of the American National Standard Writing Group S2-58 that is currently preparing a standard on the experimental measurement of mechanical impedance. The document to be produced by this committee will serve as a general guide for the user in the selection of calibration techniques and will recommend types of evaluation tests necessary for determining the suitability of transducers and associated instrumentation. A section of the S2-58 document will discuss force transducer base strain sensitivity and amplitude linearity. This paper, which will be presented at the 42nd Shock and Vibration Symposium in Key West, Florida, will contain a more comprehensive discussion.

SYMBOLS

A	Beam Cross-Sectional Area - in^2
a	Acceleration - g's
c	Damping - lbf/in/sec
c_c	Critical Damping - lbf/in/sec
d	Displacement - in
E	Modulus of Elasticity - lbf/in^2
E_k	Kinetic Energy - $lbm/in^2/sec^2$
E_x	Output Signal - mv. or pc
F	Force - lbf
f	Frequency - Hz
g	Gravitational Constant - $lbf\text{-}in/lbm\text{-}sec^2$
I	Moment of Inertia - in^4
j	$\sqrt{-1}$
K	Spring Constant - lbf/in
L	Beam Length - in
M	Moment - lbf-in
m	Mass - lbm
m_e	Effective Mass - lbm
Sx	Sensitivity - mv/lbf or pc/lbf
S_D	Sensitivity Deviation
t	Time - sec
v	Velocity - in/sec
W	Weight - lbf
W_e	Effective Weight - lbf
x	Distance Along the Beam - in
y	Deflection of the Beam - in
ym	Maximum Deflection - in
Z	Mechanical Impedance - lbf/in/sec
δ	Logarithmic Decrement
ϵ	Strain - μin/in
ρ	Density - lbf/in^3
σ	Stress - lbf/in^2
ω	Circular Frequency - rad/sec

AMPLITUDE SENSITIVITY LINEARITY

The study of dynamic structures using the mechanical impedance approach entails the measurement of the applied force. This force may vary over a wide dynamic range due to the responsiveness of the structure under test. For this reason the amplitude linearity characteristics of the measuring transducer must be established. Published specifications of force transducers do not always provide sufficient data for the mechanical impedance user. Some users may not be aware of the insufficient data that is important to make a valid measurement. The following may affect amplitude sensitivity and its deviation: preload mounting torque; different type attaching bolts; lack of standard methods of stating linearity and methods of obtaining calibration data. A standard calibration procedure must be established.

The following test procedure will allow this standardization to be accomplished: The amplitude linearity calibration is performed by vibrating the force transducer at various acceleration levels (a) with a known mass attached (m) and measuring its output signal (E_X). A standard 200 Hz frequency should be used if it is within the rating of the transducer. Calibration data points will be taken at least at octave band intervals between one and 200 lb and at 100 lb intervals over the rest of the transducer span. For transducers rated at less than one pound, data should be taken in the same manner to cover the span of the transducer.

The above calibration data will permit calculations of force transducer sensitivity as a function of applied force.

$$\text{Applied Force} \quad F = ma$$
$$\text{Force Transducer Sensitivity} \quad Sx = Ex/F$$

Since the force sensitivity is now known over the span of the transducer, its deviation can be calculated in plus or minus percent from the mean.

Sensitivity Deviation

$$S_D = \frac{Sx - S_{avg}}{S_{avg}} \times 100$$

This seems to be one of the better statistical methods for stating deviation. A calibration curve supplied with the transducer specification, however, would be most desirable. This information would allow the user to establish sensitivity deviation over his span of concern. For example, Figure 1 illustrates a transducer torqued to 25 foot pounds with a deviation of approximately ±9% when defined at 1800 pounds. The same transducer at 400 pounds is a ±3% transducer. Many specifications state sensitivity deviation at ± percent of full scale. This percentage loses significance at relatively low force levels which are normally applied during a mechanical impedance test (i.e., a transducer with a 500 ±2% pound full scale force rating would allow for a ±10 pound deviation. If a test requiring 10 pounds of applied force were required, the user of this transducer could only guarantee that the applied force was within 0 to 20 pounds). The calibration specification should also include information about preload versus torque for the type of attachment bolt recommended and mass and accelerometer NBS traceability.

To test the practicality of this procedure, quartz and piezite annular transducers were calibrated using these guidelines. Figure 2 is a photo of one transducer mounted on a dynamic exciter with the calibration mass attached. Figures 1 and 3 illustrate empirically derived force transducer sensitivities versus applied force for both transducers. These figures illustrate that increases in compressive preload caused increased sensitivity and improved

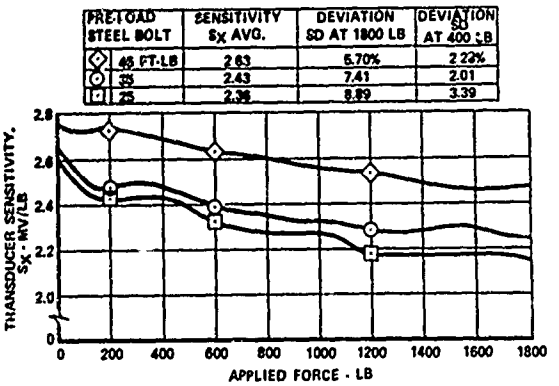

Fig. 1 - Annular Piezite Force Transducer Calibration Data

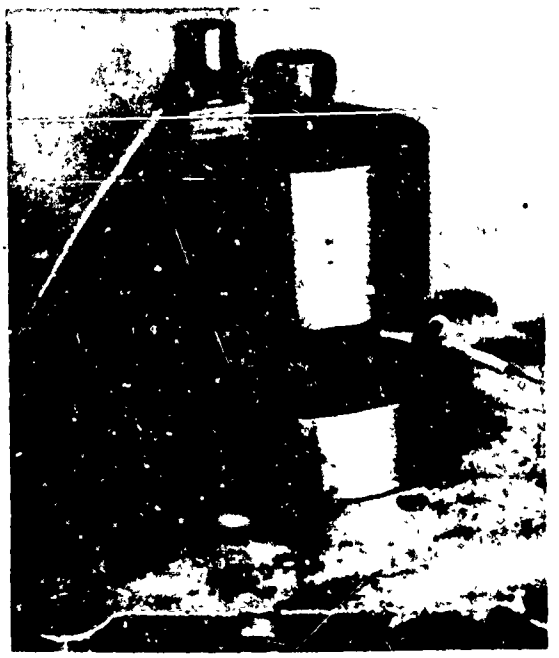

Fig. 2 - Amplitude Linearity Calibration Setup

amplitude linearity. Figure 3 illustrates the effect of bolt type on sensitivity. The steel bolt decreased sensitivity but showed better linearity compared to the berylium copper bolt.

Both static and dynamic test data were taken on the quartz force transducer. The same trend in data was consistent for both conditions; sensitivity increased with torque, and linearity improved. The main difference noted was that static calibrations consistently showed a lower sensitivity. Also, the dynamic

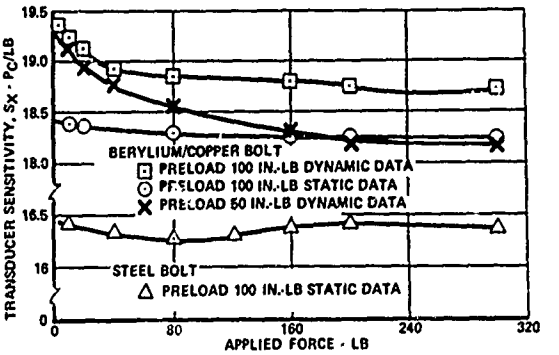

Fig. 3 - Annular Quartz Force Transducer Calibration Data

sensitivity tended to increase at low force levels at a different rate than static sensitivity.

FORCE TRANSDUCER BASE STRAIN SENSITIVITY

Determination of force transducer base-strain sensitivity involves mounting the transducer on a surface which could be stressed to measure accurately the strain at the base of the transducer. The transducer used was an annular piezite element that requires a center torque bolt for attachment.

A cantilever beam was selected as the best surface for determining strain. If all properties of the beam were known, strain could be determined both theoretically and with gages. The theoretical spring rate and effective mass for a 16-inch cantilever beam at first bending were computed as well as the first five resonant frequencies. The data was then compared with actual mechanical impedance data taken at various points along the beam. Spring rate was checked against the impedance data. The effective mass also was checked against the data. Resonant frequencies computed theroetically were very close to those appearing in the impedance data.

Holograms were made of the beam during vibration at first bending. Displacements were taken from the reconstructions of these holograms and compared with theoretical deflection values calculated using the standard cantilever beam deflection equation and sinusoidal approximation.

A mathematical model of the beam was made to further substantiate the mechanical impedance at the tip of the beam. The model

was a series of mass-spring-damper systems. The values of spring rate, effective mass and damping were based on data taken from static loading tests, logarithmic decrement or read directly from the impedance data.

After determining values of spring rate and effective mass, the transducer base strain was calculated for various tip displacement and acceleration levels. These values were compared with test data taken at these levels. With strain determined for different loads, the sensitivity of the transducer to base strain was recorded and analyzed.

BEAM ANALYSIS FOR IMPEDANCE CORRELATION

The equations used in the majority of this section stem from beam theory. The basic differential equation is for the beam's elastic curve.

$$d^2y/dx^2 = M/EI$$

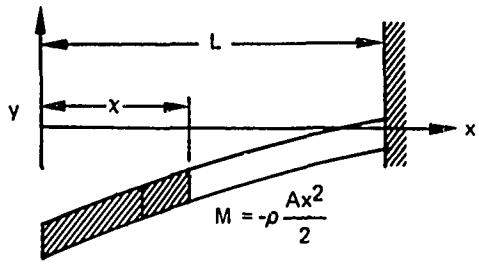

Using the boundary conditions of a cantilever beam under uniform loading, this equation can be solved and used for theoretical checks on actual cantilever beam data:

$$y = -\rho A/24EI\,(x^4 - 4L^3x + 3L^4)$$

$$y_m = -\rho AL^4/8EI \text{ at } x = 0$$

These equations are used to determine the theoretical spring rate at first bending and the effective mass. They also provide a check on natural frequencies.

The predicted spring constant for an ideal cantilever beam can be calculated as a function of length from the clamped end. The beam deflection produced by a force at a distance d from the clamp point equals:

$$y = -F/6EI\,(-d^3 + 3d^2L - 3d^2x)$$

The spring constant K at d.

$$K = 3EI/d^3$$

For example, the theoretical spring constant at the tip of a sixteen-inch steel beam with a cross-sectional area 3.0 x 0.5 in. is 886 lbf/in. Testing determined the static spring constant for this beam in a clamping device to be 562 lbf/in. Deflection inside the clamping device is the most likely cause of the discrepancy between these constants. The theoretical length would then be 17.1 inches.

The effective mass of a cantilever beam at first bending can be calculated by energy methods. The beam deflection mode shape can be described as

$$y = y_m/3\left[(x/L)^4 - 4\,(x/L) + 3\right]$$

The kinetic energy of the cantilever is

$$E_k = 1/2 \int_0^L (dy/dt)^2\,dm$$

where $dy/dt = \omega y$ and $dm = W/gL\,dx$

Integrating we get

$$E_k = 0.1283\,W\omega^2 y_m^2/g$$

This is equal to the kinetic energy of the effective mass:

$$E_k = 1/2 W_e \omega^2 y_m^2/g$$

$$m_e = 0.2566m$$

That is, a steel beam sixteen inches long with a cross-sectional area of 1.5 in^2 would have an effective mass at first bending equal to 0.00483 lbm. (W_e = 1.86 lbf.)

A second method of determining the effective mass was suggested in Reference 1. The mode shape at first bending was approximated by using

$$y = y_m\,(1 - \cos\pi x/2L)$$

Figure 4 compares this mode shape with the elastic curve. Solving the integral for kinetic energy yields a slightly different value for effective mass.

$$m_e = 0.227m$$

$$m_e = 0.00427 \text{ lbm}$$

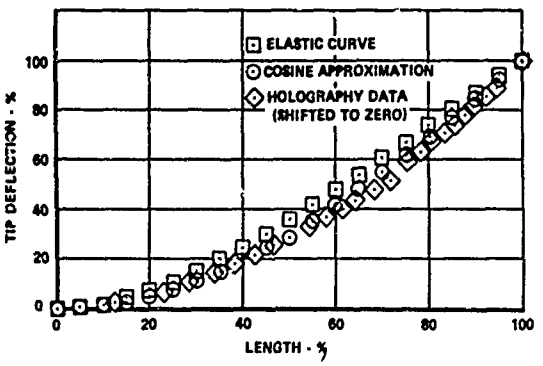

Fig. 4 - Deflection of a Cantilever Beam

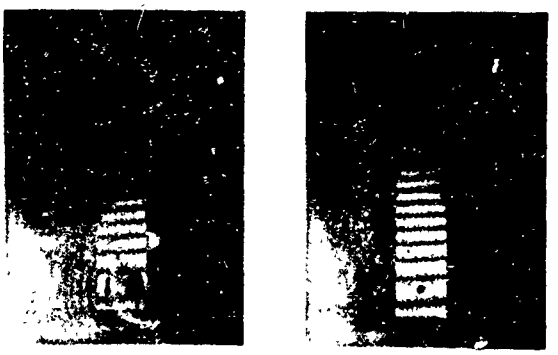

Fig. 5 - Holograms of the Cantilever Beam

To determine which deflection curve approximated more closely the mode shape at first bending, a hologram of the sixteen-inch beam was made during vibration. This study of the data from the holography curve indicates that perhaps the beam was not secure in its fixture during the mode shape holography. In general, the trend of the data is good, but the shift at the zero point indicates slight motion at the clamp. For the hologram chosen, tip deflection was 64 microinches single amplitude. Data taken near the clamp indicates approximately 1.5 microinches double amplitude with the true zero deflection point approximately two inches beyond the clamp. Shifting the zero point makes the mode shape agree closely with the cosine curve.

As shown in Figure 5, the holograms revealed no difference in the deflection with the transducer on or off the beam. This means that the preceding calculations are valid for calculating transducer base strain.

The resonant frequencies of a cantilever beam are obtained by solving the partial differential equation of motion. This will be done for a steel beam with dimensions 16 x 3 x 0.5 inches. Beam equation:

$$\frac{\partial^2 \left| EI(x)\partial^2 y/\partial x^2 \right|}{\partial x^4} = -\frac{\rho A(x)}{g}\,\partial^2 y/\partial t^2 - f(x, y, \dot{y}, t)$$

Since I and A are not functions of x, and assuming no external loading,

$$a^2\,\partial^4 y/\partial x^4 = -\partial^2 y/\partial t^2 \qquad a^2 = EIg/\rho A$$

where with appropriate boundary conditions, the nontrivial solution yields:

$$\cos z = -1/\cosh z$$

$$\text{where } z = \sqrt{\omega/a}\,L$$

which is satisfied at the roots:

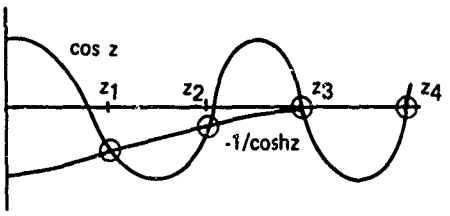

The natural frequencies are

$$\omega_n = \sqrt{EIg/\rho A}\,(z_n/L)^2$$

The first five resonant frequencies are:

$$z_1 = 1.875 \qquad \sqrt{EIg/\rho AL^4} = 114.$$

$$\omega_1 = z_1^2\,\sqrt{EIg/\rho AL^4} = 401. \quad f_1 = 63.8$$

This frequency would be 55.9 Hz if the beam were 17.1 inches long.

z_2	4.694	$f_2 = z_2^2/2\pi(114.)$	400.
z_3	7.855	f_3	1121
z_4	10.996	f_4	2200.
z_5	14.137	f_5	3620.

Two other methods of finding the resonant frequencies were investigated. The Rayleigh method used the sinusoidal approximation deflection curve. The other is the energy method, for which the beam deflection equation was used. Beam equation results agreed very well with the results of the previous section.

CORRELATION WITH IMPEDANCE DATA

An actual steel beam measuring 16 x 3 x 0.5 inches was tested for impedance with the drive point located on the centerline at different lengths from the clamped end (Figure 6). Theoretical values of spring constant, effective mass and exponential decay damping data will be compared with impedance test data. At resonance, the impedance due to the spring term and mass term cancel each other leaving only damping.

$$\overline{Z} = \overline{c} + \overline{j}\omega m - \overline{j}K/\omega$$

$$|Z| = \sqrt{c^2 + (\omega m - K/\omega)^2}$$

At resonance,

$$\omega m = K/\omega$$
$$|Z| = c$$

Since the spring constant at the tip of the cantilever is known, and the frequency at first bending is known, the effective mass can be calculated by this method also. Tip spring constant

$$K = 686 \text{ lbf/in}$$

Effective mass

$$m_e = K/(2\pi f)^2 \text{ where } f = 63.8 \text{ Hz}$$

$$m_e = 0.00427 \text{ lbm}$$

Effective weight

$$W_e = 1.65 \text{ lbf}$$

This agrees well with the effective mass (weight) calculated by the kinetic energy methods. Mass and spring constants can next be used to calculate the critical damping coefficient.

$$c_c = 2\sqrt{Km_e} \quad 3.42 \text{ lbf/in/sec}$$

With spring constant and effective mass determined analytically, damping must be derived from the logarithmic decrement. A decay curve of tip acceleration was made so that the damping could be derived. The frequency of this free vibration was at 57.9 Hz.

Fig. 6 - Strain Sensitivity Calibration Setup

Logarithmic decrement

$$\delta = (1/n-1) \ln x_1/x_n$$

From actual decay data:

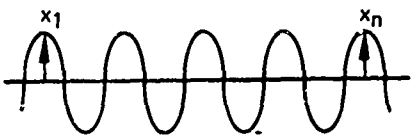

$$x_1 = 2.175$$

$$x_5 = 1.94$$

$$4\delta = \ln (2.175/1.94)$$

$$\delta = 0.0294$$

To calculate actual damping

$$c/c_c = \delta/\sqrt{\delta^2 + 4\pi^2}$$

$$c \quad 0.016 \text{ lbf/in/sec}$$

Figures 7-10 show data taken at different points along the beam. (16, 12, 8, 4 inches from the clamped end.) In Figure 7 where the beam was being excited at the tip, the theoretical spring rate, actual damping and effective

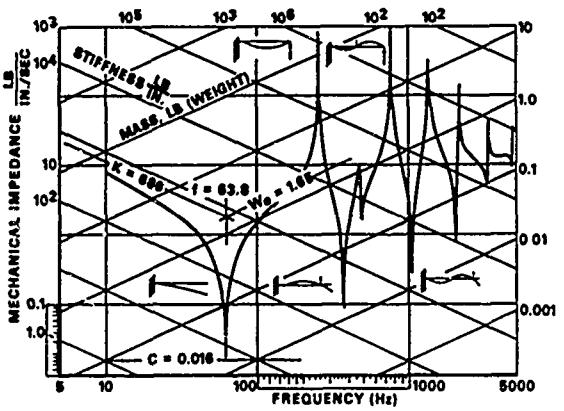

Fig. 7 - Impedance of the Cantilever Beam Drive Pt - Tip

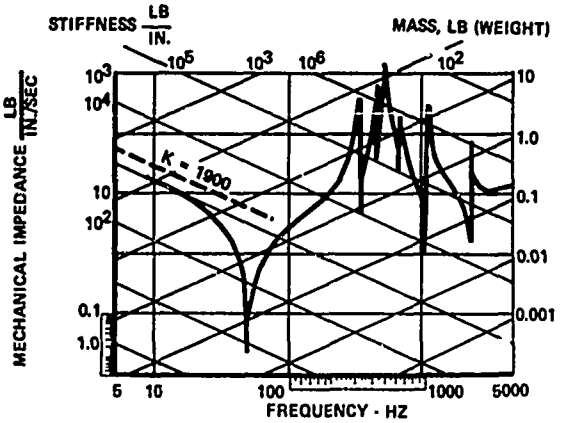

Fig. 8 - Impedance of the Cantilever Beam Drive Pt. 4 in from Tip

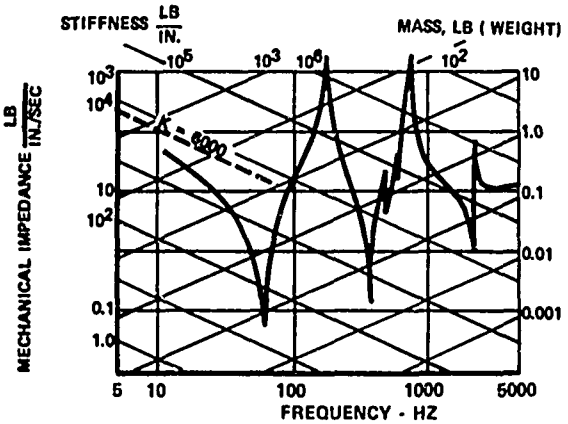

Fig. 9 - Impedance of the Cantilever Beam Drive Pt. 8 in from Tip

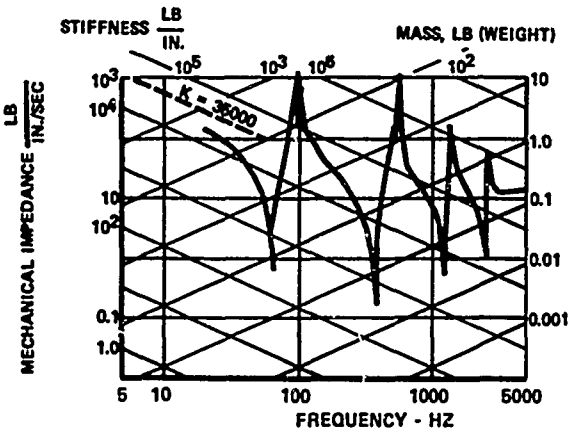

Fig. 10 - Impedance of the Cantilever Beam Drive Pt. 12 in from Tip

weight lines have been drawn. The inserts are mode shapes of the beam at the particular resonant or antiresonant point. Theoretical spring rates are shown on the three other figures. From these data it is evident that damping ratio is fairly constant along the beam.

COMPUTER SIMULATION

To further correlate the actual and theoretical impedance of the cantilever beam, a computer routine was written that broke the beam into a series of mass-spring-damper systems. Each system matched one resonant frequency on the impedance data. The impedances of all systems were added to calculate the total impedance.

The impedance of a single mass-spring-damper parallel system can be described by using a combination of real (damping) and imaginary (mass and spring) vectors.

$$\vec{Z} = \vec{c} + \vec{j}\omega m - \vec{j}k/\omega$$

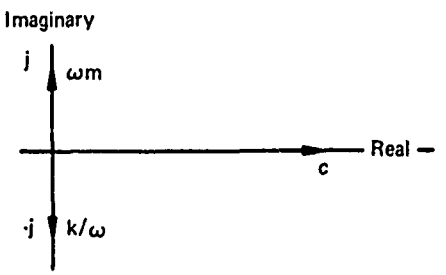

Since systems added in series must be summed as the inverse, it is easier mathematically to sum mobility, the inverse of impedance.

$$\vec{Y}_i = \frac{1}{\vec{Z}_i} = \frac{\vec{c}_i - \vec{j}(\omega m_i - K_i/\omega)}{c_i^2 + (\omega m_i - K_i/\omega)^2}$$

The real and imaginary terms can be summed separately. Then, the mobility will be the square root of the sum of the squares of the real and imaginary terms. A comparison of the computer simulation with impedance data is shown in Figure 11. It is obvious that the antiresonances are not being modeled properly. Investigation into this phenomenon using different models will continue.

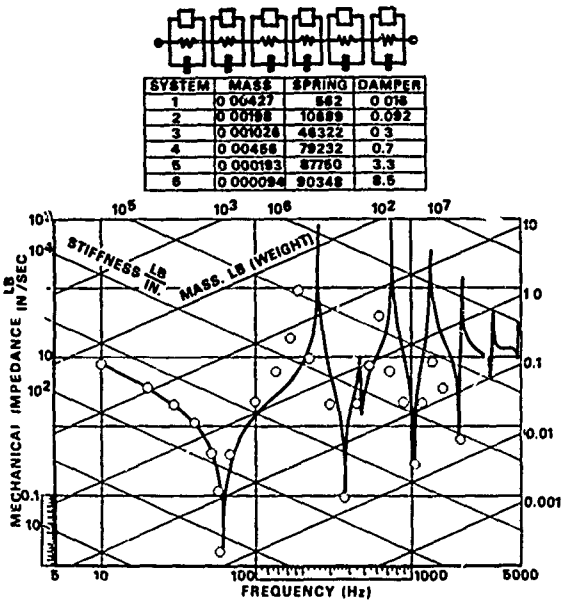

Fig. 11 - Computer Simulation - Cantilever Beam Impedance

The spring rate at first bending for the model tested was chosen as 562 lbf/in., the static spring rate. This value was chosen rather than 686 lbf/in. because of the movement inside the clamping device discussed previously. The length of the cantilever was considered as 17.1 inches. The first resonant frequency was 57.9 Hz, the free vibration value measured on the decay data. The calculated effective mass used for first bending was 0.00427 lbm.

Damping is equal to the value of impedance at each resonant point. The values of spring rate and effective mass for each of the other modes were based on the frequencies at the resonant and antiresonant points obtained from test data. In formula,

$$me_1 = K_1/\omega^2_{R1} \qquad \text{first resonance}$$

$$K_2 = m_{e1}\,\omega^2_{A_1} \qquad \text{first antiresonance}$$

$$me_2 = K_2/\omega^2_{R_2} \qquad \text{second resonance}$$

The simulation's spring rate asymptote at low frequencies is lower than the spring constant used to model the first resonant mode. This is due to the additive effects of springs in series. Most test specimens at FRDC, however, have shown the asymptote of the impedance data to be very close to the spring constant value for the fundamental mode. Spring constants of secondary modes have not lowered the asymptote appreciably. Even though the above approach seems basic for a simple cantilever system, the theoretical calculation, impedance testing and computer simulation method can be broadened to encompass more complex systems.

BEAM AS A STRAIN INPUT

With the deflection of a cantilever beam thoroughly investigated, this beam will be considered as the source of base strain input to a force transducer mounted on the beam. Output of the transducer as a function of strain for various torque loadings and rotational positions were determined. Strain was predicted as a function of effective mass times acceleration and also as a function of spring rate times tip deflection. These values were compared with actual strain readings.

CALCULATION OF STRAIN

A bar bends when subjected to a moment M. For a small beam deflection, the strain according to Hooke's law is

$$\varepsilon_x = 1/E(\sigma_x - \nu\sigma_y) = My/EI$$

Where $\sigma_y = 0$

For the calibration of a force transducer, we are interested in the strain at its mounting point at the transducer base. Data taken from strain gages located near the transducer mounting point were compared to calculated values of strain based on spring rate and effective mass in Figure 12. The beam experienced local stiffening when the transducer was mounted. Figure 12 shows the effect on strain of mounting the transducer as well as the range due to torque and rotation with the transducer mounted.

Strain in the beam is dependent on the force applied at the cantilever tip. Tip acceleration and displacement at first bending together with effective mass and spring constant yield two methods of determining force: one

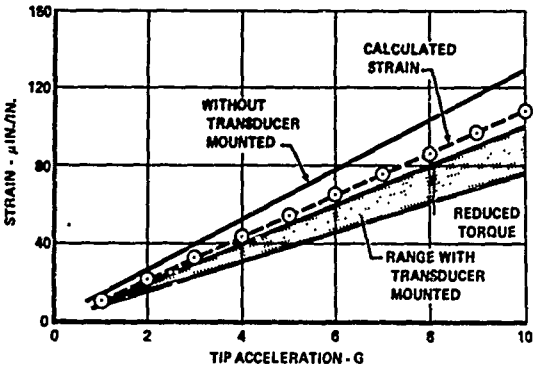

Fig. 12 - Transducer Base Strain

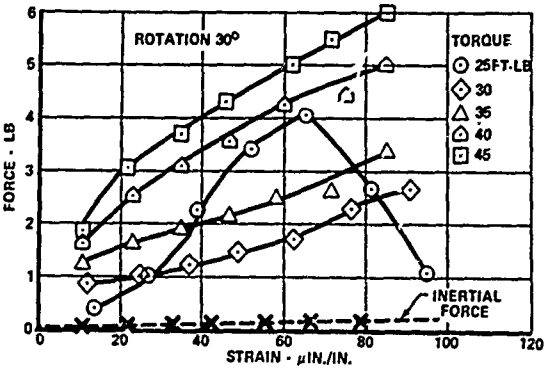

Fig. 13 - Force Transducer Output - Effect of Torque at 30°

potential and one kinetic. Peak values are obtained. The added mass of the drive rod at the tip of the beam shifts the resonant frequency lower (49 Hz) than noted for free beam vibration. This extra mass must be added to the effective mass of the beam to obtain true strain data. Electronic mass cancellation is used to correct mechanical impedance data.

RESPONSE OF A TRANSDUCER TO BASE STRAIN

Mounted on a sixteen-inch cantilever beam, a force transducer was subjected to base strain induced by vibration at first bending. The output of the transducer was recorded at different strain levels for different torque loadings and as a function of rotation around the transducer's axis. The transducer's output due to base strain was 200 times its normal inertial force output. Findings indicate a significantly higher output as torque is increased (Figure 13, 14). They also show that output is related to rotational position (Figure 15). One characteristic of output during these checks was that initial loading sometimes caused a peak transient reading. This reading then decayed to some steady-state value after a few seconds. At present, no explanation for this can be offered although the trait did depend somewhat on rotation. Further studies will be made.

Actual inertia force, shown in Figure 13, illustrates the magnitude of error due to base strain sensitivity. Most applications should avoid base strain if possible. If not, then precautions should be taken in using force data.

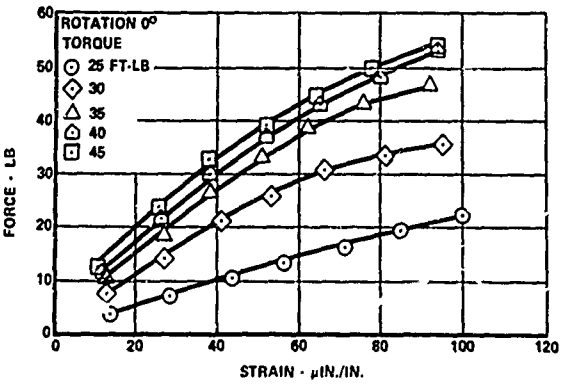

Fig. 14 - Force Transducer Output - Effect of Torque at 0°

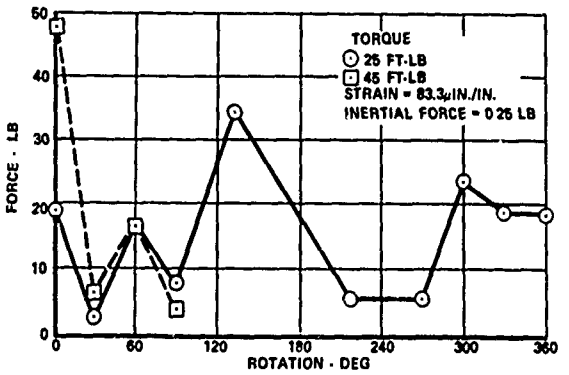

Fig. 15 - Force Transducer Output - Effect of Rotation

SUMMARY

Thus far this paper has presented two different transducer characteristics for users to consider when evaluating force transducer calibrations. The first section suggests a standardizing procedure for amplitude linearity and sensitivity deviation. The second, base strain sensitivity, suggests a procedure for determining output as a function of base strain. Cognizance of these areas will help a user determine the validity of his mechanical impedance measurements.

Studies of the cantilever beam system used for base strain sensitivity revealed a means for comparing theoretical and test results and served as an aid to simulate the mechanical impedance of this system with a math model. This same procedure could be extended to more complex systems.

FRDC IMPEDANCE TEST PROGRAMS

Mechanical impedance measurements have become a popular cost and time saving tool. This section discusses several representative impedance test programs conducted at the Pratt & Whitney Aircraft Company, Florida Research and Development Center. During these programs, considerable time and cost were saved by implementing this nondestructive test technology.

COMPARISON STUDY OF DAMPING SCHEMES

A determination of the mechanical impedance characteristics of several different louver section designs permitted selection of a practical and optimum design. Of all seven louvers tested, the "handlebar mustache" design (D) possesses the best damping characteristics. From a practical design standpoint, however, the short-hooded louver (C) possesses sufficient damping properties below 750 Hz. Figure 16 compares four louvers tested.

BURNER CAN CLAMP WEAR DIAGNOSED THROUGH IMPEDANCE MEASUREMENTS AND LASER HOLOGRAPHY

Excessive clamp wear during an engine development program prompted an investigation of burner can damping characteristics. The data from the impedance test program described critical frequencies at which mode shape holograms were taken. These holograms (Figure 17) depicted a bending mode in the 100 Hz

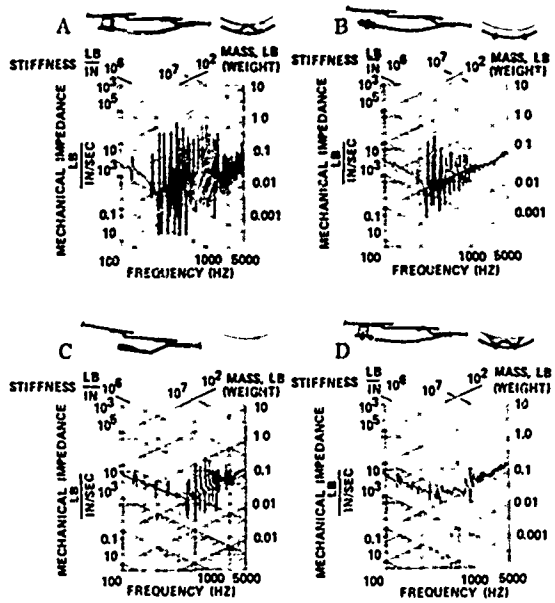

Fig. 16 - Louver Section Damping Study

frequency range that could cause clamp wear. This frequency also correlated with a critical frequency source generated by the development engine. With the test proven effective in diagnosing clamp wear, this procedure could be extended to determine if a burner section requires overhaul during prescribed maintenance schedules.

MECHANICAL IMPEDANCE DEFINITION OF CRITICAL PLUMBING BENDING MODES

Point and transfer impedance data taken on the pump plumbing (Figure 18) defined critical resonant frequencies. Laser (time average) holography was used to signature plumbing deformation at each minimum impedance drive point location so that particular component spring rates and mode shapes could be defined.

VERIFICATION OF PREDICTED ANALYTICAL PARAMETERS

Impedance measurements were used to verify analytically-predicted dynamic spring rates of a rocket engine fuel pump bearing support. The bearing support and housing were mounted for test as shown in Figure 19. Transfer impedance data was taken on the critical members of the bearing support system. Analysis of this data showed good correlation with calculated spring rates. The test results indicated that a critical speed analysis program was within design tolerances.

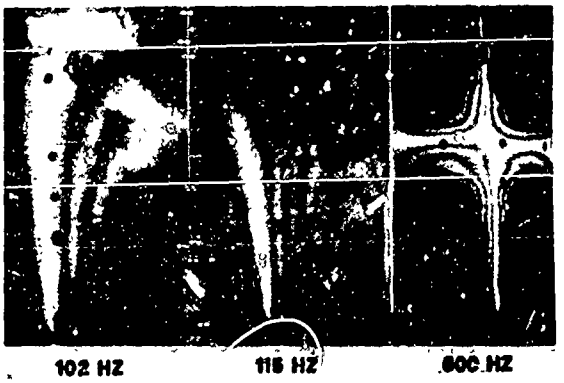

Fig. 17 - Burner Can Clamp Wear Test Setup

Fig. 18 - Pump Plumbing Mode Test Setup

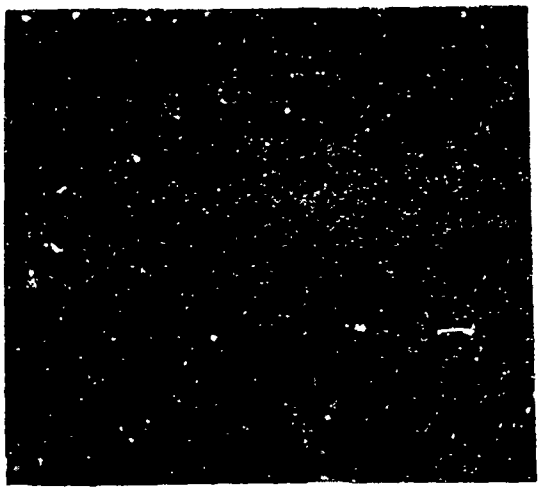

Fig. 19 - Bearing Support Test Setup

ROCKET ENGINE SIDE LOAD DETERMINED BY DYNAMIC SPRING RATE TEST

Substantial cost savings are realized by the effective use of mechanical impedance measurements. During a recent rocket engine test, for example, a standing shock wave was ingested into the nozzle of a staged-combustion rig and became attached during the run. The point of attachment could be determined as well as the side displacement when attachment occurred. To estimate the amount of side loading which caused this displacement, the spring constant of the nozzle system had to be determined. Since the engine was in the test stand and time was a very critical factor, impedance was measured at the test site. The exciter was positioned at several locations along the nozzle. Figure 20 illustrates the exciter at the tip. From impedance data taken in the 5-5000 Hz range the first bending mode of the extendible nozzle assembly was found to occur at approximately 5 Hz, the first ring mode occurred at 42 Hz. A spring rate of the nozzle system was determined by analyzing the impedance plots and constructing mathematical models from the low order modes.

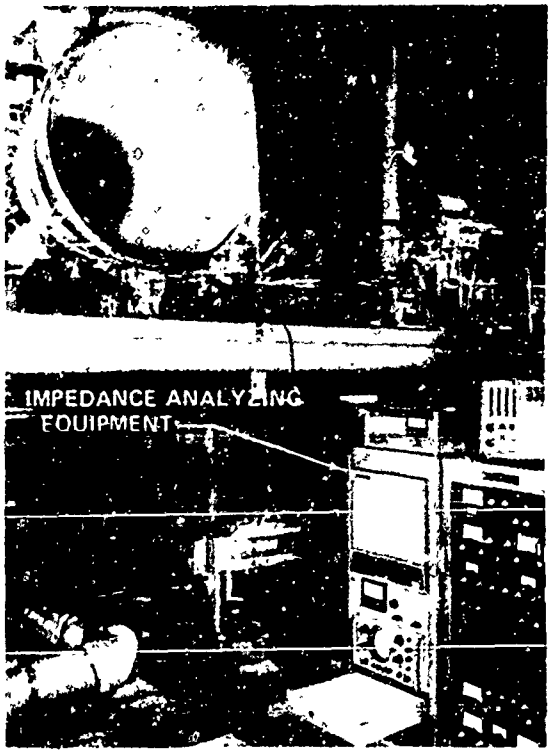

Fig. 20 - Nozzle Spring Rate Test Setup

REFERENCES

Bonesho, J.A. and Bollinger, J.G., "Self-Optimizing Vibration Damper," Machine Design, Feb. 29, 1968, pp. 123-127.

Freberg, C.R. and Kemler, E.N., Elements of Mechanical Vibration, 2nd Ed. John Wiley & Sons, Inc., 1966.

Harris, C.O., Introduction to Stress Anslysis, McMillam Co., N.Y., 1959, pp 93-94.

Wylie, C.R., Jr., Advanced Engineering Mathematics, 3rd Ed., McGraw Hill Book Co., N.Y., 1966, pp 323-326.

DISCUSSION

Mr. Bouche (Endevco): As chairman of American National Standards Institute committee S2-58 I would like to compliment Mr. Ludwig on doing a very excellent job in making these calibrations. Early in the work of this committee we recognized that these two characteristics were very important for this standards document and that additional calibration work would have to be done in order to have enough information to include in the standard. So we asked Mr. Ludwig to make these measurements, and the results are good. The amplitude linearity measurements turned out better than expected. The base-strain sensitivity turned out to be quite serious, because if there is a strain present in actual experimental measurement of the order of, say 100 microinches per inch, then large force errors could result. It would be necessary then to select locations on the test specimen where it is known that the strain environment is small.

THE MEASUREMENT OF MECHANICAL IMPEDANCE AND ITS USE IN VIBRATION TESTING*

N. F. Hunter, Jr., and J. V. Otts
Sandia Corporation
Albuquerque, New Mexico

Mechanical impedance has, in the past, been used almost exclusively as an analytical tool in the vibration field. This paper considers both the laboratory test procedures and instrumentation used to measure the impedance of structures. This is followed by both an interpretation of typical data and the utilization of this data for the following:

1) derivation of laboratory test specifications,
2) comparison of a system's impedance characteristics before and after tests to determine structural failure, and
3) electronic simulation of a structure during force controlled vibration tests.

Each of the above applications is supported by specific examples.

MECHANICAL IMPEDANCE AND APPARENT WEIGHT

Mechanical impedance (Z) is defined as the complex ratio of the driving force acting on a system to the velocity response of the system.

$$Z(\omega) = \frac{F(\omega)}{v(\omega)} \angle \phi(\omega)$$

where

$Z(\omega)$ = mechanical impedance**

$F(\omega)$ = driving force

$v(\omega)$ = velocity response

$\phi(\omega)$ = phase angle between F and v.

An alternate expression for Z is in terms of its real and imaginary components:

$$Z = \frac{F}{v} \cos \phi + j \frac{F}{v} \sin \phi .$$

If the velocity response is measured at the point of force input, the Z is referred to as driving point impedance (Z_p). Conversely, the use of velocity response at another point on the system is termed transfer impedance (Z_T). Since

$$H(\omega) = \frac{v_2}{v_1}$$

where

$H(\omega)$ = transfer function

v_1 = velocity at point of force input

v_2 = velocity at some other point on system,

then

$$Z_T = \frac{F}{v_2} = \frac{F}{H(\omega) v_1} = \frac{1}{H(\omega)} Z_p$$

where

Z_T = transfer impedance

Z_p = driving point impedance.

Apparent weight is defined as the complex ratio of the driving force and the acceleration

*This work was supported by the United States Atomic Energy Commission.

**Mechanical impedance and all related terms are a function of frequency. Hereafter, the (ω) will be omitted and hence implied.

response of the system. Acceleration is in terms of G, where one G is equal to 386 in/sec^2.

$$W = \frac{F}{G} \angle \phi$$

where

W = apparent weight

F = driving force

G = acceleration response $\left(\frac{a}{386}\right)$

$\angle\phi$ = phase angle between F and G.

Using the relationship between acceleration and velocity; $v = Gg/j\omega$, then

$$W = \frac{g}{j\omega} Z$$

where

W = apparent weight

Z = mechanical impedance

g = gravitational acceleration (386 in/sec^2)

ω = circular frequency ($2\pi f$).

The point and transfer concept applies to apparent weight the same as for mechanical impedance. Namely,

$$W_T = \frac{1}{H(\omega)} W_p$$

where

W_T = transfer apparent weight

W_p = point apparent weight

$H(\omega)$ = transfer function.

INTERPRETATION OF APPARENT WEIGHT DATA

The apparent weight characteristics of the three ideal elements (mass, dashpot, and spring) are given by the following equations.

Mass $W_m = mg = w$

Dashpot $W_d = \frac{jgc}{\omega}$

Spring $W_s = \frac{gk}{\omega^2}$

where

W = apparent weight (pounds)

g = acceleration of gravity (386 in/sec^2)

k = spring constant (#/in)

m = mass $\left(\frac{\#sec^2}{in}\right)$

w = static weight (#)

c = damping coefficient $\frac{\# sec}{in}$

ω = circular frequency ($2\pi f$).

The apparent weight characteristics expressed above are plotted in Figure 1. Knowledge of the above characteristics will often prove valuable in the interpretation of laboratory data obtained during system analysis.

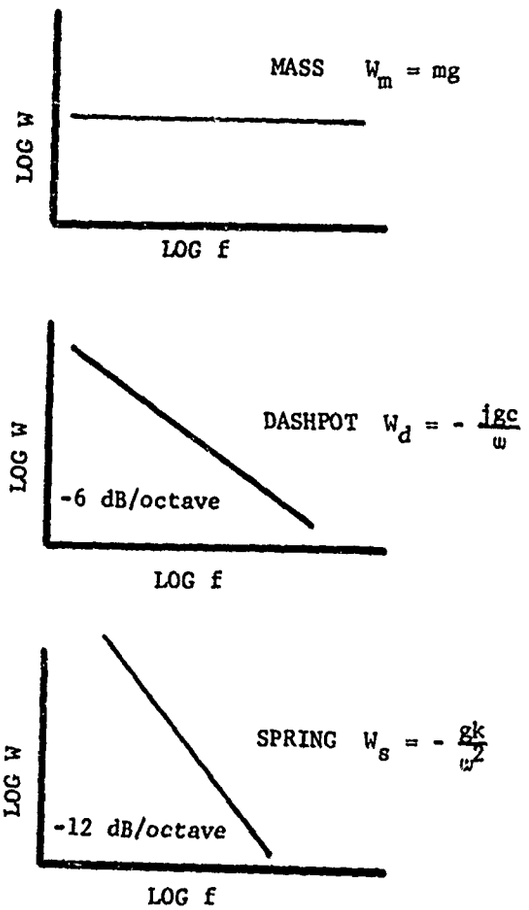

Fig. 1 - Apparent Weights of Ideal Elements

A typical apparent weight (W) plot, obtained in the vibration laboratory, is shown in Figure 2.

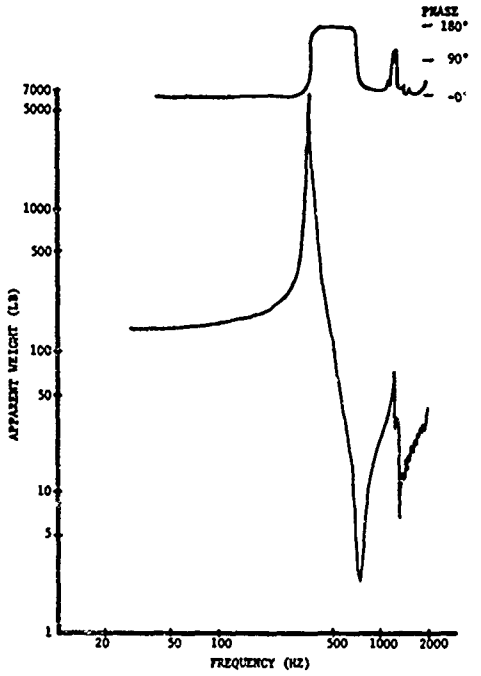

Fig. 2 - Typical Apparent Weight Plot

In this case, the amplitude of W, as well as the phase between force (F) and acceleration (G), are plotted on log-log paper as a function of frequency. This data is discussed below.

a) Low Frequencies - Rigid Body

The system is rigid over the low frequency range from 20 Hz to 50 Hz. The magnitude of the system apparent weight (W) is equal to the static weight (145#); it is constant; and the phase is zero degrees. This is the frequency range where pre-test measurement of the static weight facilitates calibration and pre-test confirmation.

b) System Anti-Resonance

The peak in W, associated with a phase of 90°, at 400 Hz signifies an anti-resonance with respect to the point of measurement. In other words, a subsystem, somewhere above the control point, is resonating. The peak of W signifies resistance to motion at the driving point (an apparent weight of 7000#).

c) System Resonance

The notch in W, associated with a phase shift from 180° to 90°, at 780 Hz signifies system resonance where the system is very non-resistant to motion (an apparent weight less than 5#).

d) Weight of Decoupled Subsystem

If one is fortunate enough to be working with a simple system, it is sometimes possible to determine the weight of the decoupled subsystem after resonance.

Consider the simplified system and its apparent weight curve depicted in Figure 3.

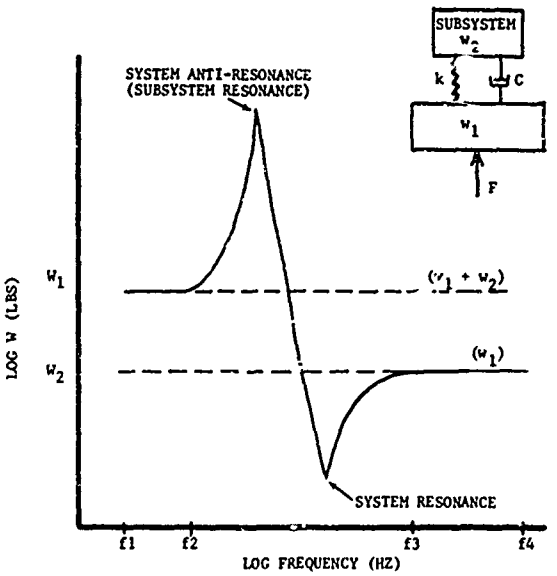

Fig. 3 - Apparent Weight Plot Showing Decoupled Mass

Over the frequency range f_3 to f_4 Hz, after W_2 has decoupled, the weight of W_2 is found as follows:

$$W_2 = W_1 - W_2 .$$

It should be noted that as a general rule the peaks and notches of apparent weight respectively correspond to subsystem and system resonances.

APPARENT WEIGHT VS MECHANICAL IMPEDANCE

Although mechanical impedance is a familiar vibration analysis parameter, apparent weight is the more efficient and convenient environmental test tool. The reasons are outlined below.

a) Accelerometers are the most common transducers used in the laboratory.

b) Apparent weight has dimensions of pounds. The fact that a system normally acts as a rigid body at low frequencies (10 to 20 Hz) means that the apparent weight is equal to the static weight within this frequency range. This provides both an easy and accurate pre-test calibrate scheme.

c) Field data is normally reported in terms of acceleration. As will be demonstrated later, apparent weight can be used in direct calculations involving field data since both involve acceleration.

d) Many vibration tests, particularly the surveys designed to determine the dynamic characteristics of a system, use a constant acceleration input control. If the control accelerometer is located at the point of force measurement, a ratio is not required. The force output is directly proportional to the apparent weight.

e) Apparent weight (along with blocked force) may be used to define the foundation's characteristics as seen by a test item [2]. In fact apparent weight may be inserted in any equations involving mechanical impedance by using

$$Z = \frac{j\omega}{g} W .$$

MEASUREMENT OF APPARENT WEIGHT

The basic requirement is measurement of the driving force and the resultant acceleration. These measurements, as well as the fixturing, are outlined below prior to considering the excitation source and the instrumentation for ratio and phase measurements.

1) Force Measurement

Commercial force transducers, as well as one developed at Sandia [1], are all acceptable. All known force transducers are moment sensitive. This must be considered in test design and data analysis. The transducer(s) must be inserted intermediate to the path of force transfer. The input force must be controlled and/or measured at the point or plane where apparent weight is desired. If the interface area is small, one force transducer is used. However, a multi-gage array will be required for systems with a large interface. The total force from a multi-gage array is obtained by summing the instantaneous output from each transducer. Note that a phase sensitive sum must be used since apparent weight is the complex ratio of force to acceleration. A DC summation (i.e., peak averaging) cannot be used since the resultant is a DC, phase insensitive, signal.

A fixture is usually required between the force transducer and the system being analyzed. Several fixture requirements are listed below:

a) The fixture must be rigid over the frequency range of interest. In addition to axial rigidity, there must be no resonances between the transducers in a multi-gage array.

b) The attachment of the transducers to the fixture must be rigid.

c) The attachment of the fixture to the system must be rigid.

d) The fixture should adapt to the test item in the same way as the field mount.

e) Commercial force transducers are moment sensitive. The fixture must be designed to minimize moments acting on the transducer.

f) Motion should as nearly as possible be confined to the axis of force input.

To summarize a, b and c above, the motion at the force transducer face must equal that at the base of the system (both amplitude and phase). When a fixture is between the force transducer and the system, the force required to drive the fixture must be subtracted from that indicated by the force transducer(s) as expressed below.

$$F_S = F_T - F_F$$

where

F_S = force into system

F_T = force indicated by transducer

F_F = force to drive the fixture.

Since the fixture (by design) is rigid, the force required to drive it can be expressed as:

$$F_F = ma = wG$$

where

w = fixture weight

G = acceleration of fixture $\left(\frac{a}{386}\right)$.

Therefore,

$$F_S = F_T - wG .$$

This subtraction can be done electronically [2]. The electronic subtraction

technique will be included in the discussion of apparent weight simulation below.

For a single force transducer, calibration is accomplished (1) through use of the voltage or charge sensitivity, or (2) by measuring the acceleration of the rigid system above the force input (at low frequencies) and using $F = ma = wG$. Multi-gage array calibration is normally by method 2 above.

2) Acceleration Measurement

Commercial accelerometers are acceptable. Measurement of point apparent weight requires that the accelerometer(s) be mounted on the test item or fixture immediately above the force transducer(s) so as to represent the acceleration at the point of force input. Transfer apparent weight requires that an accelerometer be mounted at the point of interest above the force transducer(s). Multi-accelerometer arrays are normally used to monitor acceleration of systems with a large interface. The general rule is to locate an accelerometer directly adjacent to (above) each force transducer. In order to maintain a phase sensitive acceleration signal, the multi-gage arrays are instantaneously (AC) averaged during the test. It should be re-emphasized that for point apparent weight, the acceleration required is that on the test item at the point of force input. Therefore, any fixturing must be rigid (acceleration equal in phase and amplitude to that at the point of interest on the test system). Accelerometers are calibrated according to voltage or charge sensitivity.

3) Force Generators

Several factors influence the size (power) of the vibration source. These are discussed below.

A small amount of force can be used to measure apparent weight of heavy items. For example, a 50# generator was used to analyze a 3000-lb system. However, it should be noted that the acceleration level will be extremely low for even moderate apparent weight values. A highly sensitive accelerometer will thus be required.

The size of the vibration machine required is often dictated by the size of the system interface to be analyzed. For example, multi-point force input to a test system of large diameter requires a large vibration machine.

In cases where the apparent weight is measured for the purpose of comparison (discussed later) low force input is acceptable. However, in cases where the apparent weight is to be used in conjunction with field data or environmental tests, the force and/or acceleration test levels should approximate those anticipated in field and laboratory usage. This requirement is primarily due to the non-linear characteristics of most systems.

4) Instrumentation

The instrumentation used to obtain the complex ratio of F to G is constantly being improved. The system depicted in Fig. 4 is fairly representative of the required setup.

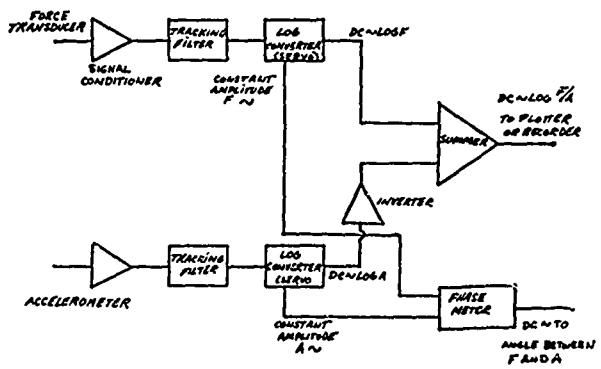

Fig. 4 - Apparent Weight Measurement System

Signal conditioning amplifiers are required for the piezoelectric force transducers and accelerometers. The F and G signals are filtered (extract fundamental) and fed to log converters whose outputs are DC signals proportional to log F and log G. These DC signals are subtracted to yield log F/G which may be recorded or plotted.

Note that the log converters used are designed for apparent weight measurement. They provide constant amplitude outputs phase coherent with the input F and G signals for phase detection. In the newer and more sophisticated apparent weight systems the tracking filtering and log converting may be done in one operation to increase system dynamic range.

The phase meter provides a meter reading and a DC output proportional to the phase difference between F and G. This DC proportional to phase may then be recorded or plotted.

5) Input Control

Primarily, apparent weight is computed during sinusoidal tests. In practice, experimental determinations using random vibration inputs have been made [3]. Using the equations

$$\mathcal{F} = |W|^2 \mathcal{G}$$

$$G_{af} = W \mathcal{G}$$

where

W = apparent weight

$\mathcal{F}$ = force spectral density (lb^2/Hz)

ϕ = acceleration spectral density (G^2/Hz)

G_{af} = acceleration force cross spectral density,

the apparent weight could be determined. Thus far, experimental techniques using the equations above have been tried at Sandia, but no test results are available. The experimental results are considered by Hunter and Otts [3].

FUNDAMENTAL EQUATIONS INVOLVING APPARENT WEIGHT

The fundamental equations used to derive random and sinusoidal test parameters will be considered prior to a discussion of specific laboratory procedures. Note, again, that apparent weight and vibration amplitude are complex functions of frequency. Therefore, the equations below must be applied at discrete frequencies over the frequency band of interest. Also note that point apparent weight will be implied unless otherwise specified.

1) Interface Apparent Weight When Two Structures Are Joined

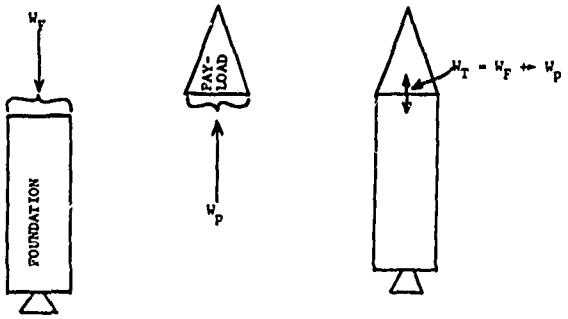

Fig. 5 - Apparent Weight of Joined Structures (At Interface)

Referring to Figure 5, a payload and foundation with apparent weights W_p and W_F, respectively, are to be joined. The total apparent weight (W_T) of the interface is the vector sum of the apparent weights of the two structures.

$$W_T = W_p + W_F$$

where

W_p = payload apparent weight

W_F = foundation apparent weight

W_T = total apparent weight.

Note that this relationship is valid only for a rigid connection at the interface. In other words, validity holds only over the frequency range where the acceleration of the two mounting surfaces is equal.

2) Vibration Response of Foundation With and Without Payload

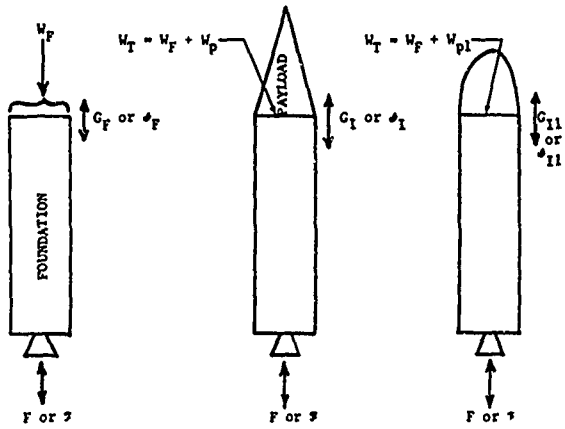

Fig. 6 - Response of Foundation With and Without Payload and With Different Payloads

Referring to Figure 6, a foundation with apparent weight W_F (at payload mounting point) is subjected to a sinusoidal force F. The acceleration response (G_F) at the mounting point results from the input F.

If a payload (W_p) is mounted to the foundation (W_F), the interface response (G_I) to the same force spectrum F is as shown below.

$$G_I = G_F \frac{W_F}{(W_F + W_p)} = G_F\left(\frac{W_F}{W_T}\right)$$

where

G_I = acceleration at interface with payload mounted (sinusoidal)

G_F = acceleration at interface without payload (sinusoidal)

W_F = apparent weight of foundation as seen by payload

W_p = apparent weight of payload as seen by foundation

W_T = interface apparent weight with foundation and payload joined $(W_F + W_p)$.

Similarly, if the force excitation were random ($\mathcal{F}$), and the random acceleration responses were ϕ_F and ϕ_I with and without the payload respectively, the following relationships would apply.

$$\phi_I = \phi_F \left(\frac{|W_F|^2}{|W_F + W_p|^2} \right) = \phi_F \left(\frac{W_F}{W_T} \right)^2$$

where

ϕ_I = PSD response at interface with payload

ϕ_F = PSD response without payload

W_F = apparent weight of foundation as seen by payload

W_p = apparent weight of payload as seen by foundation

W_T = interface apparent weight $(W_F + W_p)$.

3) Vibration Response at Interface with Different Payloads

Continuing with example 2 and Figure 6, above, the response of a different payload (W_{pl}) would be related to the response of W_p as shown below. Both sinusoidal (G_{Il}) and random (ϕ_{Il}) interface responses are considered. The same sine and random force excitations (F and $\mathcal{F}$) as in example 2 are assumed.

$$G_{Il} = G_I \left(\frac{W_F + W_p}{W_F + W_{pl}} \right)$$

$$\phi_{Il} = \phi_I \left(\frac{|W_F + W_p|^2}{|W_F + W_{pl}|^2} \right)$$

where

W_{pl} = apparent weight of different payloads

G_{Il} = sinusoidal response of payload P_1 on foundation

ϕ_{Il} = PSD response of payload P_1 on foundation

G_I = same as in example 2

ϕ_I = same as in example 2

W_F = same as in example 2

W_p = same as in example 2

4) Driving Force at Interface

If the payload-foundation interface response (G_I) is known and the foundation and payload apparent weights are measured to be W_F and W_p, respectively, the following information can be calculated.

a) Force Driving Payload

$F_p = G_I W_p$ (sinusoidal)

$\mathcal{F}_p = \phi_I |W_p|^2$ (random)

F_p = sinusoidal force driving payload at interface

$\mathcal{F}_p$ = random force spectrum driving payload at interface.

b) Force Driving Foundation

$F_F = G_I W_F$

$\mathcal{F}_F = \phi_I |W_F|^2$

where

$F_F, \mathcal{F}_F$ = sine and random force respectively driving foundation from interface.

c) Total Interface Driving Force

$F_I = G_I(W_F + W_p) = F_p + F_F$

$\mathcal{F}_I = \phi_I |W_F + W_p|^2$

$F_I, \mathcal{F}_I$ = sine and random force respectively driving foundation and payload at interface.

5) Transfer Function

Acceleration response ratio and transfer apparent weight are the two forms of transfer function which will be considered. A transfer function is the complex ratio of an input to the response at a different location and can therefore take many forms.

a) Acceleration Response Ratio Transfer Function H(ω)

Consider the test item in Figure 7. The response ratio between input at point 1 and response at point 2 is

$$H(\omega) = \frac{G_2}{G_1} \quad \text{(sinusoidal)}$$

$$|H(\omega)|^2 = \frac{\phi_2}{\phi_1} \quad \text{(random)}$$

where

$H(\omega)$ = transfer function

$G_{1,2}$ = sinusoidal acceleration

$\phi_{1,2}$ = acceleration spectral density.

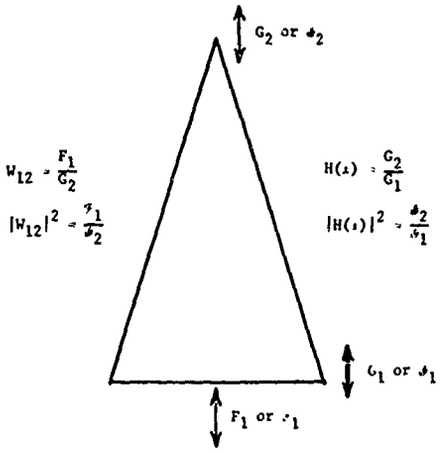

Fig. 7 - Transfer Functions

b) Transfer Apparent Weight

Again consider the test item in Figure 7. The ratio of input force at point 1 to the acceleration response at point 2 is

$$W_{12} = \frac{F_1}{G_2} .$$

From (a) above we also can write this as follows

$$W_{12} = \frac{F_1}{H(\omega)G_1} .$$

By previous definition, F_1/G_1 is defined as point apparent weight. Therefore

$$W_{12} = \frac{1}{H(\omega)} W_p$$

The basic relationships presented above will now be applied to the derivation of laboratory test specifications and procedures.

VIBRATION TEST SPECIFICATIONS AND TEST PROCEDURES AS A FUNCTION OF APPARENT WEIGHT

The fundamental equations outlined in the previous section will now be applied to various test programs. Evaluation of a system's functional and structural integrity, under field vibration environments, requires that the laboratory test be as accurate and realistic as possible. These requirements dictate that field data be used in establishing test criteria whenever applicable field data is available. Unfortunately, many times field data cannot be measured in the form required. For example, the input force spectrum at the base of a field system is difficult to obtain since force transducers must be inserted intermediate to the path of force transmission. This is normally prohibitive due to tolerance changes and/or strength changes resulting from the transducer(s). Also, apparent weight measurements on field foundations are hard to obtain due to their remoteness, size and availability. Obviously, one is forced to compromise with the ideal situation. Typical compromises, in lieu of more realistic techniques, are outlined below.

It should be noted that the purpose of this paper is to demonstrate the use of apparent weight and not to justify the techniques to which it is applied. The arguments for the various tests are thoroughly covered in cited references associated with each case discussed below.

Case #1 - Derivation of Sinusoidal Force Input Spectrum [4]

Field vibration responses of a system were measured during a large number of field tests. This data (G_P) obtained from field accelerometers located at the laboratory input control interface was analyzed in the form shown in Figure 8. This plot represents the maximum acceleration within selected frequency bands and is obtained from Sandia's VIBRAN [5] data system.

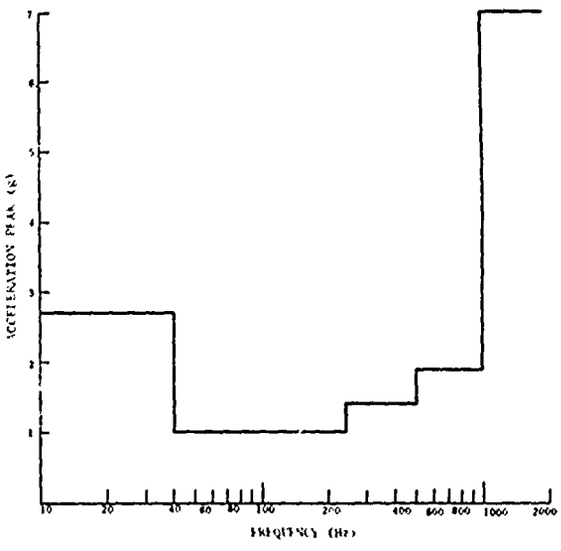

Fig. 8 - Measured Field Vibration (Maximum Response) G_P

Using example 4a from the previous section, the maximum force driving the system is

$$F_I = G_F W$$

where

F_I = force input to test system

G_F = field acceleration at input interface

W = apparent weight of test system.

In this case, the field acceleration (G_F) at the base of the test system is known from Figure 8 for each pre-selected frequency band. It is desired to calculate a constant force input F_I for each of these frequency ranges.

The system apparent weight W was measured in the laboratory and is presented in Figure 9.

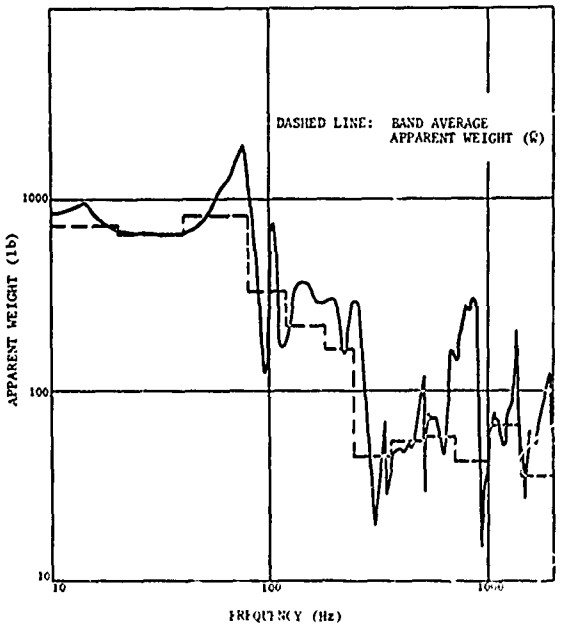

Fig. 9 - Measured Apparent Weight of Test System

As shown in Figure 9, the apparent weight over each bandwidth was biased to a minimum constant value as follows.

$$\bar{W} = W_{min} + 0.1 (W_{max} - W_{min})$$

where

$\bar{W}$ = averaged apparent weight in each band

W_{min} = minimum apparent weight in each band

W_{max} = maximum apparent weight in each band.

Minimum apparent weight corresponds to maximum acceleration response. Therefore, the apparent weight is biased to minimum values since it is to be used with maximum field acceleration.

Finally, application of $F_I = \bar{W} G_F$ resulted in the force spectrum depicted in Figure 10. (Note that the force spectrum could be faired over the frequency test range to provide a non-stepped control.) This force spectrum was used as the input control. The test item is now driven with an approximation of field force. In addition, interface acceleration was limited so as not to exceed the maximum field acceleration (G_F) from Figure 8.

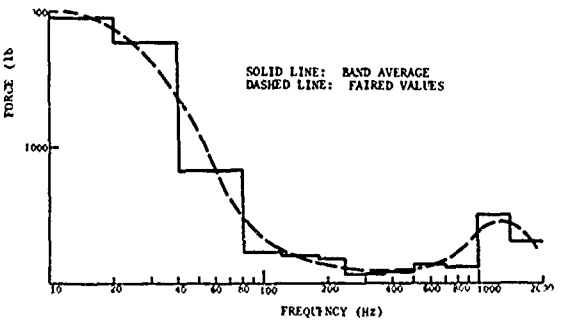

Fig. 10 - Computed Field Forces

Case #2 - Derivation of Random Force Input Spectrum [6]

As in Case #1, field vibration measurements were made during field operations with several units. A random PSD analysis of each field test was plotted. The PSD plot in Figure 11 was obtained by enveloping the maximum from the composite spectra.

Again, using example 4a (random) the force spectrum is calculated as follows

$$\mathcal{F}_I = \mathcal{G}_F |\bar{W}|^2$$

The random acceleration spectrum $\mathcal{G}_F$ was the enveloped composite spectrum in Figure 11. The system apparent weight was measured and band averaged as described previously.

$$\bar{W} = W_{min} + 0.1 (W_{max} - W_{min})$$

The band averaged apparent weight is depicted in Figure 12.

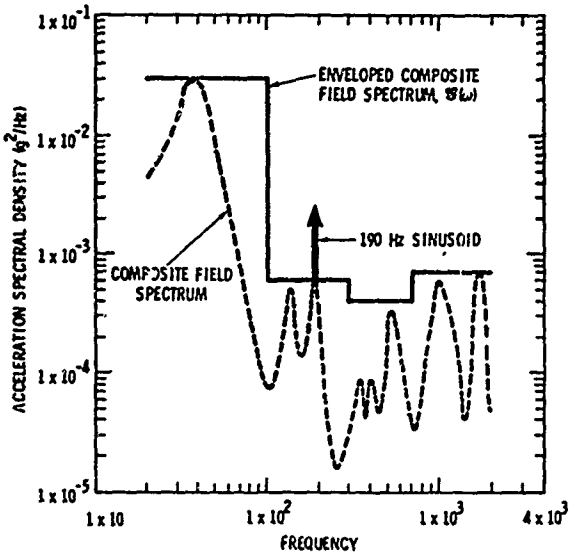

Fig. 11 - Field Acceleration Spectral Density

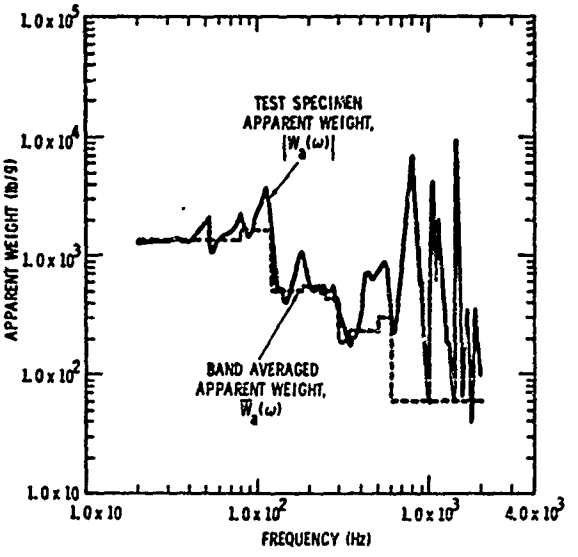

Fig. 12 - Test Specimen Apparent Weight Characteristics

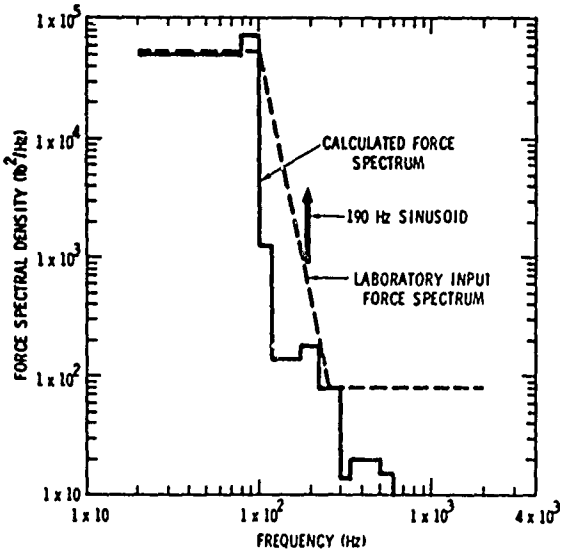

Fig. 13 - Calculated Laboratory Force Spectral Density

The $\mathcal{F}_I$ spectrum resulting from use of the above equation is shown in Figure 13.

Case #3 - Derivation of a Limit on Random Force Spectrum from Case #2 [6]

Limiting the acceleration response spectrum at a location above the control interface was also required. Unlike sinusoidal testing, there is no way to limit random spectrums with commercial or in-house electronics. It thus becomes necessary to limit the random response through proper equalization of the input force spectrum. The procedure is illustrated below.

Assume a point above the control interface is to be limited so as not to exceed a random spectrum ϕ_L during the force controlled test derived earlier. The transfer function $H(\omega)$ between the input (G_1) and limit point (G_2) can be measured in the laboratory.

$$H(\omega) = \frac{G_2}{G_1} \quad \text{(sinusoidal)}$$

$$|H(\omega)|^2 = \frac{\phi_2}{\phi_1} \quad \text{(random)} .$$

The required acceleration spectrum (ϕ_I) at the input is therefore

$$\phi_I = \frac{\phi_L}{|H(\omega)|^2}$$

where

ϕ_I = input PSD

ϕ_L = limit PSD

$H(\omega)$ = transfer function between input and limit points.

Using the definition of apparent weight, the required force spectrum is

$$\mathcal{F}_L = |W|^2 \phi_I = \left(\frac{W}{H(\omega)}\right)^2 \phi_L$$

where

$\mathcal{F}_L$ = input limit force spectral density

W = test item apparent weight

ϕ_I = input PSD

ϕ_L = limit PSD

$H(\omega)$ = transfer function as described above.

By comparison, whenever the limited force spectrum $\mathcal{F}_L$ is less than the derived spectrum $\mathcal{F}_I$, the compensation must be properly equalized. $\mathcal{F}_L$ will be used as the input spectrum over whatever frequencies it is less than $\mathcal{F}_I$.

Note that one could just as well determine transfer apparent weight between input force and acceleration response at the limit point.

$$|W_{12}|^2 = \frac{\mathcal{F}_1}{\phi_2}$$

where

W_{12} = transfer apparent weight

$\mathcal{F}_1$ = input force spectrum

ϕ_2 = response PSD.

Then, replacing ϕ_2 with ϕ_L one can find $\mathcal{F}_L$.

$$\mathcal{F}_L = |W_{12}|^2 \phi_L$$

where

$\mathcal{F}_L$ = input limit force spectral density

W_{12} = transfer apparent weight

ϕ_L = limit PSD.

As discussed previously,

$$W_{12} = \frac{F_1}{H(\omega) G_1} = \frac{W}{H(\omega)}$$

where

W_{12} = transfer apparent weight

W = point apparent weight

$H(\omega)$ = transfer function (ϕ_2/ϕ_1).

Substituting into the above yields

$$\mathcal{F}_L = \left|\frac{W}{H(\omega)}\right|^2 \phi_L ,$$

which shows that both approaches yield the same results.

Case #4 - Simulation of a Structure's Apparent Weight

Many situations arise where it is desired to insert the apparent weight of a structure into the test configuration [2]. It isn't

normally feasible to physically insert the structure, so a technique [2] has been developed whereby the apparent weight is electronically simulated. This technique simulates the blocked force and apparent weight of the test foundation according to Norton's theorem.

Electronic simulation techniques have been developed and applied at Sandia [2,3]. Basically, the technique consists of utilizing an analog computer that determines what the response of the test item would be to a force controlled input if the simulated apparent weight were physically present. It then maintains the determined acceleration response at the test item shaker interface. Full coverage of the technique and the electronics required is included in the cited references.

APPARENT WEIGHT AS NONDESTRUCTIVE TEST TOOL

Apparent weight has numerous uses in defining the mechanical characteristics of systems. These include system modeling, system comparison, and post-test diagnosis.

1) System Modeling

As discussed previously, the mechanical characteristics of a system can be interpreted from the apparent weight data. Of particular advantage are the overall system apparent weight characteristics which can be determined. The dynamic analyst uses this apparent weight data to confirm and/or modify the system model. In addition, this data can influence system design changes.

2) System Comparison

a) Comparison of Different Units

Many times the question arises as to the similarity of two units. The dynamic characteristics can be effectively compared through their apparent weights. Figure 14 shows the similarity between two units analyzed in the laboratory. Although there are minor differences, the systems are within expected tolerances.

As another example, two distinct patterns were observed as shown in Figure 15. Approximately 50 percent fell into each category. It was necessary to know which type system was used in field tests since the apparent weight characteristics were electronically simulated in laboratory tests [7,8].

b) Comparison of Same Test Unit - Different Configuration

Figure 16 is an apparent weight plot of the test unit before and after addition of a subsystem. The anti-resonant peak at about 40 Hz is unaltered, but the higher frequency (>40 Hz) characteristics have changed.

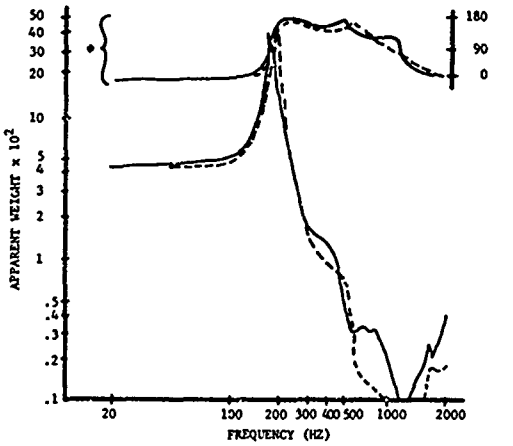

Fig. 14 - Similarity Between Apparent Weight of Two Systems (Same Design)

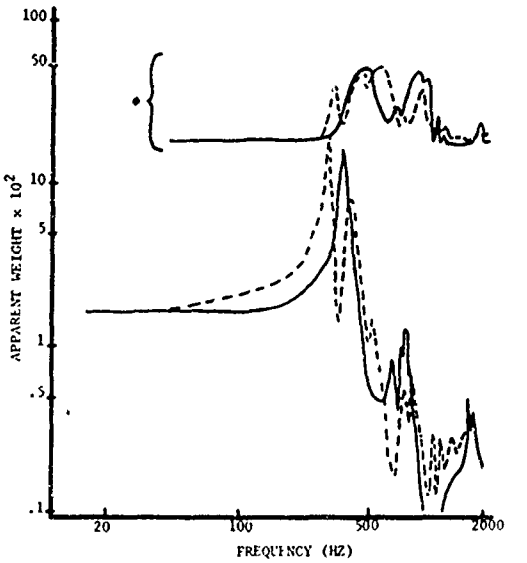

Fig. 15 - Differences Between Apparent Weight of Two Systems (Same Design)

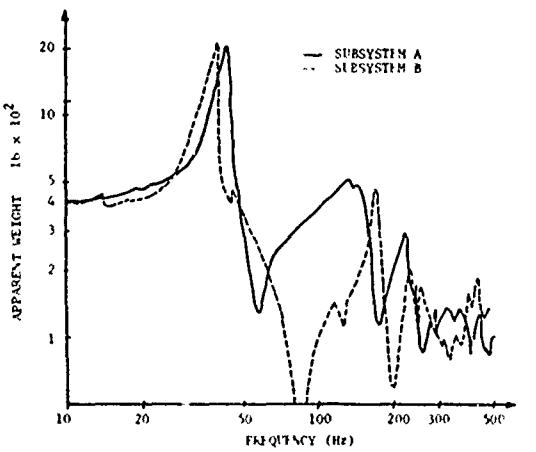

Fig. 16 - Unit Apparent Weight with Subsystems A and B

Knowledge of this type characteristic change is important when field data and apparent weight plots are used to derive laboratory test specifications as described previously.

3) Post-test Diagnosis - Detecting Unit Damage by Apparent Weight Analyses [9]

Pre-test and post-test apparent weight analyses were made on a unit which had been subjected to a vibration test program. The results are shown in Figure 17.

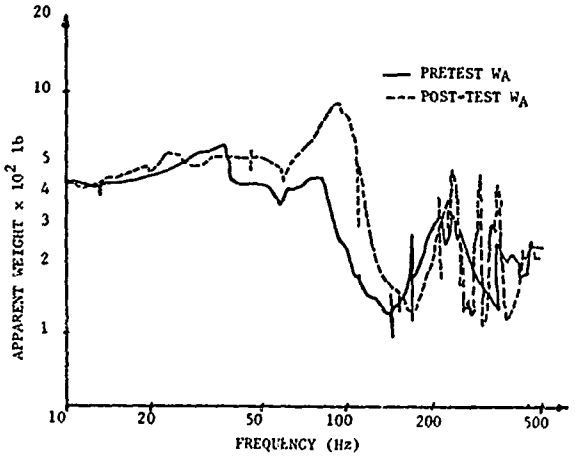

Fig. 17 - Pre-Test and Post-Test Apparent Weight

Damage during testing is evident. In this particular case the data revealed that structural failure of a support flange had occurred. The support flange was redesigned.

Pre-test and post-test comparison is becoming standard procedure on units subjected to complex test series (radiant heat, shock, vibration, etc.). Many times this allows the project consultant to evaluate test results without having to disassemble the unit for inspection.

Apparent weight is a powerful tool in vibration testing. However, it is not simple to measure this characteristic in the laboratory. Some of the problems and associated precautions were discussed previously in the section entitled "Measurement of Apparent Weight." Further consideration to this problem is given below.

1) Dynamic Range

Tracking filters, log converters, voltage amplifiers and phase meters normally have a maximum of 70 dB dynamic range. On the other hand, apparent weight plots many times exceed this range limit.

As a result, control of constant force or acceleration input across the frequency range may not be possible. Variable force or acceleration input and force-acceleration product control are solutions, but should be applied with caution since system nonlinearities can affect the test results. Problems resulting from nonlinearity are discussed below.

2) Phase Measurement

Since apparent weight is a complex ratio, care must be taken to preserve the proper phase between force and acceleration. Tracking filters and log converters do not necessarily maintain phase coherency. Also, tape machines may pose problems for phase coherent recording.

3) System Nonlinearity

A nonlinear system will exhibit apparent weight characteristics which are different, the differences normally being a function of input amplitude and/or direction of sweep.

a) Input Amplitude Effects

Figures 18 and 19 are plots of two different analyses (upsweep vs. downsweep) of the same test system. Both plots were from 1/2 g input control. All conditions (fixturing, input, etc.) were unaltered for the two tests. The results show that the data is quite repeatable. (Figures 18 and 19 on following page.)

Figure 20 depicts the results of a 5 g acceleration input control (vs. 1/2 g in Figs. 18 and 19). The consequent differences in the system characteristics are obvious.

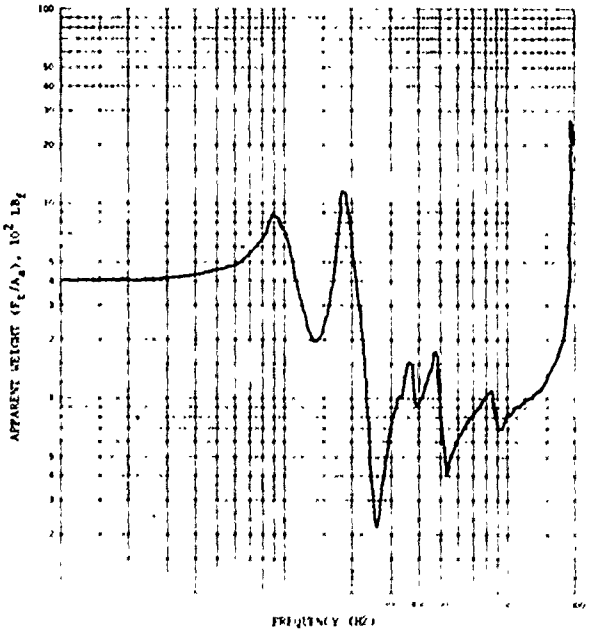

Fig. 18 - Apparent Weight of System Measured During Upsweep (1/2 g Constant Input) Compare to Figure 19

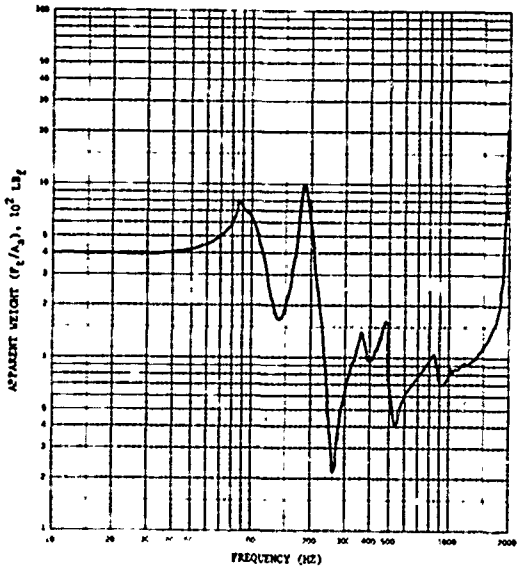

Fig. 19 - Apparent Weight of System Measured During Downsweep (1/2 g Constant Input) - Compare to Figure 18

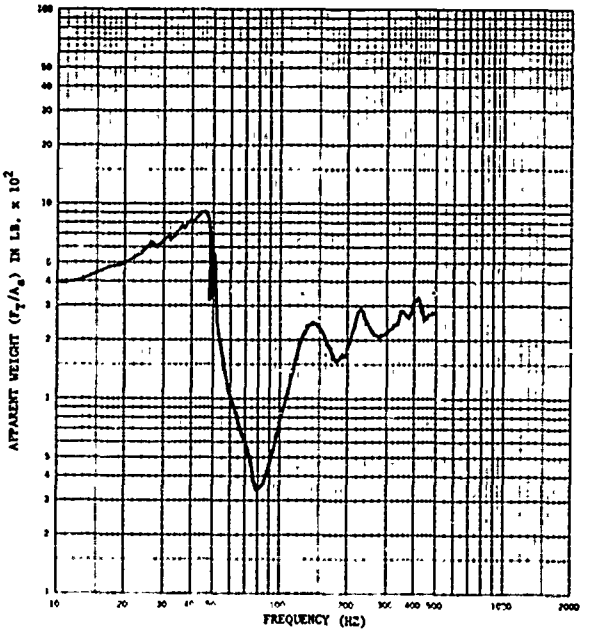

Fig. 21 - Apparent Weight of System Upsweep at 5.0 g Compare to Figure 22

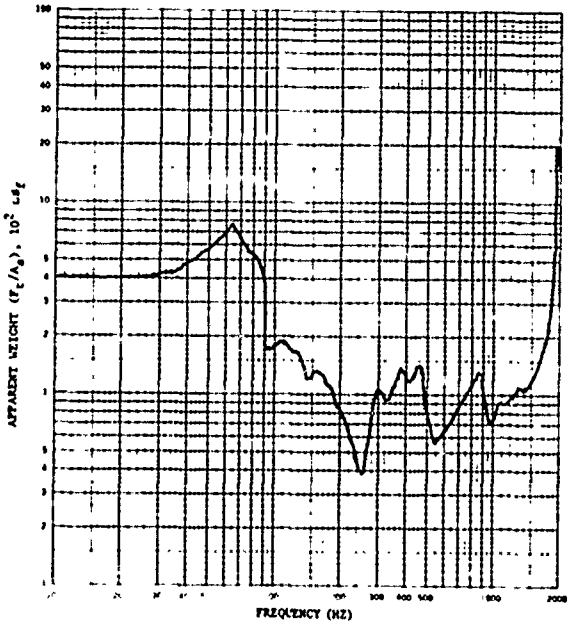

Fig. 20 - Apparent Weight of System (5g Constant Input) - Compare to Figs. 18 and 19

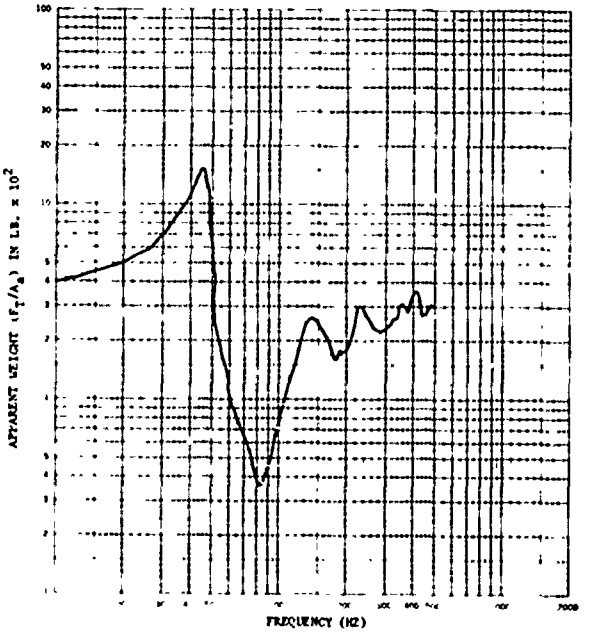

Fig. 22 - Apparent Weight of System Downsweep at 5.0 g Compare to Figure 21

b) Sweep Effects

Figures 21 and 22 compare a unit analyzed during an upsweep and downsweep, respectively. Note the difference in the anti-resonant amplitude at 50 Hz (900 vs. 1400 lb). It should be noted that such a drastic change is an exception, not a rule. However, one must be aware that this type discrepancy can occur.

CONCLUSION

Apparent weight is a valuable tool for the test engineer and dynamic analyst. The field of application covers system analysis, test specifications, test techniques and trouble shooting.

The intent of this paper has been to acquaint test and design personnel with typical applications, techniques and problems.

In particular, it should be noted that apparent weight is a relatively new tool in the vibration laboratory. Known limitations and inherent inaccuracies should be fully understood prior to application.

REFERENCES

1. M. W. Sterk and J. A. Ellison, "Development of Low Cost Force Transducer," The Shock and Vibration Bulletin, Bulletin 36, Part 6, February 1967.

2. N. F. Hunter and J. V. Otts, "Electronic Simulation of Apparent Weight in Force Controlled Vibration Tests," 22nd ISA Conference, Preprint No. P15-1-PHYMMID-67, September 1967.

3. N. F. Hunter and J. V. Otts, "Random Force Vibration Testing," The Shock and Vibration Bulletin, Bulletin 37, February 1965.

4. W. B. Murfin, "Dual Specifications in Vibration Testing," The Shock and Vibration Bulletin, Bulletin 38, Part I, Aug. 1968.

5. J. T. Foley, "An Environmental Research Study," Institute of Environmental Sciences, April 1967 Proceedings.

6. A. F. Witte and R. Rodeman, "Dual Specifications in Random Vibration Testing - An Application of Mechanical Impedance," The Shock and Vibration Bulletin, Bulletin 41, October 1970.

7. J. V. Otts, "A Study of the XW-25 Vibration Response to Structure-Borne Input from the Genie Rocket," Sandia Report SC-DR-66-186, May 1966.

8. C. E. Nuckolls and J. V. Otts, "A Progress Report on Force Controlled Vibration Testing," The Shock and Vibration Bulletin 35, January 1968.

9. R. B. Tatge, "Failure Detection By Mechanical Impedance Techniques," Acoustic Society Journal, 41:1196-1200, May 1967.

Voice: The amplitude did not matter under testing, because you had lower accelerations than in the field, In your tests did you have any problem with nonlinearities, in the system that you later discussed, where the accelerations were greater? Did that affect your apparent weight calculations?

Mr. Hunter: There are a couple of different systems here. On the system that I showed for our unit diagnosis, all of the accelerations were low. We did not use this apparent weight in deriving test specifications for any unit. In the earlier part of the paper, where I talked about deriving the test specifications for a unit, the forces and accelerations in the measurement of the apparent weight did, indeed, approximate the field measurements. If we had tried to use those later measurements just for unit diagnosis, I am sure we would have had problems, because it looked like a pretty nonlinear unit.

Voice: I have not had very good luck with phase meters and I cannot seem to get better than 10- or 15-degree resolution in the angle. Maybe it is because the signals I measure are not pure sinusoids. They are sinusoidal inputs, but the outputs are not sinusoids. Did you have any better luck than that? For me 15 degrees was a real problem. With the kind of resolution I get, it hurts if I have that much scatter.

Mr. Hunter: I think normally we have gotten better results than that, probably in the neighborhood of ± 5 degrees, but a lot depends on what you define as the resolution. If you are testing an item that is severely non-linear so that there are many second and third harmonics in the acceleration response, and if you filter that response to get a clean sine wave, the phase of the clean sine wave output can be measured pretty well. We have had good results with several different types of phase meters. However, if you want to argue the question, "What phase are you trying to measure with this noise on the signal?" that would be a different question.

Mr. Bouche (Endevco): I assume from your discussion that you are measuring point apparent weight or point acceleration impedance. Is that correct in most of these practical applications?

Mr. Hunter: The practical diagnoses of unit failure and that sort of application were really point-apparent-weight measurements using a small exciter and a single force gauge. For most of the test specification derivation work, we have been using a ring of force gauges containing perhaps 10 to 15 force gauges in a sandwich fixture arrangement and measuring resultant acceleration on a ring just above the gauges on the unit.

Mr. Bouche: Do all accererometers experience the same acceleration motion?

Mr. Hunter: Not necessarily. That is a pretty strong limitation that I should have mentioned in the discussion. We assume that all points on the test item have the same motion. If they do not, of course, an error is introduced. The amount of error depends on how much motion gradient you have across the base of the item. For most of our applications, we have tried to hold our frequency range down, e.g, below 500 Hertz, in order to get some sort of reasonable correlation between the accelerometers.

TRANSIENT TEST TECHNIQUES FOR MECHANICAL IMPEDANCE AND MODAL SURVEY TESTING

John D. Favour
Malcolm C. Mitchell
Norman L. Olson

The Boeing Company
Seattle, Washington

The historical development of transient test techniques utilizing the modern digital computer to analyze transient data to define mechanical impedance and modal survey information is discussed. Complex frequency functions, such as apparent mass and transmissibility transfer functions, are developed through ratios of Fourier transforms and digitally plotted both in rectilinear (magnitude and phase vs. frequency) and polar (Nyquist) forms. Validation of early software (prior to the advent of Fast Fourier Transforms), through mechanical impedance measurements on the Bouche aluminum beam demonstrated dynamic range and frequency accuracy superior to existing analog techniques. The operating logic of present digital software routines is discussed. Attention is drawn to the digital plotting of transfer function data in the polar (Nyquist) form, and in particular, the advantages of the annotation method developed.

The developed transient test techniques have been utilized in the analysis of spacecraft, missiles and airplane flutter model testing.

The major bending and torsional modes, and natural frequencies, of a large spacecraft structure were clearly identified via the Nyquist plotting routine. The structure was excited with a force step function and the transient response at various locations analyzed. This data is presented as a relatively straight-forward use of the technique.

A cantilevered supersonic wing flutter model was tested using a transient fast sine sweep. The structural transfer function obtained is compared to a transfer function obtained by an analog steady state vector analyzer. Because of the close spacing of modes, typical in airplane wing structures, the Nyquist presentation of the transfer function is used. This data demonstrates the ability of the transient excitation techniques and the Nyquist presentation to obtain the best estimates of normal mode response without multiple exciters when the actual response is far from being orthogonal.

BACKGROUND

During the early and mid-sixties, the aerospace industry had a love affair with the concept of "Mechanical Impedance". The Boeing Company, like all other aerospace contractors, developed a mechanical impedance measurement capability. The equipment suppliers offered a variety of equipment, all of which relied upon sinusoidal forcing functions to excite the test article. Narrow bandwidth tracking filters were generally the "heart" of the analysis equipment. Those practitioners of the "art" soon found out, amongst other things, that the accurate measurement and plotting of the mechanical impedance of a High Q, mechanical system required very slow sinusoidal frequency sweep rates and could consume from 20 to 40 minutes time to complete one plot. Furthermore,

non-linearities and drift were a problem with individual components, such as frequency converters, oscillators, tracking filters, phase detectors, etc., such that the final plot could not be expected to exhibit a high degree of accuracy. To compound these problems, the data plot, to be of any further use analytically, had to be reduced, generally by some manual means. This added to the errors and the overall time consumption. Because of this, a parallel research effort was initiated to develop an accurate and stable technique of measuring mechanical impedance, transmissibilities, transfer functions and other forms of input-output relationships generally associated with linear systems analysis techniques.

Because of some prior experience on a linear system research [1] problem, the digital computer was chosen to be the nucleus of the new mechanical impedance technique. The reasons for this were the following: a) it was stable, repeatable and accurate, b) the output data could be in both plotted and listed form, c) it permitted the utilization of non-sinusoidal excitation, thereby saving time, and d) it simplified the on-site data acquisition requirements. This research led to the development of a package of computer software entitled "IRES" (Impulse Response). The "IRES" program is designed to analyze transient or impulsive forcing functions and the resultant response data. It does so by computing the Fourier Integral Transforms of the transient forcing function and response data and subsequently ratioing the two transforms to yield the system transfer function. This is a straight-forward linear systems approach. This software program was developed prior to the development of the Fast Fourier Transform (FFT) [2] and relied upon a Fourier transform algorithm entitled "FXFORM". FXFORM permitted the solution of the Fourier Integral equation at any desirable frequency, not just integer multiples of the fundamental frequency (inverse of record length, T).

The FXFORM program provided very high resolution in the frequency domain and the ability to define very sharp peaks and notches. Figure 1 illustrates the high resolution and sharpness made possible with FXFORM. Figure 1 is an "apparent mass" measurement on the "Bouche" [3] aluminum beam measuring 3/4 in. x 3 in. x 36 in. This figure illustrates the quality of resonant frequency correspondence between theoretical and measured. Refer to Table 1.

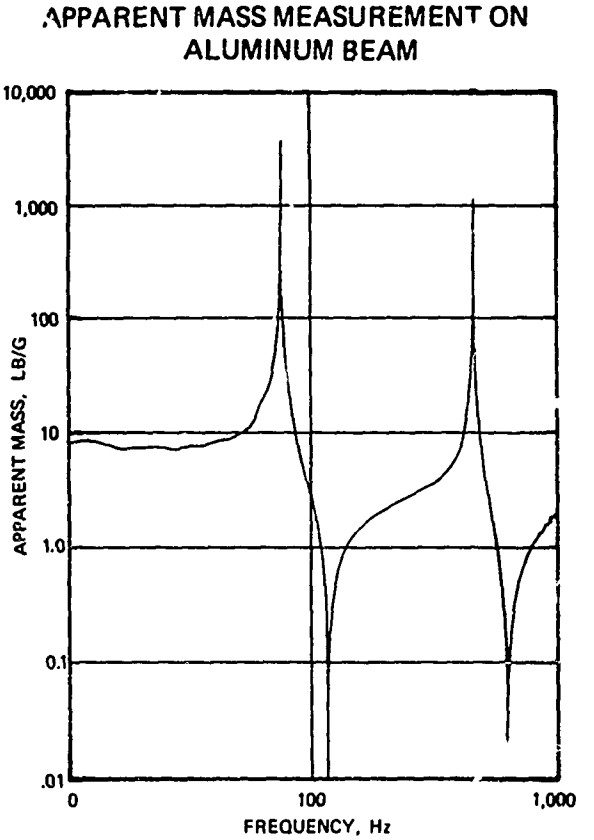

Figure 1

THEORETICAL [4] RESONANT FREQUENCY, Hz	74.5	118.6	474.4	640
MEASURED RESONANT FREQUENCY, Hz	74.3	118	459	625

TABLE 1, THEORETICAL & MEASURED RESONANT FREQUENCIES OF STANDARD BEAM

These results were superior to anything produced by our commercial analog equipment. The only disadvantage to the digital method was the data turnaround time, 24 to 48 hours after test. The test data was recorded directly in digital form by a portable analog to digital converter and tape storage unit. Three channels of data could be recorded to accommodate the necessary mass cancellation computation. Upon completion of testing, the digital magnetic tape was sent to the Central Computer Processing Center and processed on the IBM 7094 computer. This technique, developed as a result of "in-house" research, found scattered usage in many tests but failed to receive general acceptance due to the long turnaround time required and some customer reluctance to test with a "new" method.

DYNAMIC DATA ANALYSIS SYSTEM AND IRES

In 1968, a new data acquisition and analysis system designed around an XDS Sigma II digital computer was acquired. This system, the Dynamic Data Analysis System (DDAS) [5] was developed for test support and analysis of transient and random data. The system provides "on line" time and frequency domain analyses for both local and remote test operations, thereby eliminating the long turnaround time problem. The IRES program was rewritten (using the same general methodology) to be compatible with the DDAS.

The source of data inputs to the DDAS is analog FM tape containing calibration data, the forcing function, the response data and an IRIG B time code signal. Calibration and data signals are digitized by a dual channel, 10-bit-plus-sign, synchronous-sampling Analog to Digital Converter (ADC). Digitizing is initiated from the IRIG time code signal at a time and for a duration specified by program control parameters.

The digitized dual channel sinusoidal calibration signals, in conjunction with the known transducer sensitivity, calibrates the 'raw' data into engineering units and provides the cross-channel time delay or skew information, which is used to remove unwanted skew from the time domain data.

Any D.C. offset, or tare value, immediately prior to initiation of the transient test data is subsequently subtracted from test data before translation to engineering units.

The resultant transient test data is reformatted for time history plots (if desired) and Fourier transform computation.

The DDAS Fast Fourier Transform is a modified Cooley-Tukey algorighm [6] calculated in a Digital Spectrum Analyzer (DSA). The DSA is a small special purpose computer, controlled from the Sigma II Central Processing Unit (CPU). It is comprised of two 4096 word memories, one of which typically contains time domain data, and the other, a sine or cosine function. The multiply-add cycle time of this device is approximately 900 nanoseconds. The DDAS FFT algorithm requires that the time domain data to be transformed be composed of an integral power-of-two data points. Zero data values are added onto the end of the digitized time series to yield the required power-of-two values for transformation.

The individual transforms of the forcing function and responses to the forcing function may be plotted if desired.

The frequency domain transfer function is calculated as

$$T(f) = \frac{R(f)}{F(f)}$$

where $T(f)$ = Complex transfer function,

$R(f)$ = Fourier transform of response function,

$F(f)$ = Fourier transform of forcing function,

and may be plotted, listed, and or written on digital magnetic tape, for reformatting and plotting in Nyquist form as described below.

NYQUIST PLOTTING ROUTINE

With the reduced turnaround time of the IRES program on DDAS, the utilization of IRES increased quite dramatically. Those structural dynamicists and engineers, charged with the responsibility for laboratory verification of the structural and dynamic analysis of a complex structure, became increasingly interested in the possibilities offered by IRES. The only problem was that they were not happy with the rectilinear plotting of transfer function magnitude versus frequency on one page and the plotting of phase on another (Fig. 2A). Specifically, the methods developed by Kennedy and Pancu [7] were being used with analog equipment and the Nyquist or polar plot of a transfer function was most useful. The Nyquist plot permits the direct plotting of magnitude, phase and frequency (see Figure 2B). The major problem involved with Nyquist plotting, both with analog equipment as well as digital equipment, has been the proper and accurate annotation of the running parameter, frequency. A Nyquist plotting routine was added to the IRES software and the solution to the annotation problem was developed.

Transfer function data is input to the Nyquist plot routine via digital magnetic tape generated by IRES.

The frequency range for plotting is selectable by program control, allowing any desired isolated modal response to be plotted, thereby eliminating the visual confusion of multiple-overlaid modes, which would result from displaying the transfer function over its entire frequency range on a single plotted page. Modal responses to be plotted are typically selected by quick

look examination of transfer function magnitude and phase plots on a storage and display scope.

The Nyquist polar plane representation of the system transfer function is constructed from 3 variables. Frequency is the independent variable and the real and imaginary parts of the transfer function are dependent variables.

At each discrete frequency, f_i, the real and imaginary parts of the transfer function, R_i and I_i, are plotted, respectively, on the real and imaginary axes as illustrated in Figure 2B.

Discrete frequency points on the locus of the Nyquist plot are denoted by a small square (■) and consecutively connected by line segments. The set of points is plotted within a polar circle of 3 inch radius. The engineering unit equivalent of this radius is annotated on the plot.

The problem of clearly and accurately indicating running frequency was solved by numerically annotating the frequency of every 'kth' point. "K" is a value supplied to the program by the DDAS operator.

Of particular interest to the structural dynamicist is the notation of maximum rate of change of arc length with respect to frequency along the locus of the Nyquist plot. This point approximated by locating the maximum distance between discrete frequencies within the frequency range plotted.

Clearly, this approximation approaches true rate of change of arc length in the limit as $\Delta f \rightarrow 0$, hence, sufficiently fine frequency resolution is of considerable importance. Plus (+) symbols on the locus denote the two frequency points between which the maximum distance occurs.

Operator/program communications are performed at the DDAS teletype console in a conversational mode. Required control parameters a[illegible]ew in number and operator intervention is thereby minimized.

After plotting has been completed, the operator may elect to a) replot (on the same, or on a different plotter); b) terminate program execution; c) change any combination of program control parameters and r[illegible]plot from the stored data or d) read in another transfer function from the digital data tape

TRANSFER FUNCTION OF SECOND ORDER SINGLE DEGREE OF FREEDOM SYSTEM PLOTTED IN RECTILINEAR AND NYQUIST FORMS

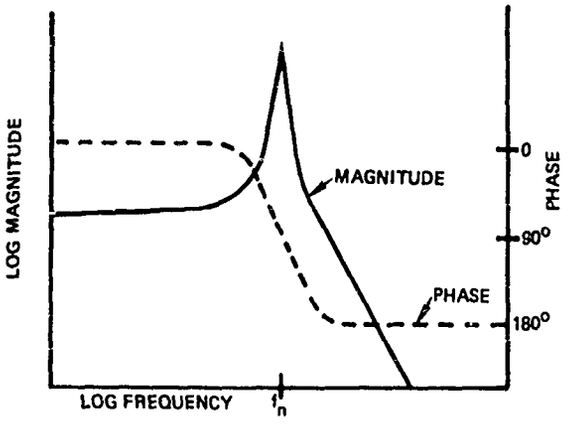

2A. COMBINED RECTILINEAR TRANSFER FUNCTION PLOTS

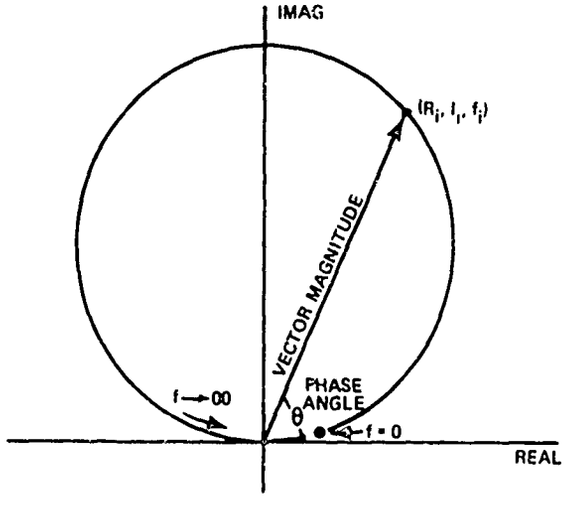

2B NYQUIST POLAR PLOT

Figure 2

UTILIZATION

The remainder of this paper is devoted to illustrating two of the many ways by which this transient test technique has been utilized. The first example illustrates verification of structural dynamics of an ultra-lightweight, spacecraft solar array structure, thru a simple "twang" test and analysis of the structural response. The second example is a more complex illustration of how transient excitation and analysis techniques have been utilized to analyze the modal response of a cantilevered supersonic wing flutter model.

SOLAR ARRAY STRUCTURE

In the spring of 1970, a test program was in the process of verifying the dynamic structural analysis of an ultra-lightweight spacecraft solar array structure. Steady state sinusoidal response or resonant searches, resonant dwells and resonant delay phenomena, were being used to verify the analysis. In conjunction with this procedure, and because of its simplicity, an additional series of "twang" tests was also conducted. In each case the test configuration, instrumentation (partial), location and method of applying the step function excitation, or twang, are shown in Figure 3. On one side of the structural frame, a woven fiberglas skin is attached. The solar cells are mounted upon this skin. For this test, a lightweight string was attached to the back side of the fiberglas skin, in the center of one of the structural subdivisions, and run over a pulley. A 1.5 pound weight was attached thereby preloading the structure. About a dozen response accelerometers were located on the structure. Two will be discussed; accelerometer A_1, located at the point of string attachment, and another accelerometer A_2, located on the frame of the structure, outboard of A_1. The preload caused both bending and torsion in the structure.

The test was conducted by simply cutting the string and thereby applying a 1.5 pound step function (release of preload) to the structure. The response acceleration signals at A_1 and A_2 were recorded on FM magnetic tape. For purpose of analysis, the force step function was synthesized on FM magnetic tape at a later time. The data was then analyzed via the IRES program, on the DDAS, and two transfer functions were computed:

$\frac{A_1(f)}{F(f)}$ = a point inertance

$\frac{A_2(f)}{F(f)}$ = a transfer inertance

Both transfer functions were plotted in Nyquist polar form, Figures 4 and 5, over a limited bandwidth of 10 to 40 Hz. Both plots indicate two separate and distinct resonant modes at 12.8 and 29.0 Hz. Clues to the identification of these two modes are clearly provided within the two polar plots. In the point measurement, $A_1(f)/F(f)$, (Figure 4) the magnitudes of the two resonant modes are quite different with the 29 Hz mode having the larger vector magnitude. In the transfer measurement, $A_2(f)/F(f)$, (Figure 5) which is more sensitive to torsional motion, the two modes are nearly equal, but in this case the 12.8 Hz mode has the larger vector magnitude. This, along with the prediction from the dynamic analysis, clearly established the identity of the 12.8 Hz mode as first torsion and the 29.0 Hz mode as first bending.

TWANG TEST SETUP FOR SOLAR ARRAY STRUCTURE

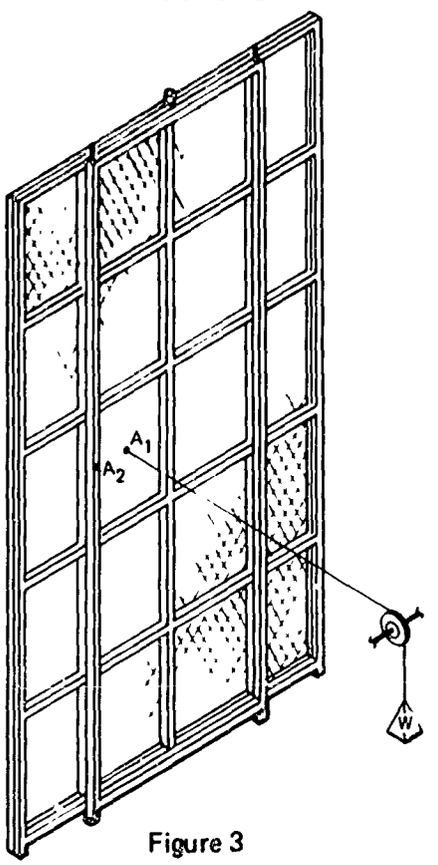

Figure 3

POINT INERTANCE MEASUREMENT,
$A_1(f)/F(f)$

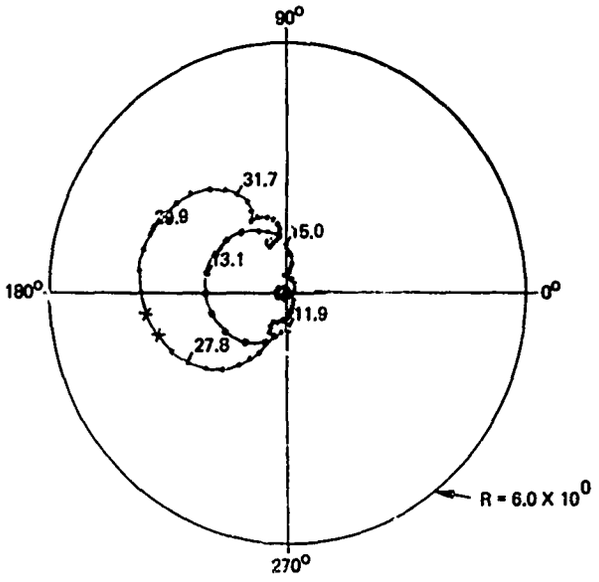

FREQ RANGE 0.1098E +02 0.4028E +02 CPS
ΔF=0.3052E + 00 CPS
0.2838E + 02 > ΔS/Δ F MAX
0.2859E + 02

Figure 4

TRANSFER INERTANCE MEASUREMENT,
$A_2(f)/F(f)$

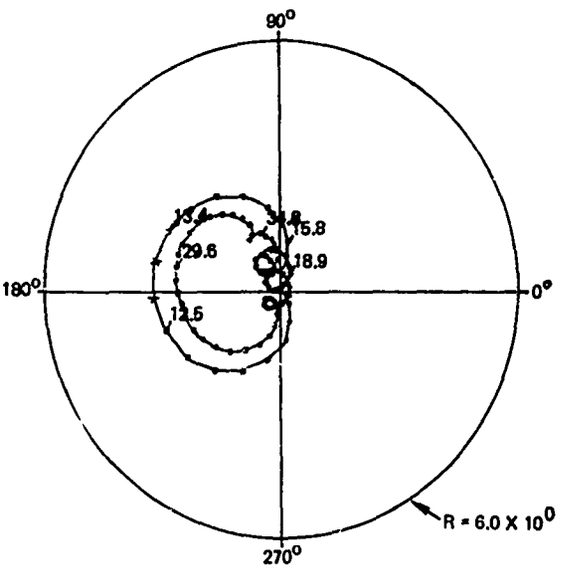

FREQ RANGE 0.9766E + 01 TO 0.4028E + 02 CPS
ΔF = 0.3052E + 00 CPS
0.1282E + 02 > ΔS/Δ F MAX
0.1312E + 02

Figure 5

By strategic location of the response transducers and the point of input forcing function, all of the dynamic modes of interest can be clearly identified through the analysis of a few simple "twang" tests.

SUPERSONIC WING FLUTTER MODEL

For preliminary evaluation of the techniques of the Fourier transform and transient excitations applied to the testing of complex airplane structures, a cantilevered wing flutter model of a supersonic airplane was chosen as a representative structure. The model was constructed primarily from fiberglas and balsa wood, with aluminum being used for the nacelle strut springs. A picture of a structure similar to the one tested is shown in Figure 6.

As a basis for judging the results of the transient testing, the model was first tested using a sinusoidal steady state vector analyzer (Aeroelastic Modal Analysis System - AMAS)[8] [9]. By setting a frequency on the frequency synthesizer the resulting complex plane vector is plotted after the system under test has reached a steady state response. This process is continued one frequency at a time until the locus of points describing a mode is plotted. This system produces excellent complex plane plots. Its main disadvantage, however, lies in long test times since it requires steady state response of the test specimen.

The excitation system consists of a voice coil weighing 20 grams placed in a constant magnetic field with no mechanical coupling between the voice coil and the field-producing structure. The voice coil is attached to and supported by the structure under test. Provided the field intensity is constant over the range of displacement of the voice coil, the derived force from this coil is proportional to its current. Using a constant current source to drive the voice coil, the coil back EMF is working into a relatively high impedance and therefore adds insignificant damping forces to the model. The force signal consists of a voltage proportional to the voice coil current and phase-coherent with it.

The response measuring system consists of an Endevco 2264 piezo-resistive accelerometer with associated power and balance units followed by a broadband instrumentation amplifier.

CANTILEVERED WING FLUTTER MODEL

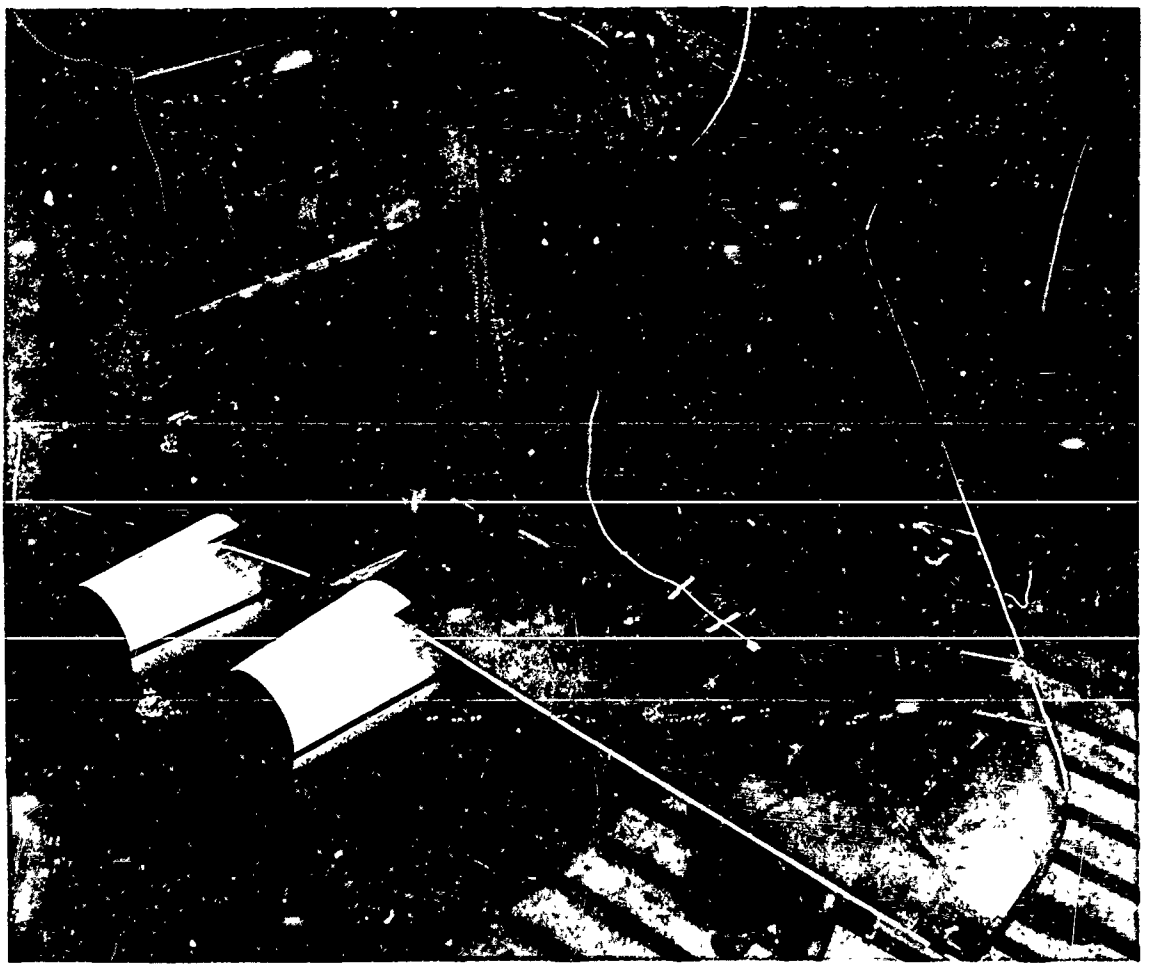

Figure 6

Figures 7 and 8 present the resulting AMAS plots for the direct inertance measurement for the first 3 modes. The method used to extract modal data follows that outlined by Kennedy & Pancu [Ref. 6] in that resonance is determined by the maximum rate of change of arc with frequency, dS/df. With the resonant frequency determined, a circle is fitted to the data around resonance from which the angle θ is determined between two vectors. This angle is used to measure the damping value from the relationship

$$\zeta = \frac{\Delta f}{f_n \tan \theta/2} ,$$

where ζ = damping ratio

f = frequency

f_n = natural frequency

θ = phase angle

This relationship is valid for low damping typical of airplane structure. For optimum results the angle θ should be kept between 10 and 30 degrees. Figure 7 details the circle fitting and calculations for the first mode and Table 2 tabulates the results from the AMAS steady state response tests. This data shows significant non-orthogonal response in modes 2 and 3.

	$\Delta f = 0.01$		
MODE	f_n	θ	2ζ
1	7.00	19°	0.017
2	10.12	32°	0.0072
3	10.28	16.5°	0.014

TABLE 2: STEADY STATE TEST RESULTS

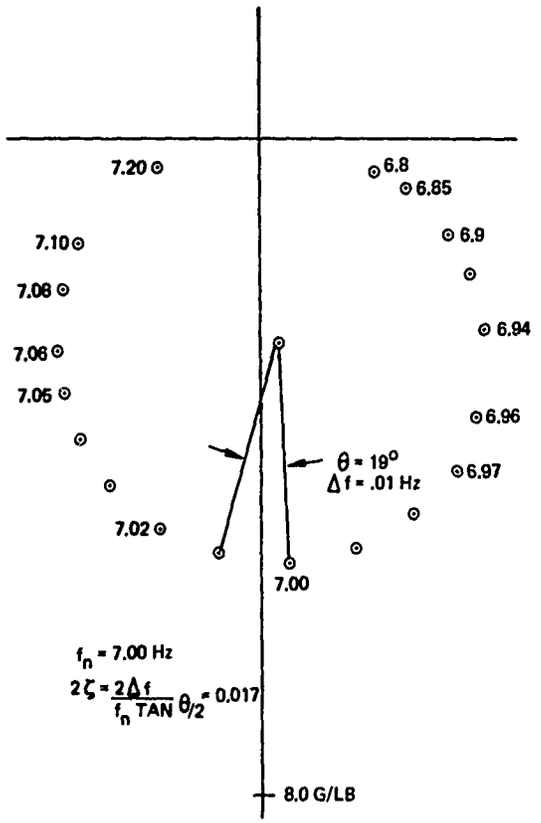

Figure 7

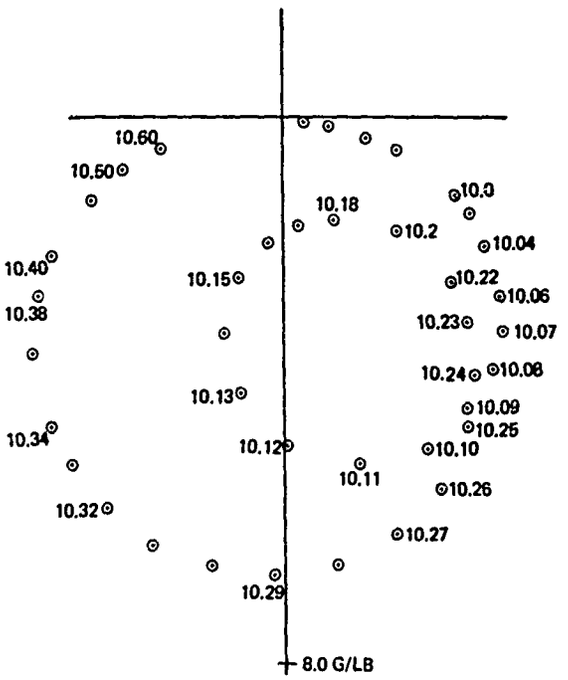

Figure 8

For the transient test a fast sine sweep was chosen as the forcing function, since it can input about two orders of magnitude more impulse, or momentum (lb-sec), into a structure as compared to using a bandwidth limited delta function (assuming the same resulting bandwidth and peak force). This is obtained because the duration of the sine sweep approaches the data sample length, T, whereas the impulsive excitation usually lasts less than 10% of T. For the fast sine sweep test, the initial or starting frequency of the sweep was chosen just below the first mode frequency and the ending frequency was picked to be somewhat above the highest mode of interest (mode 7). The resulting swept bandwidth was 5 to 50 Hz. A log sweep rate was chosen.

Since the required Δf is in the neighborhood of 0.01 Hertz, the DDAS equivalent to this is 0.00953 Hz and therefore, the required data length T is 105 seconds (real time). Taking the fast sine sweep to the limit for its duration results in about a 90 second sweep time leaving some cushion for the response to die out at the completion of the sweep, thus avoiding truncation errors.

The results of the transient fast sine sweep are shown in Figures 9 and 10 covering the first three modes. Table 3 lists the frequencies and damping obtained from the first three modes using the transient excitation.

	Δf = 0.0095		
MODE	f_n	θ	2ζ
1	7.01	23°	0.0135
2	10.12	34°	0.0063
3	10.28	23°	0.0094

TABLE 3: TRANSIENT "FAST SINE SWEEP" TEST RESULTS

TRANSIENT ANALYSIS, FIRST MODE

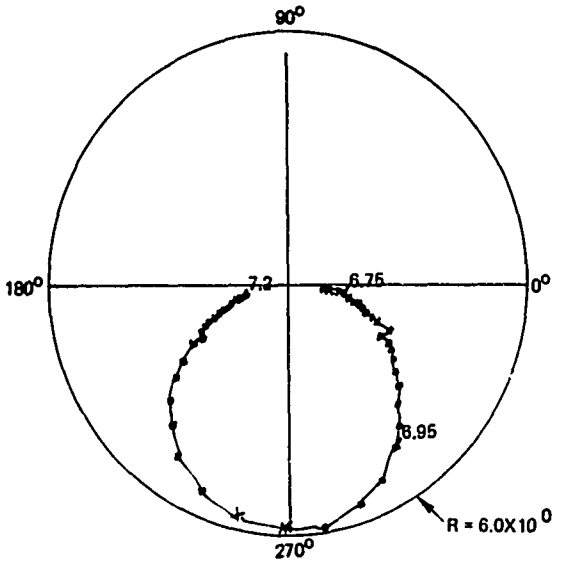

NYQUIST POLAR PLOT
FREQ RANGE 0.6500E + 01 TO 0.7250E + 01 CPS
Δ F = 0.9535E – 02 CPS

0.7010E + 01
0.7020E + 01 > ΔS/ΔF MAX

Figure 9

TRANSIENT ANALYSIS, SECOND AND THIRD MODES

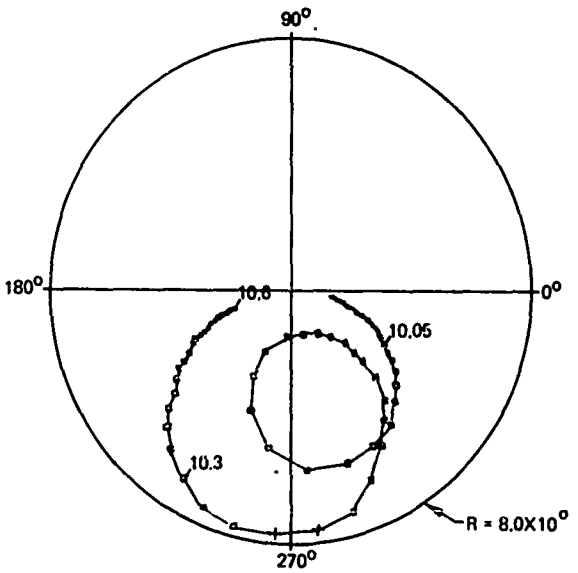

FREQ RANGE 0.9750E + 01 TO 0.1075E + 02 CPS
Δ F = 0.9535E – 02 CPS
0.1028E + 02
0.1029E + 02 > ΔS/Δ F MAX

Figure 10

The results of both methods compare favorably even though the analog system takes more test time.

The following is a discussion of additional data which can be obtained from the Nyquist plots where it can be shown that the diameter of the fitted (or constructed) circle is equal to 1/2 K, if the plot is the ratio of displacement divided by force (see Ref. 6), assuming orthogonal response. Now, for a single degree of freedom system,

$$(2\pi f_n)^2 = \frac{K}{M} = \frac{X}{F} = \frac{1}{2\zeta K} = \frac{1}{2\zeta M(2\pi f_n)^2}$$

measuring acceleration per unit force instead of displacement

$$\frac{X}{F} = \frac{-\ddot{X}}{(2\pi f)^2 F} = \frac{1}{2\zeta M(2\pi f_n)^2}$$

and at resonance, $f = f_n$,

$$\frac{X}{F} = \frac{-1}{2\zeta M},$$

where K = spring constant
M = mass
X = displacement
$\ddot{X}$ = acceleration
f = frequency
f_n = natural frequency
F = force
ζ = damping coefficient

With this relationship, the modal point mass can be measured from the plot. This method is subject first of all, to errors in the damping measurement, errors resulting from a high degree of coupling and also to errors in the absolute sensitivities of both the accelerometer and force transducers.

The alternate method of added mass is applicable to the fast sine sweeps

and the Fourier transform. Using the Nyquist form of data presentation, the resonant frequency measurement is subject to the least percentage error with respect to the other measured parameters; therefore, this method of added mass seems appropriate under the circumstances. It follows:

M_n = unknown modal mass

M_a = small added mass (known)

f_n = resonant frequency without added mass M

f_a = resonant frequency with added mass M

$$(2\pi f_n)^2 = \frac{K}{M_n} \text{ and } (2\pi f_a)^2 = \frac{K}{M_n+M_a}$$

substituting for K,

$$(2\pi f_n)^2 M_n = (2\pi f_a)^2 (M_n+M_a)$$

$$M_n[(2\pi f_n)^2 - (2\pi f_a)^2] = M_a(2\pi f_n)^2$$

$$M_n = M_a \frac{(2\pi f_a)^2}{(2\pi f_n)^2 - (2\pi f_a)^2}$$

This method is valid only for small added masses since it assumes no change in the mode shape. For the least amount of error, this calculation should be performed at a shaker location producing the best orthogonal point inertance response. If large couplings exist, the calculation is probably not worth making.

With respect to the problem of measuring the orthogonal mode shapes of an airplane, the method of multiple shakers is the best, considering the accuracy of the measured estimate. However, the method requires a considerable expenditure of effort during and in preparations for the test.

It has been shown by Pendered [10] and later by Craig [11] that the method of Kennedy-Pancu can produce inaccurate mode shape data when the degree of coupling is very high or when there is damping coupling. However, the Kennedy-Pancu method does provide data which, if used in conjunction with the determinate method of Asher [12], can set up an effective multiple shaker test. The minimum test time consumed during transient single shaker tests would allow those modes to be identified which require multiple shaker tests. The data has also been obtained in a short time period, after which the multiple shaker test can be designed and set up.

The method of estimating the orthogonal mode shape proposed here, consists of using a single shaker, the transient fast sine sweep and the Fourier transform. That is, if a series of accelerometer responses to a transient fast sine sweep excitation were recorded on magnetic tape, an estimate of the orthogonal mode shape could be obtained. First, a Nyquist plot of inertance would be calculated for each accelerometer location, using the transient fast sine sweep excitation as a common denominator. For each mode on each plot, a circle would be constructed to fit the data around resonance. A plot of the constructed circle diameters versus each location would result in the estimated orthogonal mode shape. The resonant frequency and damping for each mode would be calculated directly from one of the Nyquist plots of inertance. The measurement of modal parameters (mass) would also be performed based on the most orthogonal-looking response. The generalized parameters can then be calculated by normalizing the point of measurement to the point of maximum response using the estimated measured mode shape. Better yet, if an analytical analysis exists, the analytical generalized parameters can be normalized to the accelerometer location where the modal parameters were measured. A comparison between measured and analytical quantities could then be performed.

An interesting footnote to this investigation is the non-linear characteristic of mode 5, where a response level above a reference threshold was obtained. The relatively high force level produced a rattle in a nacelle bearing. This rattle produced the unusual AMAS steady state response of Figure 11. The fast sine sweep using a force level where the bearing rattled produced the plot of Figure 12. A lower force level produced the more usual plot shown in Figure 13.

These experiments on the flutter model wing are part of a continuing development program directed toward developing practical methods and techniques of conducting airplane ground resonance and flight flutter tests using the Fourier transform and transient excitations.

CONCLUSIONS

The techniques of mechanical impedance and structural dynamic testing thru transient excitation and digital computer analysis have been transformed from the realm of academic curiosity to existance as a realisitc, accurate and

AMAS ANALYSIS, HIGH LEVEL NONLINEAR RESPONSE

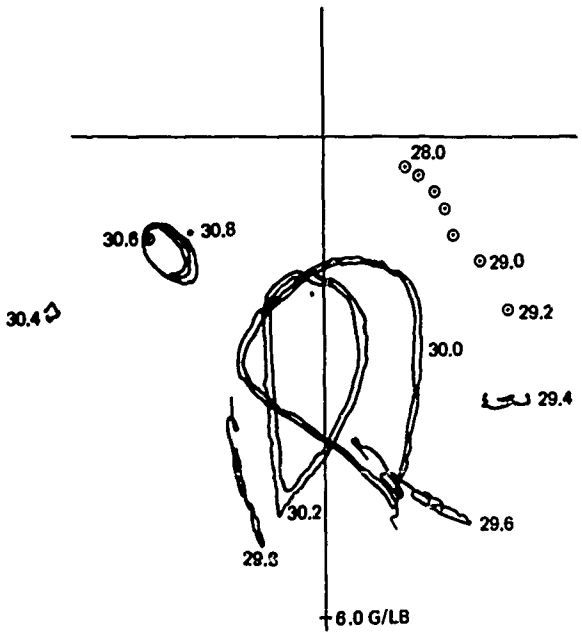

Figure 11

TRANSIENT ANALYSIS, HIGH LEVEL NONLINEAR RESPONSE

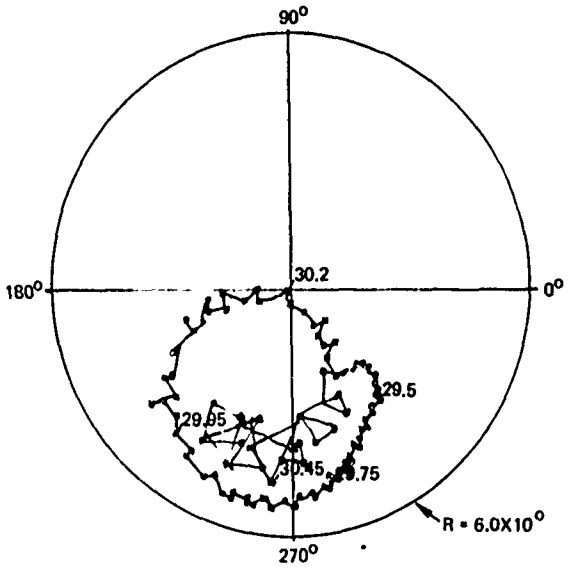

FREQ RANGE 0.2925E + 02 TO 0.3055E + 02 CPS
ΔF - 0.0535E – 02 CPS
0.3045E + 02
0.3046E + 02 >ΔS/ΔF MAX

Figure 12

TRANSIENT ANALYSIS, LOW LEVEL NONLINEAR RESPONSE

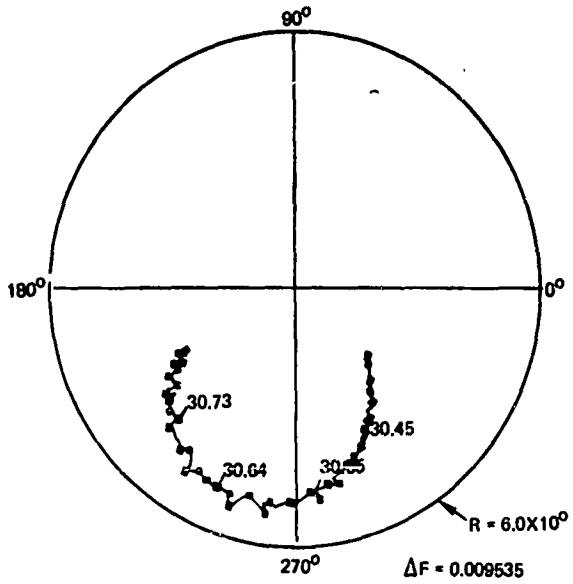

Figure 13

economical engineering tool. The work reported in this paper represents a small segment of a continuing effort to provide more economical and meaningful information from the test laboratory.

REFERENCES

[1] J. D. Favour, "Transient Data Distortion compensation", 35th Shock and Vibration Symposium, February 1966.

[2] J. W. Cooley, P.A.W. Lewis and P. A. Welch, "The Fast Fourier Transform Algorithm and Its Applications", IBM Research Report RC 1746, 1967.

[3] R. R. Bouche, "Instruments and Methods for Measuring Mechanical Impedance", 30th Symposium on Shock, Vibration & Associated Environments, October 1961.

[4] C. M. Harris and C. F. Crede, "Shock & Vibration Handbook", Volume 1.

[5] M. O. Michellich, "Dynamic Data Analysis System", 40th Shock and Vibration Bulletin, December 1969.

[6] J. W. Cooley and J. W. Tukey, "An Algorithm for the Machine Calculation of Complex Fourier Series", Math. of Comput., Vol. 19, pp 297-301, April 1965.

[7] C. C. Kennedy and C. D. P. Pancu, "Use of Vectors in Vibration Measurement and Analysis", Journal of the Aeronautical Sciences, November 1947.

[8] Instruction Manual SD1004-18B, Aeroelastic Modal Analysis System, V1 and V2, Spectral Dynamics Corporation of San Diego, 1968.

[9] Monsanto Digital Frequency Synthesizer, Model 3100A, Monsanto Electronic Instruments, West Caldwell, New Jersey, 1969.

[10] J. W. Pendered, "Theoretical Investigation Into the Effects of Close Natural Frequencies in Resonance Testing", J. Mech. Engr. Sci., V7, n 372-379, 1965.

[11] R. R. Craig, "A Study of Method for Determining Pure Modes and Frequencies of Complex Structures", Boeing Document No. T6-5558, Informal.

[12] G. W. Asher, "A Method of Normal Mode Excitation Utilizing Admittance Measurements", Proceedings - National Specialists Meeting on Dynamics & Aeroelasticity, Fort Worth Institute of Aeronautical Science, 69-76, November 1958.

DISCUSSION

Mr. Schrantz (Comsat Laboratories): What is your definition of a fast sweep-rate in terms of amplitude?

Mr. Favour: It was a constant amplitude.

Mr. Schrantz: What level?

Mr. Favour: I do not know the level on that wing. It depends upon the structure of course, but I do not know what that level was.

Mr. Schrantz: What was the sweep rate?

Mr. Favour: On that particular example it went from 5 cycles to 50 cycles in 90 seconds. Recognizing that, in order to get an analysis of 0.01 cycles delta F, we had to have 100 seconds of data. If you want to call that a transient, it really is. The sweep went from 5 to 50 cycles in 90 seconds and left about 10 seconds of residual transient to die out, so we had all the data without truncation.

PREDICTION OF FORCE SPECTRA BY MECHANICAL IMPEDANCE AND ACOUSTIC MOBILITY MEASUREMENT TECHNIQUES

R. W. Schock
NASA/Marshall Space Flight Center
Huntsville, Alabama

and

G. C. Kao
Wyle Laboratories
Huntsville, Alabama

Structural impedance, or its reciprocal mobility, has seen limited use in recent years to tailor dynamic tests of highly critical and expensive components to ensure a highly accurate control of response loads. These efforts have been generally confined to sinusoidal test simulations of rocket vehicle longitudinal and lateral modes in frequency ranges at or near the component response frequencies.

A method, described in this paper, has been developed to calculate broad frequency range vibration criteria which account for both primary and component load impedance for structures subjected to random acoustic excitation. These criteria rather than being defined in traditional motion parameters are defined in force parameters and are, therefore, termed force spectra. The force spectra were predicted by a one-dimensional equation which utilizes four types of data measured at equipment mounting locations. These data consist of: Input impedance of support structure; Acoustic mobility of support structure; Input impedance of component package; and Blocked pressure spectrum.

An experimental program was conducted to validate the prediction equation. A stiffened aluminum cylinder with the dimensions of 3 ft (diameter) x 3 ft (height) x .02 in. (skin thickness) was used in acquiring input impedances and acoustic mobilities. An 8 in. x 8 in. x 1/2 in. aluminum plate was used as a simulated component. The plate was supported by four sets of leaf springs with four loadwashers attached to the bottom of each spring for measuring loads. The blocked sound pressure spectra were obtained from microphone measurements on a rigid dummy concrete cylinder. Two equipment mounting positions were used in the tests.

All test data were acquired on-line to analog/digital acquisition systems. Computer programs were written to reduce and analyze the acquired data, and also to predict the interaction force spectra. Good agreements between the predicted and measured force spectra were obtained.

INTRODUCTION

Component packages of rocket vehicle are traditionally qualified for acoustic environments by motion-control (or response-control) testing. Vibration environments used in this type of testing are obtained by enveloping peak amplitudes of measured or predicted response data, but ignoring effects of component - primary structure coupling. Consequently, components qualified under the motion-control criteria would probably be overtested or undertested as compared to actual inflight environments. A more realistic approach would be first to determine the interaction forces between a component and its support structure, and then to test the component under the force-control environments. This approach requires a prediction technique to define the dynamic forcing criteria as indicated above. The primary objective of this paper is to present a method for predicting interaction forces between components and

corresponding support structures subjected to acoustic excitations. Such force environments which are determined in spectral forms are referred to as "Force Spectra" in this paper. Research in seeking practical techniques for defini g force-control criteria has gained considerable attention during recent years. Available results which are relevant to force-control studies are presented in References 1 through 10.

FORCE-SPECTRA EQUATION

It is assumed that dynamic responses of a structural system subjected to excitation by external forces are predominantly one-dimensional. Thus the dynamic characteristics of the structure can be represented by a one-dimensional impedance model as shown in Figure 1. In this figure, the basic unloaded structure is replaced by an equivalent structural "black box"; external loads are applied at terminals 1, 2, and component packages which are treated as load impedances, $Z_L(\omega)$, are attached to terminals 3, 4. The corresponding velocities and interaction forces at the attachment points are indicated by $V_L(\omega)$ and $F_L(\omega)$, respectively. The structural impedance model, as shown in Figure 1, can be represented by the equivalent constant-force model (Thevenin's model) and the constant-velocity model (Norton's model) as shown by Figures 2 and 3, respectively. The dynamic characteristics of the attachment points (terminals 3, 4) are represented by $Z_s(\omega)$ which is defined as the support-structure impedance, or source impedance, i.e., the impedance looking back to the left of terminals 3, 4 without any loads attached.

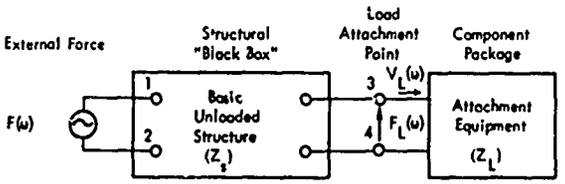

Figure 1. One-Dimensional Impedance Model of a Structural System

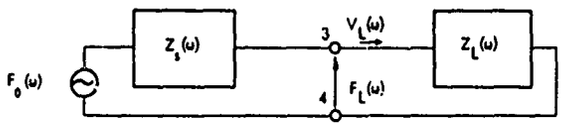

Figure 2. Equivalent-Constant Force Model

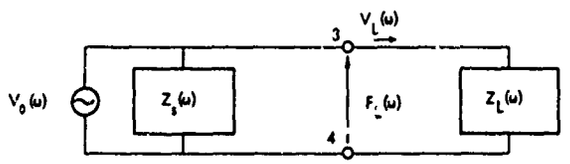

Figure 3. Equivalent-Constant Velocity Model

The driving force $F_L(\omega)$ can be shown [11] to have the following expression:

$$F_L(\omega) = V_0(\omega) \cdot \frac{Z_s Z_L}{Z_L + Z_s} \qquad (1)$$

Based on Equation (1), the component-structure interaction force spectra of vehicle structures subjected to acoustic excitations could be expressed by, [11]:

$$\Phi_L(\omega) = \Phi_p(\omega) \cdot \left| \alpha_{\dot{x}}(\omega) \right|^2 \cdot \left| \frac{Z_s Z_L}{Z_s + Z_L} \right|^2 \qquad (2)$$

Where

$\Phi_p(\omega)$ = Power spectral density (PSD) of reference sound pressure which is assumed to be constant over the surface over the component attachment locations.

$\left| \alpha_{\dot{x}}(\omega) \right|^2$ = Acoustic mobility at component mounting locations, and is defined by the ratio of the rms velocity response of a support structure and its corresponding rms sound pressure.

Due to structural complexities of rocket vehicles, precise analytical approaches to obtain the parameters defined in Equation (2) are not practical. Therefore, in order to validate Equation (2), experimental techniques were used to acquire measurements of these parameters on the selected test specimens, and to compute the force spectra quantitatively.

The accuracy of the force spectra computed in the above manner could then be checked by comparison with force responses measured from a simulated component mounted on a support structure which was subjected to random acoustic excitations. The approaches used to implement the measurement techniques outlined above are depicted in Figure 4.

TEST SPECIMENS

The support structure used in the experiment was a stiffened aluminum cylinder, as shown in Figure 5. The cylinder's dimensions were 36 in. (diameter) x 36 in. (length) x 0.02 in. (thick). The cylinder consisted of five aluminum rings and twenty-four longitudinal stringers equally spaced along the longitudinal and circumferential directions, respectively. All stiffeners were mounted to the cylinder wall by rivets.

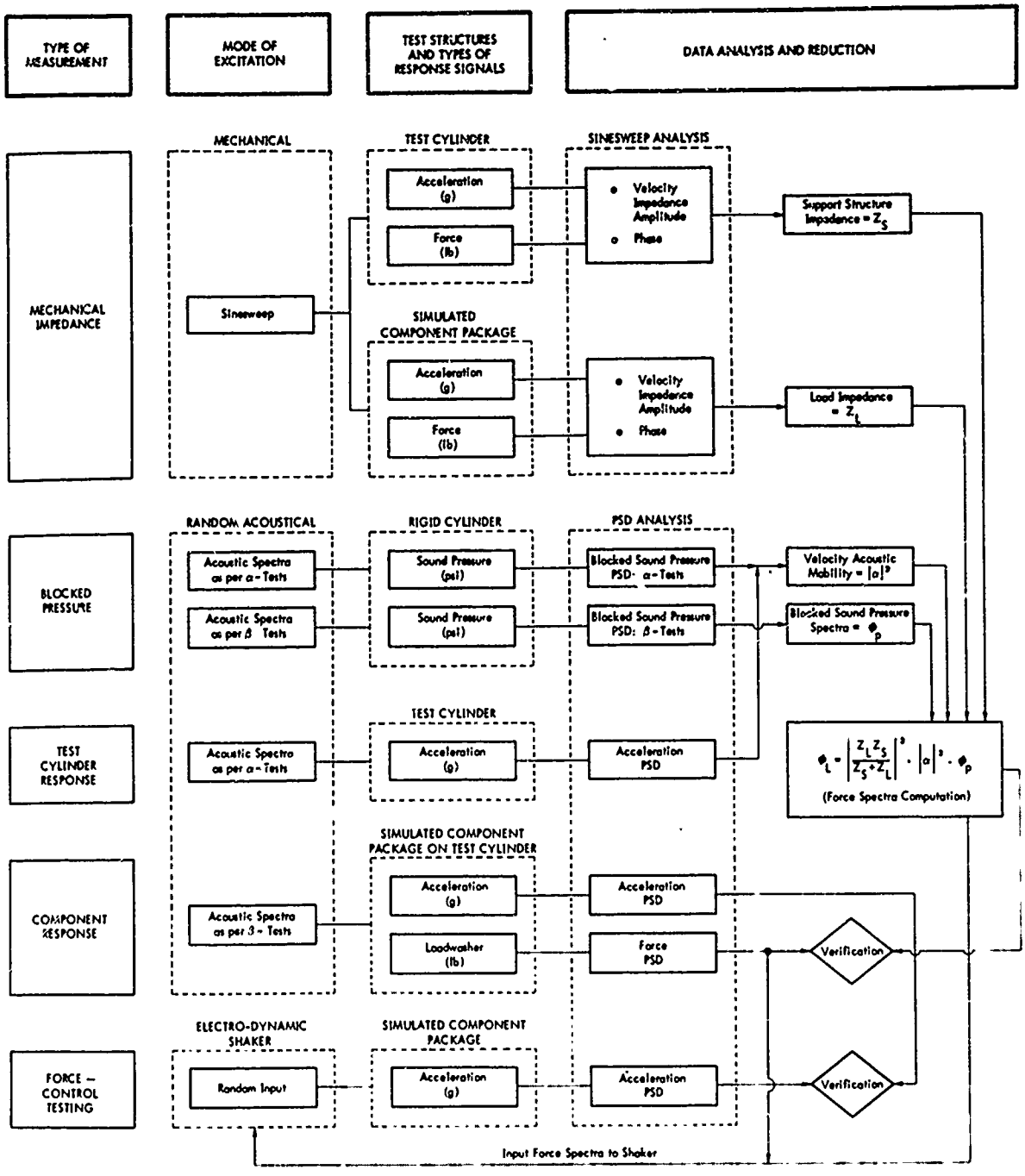

Figure 4. Block Diagram of Force-Spectra Program

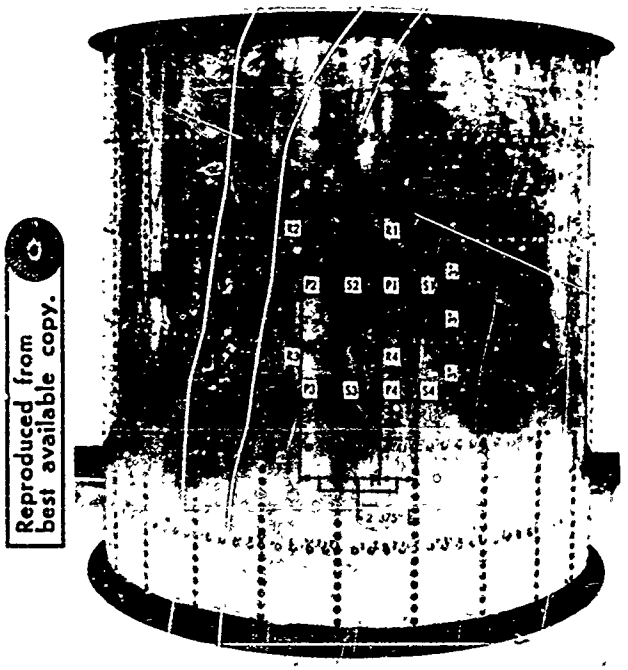

Figure 5. Stiffened Cylinder and Input Impedance Measurement Locations

The dimensions of the individual curved panels formed by the stiffeners were 6 in. x 4.75 in. Two steel rings of 1 in. x 1 in. x 1/8 in. angle section were riveted at both ends of the cylinder, and two circular sandwich plate bulkheads were bolted to these end rings by 1/4 in. diameter hex bolts and nuts. Each circular bulkhead was constructed from two steel plates of 1/8 in. thickness, separated by a 1/2 in. thick plywood section. Two component mounting positions will be discussed in this paper, and they are designated as follows:

- Positions R1, R2, R3, R4: Centers of ring frame segments
- Positions S1, S2, S3, S4: Centers of longitudinal stiffener segments

The dummy rigid cylinder consisted of reinforced concrete having dimensions of 48 in. (length) x 36 in. (diameter) x 4 in. (thick). A photograph showing the rigid cylinder is presented in Figure 12.

The simulated component package, as shown in Figure 6, consisted of a 1/2 in. aluminum plate with lateral dimensions of 8 in. x 8 in. The plate was supported by four sets of leaf springs at its corners. The bottom of each spring was fitted with a loadwasher assembly.

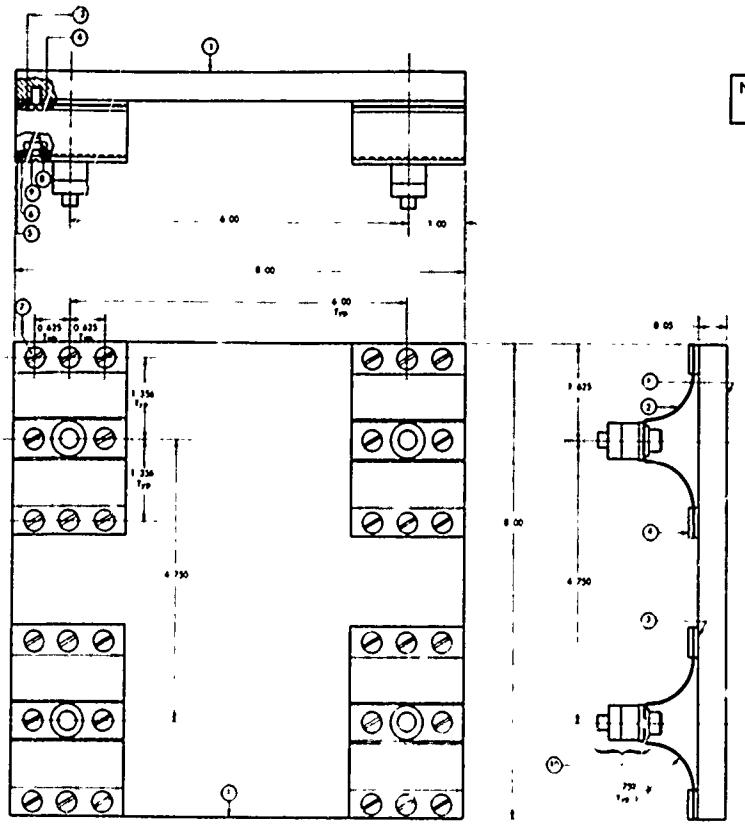

NOTE: All parts, except Item No. 2, were made of Aluminum Alloy Type 6061-T6

1. 1/2" x 8" x 8" Plate
2. 4 - 0.008 Steel Leaf Springs
3. 0.031 x 2.00 x 4.193 Strip
4. 0.063 x 0.50 x 2.00 Strip
5. 0.063 x 0.550 x 2.00 Strip
6. 0.063 x 0.550 x 2.00 Strip
7. No. 10-32 100° Flat Head Screw x 5/6" Lg.
8. No. 10-32 Hex Nut
9. No. 10-32 100° Flat Head Screw x 3/8" Lg.
10. Loadwasher Assembly; Details Shown in Figure 7

Figure 6. Dimensions of the Simulated Component Package (All Dimensional Units are in Inches)

Each assembly, as shown in Figure 7, consisted of a Kistler 901A loadwasher which was sandwiched between an anti-friction washer on the top and an aluminum mounting stud at the bottom. These elements were held together with the top clamping strips by a center bolt as shown in Figure 7. Each loadwasher was pre-compressed to approximately 1000 pounds level, so that the tensile and compressive forces induced during testing could be measured. The total weight of the component package was 3.81 pounds; the resonances of the package were measured at 110 Hz and 1200 Hz, respectively. The fundamental resonant frequency of the 1/2 in. plate was found to be 1200 Hz.

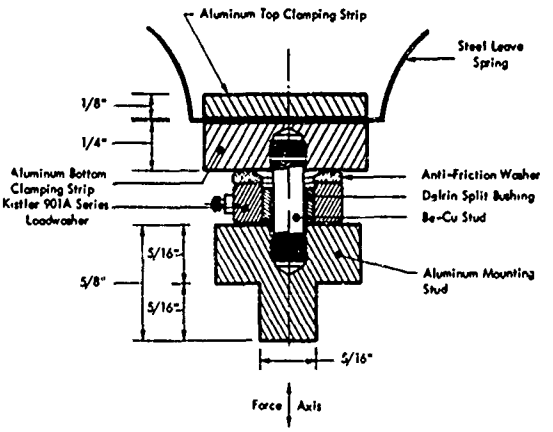

Figure 7. Details of Loadwasher Assembly

DATA ACQUISITION SYSTEM

The data acquisition systems employed in the tests are shown in Figure 8. Basically, the systems consisted of four major subsystems described as follows:

- Analog data system
- Central control system
- A/D conversion system
- Recording and displaying system

The key functions of each subsystem are described as follows:

Analog Data System

This system was comprised of transducers, such as accelerometers, microphones, strain gages, signal conditioning amplifiers and patch panels. Electrical signals produced by these transducers were conditioned by appropriate amplifiers to achieve desirable signal levels prior to the link-up with the A/D systems. A maximum of 128 data channels are available through the current system.

Central Control System

The central control system was the brain of the entire data acquisition system; it consisted of the following units:

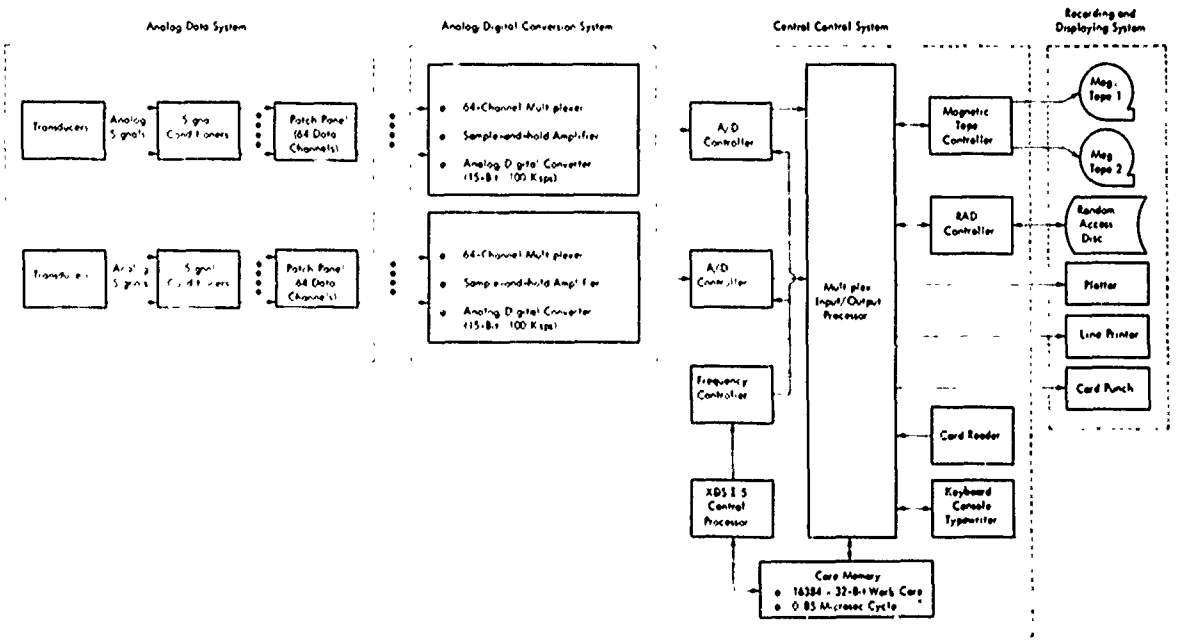

Figure 8. Block Diagram of the Analog/Digital Data Acquisition System

- XDS - SIGMA 5 Central Processor
- Core Memory Unit
- A/D Controller
- Multiplex Input/Output Processor
- Frequency Controller

The peripheral equipment used in the tests is shown in Figure 8. The main function of the central processor was to coordinate work performed by various units according to instructions as given through input devices (card reader or magnetic tapes). The input instructions established the requirements for:

- Type of analog signals to be acquired (sine or random)
- Sensitivity factors
- Number of data channels
- Sampling rate
- Frequency range
- Full-scale ranges
- Data recording or displaying formats

Each unit would then act accordingly to specific instructions during the length of a data acquisition process.

A/D Conversion System

There were two A/D conversion units which formed part of the data acquisition system. Each unit consisted of the following equipment:

- One 64-channel multiplexer
- One sample-and-hold amplifier
- One analog/digital converter (15 bit, 100 K sps)

The multiplexer's function was to transmit incoming analog signals sequentially to the sample-and-hold amplifier at a predetermined rate. The amplifier sampled the signal and applied a gain of 1, 2, 4 or 8 (as selected by the digital program) to convert the signal to a desired range. The digitized signals were stored temporarily in the core unit, and then transferred to other recording or display devices upon receiving commands from the central processor.

Recording and Displaying Systems

The recording system consisted of two magnetic tapes and one random access disc for storing digital data received from the core memory unit. Other output formats could also be obtained by plotting or punched cards, as desired.

MEASUREMENT APPROACHES

Impedance data for the support structure were acquired by the impedance measurement systems as shown schematically in Figure 9. Three types of signal were acquired for each measurement point. These signals consisted of:

- Force signal
- Acceleration signal
- Constant Amplitude Reference Frequency Signal (COLA).

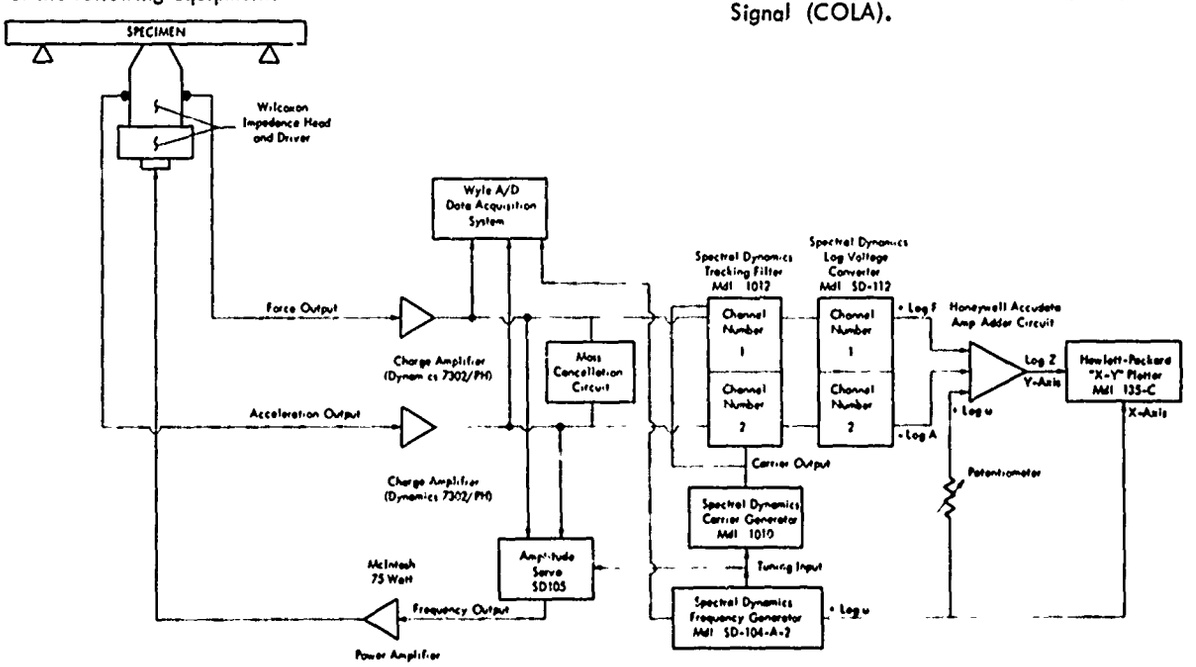

Figure 9. Instrumentation Block Diagram of the Mechanical Impedance Measurement System

The force and the acceleration signals were obtained by employing an impedance head which was bonded to the aluminum cylinder by Eastman 910 or commercial dental cement. All measurements were made in the frequency range from 40 Hz to 2000 Hz with sinesweep forcing techniques. The sweep rate was set at one octave per minute for all test runs. During each test, controls were exercised to maintain minimum force and acceleration levels by the amplitude servo monitor in order to achieve high signal levels throughout the frequency range of interest. Wilcoxon impedance heads Z-602 and Z-13 were used to measure impedances at Locations R and S, respectively.

The measurements of the component package impedances utilized the instrumentation set-up as shown in Figure 10. The component package was mounted on a shaker (Ling Model No. 286), as shown in Figure 11, which was used to provide input forces for driving the component. Response signals were obtained from two accelerometers, A1 and A2, mounted on the center of the 1/2 in. plate and the base plate, respectively. The force signals were generated by the outputs of individual loadwashers. The input impedance signals consisted of COLA, force and A2 responses; whereas, the transfer impedance signals consisted of COLA, force and A1 responses.

The measurements of vibro-acoustic data were conducted in Wyle Laboratories' 100,000 cu ft reverberation room. The acoustic mobility measurements consisted of measuring sound pressure near the surface of a concrete cylinder, and simultaneously acquiring the response data at the component mounting positions of the aluminum cylinder. The two cylinders were placed near the center of the reverberation room and were spaced 10 feet apart from each other. A control microphone, used to acquire the reference sound pressures, was located near the center of the room and 10 feet above the floor level. Figure 12 shows the relative positions of the microphones and the test cylinder in the reverberation room. Blocked sound pressure

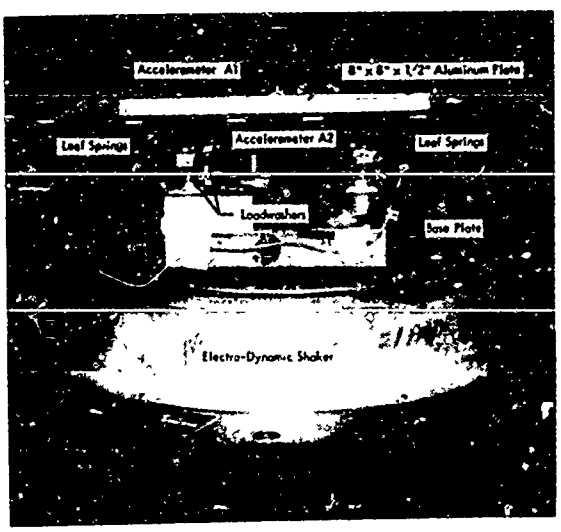

Figure 10. Measurement of Component Package Impedance

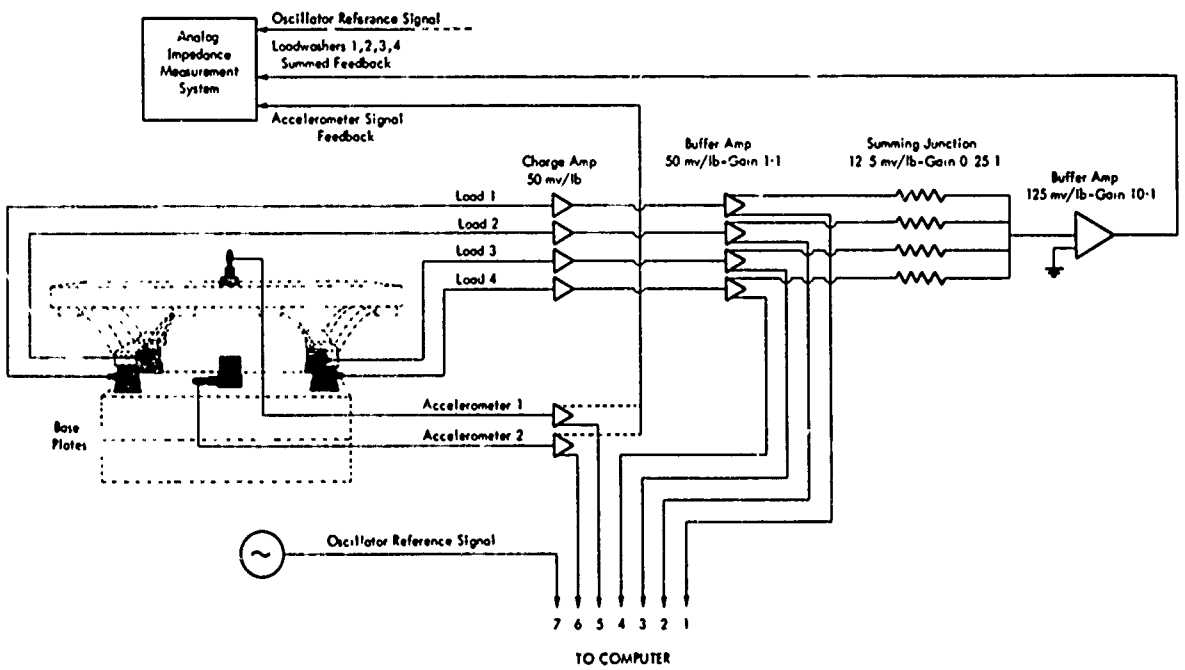

Figure 11. Instrumentation Block Diagram for Impedance Measurement of the Component Package

signals were acquired by four microphones which were placed about 1/4 in. above the surface of the concrete cylinder. The center distances between microphones were set identical to that of the component mounting positions (6 in. x 4.75 in.).

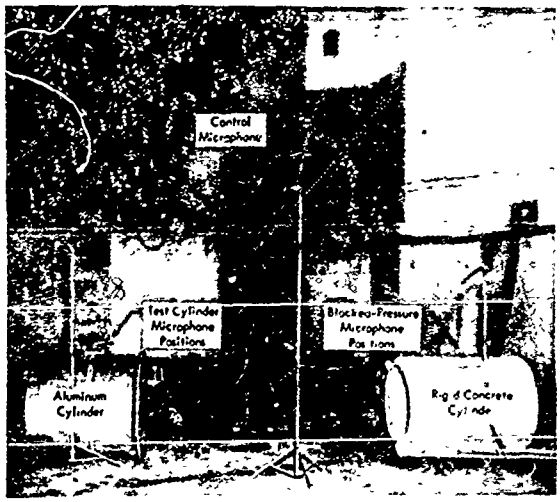

Figure 12. Relative Positions of Test Cylinders and Microphones in the Reverberation Room

To obtain the response data of the aluminum cylinder for computing acoustic mobilities, the average acceleration responses at the R and S locations were required. The average responses at these locations were obtained by placing four Endevco Type 2226 accelerometers at positions indicated below:

R1, R2, R3, R4

S1, S2, S3, S4

Following the acoustic mobility measurements, the component package was mounted on the aluminum cylinder at locations R and S, respectively, for acoustic testing. A typical test position of the component is shown in Figure 13. The blocked pressures were acquired by four microphones located near the surface of the concrete cylinder. The interaction forces between the component and the aluminum cylinder were sensed by the Kistler loadwashers; and the responses of the plate were acquired by an Endevco Type 2226 accelerometer. Instrumentation employed in the vibro-acoustic tests is shown in Figure 14.

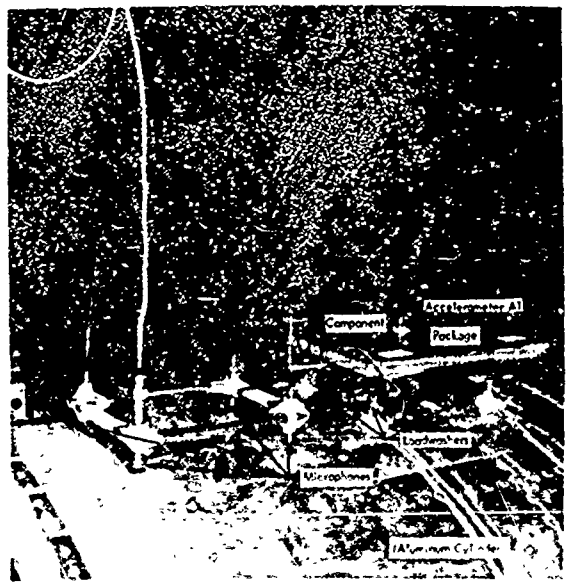

Figure 13. Measurement of Component Package Responses

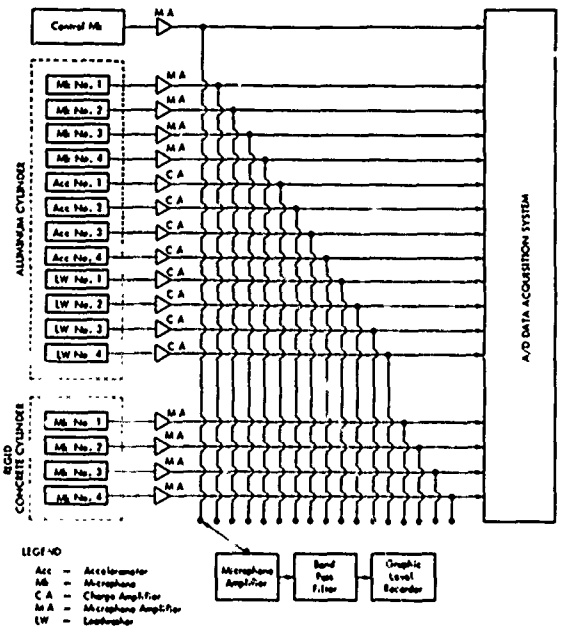

Figure 14. Instrumentation Block Diagram for Vibro—Acoustic Experiments

REDUCTION OF MEASURED DATA

The acquired data may be classified into two general categories: the sinesweep data; and the random data obtained from the vibro-acoustic tests. These data were subsequently analyzed to obtain: the component package impedance, support structure impedances, acoustic mobilities, blocked sound pressure spectra and the measured force spectra. The reduced data were stored on magnetic tapes and were used as "inputs" to compute the predicted force spectra.

The component impedance was obtained by dividing the total force acting on the component by the velocity response of the base plate (A2). The total force was obtained by summing the loadwasher responses. The component impedance plot is shown in Figure 15. The resonant frequencies of the component as seen from the shaker are located at 110 Hz and 1200 Hz. The latter frequency is the fundamental frequency of the 1/2 in. plate.

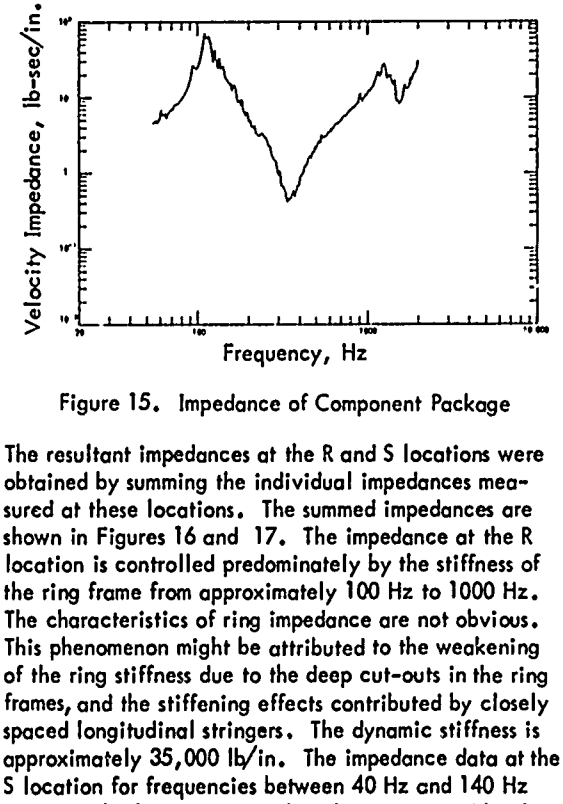

Figure 15. Impedance of Component Package

The resultant impedances at the R and S locations were obtained by summing the individual impedances measured at these locations. The summed impedances are shown in Figures 16 and 17. The impedance at the R location is controlled predominately by the stiffness of the ring frame from approximately 100 Hz to 1000 Hz. The characteristics of ring impedance are not obvious. This phenomenon might be attributed to the weakening of the ring stiffness due to the deep cut-outs in the ring frames, and the stiffening effects contributed by closely spaced longitudinal stringers. The dynamic stiffness is approximately 35,000 lb/in. The impedance data at the S location for frequencies between 40 Hz and 140 Hz appear to be low in magnitude; this was caused by the low acceleration outputs of the Z-13 head. The low-frequency stiffness (between 140 Hz and 500 Hz) is estimated as 10,000 lb/in. Major resonant and anti-resonant frequencies occur in the frequency range from 600 Hz to 1500 Hz. In general, data above 140 Hz appear to be valid.

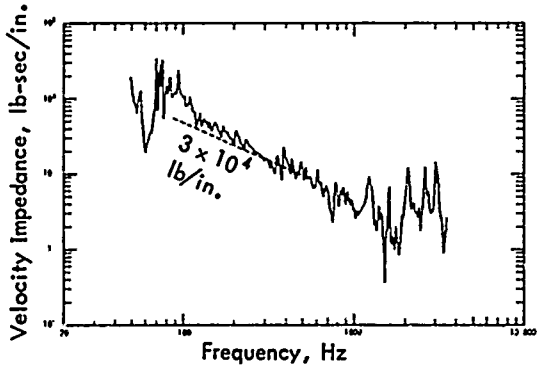

Figure 16. Summed Impedance at Location R

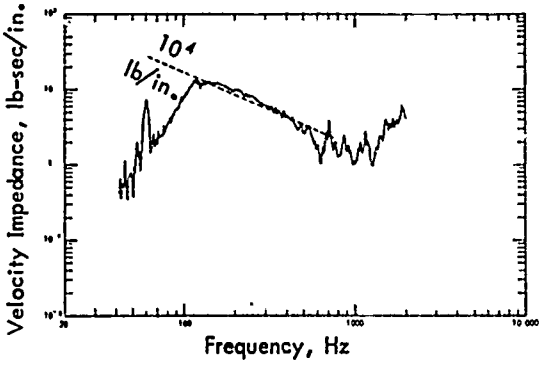

Figure 17. Summed Impedance at Location S

The analyzed results from the random data acquired during the vibro-acoustic tests are expressed in terms of the acoustic mobility data as shown in Figure 18 and the blocked pressure data as shown in Figure 19.

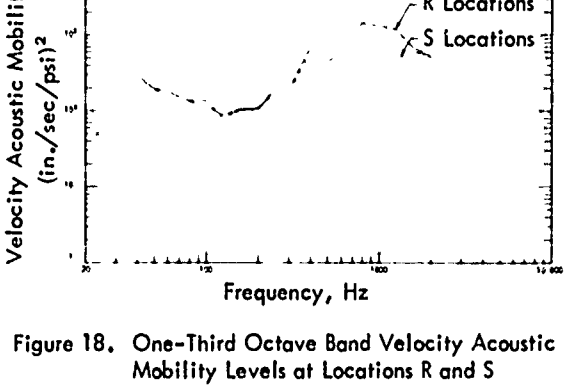

Figure 18. One-Third Octave Band Velocity Acoustic Mobility Levels at Locations R and S

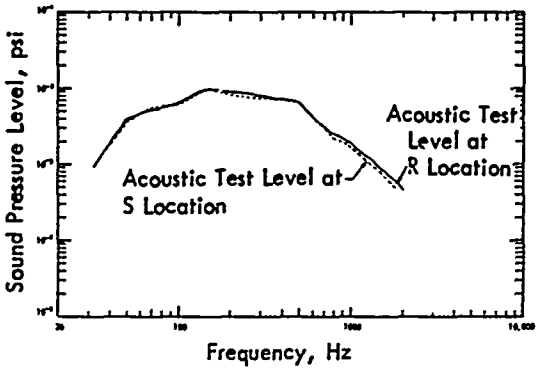

Figure 19. One-Third Octave Band Blocked Pressure Levels at R and S Locations

In general the frequency intervals at which results have been obtained from the mechanical impedance, blocked pressure, and acoustic mobility spectra are not the same. It was necessary, therefore, to convert the three spectra to the same frequency intervals by averaging and interpolating in each spectrum such that they were all reduced to identical frequency intervals determined by the widest interval of the three spectra at any point in the frequency range. Since the random data analysis was at constant bandwidth and the sinesweep data were collected on a variable frequency interval basis, the final frequency interval was determined by the random analysis at low frequencies and by the sine-sweep analysis in the upper part of the range.

DISCUSSION OF RESULTS

Based on the input data as described in the previous section, the force spectra were computed for the R and S locations. The computed results are presented in Figures 20 and 21, respectively. The measured force responses are also presented in the same figures for comparison. The rms values of these factors have been computed and are tabulated in Table I.

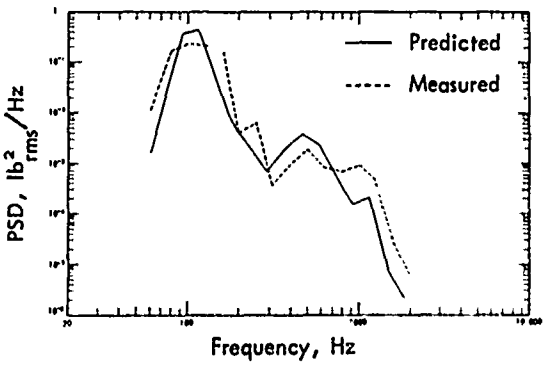

Figure 20. Comparison of Predicted and Measured Force Spectra (1/3 Octave PSD) at Location R: OASPL - 136 dB

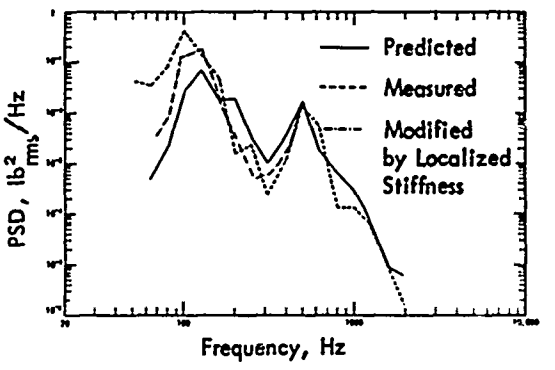

Figure 21. Comparison of Predicted and Measured Force Spectra (1/3 Octave PSD) at Location S: OASPL - 136 dB

TABLE I. Comparison of RMS Force Magnitudes

Equipment Mounting Location	Reference Acoustic Test Level dB *	RMS Force, Lb (50-2000 Hz)	
		Predicted	Measured
R	136	4.43	4.41
S	136	2.50 (4.40)†	4.26

* dB = Re 2×10^{-5} N/m^2

† Predicted force based on modified support-structure stiffness

Generally speaking, the force comparison at location R is considered quite satisfactory both in rms values and spectral characteristics. The comparison at the S location shows poor agreement for frequencies below 140 Hz. Such discrepancies are attributed to the errors incurred in the measurement of impedances of the support structure at the S locations.

The problems associated with impedance measurements originated from two main sources; namely, in the electronics of the impedance measurement equipment and the localized structural effects at measurement points. Based on the experience of the present program, the acceleration outputs from the Z-13 head appeared to be low at low frequencies. Consequently, it was found that impedance data measured at S locations are not valid below 140 Hz. The rocking and pitching motions generated by impedance heads during sinusoidal excitations would also affect the accuracy of the measured data.

The localized structural effects are attributed to the application of the dental cement in bonding impedance heads, or the mounting studs used to connect the component package to the support structure. Cement putties, depending on their sizes and the mixture ratios of the cement powder and its solvent, would tend to generate higher stiffnesses and increased modal masses at these points. Such effects would create higher stiffnesses. This is particularly true for very flexible structures, such as measurement locations at S.

At low frequencies, the increase in stiffnesses attributed to dental cement putties could be estimated by the following equation:

$$k_1 = k_2 \Big/ \left[\left(\frac{f_2}{f_1} \right)^2 - 1 \right] \qquad (3)$$

where

k_1 = localized stiffness

k_2 = stiffness of the component package (4760 lb/in.)

f_1 = resonant frequency of the component–support structure system

f_2 = resonant frequency of the component package (110 Hz)

The value of f_1 is estimated as 100 Hz from Figure 21. Thus the localized stiffness of the support structure is:

$$k_1 = \frac{4760}{0.21} = 2.27 \times 10^4 \text{ lb/in.}$$

The above value indicates an increase of stiffness which is 2.27 times greater than the originally measured value (10^4 lb/in.).

The predicted force spectrum, which is computed based on the modified stiffness, is plotted against the measured force in the frequency range of 50 Hz to 400 Hz. Significant improvements in amplitude accuracies have been achieved.

FORCE-CONTROL SHAKER TESTING EXPERIMENTS

The objective of the shaker testing was to determine the accuracy of the predicted forces as applied to the testing of component packages. The assessment of accuracies was based on the comparisons of component responses obtained in the vibro-acoustic tests with those obtained from shaker testing by controlling input forces through loadwashers. Instrumentation and testing equipment employed in the tests are illustrated by the block diagram as shown in Figure 22. The Ling Electronics Automatic Spectral Density Equalizer/Analyzer Model ASDE-80 was used to control the test system and to perform the following functions:

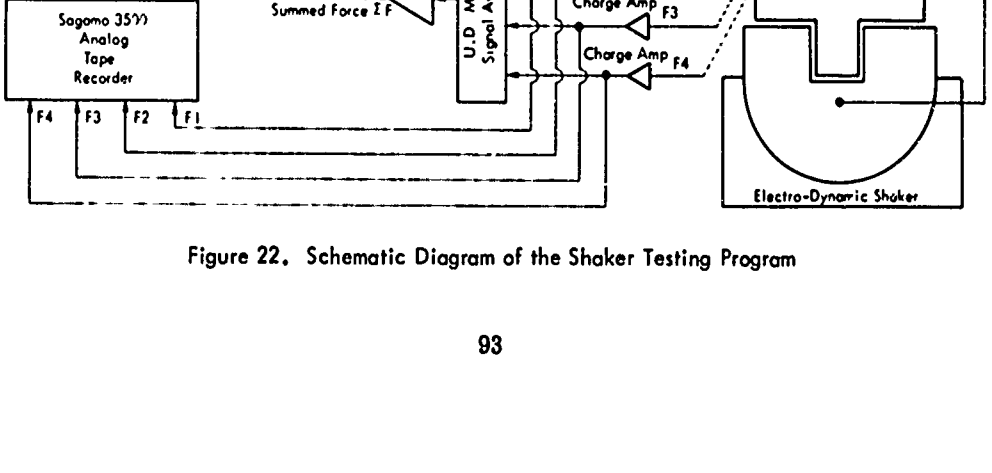

Figure 22. Schematic Diagram of the Shaker Testing Program

- To generate input force spectra for vibration tests;
- To measure the PSD of feedback signals from loadwashers on a continuous basis; and,
- To provide automatic control of the feedback PSD's by the use of automatic servos.

A control spectrum was shaped in the frequency range of 10 Hz to 2025 Hz by 85 separate servo control channels according to the specified bandwidths of the ASDE-80. The PSD's of the control forces were based on:

a) The predicted force spectra; and,

b) Loadwasher outputs obtained from vibro-acoustic tests.

The comparisons of the component package responses at locations R and S are presented in Figures 23 and 24, respectively. In the discussion of the response characteristics, the following terminologies are defined:

- Measured Response (MR) — Response measured from a vibro-acoustic test
- Test Response by Predicted Force (TRPF) — Response generated by predicted force spectra
- Test Response by Measured Force (TRMF) — Response generated by measured loadwasher outputs during a vibro-acoustic test.

In Figure 23, the MR correlates satisfactorily with the TRMF for frequencies below 300 Hz and between 800 Hz and 1200 Hz. The comparison between MR and TRPF show reasonably good agreements for frequencies below 200 Hz, but large discrepancies occur between 200 Hz and 1200 Hz. The increase in response amplitudes between 1200 and 2000 Hz was attributed to resonant vibrations of the base plates.

In Figure 24, the MR and TRMF are in satisfactory agreement for frequencies below 200 Hz and between 800 and 1200 Hz. The TRPF is in poor agreement with the MR below 800 Hz. This was certainly, in part, caused by the errors incurred in the predicted for force spectrum below 140 Hz. But, it correlated well for frequencies between 800 Hz and 1200 Hz. Large amplitude discrepancies between 1200 Hz and 2000 Hz were caused by resonant vibrations of the base plates.

The results of the force-control testing are not quite as encouraging as compared to that of the force spectra prediction. The possible causes for the large amplitude discrepancies in the component responses are presented as follows.

- Input Forces — The difference in the frequency-bandwidth resolutions between the narrow band PSD analysis (approximately

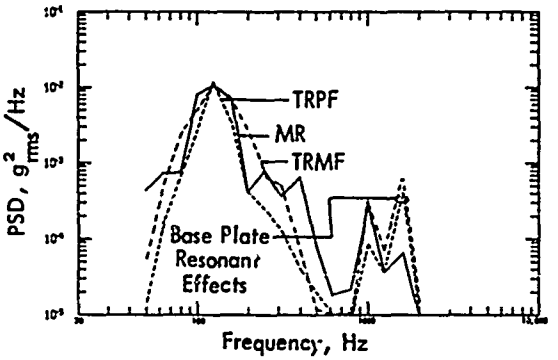

Figure 23. Comparison of Component Responses at R Location (1/3-Octave Frequency Band)

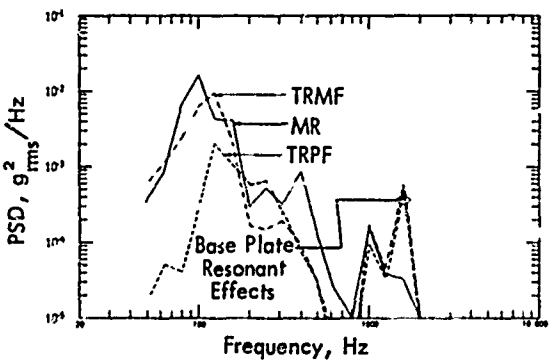

Figure 24. Comparison of Component Responses at S Location (1/3-Octave Frequency Band)

8 Hz) and the ASDE-80 (25 Hz) could change the input forcing characteristics, thereby creating different component responses.

- Dynamic Range of the Control System — The maximum dynamic range of the control system was estimated as 40 dB which, in many instances, was considered inadequate for controlling responses of high Q systems.
- Control Correction Time — The analog control system requires a minimum of 5 seconds to correct a 40-50 dB change. The correction time may have been too slow for the structural systems that were tested.

CONCLUSIONS

The following conclusions may be drawn from the results of the experimental program:

- The Force-Spectra equation can be used to predict interaction forces between support structures and component packages with reasonable accuracy provided that sound estimates can be made of:

- Input Impedance of Support Structure
- Input Impedance of Component Package
- Acoustic Mobility at Mounting Location
- Effective Acoustic Pressure on Support Structure

- The increase in localized stiffness at the component mounting locations due to the application of dental cement will significantly alter the characteristics of measured impedances. Therefore, it is important that input impedances of support structures should be determined as close to actual mounting conditions as possible.
- When corrections were made to account for stiffening effects due to localized supports, the predicted rms forces were found to be higher than the measured forces.
- Since the coupling effects between a component package and its supporting structure are included in the final vibration criteria, the effects of overtesting and undertesting on component packages can be avoided.
- Digital approaches to measure mechanical impedances and acoustic mobilities have been proved to be practical and feasible in providing dynamic information for the computation of dynamic environments.
- Improvements in mechanical impedance measurements are required to achieve desired measurement accuracies.
- The analog control system used in performing shaker testing lacked the needed dynamic ranges and correction time. This has caused poor agreement between component responses obtained from the shaker testing, and the vibro-acoustic testing.

  However, it is felt that response agreements could be improved if a digital control system were used. Current digital control systems can provide 60 dB dynamic range with a correction time of less than one second. Frequency resolutions from 4 Hz to 8 Hz are obtainable.

ACKNOWLEDGMENTS

This work was supported by National Aeronautics and Space Administration, Marshall Space Flight Center, under Contract No. NAS8-25811.

REFERENCES

1. Schock, R., "Utilization of Force-Spectra Technique for Dynamic Environmental Prediction and Test," To be published in Shock and Vibration Digest.

2. Kao, G., and Sutherland, L.C., "Development of Equivalent One-Dimensional Acoustic Force Spectra by Impedance Measurement Techniques," Wyle Laboratories Research Report WR 69-11, May 1969.

3. Jones, G., and On, F., "Prediction of Interface Random and Transient Vibratory Environments through the Use of Mechanical Impedance Concepts," The Shock and Vibration Bulletin No. 40, Part 3, pp. 79-88, December 1969.

4. Kana, D., "Response of a Cylindrical Shell to Random Acoustic Excitation," AIAA Journal Vol. 9, No. 3, pp. 425-431, March 1971.

5. Ballard, W.C., Casey, S.L., and Clausen, J. C., "Vibration Testing with Mechanical Impedance Methods," Sound and Vibration, pp. 10-21, January 1969.

6. On, F.J., "A Verification of the Practicality of Predicting Interface Dynamical Environments by Use of the Impedance Concept," The Shock and Vibration Bulletin No. 38, Part 2, pp. 249-260, August 1968.

7. Nuckolls, C.E., and Otts, J.V., "A Progress Report on Force Controlled Vibration Testing," The Shock and Vibration Bulletin No. 35, Part 2, pp. 117-130, January 1965.

8. Murfin, W.B., "Dual Specifications in Vibration Testing," The Shock and Vibration Bulletin No. 38, Part 1, pp. 109-113, August 1968.

9. Otts, J.V., "Force Controlled Vibration Tests: A Step Toward Practical Application of Mechanical Impedance, " The Shock and Vibration Bulletin No. 34, Part 5, pp. 45-52, February 1965.

10. Noiseux, D.J., and Meyer, E.B., "Applicability of Mechanical Admittance Techniques," The Shock and Vibration Bulletin No. 38, Part 2, pp. 231-238, August 1968.

11. Kao, G.C., "Prediction of Force Spectra by Mechanical Impedance and Acoustic Mobility Measurements Techniques," Wyle Laboratories Research Report WR 71-16, September 1971.

DISCUSSION

Mr. Shoulberg (General Electric): Are you proposing to average your force at the four input points?

Mr. Schock: Yes, the force spectra are averaged, but the total impedance is the summation of the impedances at the four input points.

DYNAMIC DESIGN ANALYSIS

VIA THE BUILDING BLOCK APPROACH

Albert L. Klosterman, Ph.D. and
Jason R. Lemon, Ph.D.
Structural Dynamics Research Corporation
Cincinnati, Ohio 45227

The availability of mechanical impedance testing equipment for determining the dynamic characteristics of structures has caused considerable interest in describing a complex component from test results. However, the direct use of digitized response data for highly resonant, multi-input/output components yields unsatisfactory results when used for further analytical total system investigations. This paper describes how the response data can be used to describe the component under test and the mathematical formulation necessary to represent the equations of motion of the total system. The procedures are then applied to large complex mechanical machinery to perform a total system dynamic design analysis.

INTRODUCTION

Several authors have attempted to use experimentally measured impedance data to represent various components in a total system dynamic analysis. [1, 2, 3, 4]. However, in cases where the component under test is highly resonant and has multiple connection points, the direct use of this response data is unsatisfactory [1,3]. Small errors in the measured data are unavoidable with any of the present or proposed test equipment. When these multi-input/output subsystems are included in the total system dynamic analysis, the errors will be greatly magnified whenever differences of nearly equal large quantities occur in the calculations. This work illustrates techniques which can be used to determine an analytical representation of the dynamic characteristics of a system from the response data so that the above mentioned errors are avoided. In particular, response data is used to set up a modified real or complex "modal" representation of the system under test. Although the modified modal representation is not completely general, it is convenient to manipulate and has been used satisfactorily to represent highly resonant components. These representations can then be combined with appropriate mathematical representations of other components to perform a total system dynamic analysis.

Reliable representation of components from dynamic test results allows for the complete implementation of a dynamic design analysis procedure which parallels the design process, where major structural components or substructures, are often designed or analyzed by different engineering groups or at different times. Therefore the design or analysis of each component could proceed as independently as possible with due consideration being given to the final coupling of substructures to form the complete structure. Groups which are designing the extremely complex components could rely on impedance test results while groups designing structurally simpler components could use analytical finite element investigations. The results of the dynamic analysis on each component can then be evaluated by the department with system responsibility to evaluate total system dynamic performance before the system is completely assembled. Therefore full implementation implies meaningful specifications on the dynamic performance of each component.

This procedure is also attractive because each component is represented in

terms of a reduced number of modal degrees of freedom. Therefore the degrees of freedom of the final mathematical model are significantly reduced with respect to the total physical degrees of freedom. This allows the development of a mathematical model which is flexible enough to predict the necessary phenomena under investigation, but small enough to be easily manipulated.

DETERMINATION OF DYNAMIC CHARACTERISTICS FROM RESPONSE DATA

In order to determine a modal representation of the dynamic characteristics, consider the equations of motion for steady state harmonic motion assuming the presence of hysteretic damping:

$$[M][\ddot{q}] + i\,[D][q] + [K][q] = [F]e^{i\beta t} \quad (1)$$

Normally the assumption of proportional damping is made where damping is assumed proportioned to stiffness and/or mass, in order to uncouple the equation of motion with modal coordinates. However, this assumption is not necessary if complex modes are used in the solution of the equations of motion [1]. To determine the steady state response due to sinusoidal excitation $[f]=[F]e^{i\beta t}$ seek a solution in the form $[q]=[Q]e^{i\beta t}$ to obtain:

$$\left[[K + i\,D] - \beta^2[M]\right]\,[Q] = [F] \quad (2)$$

Let $\beta^2 = \lambda$ and consider the homogeneous equation:

$$\left[[K + i\,D] - \lambda\,[M]\right]\,[Q] = [0] \quad (3)$$

This set of equations has a non-trival solution if

$$\det\,\left[[K + i\,D] - \lambda\,[M]\right] = 0 \quad (4)$$

There is a set of "n" complex eigenvalues λ_r and associated complex eigenvectors $[\pi^r]$ which satisfies this homogeneous equation:

$$[K + i\,D][\pi^r] - \lambda_r[M][\pi^r] = [0] \quad (5)$$

These complex modes depend on [K], [M] and [D] and differ from the real normal modes which depend only on [K] and [M]. Orthogonality of the above complex modes is easily shown and results in the following equations:

$$[\pi^r]^T[M][\pi^s] = [0] \quad \text{for } r \neq s$$

and

$$[\pi^r]^T\,[K + i\,D][\pi^s] = [0] \quad (6)$$

It can be easily shown [1] that the solution to the equations of motion can be written in terms of the complex modes as follows:

$$[Q] = \sum_{r=1}^{n} \frac{[\pi^r]^T[F][\pi^r]}{[\pi^r]^T[K + i\,D - \beta^2 M][\pi^r]} \quad (7)$$

or

$$[Q] = \sum_{r=1}^{n} \frac{[\pi^r]^T[F][\pi^r]}{m_r(\beta_r^2 - i\beta_r^2 g_r - \beta^2)} \quad (8)$$

where $[\pi^r]$ and m_r are complex modal parameters. The above modal parameters can be determined by various testing procedures and data analysis techniques. Some of the common methods are the following:

1) Use of multiple shakers
2) Least square curve fitting
3) Graphical curve fitting
4) Eigenvector search techniques

Reference [1] lists a fairly complete overview of the available techniques. Space does not permit a complete description of the above techniques here, however for completeness, one of the basic techniques will be reviewed.

The procedure is basicly similar to the method of Kennedy and Pancu [5], but extended to include complex modes [1]. A typical polar plot of the response of a highly resonant component is shown in Figure 1.

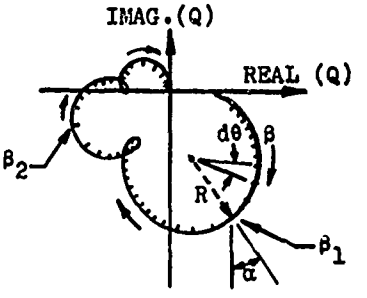

Figure 1 - Typical polar plot of a highly resonant system

It can be shown that each β_r is a frequency where the rate of change of the arc length with respect to frequency is a maximum. Once each of these frequencies is located, a circular arc can be fit to this portion of the curve and the value of

$$\left(\frac{d\beta^2}{d\theta}\right) \quad \text{at } \beta=\beta_r$$

can be determined. It can be shown that the value of g_r can then be determined from the following equation:

$$g_r = \frac{1}{\beta_r^2} \left(\frac{d \beta^2}{d \theta_r} \right) \text{ at } \beta = \beta_r \quad (9)$$

By constructing a normal to the curve at $\beta = \beta_r$ and recording the angle α, the components in the complex eigenvalue can be determined from the following equations:

$$\frac{\pi_j^r \pi_k^r}{m_r} = \beta_r^2 [U^r + i V^r] \quad (10)$$

where

$U^r = g_r 2R \cos \alpha$

$V^r = g_r 2R \sin \alpha$

R = the radius of curvature at $\beta = \beta_r$

(Note: m_r can be normalized to any value desired)

By a close examination of Equation (8) it is recognized that for a particular frequency range, the component can be adequately represented by the modes which are resonant in this range and the complex flexibility of the modes above the range of interest. Therefore, represent the dynamic flexibility equation $[Q] = [G(i\beta)][F]$ in the following form:

$$[Q] + [G^M(i\beta)][F] + [Z][F] \quad (11)$$

Where $[G^M(i\beta)]$ is determined from the resonant modes and [Z] is the complex flexibility of the higher modes of vibration. The complex flexibility matrix [Z] can be obtained by subtracting the modal response representation, determined by polar plots, from the total response data. e.g.

$$[Z][F] = [Q] - [G^M(i\beta)][F] \quad (12)$$

The best accuracy for this calculation is usually obtained at a frequency where

$G_{ij}^M F_j = 0$ (i.e. near anti-resonances in the modal response representation)

DETERMINING THE EQUATIONS OF MOTION OF THE TOTAL SYSTEM

The technique of setting up the equations of motion in terms of modal coordinates was pioneered by Hurty [6], but further advances have resulted in the practical implementation of the method for experimental data [1,7]. The method will be illustrated for zero damping, but is easily extended to damped system. Let the degrees of freedom at the points of connection to other components be designated by the vector [Q]. Then the motion of these points is related to the modal coordinates γ_r of the component by the equation:

$$[Q] = [\pi][\gamma] \quad (13)$$

The equation of motion for the generalized modal coordinate, γ_r is:

$$(-\beta^2 m_r + k_r) \gamma_r = [\pi_r]^T [F] \quad (14)$$

[F] is the vector of forces applied to the substructure and $[\pi_r]$ is the eigenvector abbreviated to include only the coordinates at the connection points, and those where additional external forces are applied.

In order to set up the mass and stiffness matrices for the entire assembly, Equations (13) and (14) can be implemented in the following manner. The equations of motion for the s^{th} component can be described in terms of modal coordinates as:

$$\left[[k^s] - \beta^2 [m^s] \right] [\gamma^s] = [\pi^s]^T [F^s] \quad (15)$$

where $[F^s]$ is the external forces applied to the s^{th} component. The uncoupled equations of motion for the total systems are:

$$\left[\begin{bmatrix} k^1 & & & \\ & k^2 & & \\ & & \ddots & \\ & & & k^n \end{bmatrix} - \beta^2 \begin{bmatrix} m^1 & & & \\ & m^2 & & \\ & & \ddots & \\ & & & m^n \end{bmatrix} \right] \begin{bmatrix} \gamma^1 \\ \gamma^2 \\ \vdots \\ \gamma^n \end{bmatrix} = \begin{bmatrix} [\pi^1]^T [F^1] \\ [\pi^2]^T [F^2] \\ \vdots \\ [\pi^n]^T [F^n] \end{bmatrix} \quad (16)$$

where

$$[Q^1] = [\pi^1][\gamma^1]$$
$$[Q^2] = [\pi^2][\gamma^2]$$
$$\vdots \qquad (17)$$
$$[Q^n] = [\pi^n][\gamma^n]$$

When the components are connected, constraint equations are necessary to relate the various physical coordinates [Q] at the connection points. Let these constraint equations be represented as:

$$[H]\begin{bmatrix} Q^1 \\ Q^2 \\ \vdots \\ Q^n \end{bmatrix} = [0] \qquad (18)$$

Substitute Equation (17) into Equation (18) to obtain:

$$[H]\begin{bmatrix} \pi^1 & & & \\ & \pi^2 & & \\ & & \ddots & \\ & & & \pi^n \end{bmatrix}\begin{bmatrix} \gamma^1 \\ \gamma^2 \\ \vdots \\ \gamma^n \end{bmatrix} = [0]$$

or

$$[C]\begin{bmatrix} \gamma^1 \\ \gamma^2 \\ \vdots \\ \gamma^n \end{bmatrix} = [0]$$

When the components are connected, the total degrees of freedom are reduced by the number of equations of constraint. Therefore, break the total degrees of freedom into independent $[\gamma_I]$ and dependent $[\gamma_D]$ coordinates.

$$[C_D \vdots C_I]\begin{bmatrix} \gamma_D \\ \gamma_I \end{bmatrix} = [0]$$

$$\therefore [C_D][\gamma_D] = -[C_I][\gamma_I]$$

$$[\gamma_D] = -[C_D]^{-1}[C_I][\gamma_I]$$

Therefore,

$$\begin{bmatrix} \gamma_D \\ \gamma_I \end{bmatrix} = \begin{bmatrix} -[C_D]^{-1}[C_I] \\ \hline I \end{bmatrix}[\gamma_I] \qquad (19)$$

Write Equation (19) as:

$$\begin{bmatrix} \gamma_D \\ \gamma_I \end{bmatrix} = [\sigma][\gamma_I]$$

where

$$[\sigma] = \begin{bmatrix} -[C_D]^{-1}[C_I] \\ \hline I \end{bmatrix}$$

Therefore, Equation (16) becomes:

$$\left[[\tilde{k}] - \beta^2[\tilde{m}]\right][\sigma][\gamma_I] = [\pi]^T[F]$$

or

$$\left[[\sigma]^T[\tilde{k}][\sigma] - \beta^2[\sigma]^T[\tilde{m}][\sigma]\right][\gamma_I] = [\sigma]^T[\pi]^T[F] \qquad (20)$$

This set of equations can then be solved to determine the natural frequencies, mode shapes, frequency response, etc.

The basic approach taken with the previous technique is to approximate a continuous system which has a infinite number of modes by a system which has a finite number of modes. Use of a smaller number of modes to represent a dynamical system always results in a loss of mass, a loss of flexibility, or both. Through practical experience, it has been observed that frequently the flexibility of component modes outside the frequency range of interest are important in the overall simulation, whereas the inertial properties are not. Therefore the following technique has been devised to include the flexibility of a higher modes without including the inertial properties.

The sinusoidal response of a particular component can be represented in modified dynamic flexibility form as:

$$[Q_c] = [\pi][\gamma] + [Z][F_c] \qquad (21)$$

where

$[Z]$ is the residual flexibility of the modes of vibration not included in the modal coordinates $[\gamma]$.

$[F_c]$ is forces at the connection points.

Also the following relationship exists between forces on modal coordinates and forces applied at the connection points.

$$[F_\gamma] = -[\pi]^T[F_c] \tag{22}$$

Multiply Equation (21) through by $[Z]^{-1}$ to obtain:

$$[F_c] = [Z]^{-1}[Q_c] - [Z]^{-1}[\pi][\gamma] \tag{23}$$

Substitute Equation (23) into Equation (22) to obtain:

$$[F_\gamma] = -[\pi]^T[Z]^{-1}[Q_c] + [\pi]^T[Z]^{-1}[\pi][\gamma] \tag{24}$$

Hence, Equations (23) and (24) become:

$$\begin{bmatrix} F_\gamma \\ F_c \end{bmatrix} = \begin{bmatrix} \pi^T Z^{-1} \pi & -\pi^T Z^{-1} \\ -Z^{-1}\pi & Z^{-1} \end{bmatrix} \begin{bmatrix} \gamma \\ Q_c \end{bmatrix} \tag{25}$$

Equation (25) represents the stiffness matrix form of an additional element which can be included in the mathematical model in order to represent the residual flexibility of a particular component. The inclusion of this element into the mathematical model has significantly improved the simulation for numerous practical cases. In some of the more critical cases the inclusion of residual flexibility has meant the difference between excellent correlation and no correlation. Therefore, either a large number of modes should be included to account for all important flexibilities, or residual flexibility should be added to approximate the effects of the omitted higher modes.

The above technique was illustrated for the case where the modes were determined from a free-free excitation test (i.e. the connection points were unrestrained). Procedures have also been developed and will be published at a later time for using the modal properties generated from excitation tests where some or all of the connection points are restrained during testing. In some cases this technique is attractive for the following reasons:

1) The free-free zero frequency modes which are sometimes difficult to determine, are eliminated.

2) A fewer number of modes are needed to obtain an adequate representation if the component is tested in a manner similar to the state in which it will be mounted in the entire assembly.

However, to determine all the necessary parameters from the experimental test, when the component is restrained, a sophisticated mounting system is required which will monitor the forces at the connection points which are restrained. In the case where constrained modes are used to represent a particular component it can be shown that the residual mass of the constrained coordinates also has a rather significant effect on the system simulation.

APPLICATION - LARGE MOTOR SIMULATION

In order to evaluate the use of this approach to studying the dynamic characteristics of complex mechanical machinery, SDRC and U.S. Steel Marketing undertook an analysis of a 1750 HP electric motor. An overall view of the motor is shown in Figure 2.

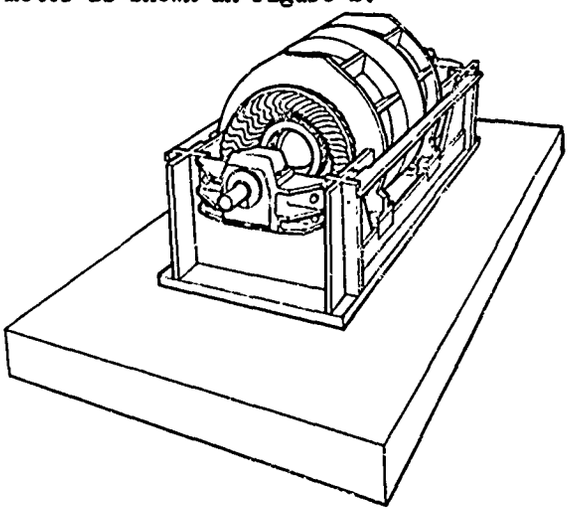

Fig. 2 - 1750 HP Electric Motor Foundation System Which Was Analyzed.

The system was divided into the following components which are shown in Figure 3.

1) Motor Base
2) Rotor
3) Fluid Film Bearings
4) Stator
5) Foundation

The motor base and rotor were modeled with finite element techniques and their individual modal characteristics determined. The other components were tested to determine their respective character-

istics.

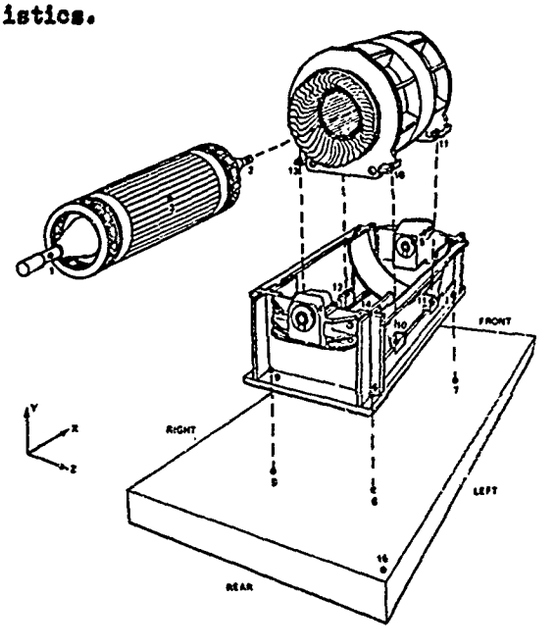

Fig. 3 - Components Selected for the Dynamic Design Analysis.

The motor base was represented with 6 rigid body zero frequency modes, 7 flexural modes and the residual flexibility of all other modes. Correlation between the computer model and the test results on the base alone are shown in Figure 4.

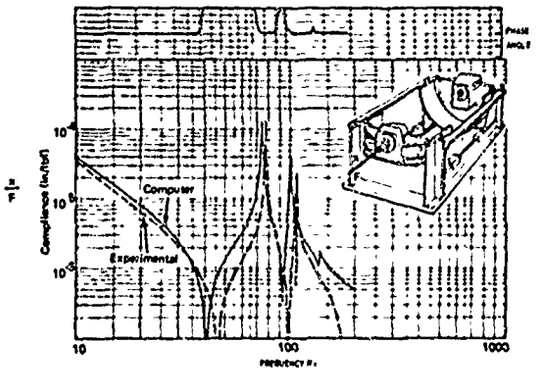

Fig. 4 - Typical Free-Free Base Frequency Response.

The rotor was represented with 6 rigid body zero frequency modes and 3 flexural modes. The correlation between the computer model and test results for the rotor are shown in Figure 5.

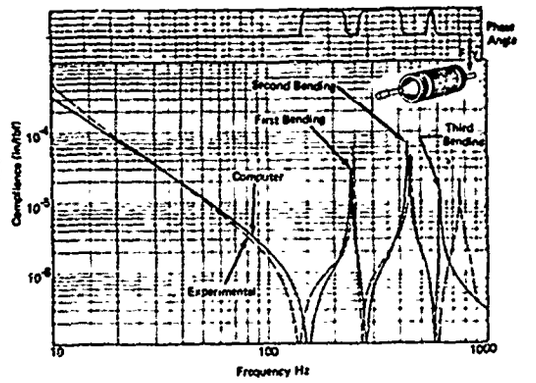

Fig. 5 - Typical Free-Free Rotor Frequency Response.

The fluid film bearings were tested and represented by a simple spring-dashpot model. The comparison of a typical analytical model to test results are shown in Figure 6.

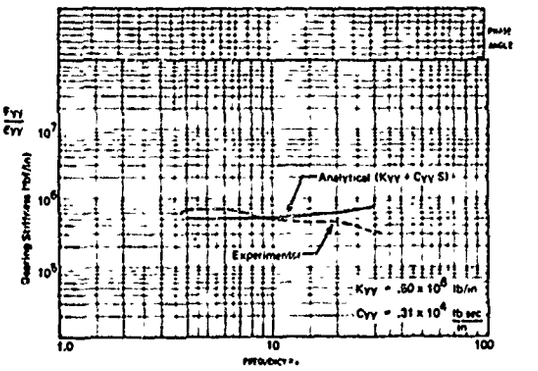

Fig. 6 - Typical Bearing Frequency Response.

The stator was tested and represented with 6 rigid body zero frequency modes and the residual flexibility of all other modes. The comparison of the test data to the analytical representation for a typical plot is shown in Figure 7.

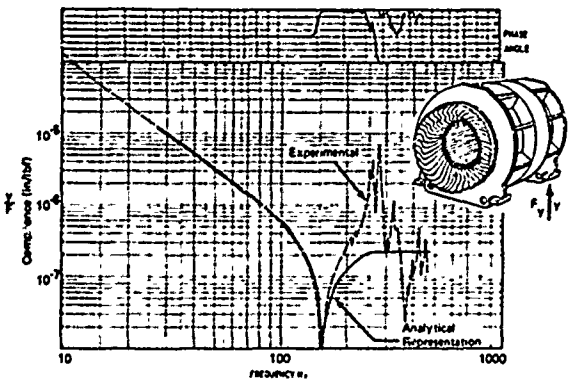

Fig. 7 - Typical Free-Free Stator Frequency Response.

The foundation was tested and represented by 6 rigid body zero frequency modes and 6 flexural modes. The comparison of the test data to the analytical representation is shown in Figure 8.

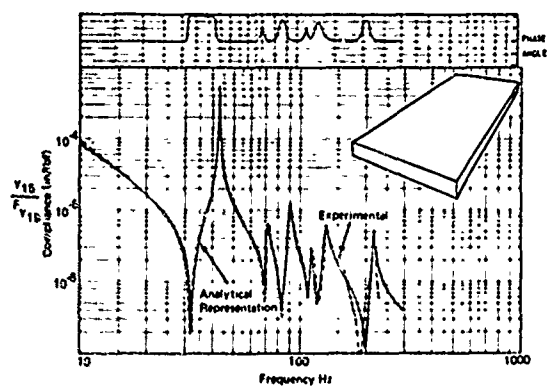

Fig. 8 - Typical Free-Free Foundation Frequency Response

Since a relatively crude model was used for the stator, it is worthwhile to combine this component with the motor base to see if meaningful results can be obtained with just these two components. The forces assumed at the connection points for the motor base and stator model are shown in Figure 9. The test results of the motor base and stator combination are compared to the component mode model in Figures 10 and 11.

The total system was then assembled mathematically and the forces assumed at the connection points are shown in Figure 12. The total system response is compared to the computer predicted response in Figures 13 and 14.

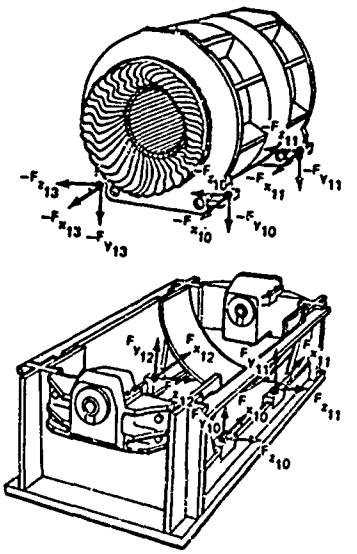

Fig. 9 - Stator and Base Free Body Diagram showing forces at the connection points.

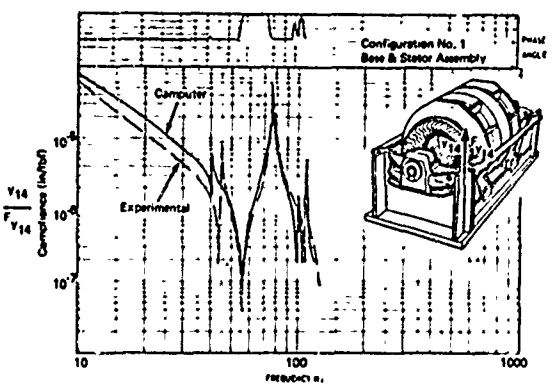

Fig. 10 - Predicted and Measured Frequency Response of Base-Stator Assembly.

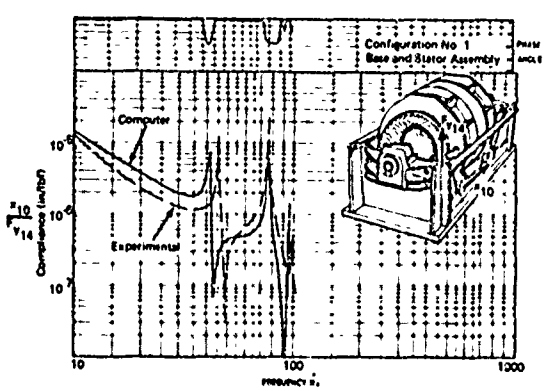

Fig. 11 - Predicted and Measured Frequency Response of Base-Stator Assembly.

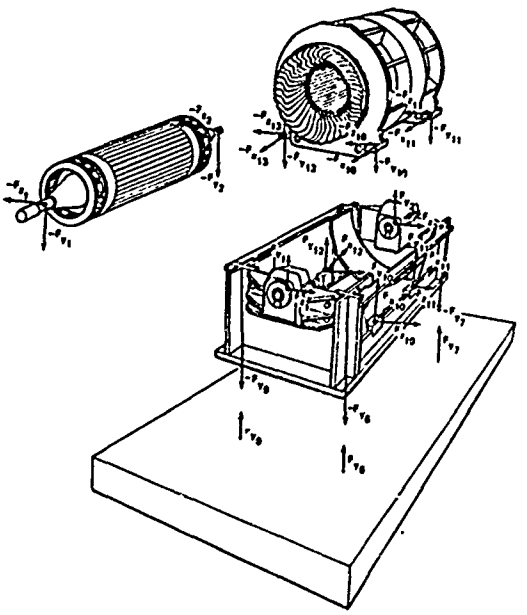

Fig. 12 - Base, Stator, Rotor and Foundation Free Body Diagram

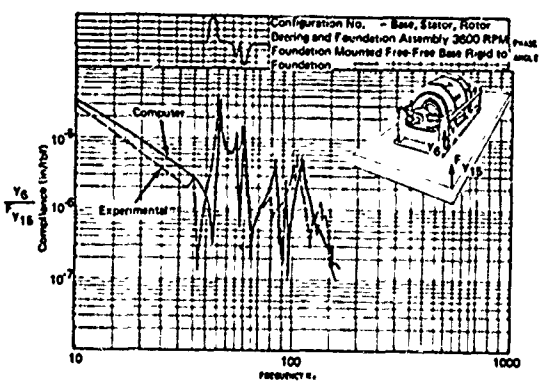

Fig. 13 - Predicted and Measured Frequency Response of Base, Stator, Rotor and Foundation System.

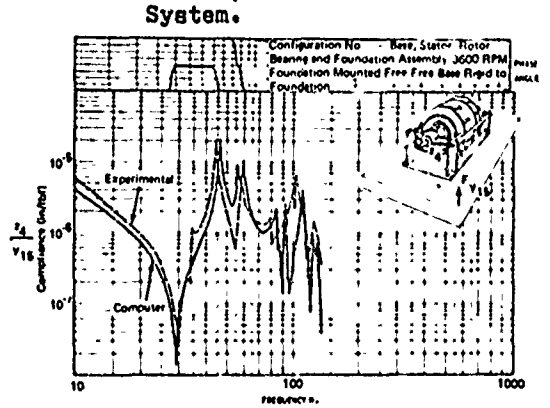

Fig. 14 - Predicted and Measured Frequency Response of Base, Stator, Rotor and Foundation System.

CONCLUSIONS

The use of a modified modal representation has been shown to be an adequate representation of the dynamic characteristics of each component for performing a total system dynamic analysis. The modified modal representation can be determined from either test data or an analytical investigation. Reliable representations determined from test results allows for the complete implementation of a "building block approach to dynamic analysis" which is extremely attractive since it is practically feasible for large complex systems and parallels the substructuring design process.

REFERENCES

[1] Klosterman, A.L. - "On the Experimental Determination and Use of Modal Representations of Dynamic Characteristics", Ph.D. Dissertation, University of Cincinnati 1971.

[2] Klosterman, A.L. & Lemon, J.R. - "Building Block Approach to Structural Dynamics", ASME Publication, 1969 VIBR - 30.

[3] Wright, D.V. - "Sound Radiation and the Force Ratios of Foundation Structures", Paper presented at Ship Silencing Symposium, Groton, Conn. May 21, 1963, Page 1015.

[4] Ballard, W.C., Casey, S.L. & Clausen, J.D. - "Vibration Testing with Mechanical Impedance Methods", Sound and Vibrations, January 1969.

[5] Kennedy & Pancu - "Use of Vectors in Vibration Measurement and Analysis", Journal of Aeronautical Sciences, Vol. 14, No. 11 November 1947.

[6] Hurty, Walter - "Dynamic Analysis of Structural Systems Using Component Modes," AIAA Journal, Volume 3, No. 4 April 1965.

[7] MacNeal, R.H.(ed) - "The Nastran Theoretical Manual", NASA SP-221, September, 1970.

MOBILITY MEASUREMENTS FOR THE VIBRATION ANALYSIS OF CONNECTED STRUCTURES

D.J. Ewins and M.G. Sainsbury
Imperial College of Science and Technology,
London, England

The mobility or impedance coupling technique is widely used for the vibration analysis of structures which comprise an assembly of connected components. Its application is straightforward when the components are amenable to theoretical analysis, but if certain components are too complex to be analysed their mobilities must be obtained experimentally. Standard 'impedance' testing methods are generally inadequate for measuring the required multidirectional mobility data, and the work described in this paper is an attempt to develop techniques for obtaining such data. Measurements have been made on a freely supported beam and on a resiliently mounted block, and these data have been used to predict the response of the system formed by bolting the beam and the block together. The results illustrate the importance of obtaining sufficiently complete and accurate data if mobility measurements are to be used for the vibration analysis of connected structures.

INTRODUCTION

Vibration analysis of complex structures which comprise an assembly of connected components is often made using the mobility or impedance coupling technique. This approach permits analysis of each component individually and then couples them together by matching forces and velocities at each connection point, which is considerably more convenient than attempting to analyse the complete structure at once. It is in fact a standard technique in dynamic analysis. However, it often happens that one (or more) of the components is itself too complex to be analysed directly and for such a case, recourse may be made to an experimental approach in order to obtain the mobility data which is required for the analysis of the complete assembly. This paper is concerned with the development of experimental techniques suitable for measuring this data.

When the mobility coupling technique is applied analytically, it is customary to consider as many co-ordinates at each connection point as are necessary to realistically describe the conditions at that junction. The motion of a point on a structure is completely defined by six co-ordinates, three translational and three rotational, but in the analysis of specific cases it is often possible to ignore some of these by virtue of the symmetry of the structure. In the simplest case where motion is known to occur in a single direction, such as a mass moving in a straight line, then only one co-ordinate is required. In practice, this degree of symmetry is seldom encountered, especially with the complex engineering structures that we are considering, so vibration analysis using a single co-ordinate is usually unrealistic. However, in many practical cases, motion is confined to a single plane involving vibration in three directions - two translation and one rotation - and for these it is necessary and sufficient to include three of the six co-ordinates in the analysis of vibration.

Such considerations are made regularly in theoretical vibration analysis

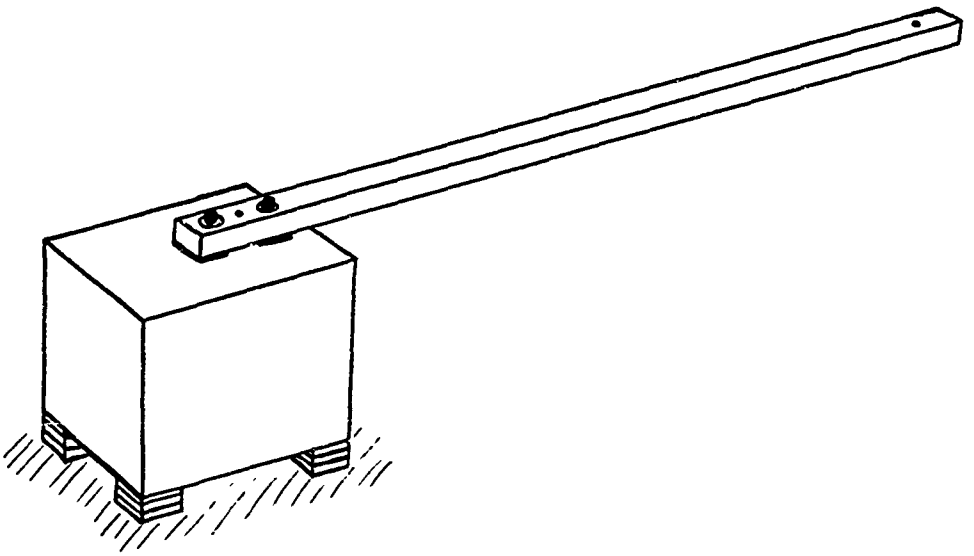

Fig. 1 BLOCK AND BEAM ASSEMBLY

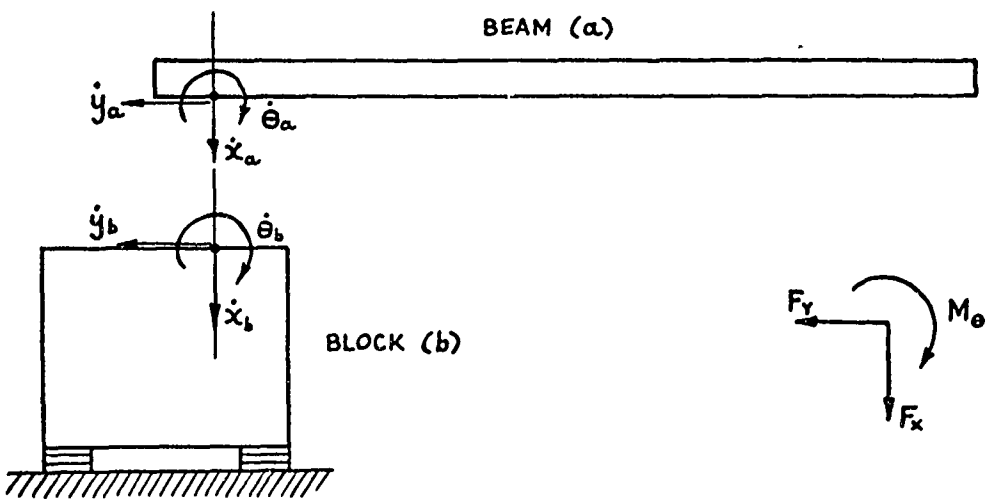

Fig. 2 CO-ORDINATES FOR COUPLING BEAM AND BLOCK

but are seldom included in those exercises which make use of experimental data for one of the components. Standard 'impedance' testing techniques are confined to measuring mobility in a single direction and are generally inadequate for the acquisition of such complete data as are required for a realistic analysis of a complex structure. This limitation has been identified already [1], [2] and previous work has demonstrated the difficulty and extent of the task of measuring the complete 6 x 6 mobility matrix for a structure [2]. However, as mentioned above, many practical structures do have a certain degree of symmetry and this permits us to confine our attention to motion in one plane and to consider only three co-ordinates at a time. The mobility data required in this case constitutes a 3 x 3 matrix which is considerably easier to handle than the complete 6 x 6 matrix.

This paper describes a case study made to assess the feasibility of using experimental data to analyse connected components and employs a particular structure composed of two components as an example. The first stage was to specify those mobility data which are required in order to analyse the vibrations of the assembled structure. Next, an experimental technique was developed for obtaining these data to the required accuracy. Finally, predictions of the dynamic characteristics of the assembled structure based on measurements of the individual components were compared with measurements made on the structure itself.

CASE STUDY

The structure treated in this study comprised two simple components. The first was a solid steel block 9" x 9" x 12" resting on four identical rubber pads, one under each corner, while the second was a uniform rectangular steel beam 1½" x 2" x 72". The assembled structure was formed by attaching the beam to the block in such a way as to obtain symmetry in one vertical plane but not in the other, as shown in Figure 1. Interest was confined to vibrations in the vertical plane containing the longitudinal axis of the beam, although a similar analysis could be made for motion in the other planes.

THEORETICAL APPROACH

In order to predict theoretically the vibration properties of the assembly formed by these two components, use is made of the mobility coupling technique. By considering each of the components individually, we may derive mobility expressions for each of these which relate the velocities at the point of connection to forces and couples applied at that point. This data may be presented generally by the matrix equation:

$$\{\dot{X}\} = [Y]\{F\} \quad \text{or} \quad \{F\} = [Z]\{\dot{X}\} \qquad (1)$$

where $[Y]$ is the mobility matrix and $[Z] = [Y]^{-1}$ is the impedance matrix for that point on the structure, $\{\dot{X}\}$ is a vector of velocities in the co-ordinate directions included and $\{F\}$ is the vector of forces (or couples) in those directions. These matrices and vectors, and all those which follow, have complex elements in order to describe both the amplitude and the phase of the various quantities represented.

Equations for two components (a and b) connected together may be related by virtue of the fact that at the connection point their respective velocities must be identical, so that

$$\{\dot{X}_a\} = \{\dot{X}_b\} = \{\dot{X}\} \qquad (2)$$

Furthermore, by considering equilibrium at the point of connection,

$$\{F_a\} + \{F_b\} = \{P\} \qquad (3)$$

where $\{P\}$ is an externally applied force.
Combination of equations (2) and (3) leads to an expression for the mobility of the combined structure at the connection point $[Y_c]$:

$$[Y_c] = \left([Y_a]^{-1} + [Y_b]^{-1}\right)^{-1} \qquad (4)$$

As mentioned earlier, as many as six co-ordinates may be necessary to define the motion of a point on a structure (in which case the order of these matrices and vectors would be 6), but in this case, as in many others, we may limit our interests to a limited number of these. Figure 2 shows the connection point for each component and indicates those co-ordinates and forces which should be included. Because of the symmetry of the structure, the other three co-ordinates (which include

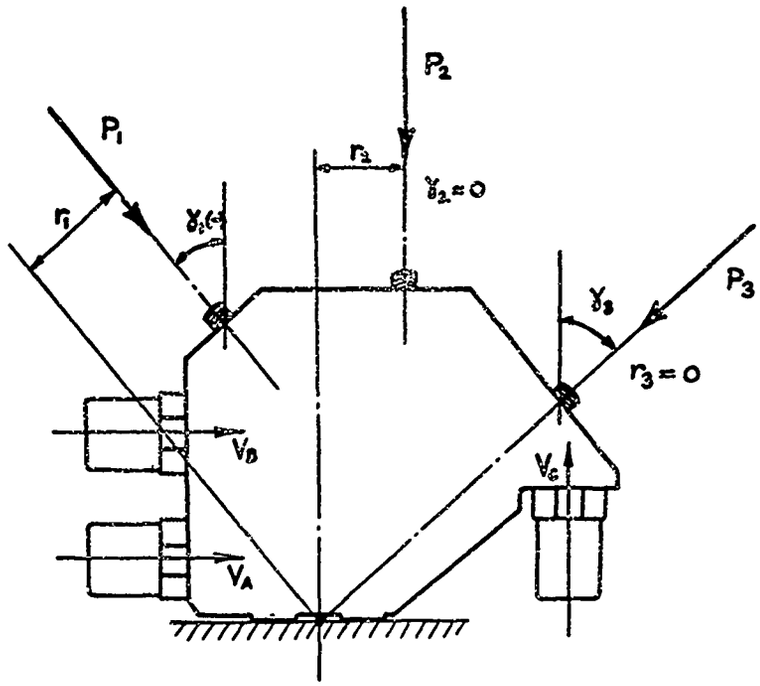

FIG. 3(a) EXCITING BLOCK MK 1 (Not to Scale)

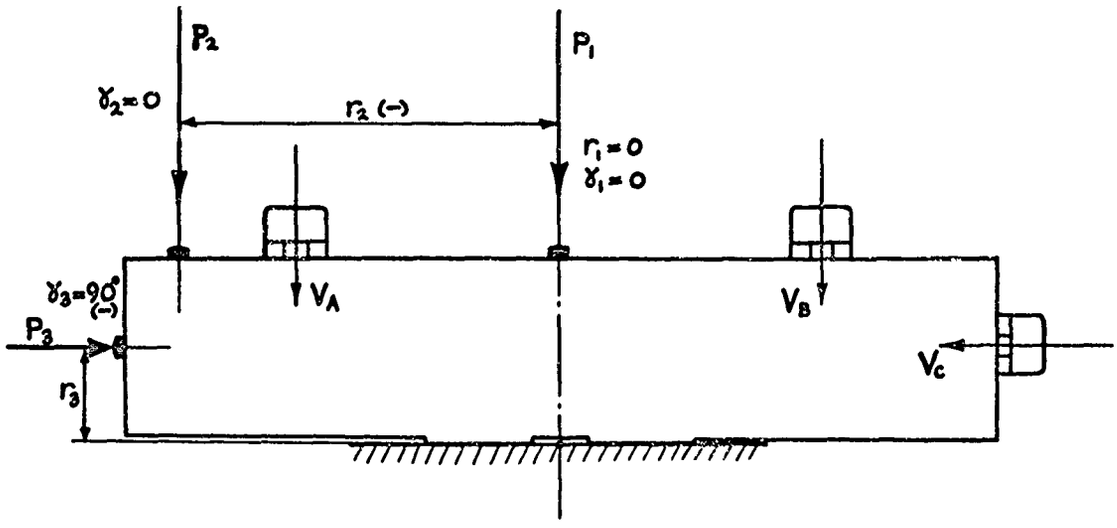

FIG. 3(b) EXCITING BLOCK MK 2 (Not to Scale)

motion out of the plane of the paper) may be ignored in this analysis or, if required, treated separately. Thus the equations defining the mobility matrix above (1) are in this case:

$$\begin{Bmatrix} \dot{x} \\ \dot{y} \\ \dot{\theta} \end{Bmatrix} = \begin{bmatrix} Y_{xx} & Y_{xy} & Y_{x\theta} \\ Y_{yx} & Y_{yy} & Y_{y\theta} \\ Y_{\theta x} & Y_{\theta y} & Y_{\theta\theta} \end{bmatrix} \begin{Bmatrix} F_x \\ F_y \\ M_\theta \end{Bmatrix} \qquad (5)$$

The object of this analysis is to predict the vibration characteristics of the complete assembly formed by the two components, and this information is contained in the assembly mobility, $[Y_c]$. It will be seen from equation (4) that this technique involves a number of matrix inversions and these can be the source of some difficulty in numerical applications. In the first instance, the component mobility matrices $[Y_a]$ and $[Y_b]$ become ill-conditioned and are difficult to invert at frequencies close to one of their respective natural frequencies. A similar limitation applies to the combined expression $([Y_a]^{-1} + [Y_b]^{-1})$ which also has to be inverted. Secondly, it is known that operations involving the mobility matrices can be sensitive to small errors in the individual mobility expressions, and this feature must be taken into account when experimental data is to be incorporated.

Theoretical expressions for the component mobility matrices were derived by standard methods [3], although it was necessary to use experimentally derived data for the dynamic stiffness and damping capacity of the rubber pads which support the steel block. Calculations were made using these expressions and the results are presented later in the paper. A further series of calculations were made to predict the mobility of the assembled structure, again using the mobility coupling technique, and these will also be presented and discussed later, together with corresponding results from the experimental approach.

EXPERIMENTAL APPROACH

We shall now consider a situation in which mobility data for the individual components are to be determined solely from experimental measurements, as opposed to theoretical analysis. This is a matter of necessity when dealing with particularly complex structures.

In exactly the same way that it was considered necessary to include three co-ordinates in the theoretical approach, so it is necessary to include all three in an approach using experimental data. The requirement for such comprehensive data may not be met using conventional methods of measuring mobility (collectively referred to as 'impedance tests') as these are insufficiently developed to provide either the completeness or the accuracy demanded for this application. In all but very exceptional cases, mobility measurements are confined to those expressions which relate response to a translational force in a direction normal to the surface of the structure under test. The response to applied couples or in-plane forces is not generally measured so that the mobility matrices required here may not be obtained directly from current experimental methods.

One previous worker has attempted to measure the complete mobility matrix and has developed a twin shaker unit to apply either a direct force (with the two shakers in phase) or a couple (with them in antiphase) to the structure [2]. An alternative solution to the problem of rotational excitation is being explored in the design of a torsional electromagnetic shaker, but this is at an early stage of development. A third approach is provided by the technique described in this paper which is based upon the use of a single shaker and other standard impedance testing equipment with the minimum of specially designed attachments. The aim of this measurement technique is to determine the 3 x 3 structural mobility matrix described above in relation to the case study which is used here as an example, and is achieved in the following way.

There are nine elements of the mobility matrix to be determined and these are obtained by measuring the three responses ($\dot{x}$, $\dot{y}$ and $\dot{\theta}$) to each of three different excitation conditions. Thus three tests over the chosen frequency range are required and in each of these the shaker is attached so that a different combination of the three reference forces (F_x, F_y and M_θ) is applied to the structure. Knowing these specific combinations, it is then possible to extract the responses to each of these forces individually and thus derive the required mobility matrix. Details of the specific shaker attachment arrangements used are discussed in the next section.

It is clear that whatever technique is employed to measure this mobility data, there is a vast quantity of

information to be handled. Essentially, all that is required from the exercise is a prediction of the vibration properties of the assembled structure and all the mobility measurements made on the separate components are of no inherent interest beyond that of enabling the calculation of the assembly properties. The mobility coupling process (i.e. application of equation (4)) is applied at each of a number of discrete frequencies using the component data measured at those frequencies. Thus it is convenient if such data are in a digital format rather than analogue (i.e. in the form of graphs). Since there is considerably more of this intermediate data than is eventually required to describe the assembly properties, it is most conveniently acquired and stored in digital form, either on punched tape or in the memory of a digital computer which is subsequently employed to carry out the matrix manipulations for extracting the required information. This requirement indicates the suitability of the digital transfer function analysers currently available which may be readily interfaced with a small digital computer to provide an automatic testing facility.

MEASUREMENT TECHNIQUE

Based upon the concept of a single shaker technique for measuring multidirectional mobility data, a number of specific configurations for attaching the shaker were investigated. It was necessary in all of these to attach an 'exciting block' to the point of interest on the structure and to connect the shaker to this block in different ways so as to exert the chosen excitation conditions to the structure. The first design for this block is illustrated in Figure 3(a). The shaker was attached to the block in each of the directions indicated by P_1, P_2 and P_3 in turn, and the corresponding components of the excitations in the three directions (F_x, F_y and M_θ) are given by the matrix equation:

$$\begin{Bmatrix} F_x \\ F_y \\ M_\theta \end{Bmatrix}_i = \begin{Bmatrix} \cos\gamma_i \\ \sin\gamma_i \\ r_i \end{Bmatrix} P_i \quad \text{or} \quad \{F\}_i = \{\Gamma\}_i P_i \qquad i=1,2,3 \tag{6}$$

For each shaker position, measurements were made at specific frequencies of the input force and the three responses, and from the collected results of all three runs the required mobility expressions could be derived as follows. The response was measured at three convenient stations on the block and by assuming the block to be rigid, these could be related to the response of the structure itself in the three reference directions by means of a simple geometric transformation:

$$\begin{Bmatrix} \dot{x} \\ \dot{y} \\ \dot{\theta} \end{Bmatrix} = [T] \begin{Bmatrix} V_A \\ V_B \\ V_C \end{Bmatrix} \quad \text{or} \quad \{\dot{X}\} = [T]\{V\} \tag{7}$$

For each excitation position, we may write

$$\{\dot{X}\}_i = [T]\{V\}_i = [Y]\{F\}_i$$
$$\therefore \{\dot{X}\}_i = [Y]\{\Gamma\}_i P_i \tag{8}$$

or

$$[T]\frac{1}{P_i}\{V\}_i = [Y]\{\Gamma\}_i$$
$$\therefore [T]\{Y_{app}\}_i = [Y]\{\Gamma\}_i \tag{9}$$

where $\{Y_{app}\}_i$ is a vector of apparent mobilities and $\{\Gamma\}_i$ is the force transformation vector for the i^{th} excitation position. Combining the three equations for i = 1, 2, 3 gives

$$[T][Y_{app}] = [Y][\Gamma]$$

or

$$[Y] = [T][Y_{app}][\Gamma]^{-1} \tag{10}$$

relating the measured quantities with the required properties.

The first stage in assessing the suitability of the proposed exciting block design was a check on the sensitivity of the numerical manipulation described by equation (10) to realistic errors in the measured data. This was performed numerically by taking a specific mobility matrix for the structure, computing the apparent mobilities that would be observed in the three runs with the exciting block, polluting this data with random or systematic errors typical of those which might be expected from the experimental equipment used and then recomputing the structure mobility with this polluted data. It was soon found from this exercise that the exciting block shown in Figure 3(a) would not be suitable for obtaining the required mobility data because errors in measured quantities of the order to 0.01% in amplitude and 0.01° in phase were sufficient to generate large errors in the computed mobilities (in excess of 5 dB). Accordingly, alternative designs for the exciting block were investigated and the one finally adopted for all the tests reported here is shown in Figure 3(b). This has a

simpler transformation to the reference co-ordinates and the checks on error sensitivity described above indicated that a measurement accuracy of 1% in amplitude and 1° in phase was usually sufficient to maintain an accuracy of better than 1 dB in the mobility of the structure computed from equation (10).

In addition to the basic force transformation from the shaker positions to the reference co-ordinates, it was also considered necessary to allow for the presence of the exciting block and the transducers mounted on it between the force measuring transducer and the structure. By assuming the block to behave as a rigid mass, it is possible to incorporate this correction in the transformations described above and the complete equation relating measured and required data then becomes:

$$[Y] = [T][Y_{app}]\left([\Gamma] - j\omega[M][T][Y_{app}]\right)^{-1} \quad (11)$$

where [M] is an inertia matrix for the specific exciting block.

Consideration of mobilities in more than one direction leads to an appreciation of some of the limitations of conventional impedance testing. In particular, it is noted that if a structure is not symmetrical, or is not excited through its mass centre, there will often be a significant response in directions other than that in which the forcing is being applied. If this effect is not properly allowed for, erroneous results can easily be obtained. For example, in measuring the mobility at the end of a simple cantilever beam it is found that there is a significant rotational response to an applied transverse force. In most cases, the shaker and its connection are not completely free to accommodate this rotation and as a result, they impose a restraint on it. This is equivalent to applying a couple to the end of the beam in addition to the intended force. This couple is not measured, but the response which is measured is the sum of that generated by the force and the couple and is not the information which is sought. In order to overcome this difficulty, it is generally sufficient to incorporate a 'decoupling rod' between the shaker and the structure which has a low stiffness in all directions other than that in which it is desired to apply excitation [4] and accordingly, this has been adopted as standard practice in all tests of the current study. A series of measurements were made to indicate the importance of using such a device. The results are given in Figure 4 which shows measurements of the response of the steel block using a range of decoupling rods and clearly demonstrates the limitations of a direct connection between the shaker and the structure.

In order to measure and process the data required in this exercise, a digital transfer function analyser (DTFA) was used in conjunction with a small digital computer to form an integrated system, described in reference [5]. Measurements were made at discrete frequencies in a chosen range (as opposed to a continuous sweep through that range) and the computer was programmed to select these frequencies, control the DTFA while it measured each of the transducer outputs in turn, and then store or output these results for subsequent processing. The amount of information which has to be acquired in order to derive the required mobility is considerably in excess of the actual data to be determined for the assembled structure. In order to compute the amplitude and phase of one mobility expression for the complete assembly, it is necessary to measure a total of 24 quantities on the components. Thus, while the information sought may be handled or presented in the form of a graph, the same is not true of the intermediate data and because of this it was decided that the automatic data handling facility was an essential feature of this measuring technique.

RESULTS

The measurements which were made on the individual components - the steel block on rubber pads and the freely supported beam - were carefully checked against theoretical predictions of their mobilities. Care was taken to ensure a high degree of accuracy throughout the experiment. The volume of the complete set of results (a total of 18 graphs for the two components) prohibits their inclusion here. However, two of the nine mobility expressions for each component are illustrated in Figures 5 and 6, for the block and beam respectively. In each case, the two examples shown represent the best and the worst correlation between theory and experiment, and apart from some difficulties encountered with signal noise at the low frequencies (below 50 Hz), the results are considered to be satisfactory.

The complete mobility data for the two components were then used in conjunction with equation (4) to predict the mobility of the assembled structure formed by connecting them together as shown in Figure 1. This process

derives the 3 x 3 mobility matrix for the assembled structure and from these data the specific information that is required may be extracted. In many cases the properties of greatest interest are the natural frequencies of the structure, and these may be conveniently described by a single mobility expression.

For the case being studied here, the direct mobility of the assembly in the x direction was computed from the component measurements and is shown in Figure 7 alongside the corresponding data obtained by measurements made direct on the assembled structure. There is an unexplained discrepancy between the two results in the magnitude of the third natural frequency (near 90 Hz) but otherwise the agreement is quite close. Perhaps the most significant result, however, is that illustrated in Figure 8 which again shows the mobility of the assembled structure predicted from the measured component mobilities, but in this case we have used the limited data which might be obtained from a conventional impedance test. This result is obtained by application of the mobility coupling technique but with only a single co-ordinate included in the analysis (in this case, the x co-ordinate). The errors in the natural frequencies predicted by this over simplified approach are quite striking, and they clearly indicate the need for the more complete data which has been measured by the method described above.

A final result given in Figure 9 shows the measured mobility of the assembled structure compared with that predicted entirely from theoretical analysis. Such an approach was only possible in this case because of the simplicity of the two components. The result illustrates the important point that even for such simple structures as were used in this study, agreement between theoretically predicted and experimentally measured characteristics is not remarkable. In fact, the data predicted from the component mobility measurements shows better agreement than that predicted from theory.

DISCUSSION

We have shown that it is both possible and practical to predict the vibration characteristics of an assembly of connected components using experimentally measured mobility data. However, it must be emphasised that such an approach is only reliable when the measured data is sufficiently complete and accurate and this requirement is not usually satisfied by conventional impedance testing techniques.

At the outset of a theoretical vibration analysis it is necessary to consider which co-ordinates must be included in order to satisfactorily define the motion of the components concerned. Only exceptional cases demand all six co-ordinates at each point of connection between components, but on the other hand, very few may be treated with only a single co-ordinate. Exactly the same considerations must be made for an analysis which employs experimentally obtained data. There are many applications in which one or more components may not be analysed directly because of their complexity and for which experimental measurement of mobility data is undertaken. The majority of mobility measurements are made with standard 'impedance testing' techniques and these are often totally inadequate for the application of such data to a mobility coupling exercise. Standard testing is usually confined to a single direction - that normal to the structure in most cases - while mobility data in other directions can be of equal or even greater importance. This fact is illustrated by the case studied here where exclusion of the rotation co-ordinate, θ, results in a marked deterioration in the quality of the predictions (cf. Figures 7 and 8).

While it is essential to include as many co-ordinates as are necessary, it is also important to ensure that the unimportant ones are omitted. The reason for this is that as the order of the matrices increases (by the inclusion of more co-ordinates in the analysis), so does the sensitivity of the numerical operations to small errors. Thus it is possible to gain no benefit from the inclusion of an extra co-ordinate (providing this is a relatively unimportant one) without simultaneously improving the accuracy of the measured quantities.

In the majority of cases, it will be necessary to measure mobility data in more than one direction. The two main problems encountered in making these measurements are (i) the application of a couple, and (ii) the application of in-plane forces, to the structure under test. The first of these may be overcome by using a torsional shaker or by using a twin shaker system but the second is very difficult to overcome. In some cases, it is possible to excite with a force parallel to the surface but raised above it by an amount sufficient to accommodate the

shaker. This gives rise to an applied couple in addition to the desired force and although this may be small, the response due to it could be of the same order of magnitude (even greater) as that due to the force. Thus unless the response to a couple (i.e. the rotational mobility data) is known, this technique must be used with a degree of caution.

One general solution to these difficulties is the experimental technique described in this paper, where it is accepted that the required mobility data may not be measured directly but must be extracted from a series of carefully controlled and designed experiments. By this approach, it is possible to determine the mobility matrix for a component using a single shaker in conjunction with an 'exciting block' which is attached to the test structure, and other standard equipment. However experience has shown that care must be exercised in the design of the exciting block in order to maintain an acceptable degree of accuracy in the final results. It is also an accepted feature of the technique that a large amount of data has to be measured, acquired and processed in order to obtain relatively little desired information. Since it is likely that this data is itself required for detailed analysis (as for the mobility coupling in this example), then it is convenient to present it in a digital format, readily stored on punched tape and available for further computation. Thus it was decided that an automatic instrumentation system based on a digital computer and digital transfer function analyser was necessary for efficient application of the technique.

CONCLUSIONS

It has been shown that vibration analysis of an assembly of connected structures may be made using experimentally measured mobility data for the components. However, this approach is only practicable when the measured data is sufficiently accurate and complete for the structure in question. This requirement demands the measurement of mobility data in more than one direction for most practical structures.

An experimental technique using a single shaker has been described for measuring mobility in up to three directions and this has been tested in a case study of two connected components. The results of the exercise confirm that the experimental method is satisfactory and that the additional complexity involved in multi-directional measurement is essential to a realistic analysis of typical engineering structures.

ACKNOWLEDGEMENT

The authors wish to thank the Ministry of Defence (Admiralty Engineering Laboratory) for the sponsorship of the contract under which this work was conducted.

Thanks are also due to Solartron Ltd. who supplied the computer-controlled transfer function analyser for making the measuremerts.

REFERENCES

1. D.U. Noiseux and E.B. Meyer, "Applicability of mechanical admittance techniques," Shock and Vibration Bulletin, 38, 1968.
2. J.E. Smith, "Measurement of the total structural mobility matrix," Shock and Vibration Bulletin, 40, 1970.
3. R.E.D. Bishop and D.C. Johnson, The Mechanics of Vibration, Cambridge University Press, 1960.
4. Kerlin and Snowdon, "Driving Point Impedance of Cantilever Beams," JASA, Vol.47 No.1(Pt 2) 1970.
5. A. Martin and C. Ashley, "A computer controlled digital transfer function analyser and its application in automobile testing," Society of Environmental Engineers Symposium on Dynamic Testing, 1971.

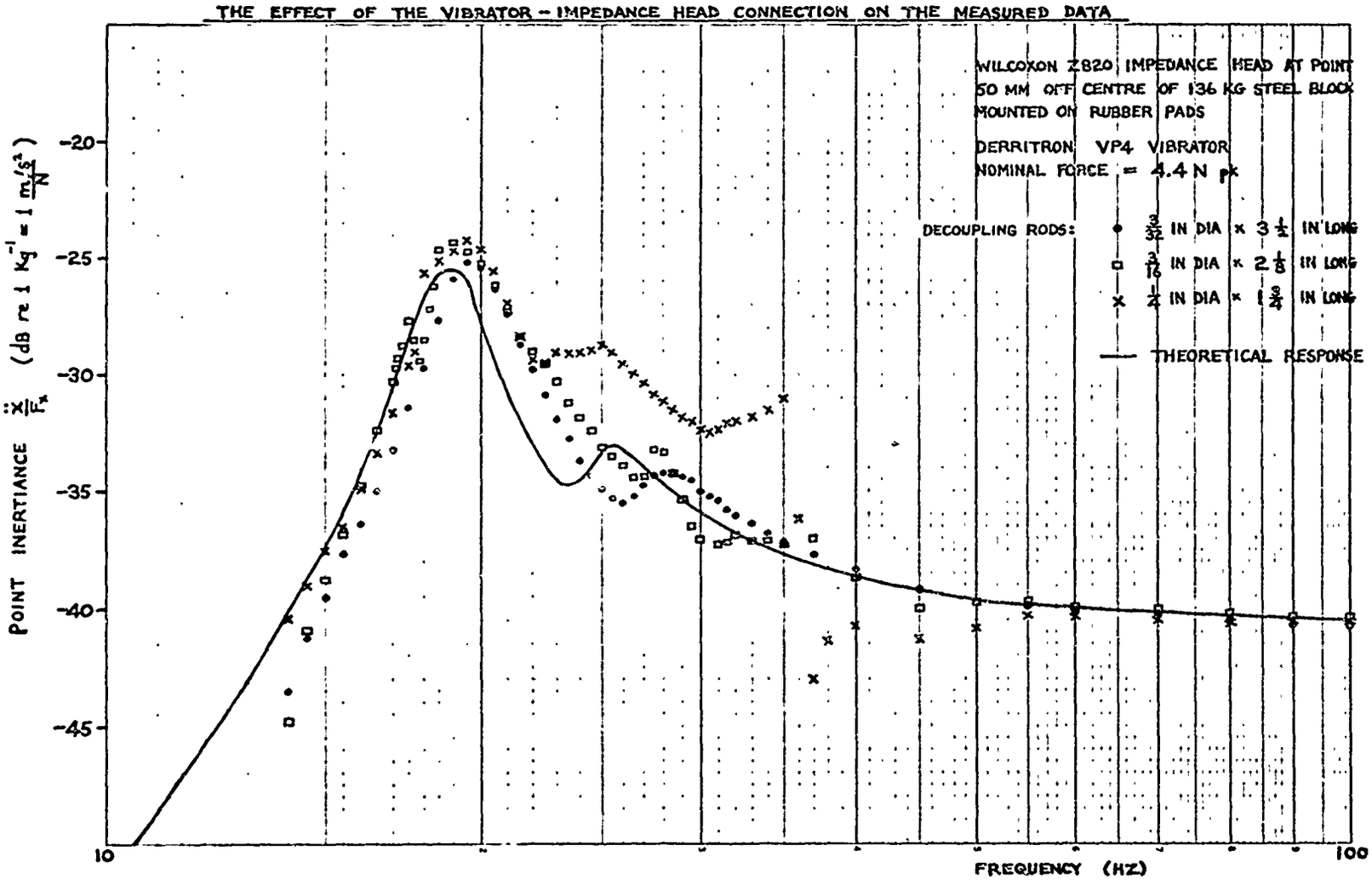
THE EFFECT OF THE VIBRATOR - IMPEDANCE HEAD CONNECTION ON THE MEASURED DATA
WILCOXON Z820 IMPEDANCE HEAD AT POINT 50 MM OFF CENTRE OF 136 KG STEEL BLOCK MOUNTED ON RUBBER PADS
DERRITRON VP4 VIBRATOR
NOMINAL FORCE = 4.4 N pk
DECOUPLING RODS: ● 3/32 IN DIA × 3 1/2 IN LONG
□ 3/16 IN DIA × 2 1/8 IN LONG
× 1/4 IN DIA × 1 3/4 IN LONG
THEORETICAL RESPONSE
POINT INERTIANCE ẍ/F_x (dB re 1 Kg⁻¹ = 1 m/s²/N)
-20
-25
-30
-35
-40
-45
10
100
FREQUENCY (HZ)

FIG. 4

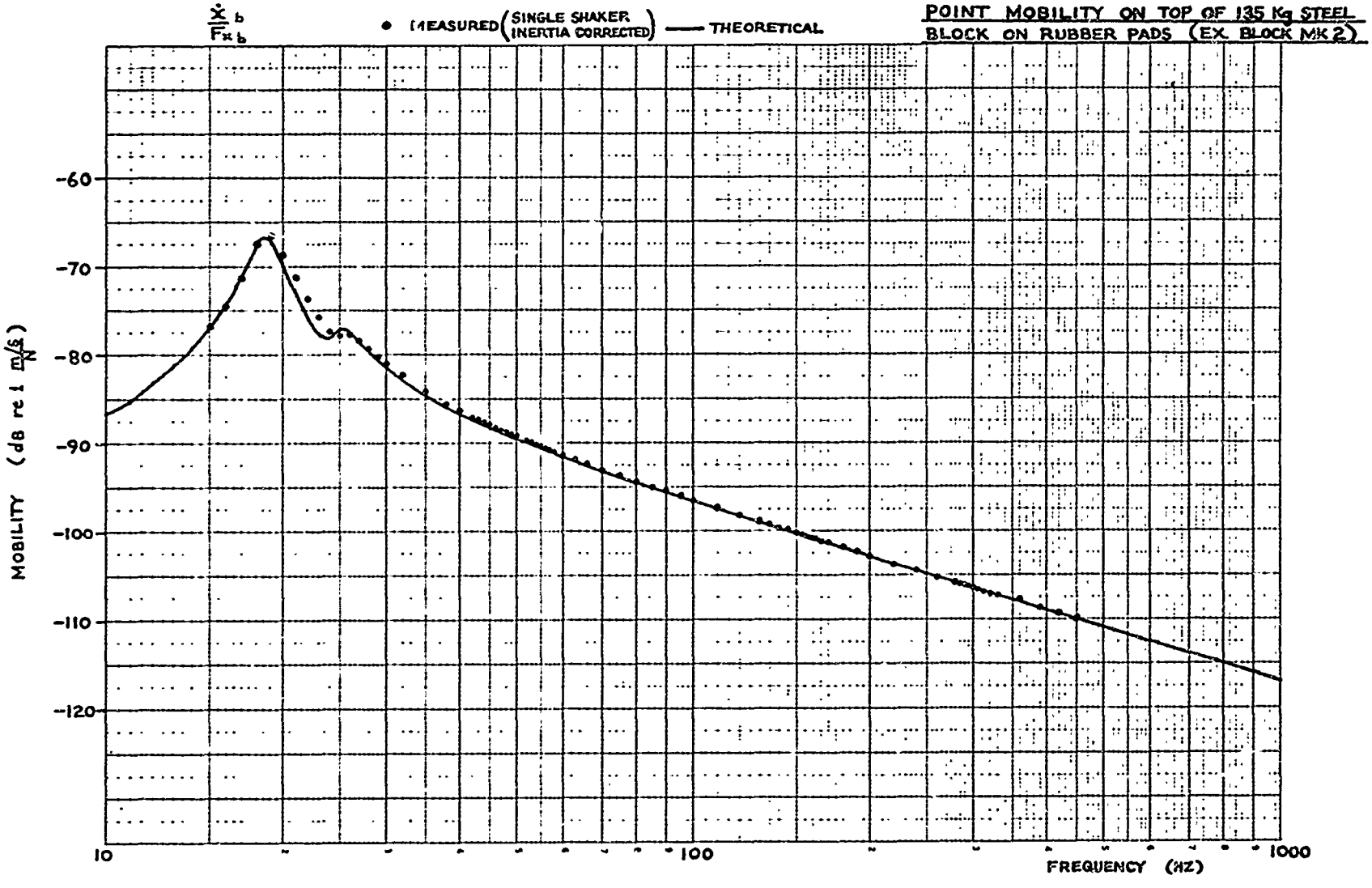
$\frac{\dot{X}_b}{F_{x_b}}$
• MEASURED (SINGLE SHAKER INERTIA CORRECTED)
— THEORETICAL
POINT MOBILITY ON TOP OF 135 Kg STEEL BLOCK ON RUBBER PADS (EX. BLOCK MK 2)
MOBILITY (dB re 1 m/s/N)
-60
-70
-80
-90
-100
-110
-120
10
100
1000
FREQUENCY (HZ)

FIG. 5(

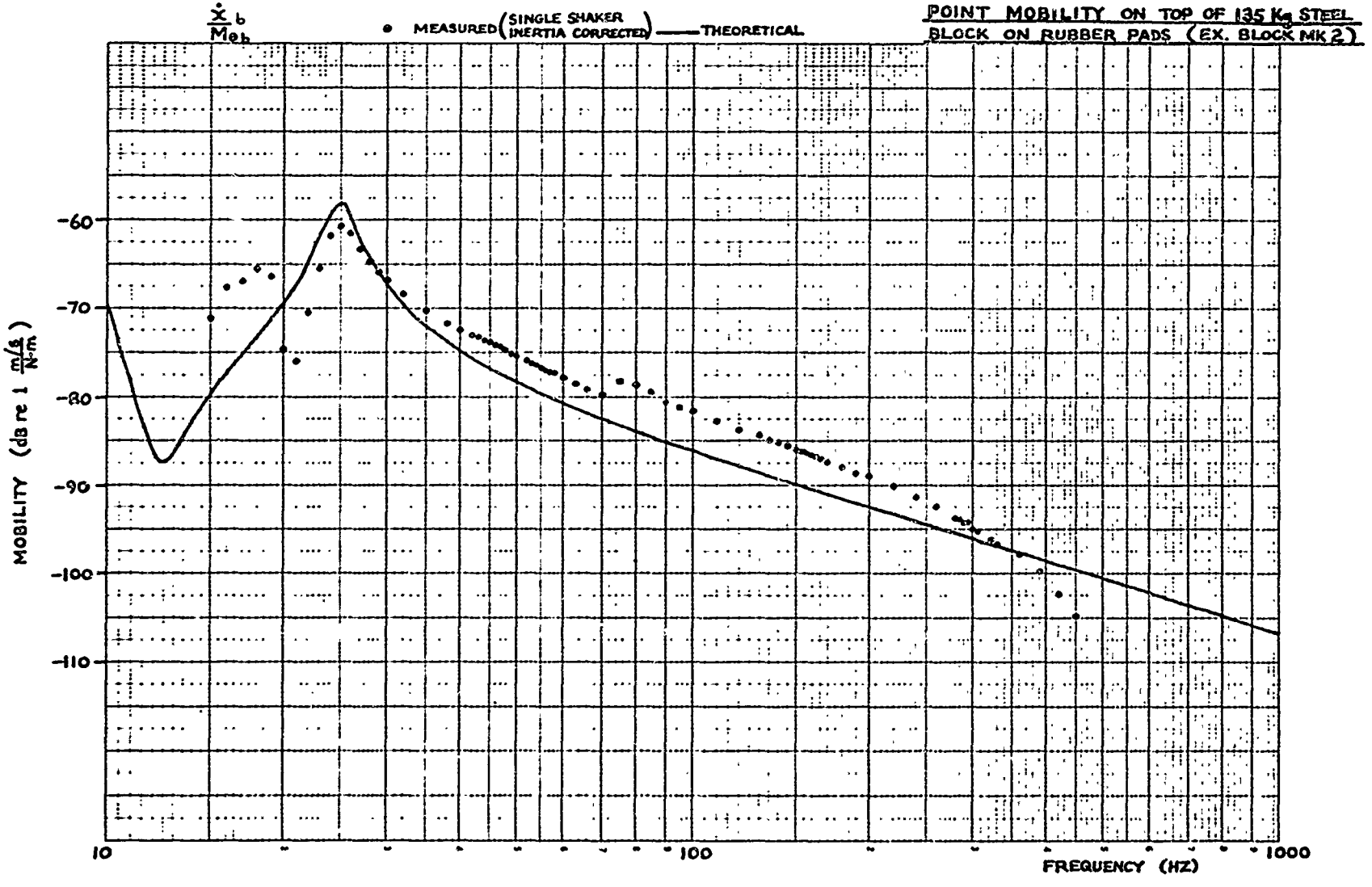
$\frac{\dot{x}_b}{M_{eb}}$
MEASURED (SINGLE SHAKER INERTIA CORRECTED)
THEORETICAL
POINT MOBILITY ON TOP OF 135 Kg STEEL BLOCK ON RUBBER PADS (EX. BLOCK MK 2)
MOBILITY (dB re 1 $\frac{m/s}{N\cdot m}$)
-60
-70
-80
-90
-100
-110
10
100
1000
FREQUENCY (HZ)

FIG. 5(b)

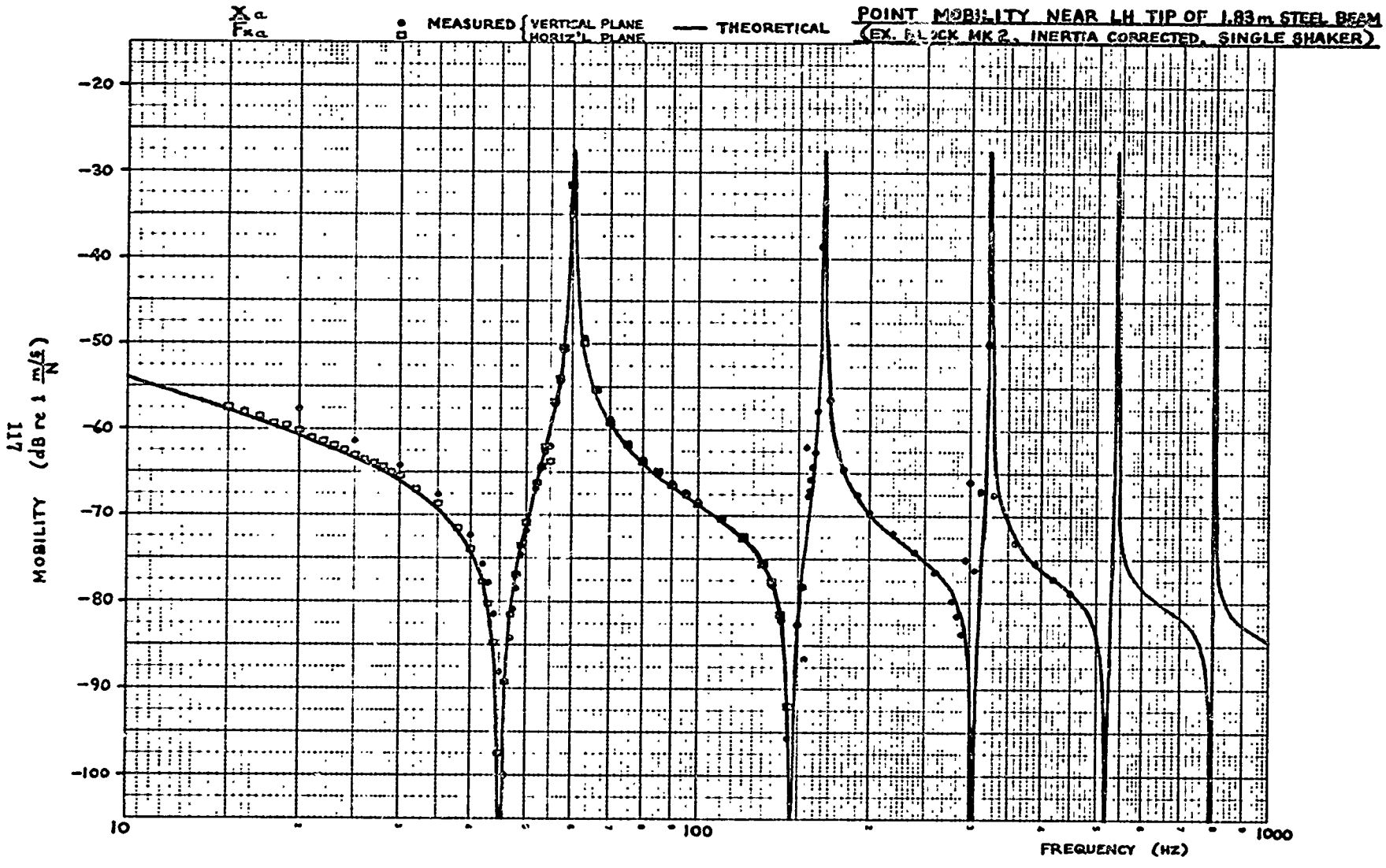
POINT MOBILITY NEAR LH TIP OF 1.83m STEEL BEAM
(EX. BLOCK MK 2, INERTIA CORRECTED, SINGLE SHAKER)
MEASURED { VERTICAL PLANE
HORIZ'L PLANE
THEORETICAL
MOBILITY (dB re 1 m/s/N)
-20
-30
-40
-50
-60
-70
-80
-90
-100
10
100
1000
FREQUENCY (Hz)

FIG. 6(a)

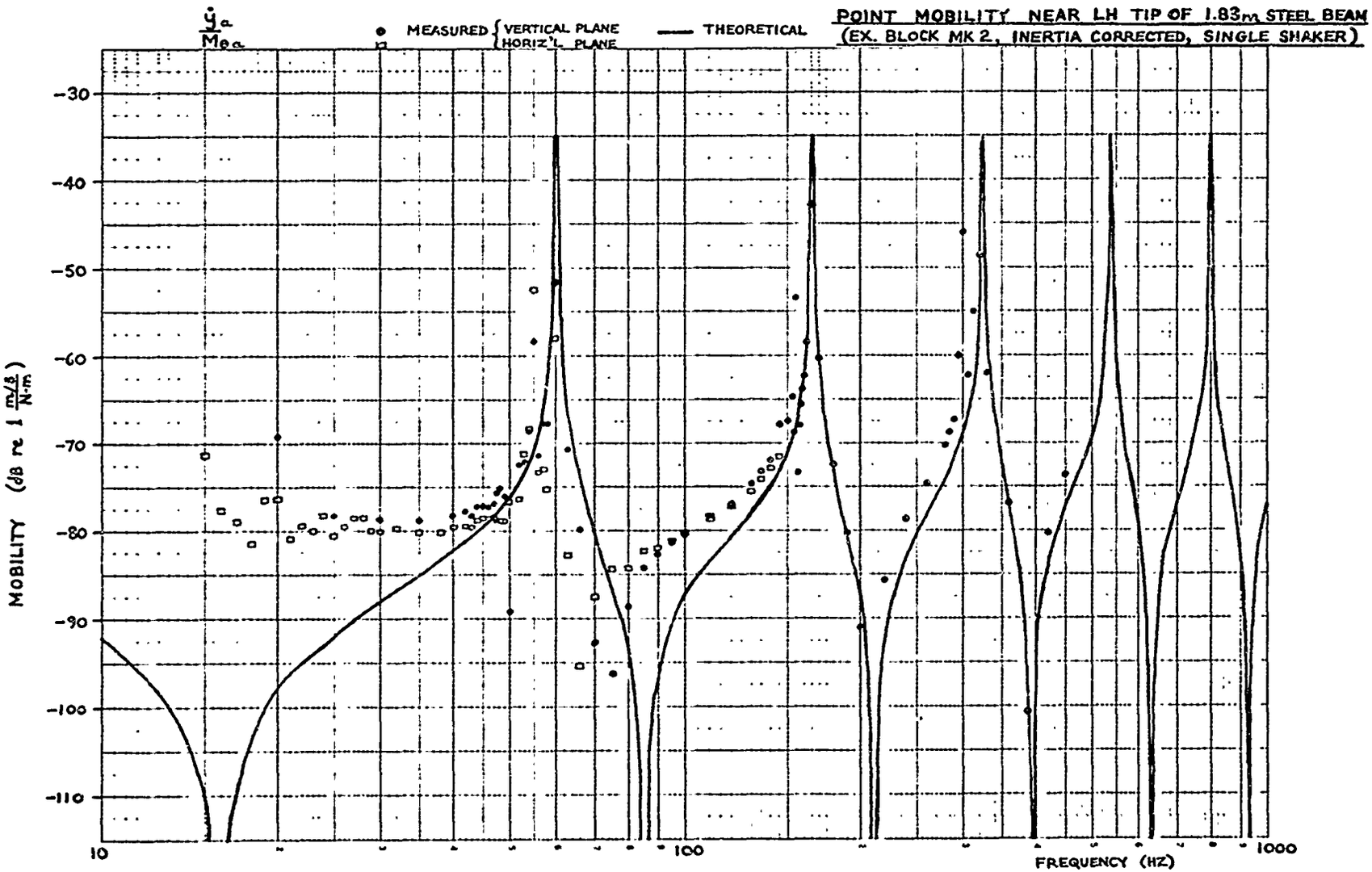
POINT MOBILITY NEAR LH TIP OF 1.83m STEEL BEAM
(EX. BLOCK MK 2, INERTIA CORRECTED, SINGLE SHAKER)
MEASURED { VERTICAL PLANE / HORIZ'L PLANE
THEORETICAL
MOBILITY (dB re 1 m/s / N-m)
-30
-40
-50
-60
-70
-80
-90
-100
-110
10
100
1000
FREQUENCY (HZ)

FIG. 6(b)

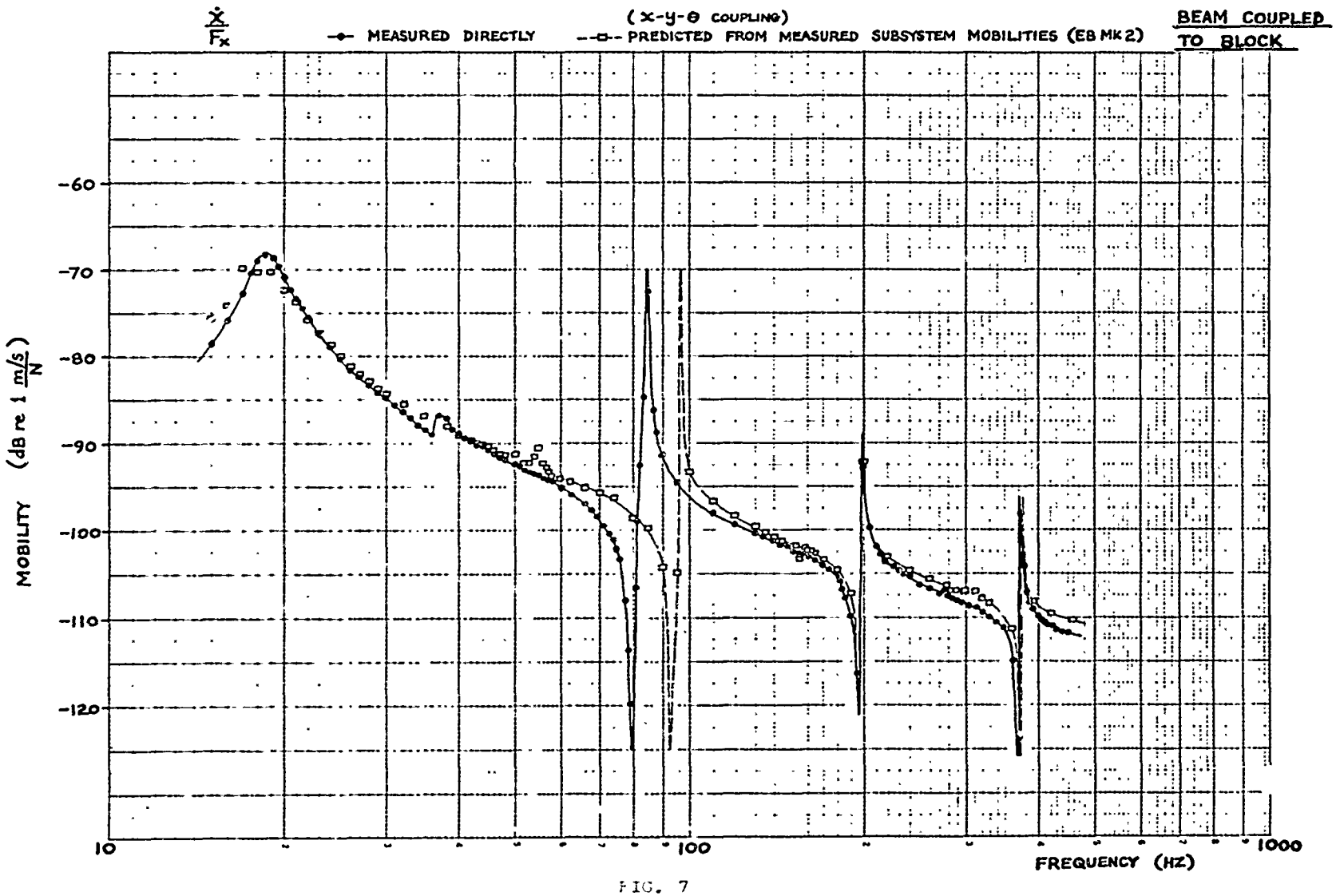
$\frac{\dot{X}}{F_x}$
(x-y-θ COUPLING)
MEASURED DIRECTLY
PREDICTED FROM MEASURED SUBSYSTEM MOBILITIES (EB MK2)
BEAM COUPLED TO BLOCK
MOBILITY (dB re 1 $\frac{m/s}{N}$)
-60
-70
-80
-90
-100
-110
-120
10
100
1000
FREQUENCY (HZ)

FIG. 7

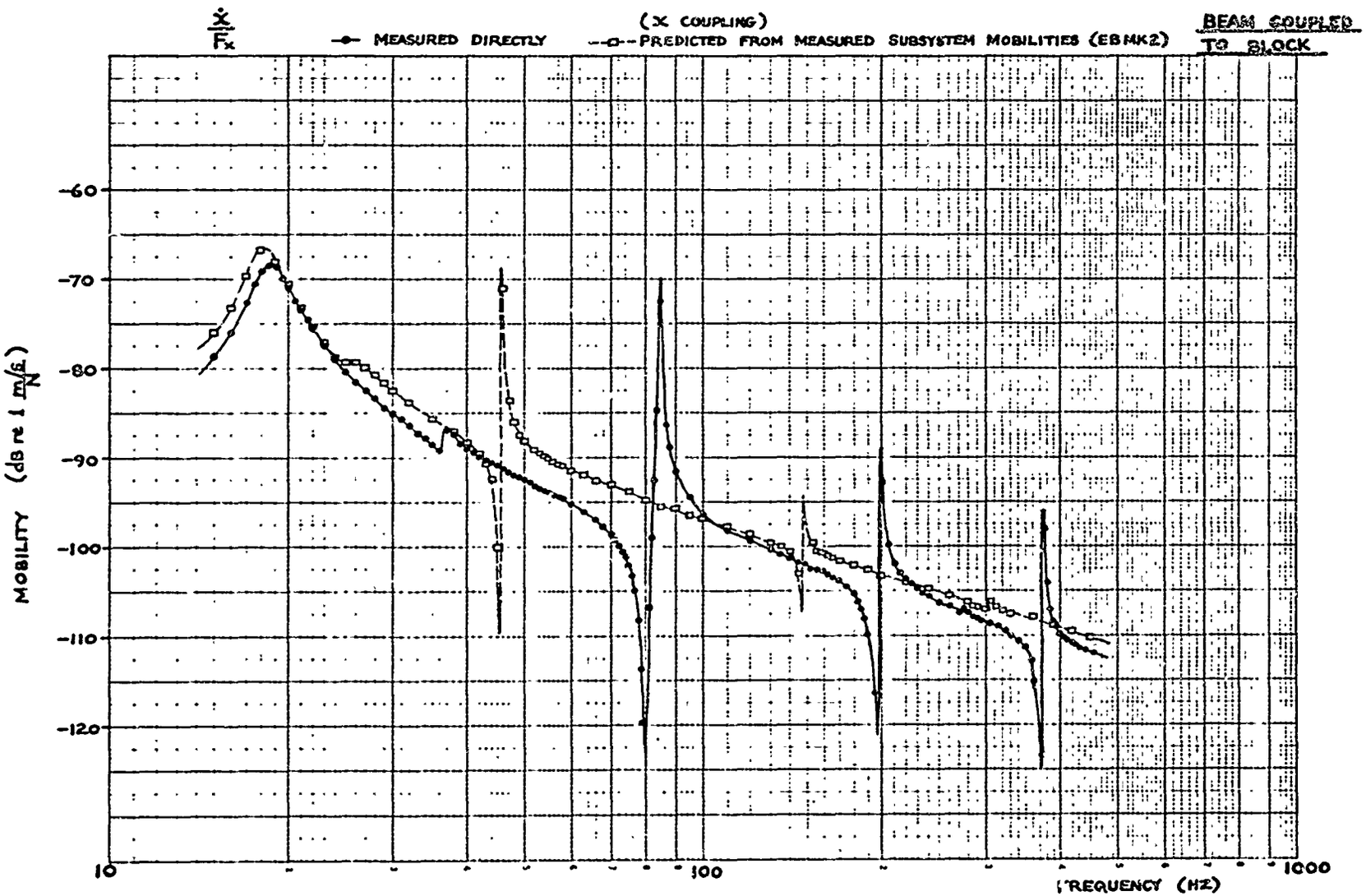
$\frac{\dot{x}}{F_x}$
(X COUPLING)
MEASURED DIRECTLY
PREDICTED FROM MEASURED SUBSYSTEM MOBILITIES (EBMK2)
BEAM COUPLED TO BLOCK
MOBILITY (dB re 1 $\frac{m/s}{N}$)
-60
-70
-80
-90
-100
-110
-120
10
100
1000
FREQUENCY (HZ)

FIG. 8

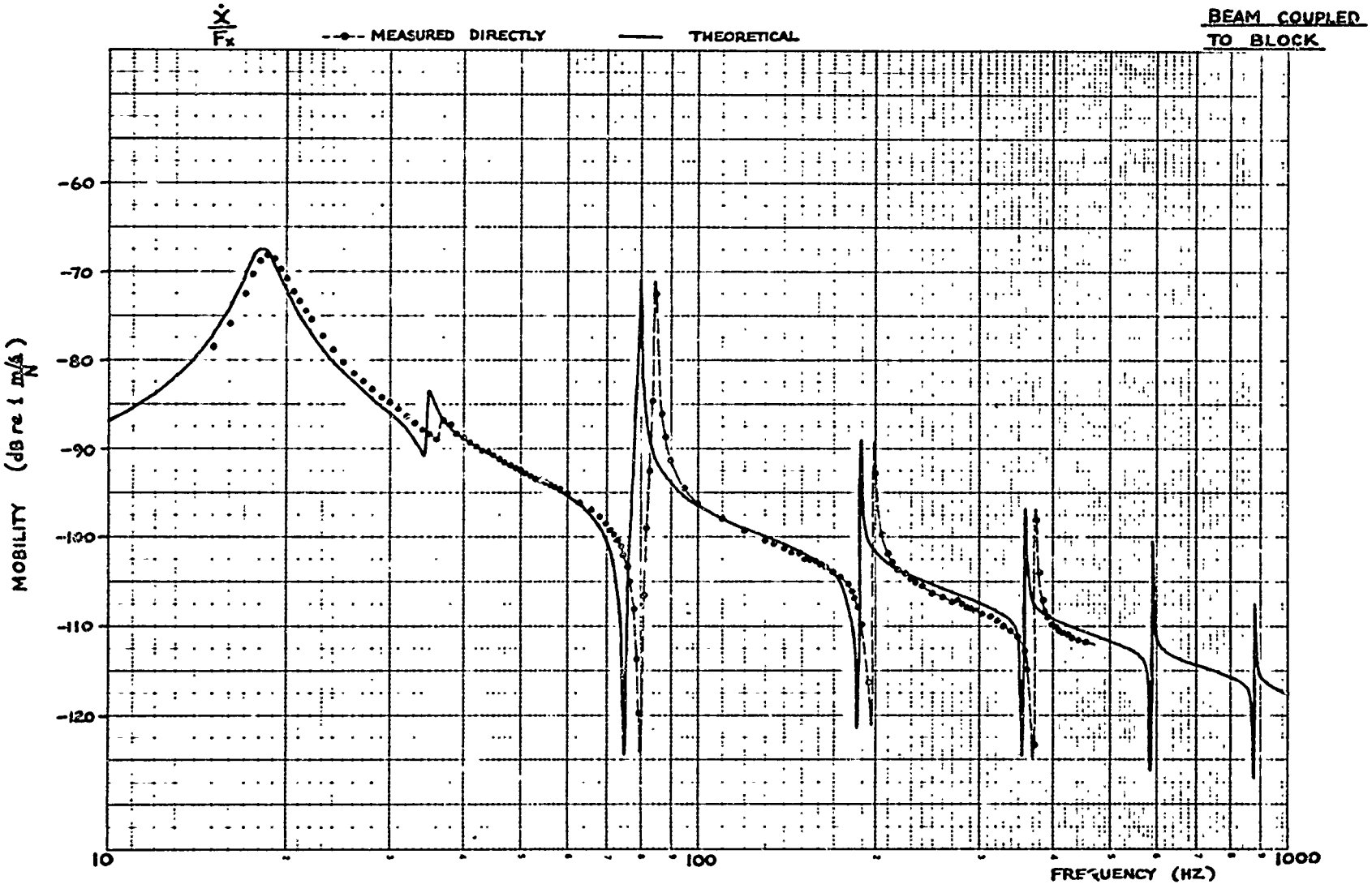
$\frac{\dot{x}}{F_x}$
MEASURED DIRECTLY
THEORETICAL
BEAM COUPLED TO BLOCK
MOBILITY (dB re 1 $\frac{m/s}{N}$)
-60
-70
-80
-90
-100
-110
-120
10
100
1000
FREQUENCY (HZ)

FIG. 9

Voice: Could you say something about the time required to compute the measurements from the raw data?

Mr. Ewins: On the full 3 x 3 matrix, we have not used the PDP-8 for that calculation. The system that you saw in the photograph was the preproduction prototype. There is only one in existence, and the store that is attached to it is not sufficient to do the matrix calculation. We have been using that for running the test, for storing the data and putting the data onto paper tape which we feed into our CDC computer. The actual computation time in a CDC is a matter of seconds - less than a minute. If we were to use the PDP-8, it is not sufficient to store all the data. We need an extra magnetic tape or extra disc storage. It would presumably take somewhat longer, but, using the PDP-8 to interface with a larger computer, it is a very short time -- on the order of a minute.

Mr. Bouche (Endevco): Is there some practical solution to your noise problems at low frequencies such as using accelerometers with higher sensitivity or narrow band filtering?

Mr. Ewins: The accelerometers that we used had a sensitivity of 300 picacoulombs per g. I do not think we could use more sensitive ones. The digital transfer function analyzer does the filtering in a quasi-digital manner. It handles a very high noise level very well. The problem was that the mobility levels we were measuring were so low at these low frequencies that they just could not be handled. The main difficulty on the beam example, where we had rather poor agreement between the theoretical curve and the measured one was that it was in the region of the first antiresonance where you have effectively zero mobility. It was in getting this antiresonance through that we ran into the noise problems at about 15 Hz. I think it was probably an extreme condition for the equipment to be tried on.

LIQUID-STRUCTURE COUPLING IN CURVED PIPES - II

L. C. Davidson and D. R. Samsury
Machinery Dynamics Division
Naval Ship Research and Development Center
Annapolis, Maryland

The coupled vibrational characteristics of a pipe assembly comprised of straight sections and uniform bends arranged in a nonplane configuration have been analyzed. The results indicate a significant level of coupling between the plane compressional wave in the contained liquid and beam responses of the pipe. Experiments confirm the general level of coupling but indicate some difficulty in predicting the fine detail of frequency response.

BACKGROUND

Liquid transfer systems continue as a major class of machinery recognized as a serious noise problem. A principal cause of this noise is the pump which, in doing work on the liquid, produces a dynamic pressure pulsation. Because of the relatively low frequency, this pulsation is transmitted through the liquid as a plane compressional wave. To the pipe, and any other structure encountered, this pressure is an exciting force. In a straight pipe the structural response is a radial extension or breathing of the pipe wall. In the frequency range of interest, which is well below the breathing resonance, this mechanism does not transmit a significant amount of energy. It must be considered, however, for its apparent effect on the compressibility of the liquid and attendant change in the sonic velocity.

In a curved pipe the change in direction of the plane wave front produces a transverse force on the pipe wall which has been shown to be an effective coupling mechanism between the longitudinal wave in the liquid and beam responses of the pipe.

Reference [1] described a technique for deriving and a matrix iteration technique for solving the differential equations describing the uniformly curved liquid filled pipe in the plane of the bend (8 degrees of freedom). Experimental results confirmed a significant level of liquid-structure coupling.

This work has now been extended to nonplane pipe configurations and, additionally, a closed form approximation to the differential equations has been obtained.

The structure shown in Fig. 1 was analyzed and its frequency response, in the form of mechanical mobility, computed. Of particular interest were the transfer mobilities from an acoustic input at the "free" end to structural responses at the flanged end. Several of these were measured and the results generally confirm the analysis. The experimental procedure necessarily employs novel measurement techniques.

MATHEMATICAL ANALYSIS

The computations performed in this work rest on the ability to characterize each component of the structure by

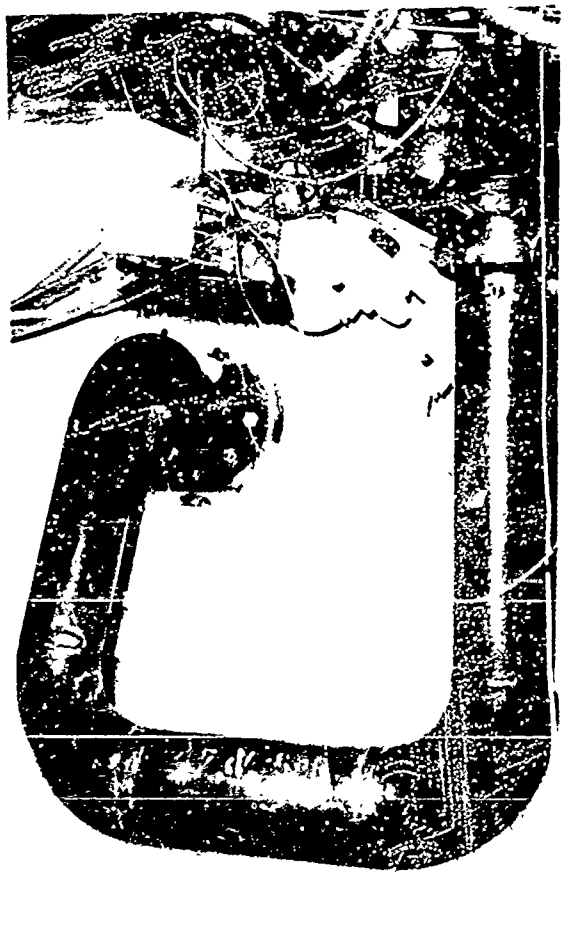

Fig. 1 - Liquid Filled Pipe Configuration

its transmission matrix. The choice of components follows naturally from the fabrication of the actual structure. The structure consists of four straight pipes and three 90° elbows as shown in Figs. 1 and 2. The object of the analysis is to obtain transmission matrices for these components and with them construct the system mathematically. The advantage of formulating the problem in terms of transmission matrices is that the complete structure (including physical boundary restraints) may be synthesized by multiplication of the component transmission matrices in the appropriate order. Due to the complexity of the structure's geometry, coordinate system rotations are necessary to obtain a result describing the desired structure. This is done by including rotation matrices at proper intervals during the synthesis. Finally, the overall transmission matrix which results from the synthesis can be manipulated to yield the mobility parameters of the structure [2,3] .

In Fig. 2 weld joints are indicated by heavy lines. The numbers shown at the ends of the structure and at each weldment facilitate identification of each component and serve as indices for their transmission matrices.

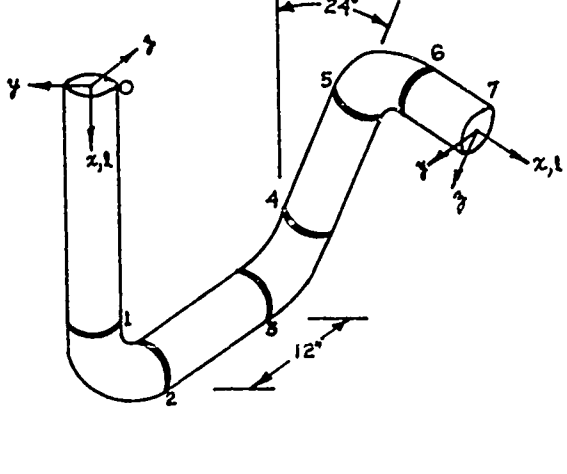

Fig. 2 - Piping Arrangement Coordinate System

A right hand coordinate system is chosen and oriented so that the x-axis is always directed along the centerline of straight sections or tangent to the centerline of elbows. The z-axis is always directed toward the origin of the radius of curvature of any "straight-elbow-straight" section of the structure and thus always lies in the plane containing a section of this type. In this structure those sections are (3) - (0), (5) - (2) and (7) - (4) . Therefore, the right hand triad rotates about the x-axis as one travels from (0) to (7) and hence the necessity of rotation matrices as indicated above.

A transmission matrix relates the forces, moments, displacements and rotations at one point in a component (or structure) to the same quantities at another point. Stated mathematically

$$Z_i = U Z_{i-1} \qquad (1)$$

or

$$\begin{bmatrix} d \\ f \end{bmatrix}_i = \begin{bmatrix} t_1 & t_2 \\ t_3 & t_4 \end{bmatrix} \begin{bmatrix} d \\ f \end{bmatrix}_{i-1} \qquad (2)$$

where U is the transmission matrix and Z is a state vector. Eq. (2) shows the relation in partitioned form where

$$d = \begin{bmatrix} u \\ v \\ w \\ \phi \\ \psi \\ \vartheta \\ l \end{bmatrix} \qquad f = \begin{bmatrix} N \\ V_y \\ V_z \\ T \\ M_y \\ M_z \\ P \end{bmatrix} \qquad (3)$$

The quantities in Eq. (3) are defined as follows:

u,v,w - displacements along x,y and z axes respectively.

ϕ, ψ, ϑ - rotations about the x,y and z axes.

l - displacement of a fluid particle along x axis.

N, V_y, V_z - normal and shear forces along x,y and z axes.

T, M_y, M_z - torsion and bending moments about x,y and z axes.

P - force on fluid along x axis (pressure not used to avoid unit inconsistencies)

It follows that U is a 14 x 14 square matrix and each of the submatrices in Eq. (2) is 7 x 7. For this problem

$$i = 1,2,....7$$

and U is a rearward transmission matrix [2]

Obtaining the transmission matrix for a straight pipe section filled with liquid is facilitated by [3] , where transmission matrices for a straight beam under axial, bending and torsional loads are catalogued. Combining them yields a 12 x 12 transmission matrix which does not include the presence of the liquid. However, by considering the liquid to behave as an elastic beam with no bending or torsional stiffness, a 2 x 2 transmission matrix relating l and P at the ends of the pipe is obtained by analogy to the catalogued matrix for an axially loaded beam. This is done by replacing E, Young's modulus, by B, the effective bulk modulus of the fluid [4] . These matrices can then be combined to form a 14 x 14 transmission matrix for the liquid-filled pipe if the mass of the pipe μ', and the liquid, μ'' , are added in those elements of U describing bending behavior.

Unfortunately, the 14 x 14 transmission matrix for the liquid-filled elbow in closed form is not as readily obtained. However, the literature does provide guidelines. Reference [3] gives the transmission matrices for rigid elbows with distributed mass and for massless, elastic elbows. In the case of the massless elastic elbow, the effects of shear deformation are neglected. (These effects are accounted for in this work.) Neither of these models is sufficient but they do serve as a starting point to obtain the desired matrix. The massless model is rejected for obvious reasons and, although previous unreported mathematical analysis indicated that large increases in stiffness do not significantly change the behavior of short radius elbows, the conclusion that infinite stiffness may therefore be assumed is erroneous. Assuming the elbow to be rigid causes the submatrix t_2 in Eq. (2) to be null. Although the actual values of the elements in t_2 are small in comparison to other elements of U (on the order of 10^{-6}), their contribution in synthesizing the complete system is significant.

Therefore, rather than trying to amend and append existing forms of U for the elbows, a derivation from first principles is used.

Consider the free-body diagram of a differential element of a liquid-filled elbow in Fig. 3. By writing the equilibrium equations and the appropriate elasticity equations that relate forces and moments to displacements and

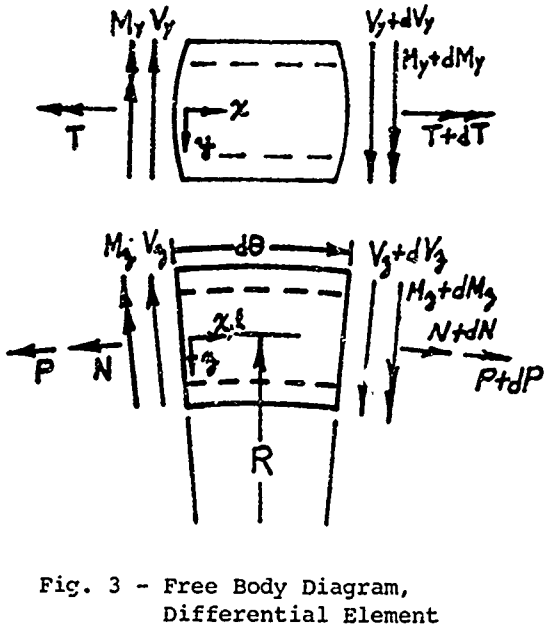

Fig. 3 - Free Body Diagram, Differential Element

rotations through the elastic properties of the elbow and which reflect the presence of the liquid, a set of first order, linear differential equations with constant coefficients results [3]. This set of equations, 14 in number, is shown in Eq. (4).

$$\frac{dZ}{ds} = As \tag{4}$$

Z is defined in Eq. (3), A is the 14 x 14 matrix of constant coefficients and s = Rθ, R being the radius of curvature of the elbow and θ the angle the elbow turns. The matrix A is shown in Eq. (4a).

Equation (4) is analogous to the linear, first order different equation

$$\frac{dz}{ds} = as$$

whose solution, given $z(0) = z_o$, is

$$z = e^{as} z_o$$

Similarly, the solution to Eq. (4) is

$$Z = e^{As} Z_o \tag{5}$$

Where Z_o is the state vector at S = 0 and

$$e^{As} = U \tag{6}$$

is the desired transmission matrix. Further, since

$$e^{as} = 1 + \frac{(as)}{1!} + \frac{(as)^2}{2!} + \cdots$$

$$\frac{d}{d\theta}\begin{bmatrix} u \\ v \\ w \\ \phi \\ \psi \\ \vartheta \\ \ell \\ N \\ V_y \\ V_z \\ T \\ M_y \\ M_z \\ P \end{bmatrix} = \left[\begin{array}{ccccccc|ccccccc} 0 & 0 & 1 & 0 & 0 & 0 & 0 & R/EA' & 0 & 0 & 0 & 0 & 0 & 0 \\ 0 & 0 & 0 & 0 & 0 & R & 0 & 0 & RX/GA' & 0 & 0 & 0 & 0 & 0 \\ -1 & 0 & 0 & 0 & -R & 0 & 0 & 0 & 0 & RX/GA' & 0 & 0 & 0 & 0 \\ 0 & 0 & 0 & 0 & 0 & 1 & 0 & 0 & 0 & 0 & R/GJ & 0 & 0 & 0 \\ 0 & 0 & 0 & 0 & 0 & 0 & 0 & 0 & 0 & 0 & 0 & R/EKI_y & 0 & 0 \\ 0 & 0 & 0 & -1 & 0 & 0 & 0 & 0 & 0 & 0 & 0 & 0 & R/EI_z & 0 \\ 0 & 0 & 1 & 0 & 0 & 0 & 0 & 0 & 0 & 0 & 0 & 0 & 0 & R/BA'' \\ -\mu R\omega^2 & 0 & 0 & 0 & 0 & 0 & 0 & 0 & 0 & 1 & 0 & 0 & 0 & 0 \\ 0 & -\mu R\omega^2 & 0 & 0 & 0 & 0 & 0 & 0 & 0 & 0 & 0 & 0 & 0 & 0 \\ 0 & 0 & -\mu R\omega^2 & 0 & 0 & 0 & 0 & -1 & 0 & 0 & 0 & 0 & 0 & -1 \\ 0 & 0 & 0 & -\mu i_x^2 R\omega^2 & 0 & 0 & 0 & 0 & 0 & 0 & 0 & 0 & 1 & 0 \\ 0 & 0 & 0 & 0 & -\mu i_y^2 R\omega^2 & 0 & 0 & 0 & 0 & 0 & R & 0 & 0 & 0 \\ 0 & 0 & 0 & 0 & 0 & -\mu i_z^2 R\omega^2 & 0 & 0 & -R & 0 & -1 & 0 & 0 & 0 \\ 0 & 0 & 0 & 0 & 0 & 0 & -\mu' R\omega^2 & 0 & 0 & 0 & 0 & 0 & 0 & 0 \end{array}\right] \begin{bmatrix} u \\ v \\ w \\ \phi \\ \psi \\ \vartheta \\ \ell \\ N \\ V_y \\ V_z \\ T \\ M_y \\ M_z \\ P \end{bmatrix} \tag{4a}$$

it can be shown that the matrix equation

$$e^{As} = I + \frac{(As)}{1!} + \frac{(As)^2}{2!} + \cdots \qquad (7)$$

I being a unit matrix, is a valid representation of the transmission matrix. Eq. (7) is used to obtain U for the elbow.

Two approaches to finding U are available at this point and both are used. In the first, the elements of A can be computed numerically, the powers of A found and Eq. (7) formed using enough terms in the series to insure accuracy. Although A is complex (E,G and B, Young's, shear and bulk modulus respectively, are given small phase angles to represent damping), Eq. (7) converges absolutely [5] and hence it is only necessary to choose a criteria for accuracy that determines the number of terms necessary to be included. In this work, the criteria chosen is that the elements of the nth partial sum in Eq. (7) exceed the corresponding elements of the (n + 1) term by 10^6 in ratio. For the elbow considered, 10 terms of the series are necessary to satisfy this requirement.

This technique has been used to find U for an elbow where only degrees of freedom in the plane of curvature are considered [1], yielding U as an 8 x 8 matrix. The method has been extended in this investigation to include all degrees of freedom and yield U as a 14 x 14 matrix. The difficulty that arises in using this approach is not accuracy or complexity but economy of time.

The second method which results directly from the difficulty cited above is to find U in closed form. The approach is similar to that above in that Eq. (7) is used. Here, however, the elements of A are written symbolically and the powers of A up to the tenth term are obtained by performing the necessary matrix multiplications by hand. The partial sum is formed and each element contained in the resulting matrix is examined to determine what function or combination of functions the elemental series represents based on what the available terms imply. A problem arises here since each elemental series is of such complexity as to defy complete identification in terms of known functions. To ease the situation, only those terms in each elemental series containing a single stiffness parameter (E, G or B) to the first power in the denominator (or not at all) are retained. Under these conditions, only those terms of each elemental series which were readily identifiable with known functions at the outset still remain.

Futher simplification is made by examining with this second method the cases of a rigid liquid-filled elbow with distributed mass (E,G, and B infinite) and a massless elastic elbow. In the case of the rigid elbow with mass, comparison of numerical results with results obtained by the first technique outlined above reveals that in the submatrix t_3 of Eq. (2) the elements correspond exactly with the exception of the element at row 11, column 3 of U . This element vanishes in the rigid elbow with mass and is small (in comparison to all other elements in t_3) but nevertheless nonzero using the numerical method first presented. By including in this element stiffness terms according to the criteria above and leaving all other elements in t_3 unaltered, this element also compares well (but not exactly). It is concluded, then, that in t_3, with the single exception noted, the terms used to represent U in closed form correspond to those for a rigid elbow with distributed mass. That is, stiffness parameters need not appear in t_3, at least in the frequency range of interest (20-550 Hz) for the elements indicated.

For the massless elastic elbow (μ', μ'' and $\mu = \mu' + \mu''$ vanish), comparison with the numerical method first presented reveals that all elements of submatrix t_2 compare exactly. Further, in both techniques the elements are constants over the frequency range of interest. It is concluded that no frequency dependent terms need be retained in t_2 in approximating U in closed form and those which do appear correspond to the elements in t_2 for a massless elastic elbow.

Finally the two limiting cases indicate to a limited extent the partial form of some of the elements in t_1 and t_4. Their final form and the form of those elements which vanish in these cases are obtained as described above.

Having obtained the required transmission matrices, the synthesis process is a simple one. Consider for example the interface of straight pipe and elbow at point 6 in Fig. 2. Continuity requires that the displacements and rotations of the elbow at this point be equal to those of the straight pipe. Having adopted the force and moment sign convention that positive forces on positive faces are positive as well as negative forces on negative faces and again invoking continuity it is seen that the state vectors of the elbow and straight section are equal. Thus, if $Z_{7S} = U_{76}Z_{6S}$ and $Z_{6E} = U_{65}Z_{5E}$ and since $Z_{6S} = Z_{6E}$ it is correct to write $Z_7 = U_{76}U_{65}Z_5$ where S and E have been dropped.

This process can be continued until point (0) is reached yielding

$$Z_7 = U_L U_{76} U_{65} U_{54} R_4 U_{43} R_3 U_{32} U_{21} U_{10} Z_0 \quad (8)$$

or

$$\begin{bmatrix} d_7 \\ f_7 \end{bmatrix} = \begin{bmatrix} t_1 & t_2 \\ t_3 & t_4 \end{bmatrix} \begin{bmatrix} d_0 \\ f_0 \end{bmatrix} \quad (9)$$

where the matrices R_3 and R_4 are rotation matrices ensuring proper orientation of the coordinate triad as outlined above and the form of the state vectors is defined in Eqs. (2) and (3). The matrix U_L is the transmission matrix of the flange and plate assembly shown in Fig. (5).

Equation (9) may be transformed to a mobility matrix

$$\begin{bmatrix} V_0 \\ V_7 \end{bmatrix} = j\omega \begin{bmatrix} t_3^{-1} t_4 & t_3^{-1} \\ -t_2 + t_1 t_3^{-1} t_4 & t_1 t_3^{-1} \end{bmatrix} \begin{bmatrix} f_0 \\ f_7 \end{bmatrix} \quad (10)$$

since in general $V = j\omega d$. In Eq. (10) the upper and lower left hand submatrices have been multiplied by (-1) since f_0 in transmission notation is the negative of f_0 in mobility notation.

The computed results presented in this report were facilitated by the use of a general purpose computer program [6] which allows convenient matrix manipulation and includes a graphing subroutine. In all figures shown herein the subscript 7 has been interposed to 1 for consistency with available literature [3]. Finally, it is noted that mobility parameters obtained using the numerical technique to find U for the elbow compared almost exactly to those obtained using the U matrix of the elbow in closed form.

EXPERIMENTAL MEASUREMENTS

The pipe configuration of Fig. 1 was fabricated from standard 4-inch I.D. seamless steel pipe and 6-inch radius elbows (90°). The structure was filled with lubricating oil and tested by measuring four transfer mobilities. In each case excitation of the structure was produced by an airborne sound generator suspended above the unflanged end of the pipe and acoustically coupled through a rigid cone adaptor. During tests an air gap of approximately 1/64-inch was maintained between the cone and pipe. Two wall mounted microphones in the cone provided for detection of the excitation pressure and also indicated the frequency range over which a plane wave was present, as shown in Fig. 4.

Structural details of the flanged end are shown in Fig. 5. Structural responses at this end were detected with the pair of accelerometers which can be seen on the plate structure in Fig. 1. As arranged, their sum detects translation along the x-axis; their difference, rotation about the y-axis (ψ). These were moved to positions corresponding to 9 and 3 o'clock on the flange to detect rotation about the z-axis (θ).

The fluid response at the flanged end was detected with a wall mounted hydrophone which can be seen on the underside of the pipe in Fig. 1. This pressure detector, being very near the "free" surface effected by the rubber membrane

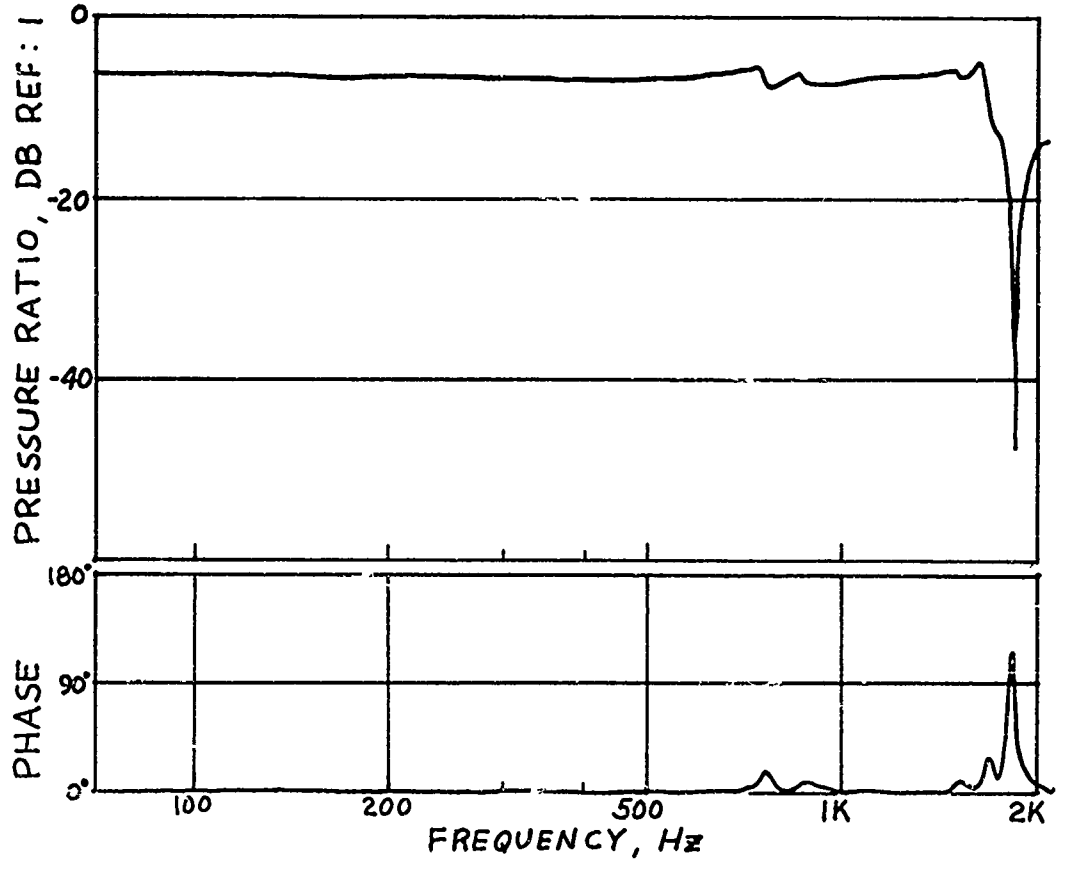

Fig. 4 - Pressure Distribution in Adaptor Cone

(Fig. 5), is loaded by inertial characteristics of a short liquid column and, therefore, serves as an acceleration detector.

For computational purposes the blocking structure was assumed to be characterized by a diagonal mobility matrix. Mobilities in the plane of the plate structure were assumed to be ideal stiffnesses, dependent only on structural geometry and material properties. The mobilities out of the place (translation along the x-axis, rotation about the y-and z-axes) were measured with the apparatus of Smith [7] . This technique involves the use of a specially designed exciter, Fig. 6, and required only acceleration response measurements. For low mobility structures, such as encountered here, no correction to the measured data is required. Two of these measurements are presented in Figs. 7 and 8. From these, appropriate spring rates were obtained for use in the computations. These measurements were subject to a poor signal to noise ratio which accounts for the departure from spring-like behavior at low frequencies.

Figures 9 and 10 present a comparison of computed and measured transfer mobilities for the coupled structure of Fig. 1. The complete 14 x 14 mobility matrix was computed but only those parameters involving liquid-structure coupling and considered significant from a noise transmission viewpoint were measured. In all cases the mean levels of computed and measured mobility spectra agreed quite well, indicating that the coupling mechanism was accurately represented. Agreement in detail of the rotational mobilities is considered reasonable for a structure of this

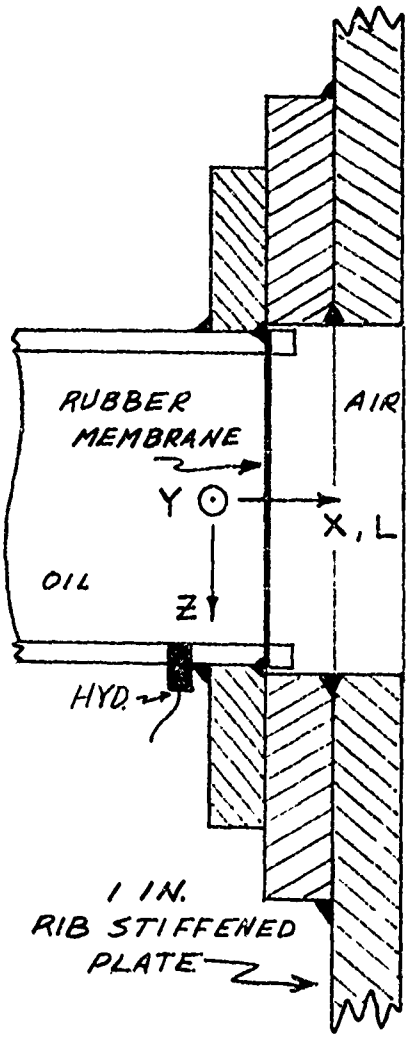

Fig. 5 - Physical Restraint and Coordinate System at Flanged End

complexity. The translational response, however, shows some rather large discrepancies. A possible explanation for the peaks which occur in the 100 to 200 Hz range of the measured data and also for the generally poor agreement at low frequencies, is that accelerometer response due to rotation was large in these regions. However, translational measurements were made with accelerometers in both 12-6 and 9-3 o'clock positions and they were nearly identical. This would not be the case

Fig. 6 - Mobility Measurement Apparatus

if rotational response was the problem since the rotations were not the same in the two planes.

The final frequency response in this group is the transfer through the liquid column. This also indicates some difficulty in establishing the exact detail of response, but it is not likely that the response transducer (hydrophone) is at fault since this measurement technique has been employed successfully in a wide range of applications. Rather, it is thought that structural details such as the bolted flange and welded joints, which are not considered in the analysis, produce these errors.

The significance of liquid structure coupling as a noise transmission mechanism can be appreciated by comparing the responses at the plate structure due to the liquid input (pressure x area) and due to a force applied directly to the free end of the pipe

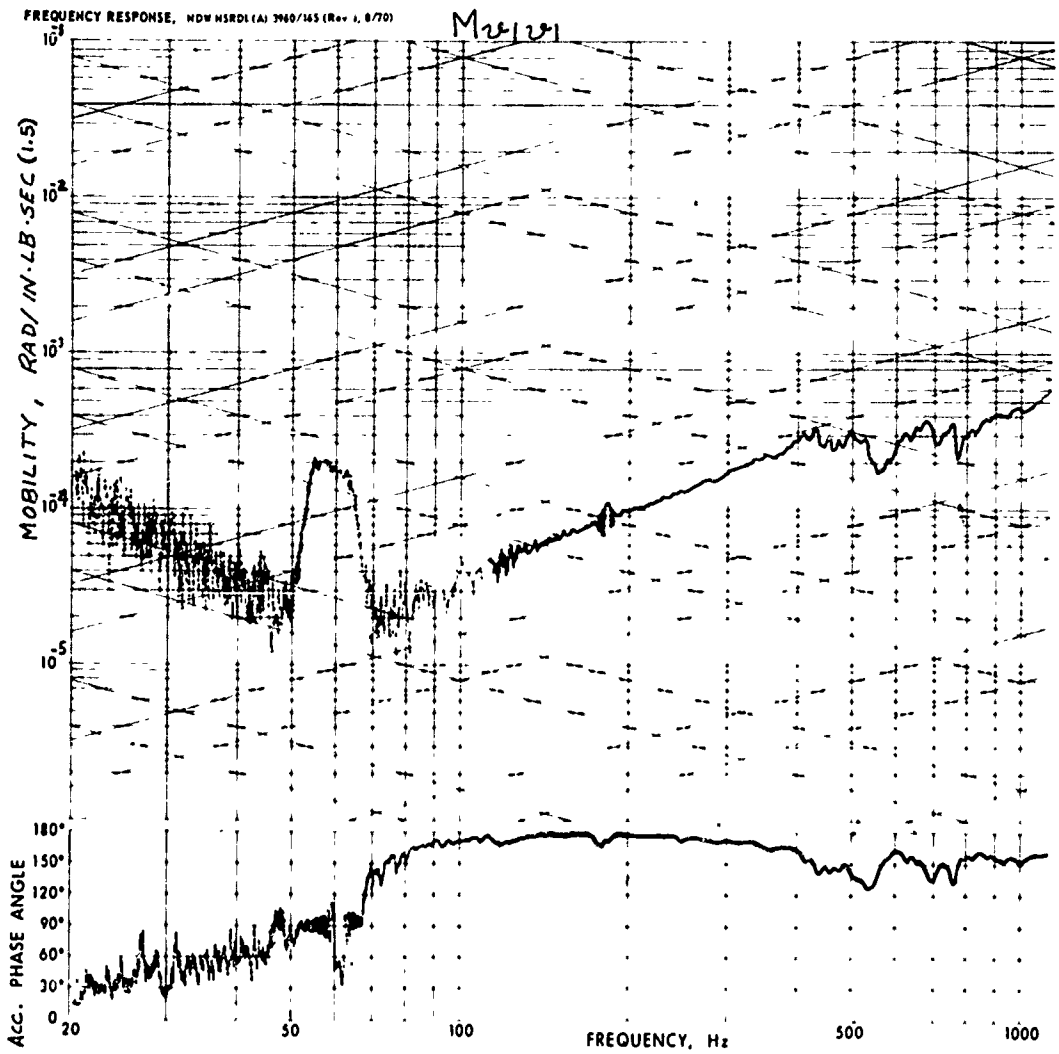

Fig. 7 - Measured Rotational Mobility, Blocking Structure

(Figure 11). It is seen that the response due to liquid-structure coupling is as high or higher than that due to direct force throughout most of the spectrum. Since all coupling occurs in the elbows, this depends on their placement relative to the pressure distribution in the pipe. This high level of coupling, however, has been found to be the normal situation.

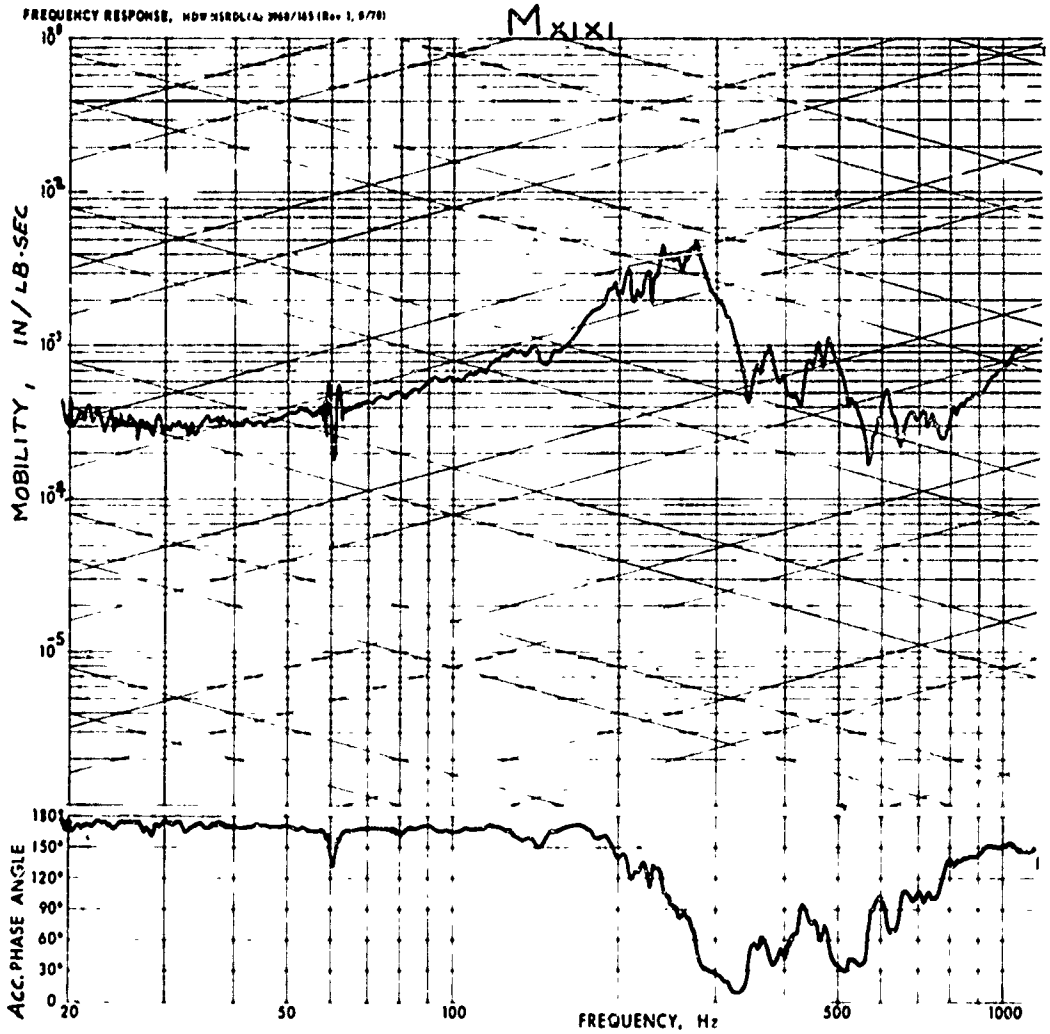

Fig. 8 - Measured Translational Mobility, Blocking Structure

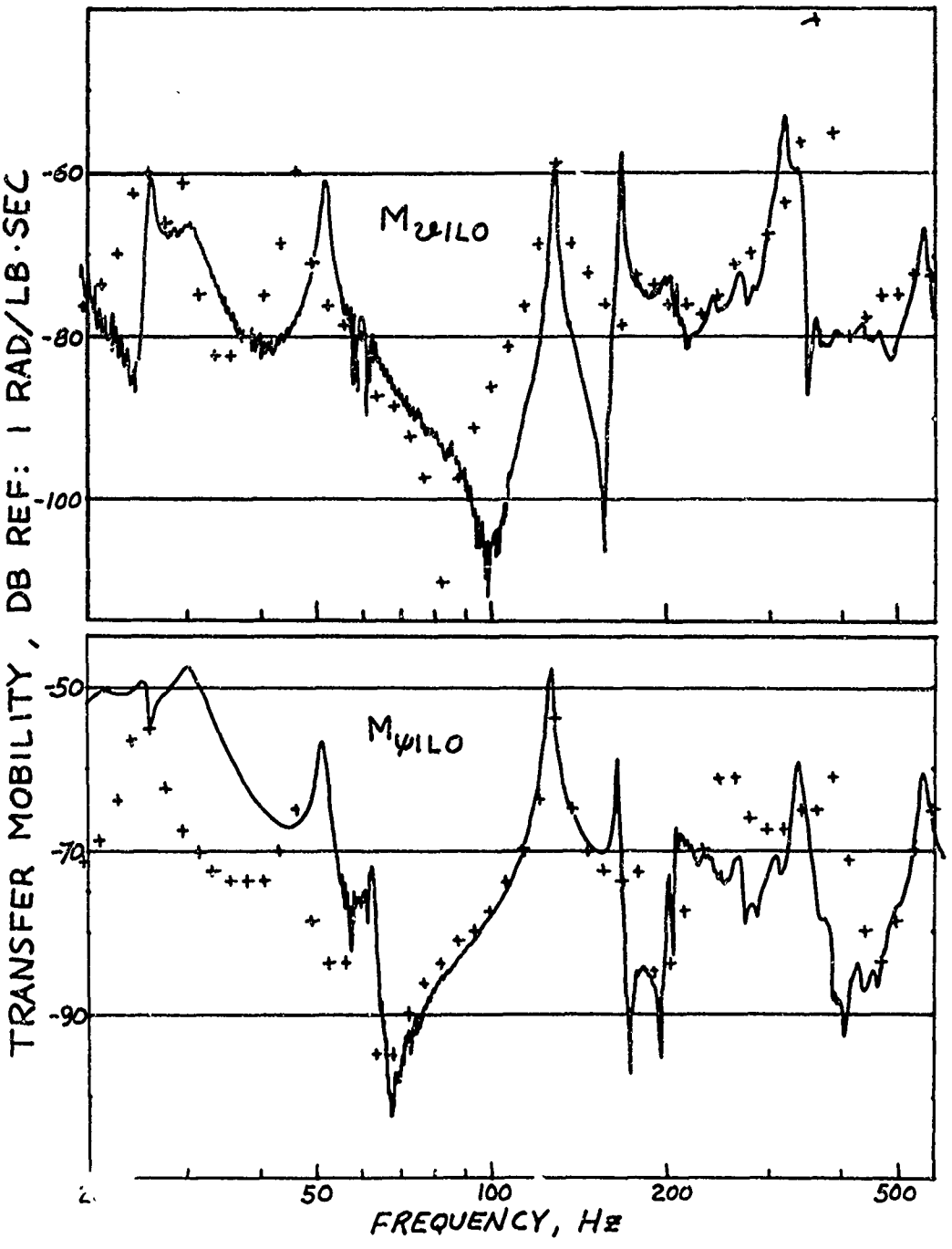

Fig. 9 - Transfer Mobilities, Liquid Filled Pipe

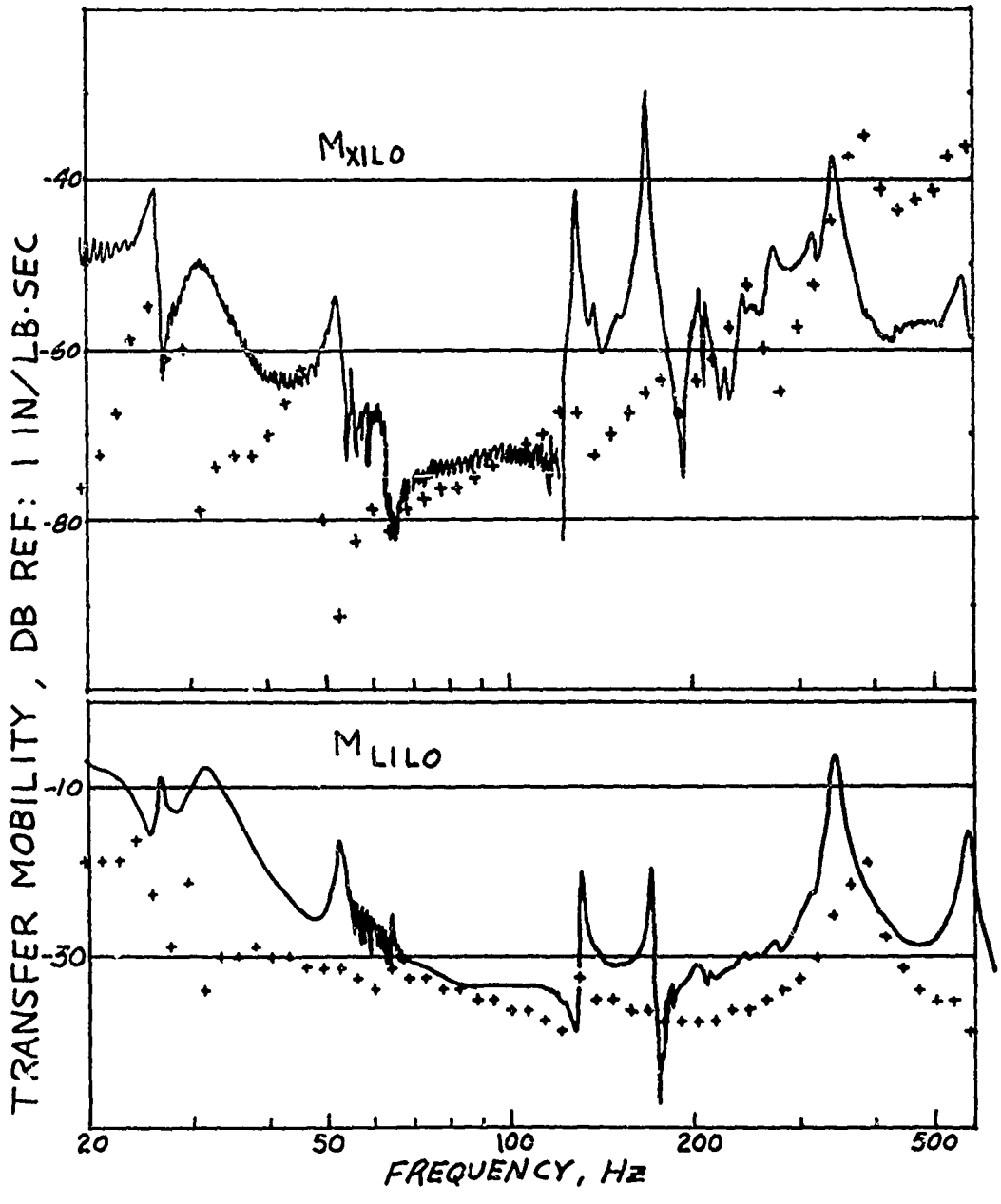

Fig. 10 - Transfer Mobilities, Liquid Filled Pipe

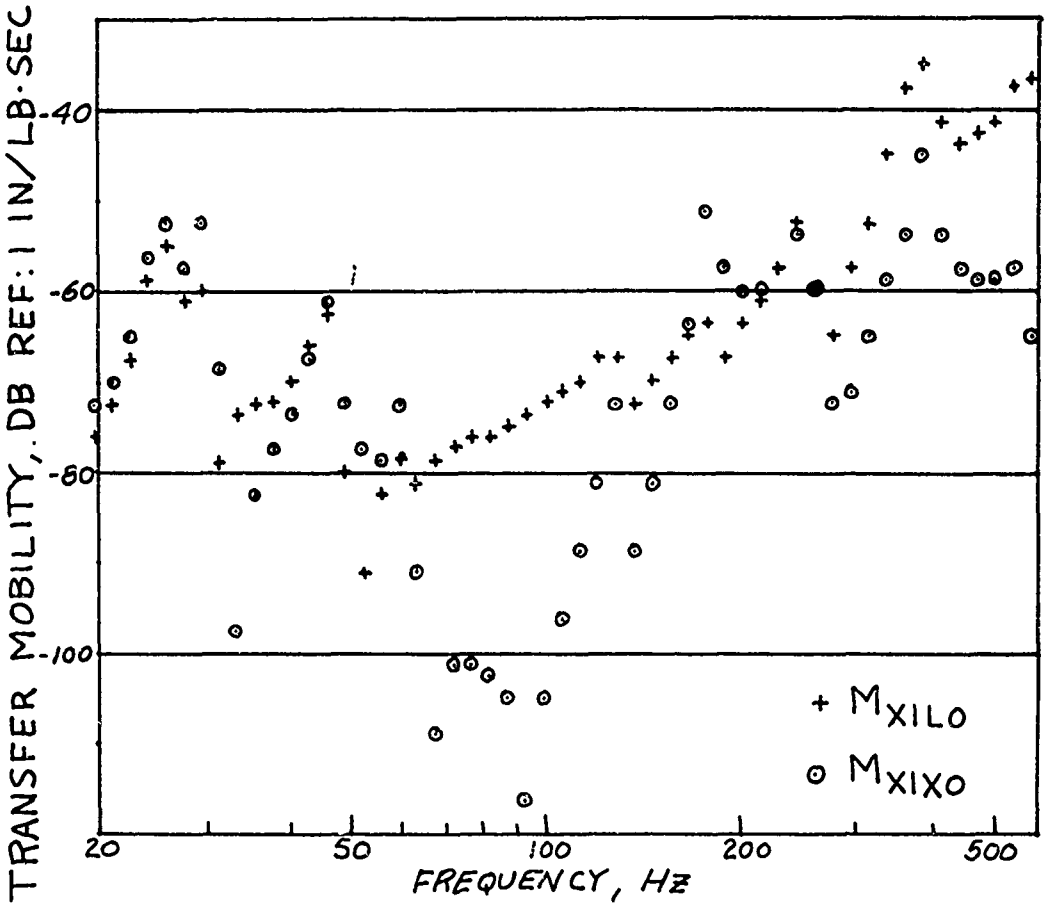

Fig. 11 - Transfer Mobilities, Relative Response Due to Liquid and Structural Excitation

REFERENCES

1. L. C. Davidson and J. E. Smith, "Liquid-Structure Coupling in Curved Pipes," The Shock and Vibration Bulletin, No. 40, Part 4, pp. 197-207.

2. Sheldon Rubin, "Review of Mechanical Immitance and Transmission Matrix Concepts," (Presented at 71st Meeting of Acoustic Society of America, Boston, Mass., 1966).

3. E. C. Pestel and F. A. Leckie, Matrix Methods in Elastomechanics, pp. 138-152, McGraw-Hill Book Co., Inc., New York, 1963.

4. E. J. Waller and L. E. Hove, "Liquidborne Noise Reduction, Final Report of Contract NObs 86437," School of Civil Engineering Research Publication No. 8, Oklahoma State University, February 1963.

5. Erwin Kreyszig, Advanced Engineering Mathematics, pp. 604-606, John Wiley and Sons, Inc., New York, 1962.

6. D. R. Jordon, A General Digital Computer Program, CODAT, for Solving Noise Transmission Problems," MEL R&D Rept 548/66, March 1967.

7. J. E. Smith, Measurements of the Total Structural Mobility Matrix," The Shock and Vibration Bulletin, Bulletin No. 40, Part 7, pp. 51-84.

Voice: Did the resonance of the fluid in the column correspond to what normally would occur?

Mr. Samsury: The prediction is on the mark as compared to the measurement. What this means is that the model is a good model.

Voice: I just wondered if you saw two compliances that dropped the frequencies a little bit lower than your calculated points.

Mr. Samsury: If anything, in generating transmission matrices to perform the theoretical analysis we had problems with respect to having a much stiffer system than we should. It took a little refining of the model to make it work.

Voice: I think you misunderstood the question.

Mr. Samsury: Yes, I did misunderstand what you meant. In the coefficient matrix of this 14 x 14 set of equations, the bulk modulus is involved in one of the liquid terms. The bulk modulus is determined on the basis of effective bulk modulus which reflects the material of which the pipe is made. In other words, yes the compliance of the system containing the fluid is included in the sound speed in the fluid.

TRANSPORTATION AND PACKAGING

A SURVEY OF THE TRANSPORTATION SHOCK AND VIBRATION INPUT TO CARGO

F. E. Ostrem

GENERAL AMERICAN RESEARCH DIVISION
GENERAL AMERICAN TRANSPORTATION CORPORATION
NILES, ILLINOIS

The shock and vibration environment encountered by cargo during transportation is reviewed. Available data describing the environment on trucks, railcars, ships and aircraft is summarized. The vibration environment is described in terms of probability of occurrence of peak accelerations (within selected frequency bands) as a function of frequency. Peak acceleration levels, 99.5%, 99%, 98%, and 90% probability levels are presented for particular vehicles covering a wide range of operating conditions. Curves are presented to show the effect of direction, load, location and speed on the environment. The shock environment is described in terms of shock spectra. Shock spectra are presented for typical events encountered during transportation, such as trucks crossing railroad tracks and backing into loading docks, railcars crossing railroad switches and railcar coupling events.

INTRODUCTION

In order to design an efficient and economical package or container to safely transport goods and material, detailed information on the transportation environment must be available. Such information is also useful for developing tests to assess the ability of new or existing packages and containers to protect or contain the contents during transportation. Designs or tests based on valid quantitative data can be cause for debate only as a result of a change in the transportation system or condition. The design or tests based on estimates or judgement are always subject to question.

Although extensive data is available on the transportation environment, the information is widely scattered and fragmented. This is a result of the approach to the transportation environment which has generally been to measure the response of cargo with little concern for the actual inputs. As such, only occasionally is there relevant data on the environment and this must be sought out in each report. Few programs have been conducted with a view toward providing basic descriptions of the transportation environment.

A survey study recently completed for the Office of Hazardous Materials of the Department of Transportation has compiled, reviewed and assessed currently available information describing the environmental conditions encountered by cargo during transportation(1). The information will be used to develop performance tests for evaluating containers used in the shipment of hazardous materials. This paper summarizes the data on two of the transportation environmental conditions, namely shock and vibration. The data covers shipments by the major transportation modes (rail, air, road and water).

Although a wealth of data exists describing the shock and vibration environment for the various modes, only selected data which presents the latest in measurement and analysis techniques is presented in this paper. More detailed information on the transportation environment is presented in Ref. (1).

VIBRATION

The vibration environment, in most studies, is defined as the motion of the surface supporting the cargo, i.e., the motion of the cargo floor of the vehicle directly adjacent or beneath the cargo. For a container restrained or in contact with the floor, this is assumed to be the input to the container. However, even this description of the environment is open to question. Measurements taken next to the container or cargo can differ from actual load inputs. It has been demonstrated in controlled laboratory tests employing a road simulator (tethered truck)(2) that although the accelerations measured directly on rigid weights

(representing the cargo load) were low when compared to the unloaded condition at the same location, the accelerations at locations removed from the neighborhood of the load were not affected much by the presence of the load. Therefore, the cargo load and the proximity of the transducers will influence the measurements, and the currently employed method of describing container input may be very conservative. A more accurate determination of load inputs would require measurements (with load cells) at the container/cargo floor interface. Other techniques are required in the event the cargo leaves the cargo floor, e.g., loose cargo.

In many of the vibration studies conducted, only measurements in the vertical direction are reported, since this direction is assumed or has been determined to be the severest. This is justified for general cargo which is loaded onto vehicles regardless of directions or labels (e.g., this side up). The vibrations are assumed to be capable of being applied to any surface of the container and thus only the direction of severest vibration environment is measured.

Road Vehicles

Typical sources of vibration to road vehicles include road surface roughness, engine, transmission and drive assembly, wheel unbalance, wheel shimmy, and wind gusts. Except for the road inputs and occasionally wind gusts, the vibration due to the other sources are kept low as a result of proper design and maintenance. For poorly maintained vehicles operating on the road, the other sources can exist and present a major source of vibration. Unfortunately, in most studies of the vibration environment on road vehicles, the vehicles are carefully selected and in excellent condition, thereby eliminating many of the potentially severe sources of vibration.

Semi-Trailers - An extensive measurement program of the vibration environment on a flatbed tractor-trailer is reported in Ref. (3). Measurements were made at various locations on the cargo floor of an unloaded tractor-trailer combination and with cargo consisting of a radioactive materials cask weighing 15 tons.

Sixteen different road conditions were encountered and identified in the study and these were traversed at different speeds. Representative data are presented for each of these conditions in the report. Probability factors were developed in the study to account for the various speed and road type combinations likely to be encountered in a cross-country trip.

The data were analyzed with a series of filters having the following bandwidths:

Bandwidth	Center Frequency
0 - 2-1/2 Hz	1-1/4 Hz
2-1/2 - 5	3-3/4
5 - 10	7-1/2
10 - 15 Hz	12-1/2 Hz
15 - 23	19
23 - 30	26-1/2
30 - 44	37
44 - 63	53-1/2
63 - 88	75-1/2
88 - 125	106-1/2
125 - 175	150
175 - 238	206-1/2
238 - 313 Hz	275-1/2 Hz

Results of the analyses are summarized in Fig. 1 for the loaded trailer. The data have been plotted at the center frequencies of the filters used in the analyses and present the probabilities of peak accelerations being less than a given value for that frequency band. The figure summarizes measurements made at various locations on the cargo floor in the vertical direction only, since these were determined to be governing. It was concluded from this study that the environment over most roads consists of low-level complex vibration upon which are superimposed a great number of repetitive shock pulses.

A question frequently raised in the description of the transportation environment is the duration of time that the various frequencies are excited. This has been determined by evaluating data reported for a typical road condition and speed. In the study described above, additional information concerning the number of peaks counted in each bandwidth is given. These peaks are presented below for the unloaded tractor-trailer travelling on level concrete at a speed of 50 miles per hour. The data have been normalized first to the lowest frequency and then to the frequency having the highest peak count ratio to frequency ratio.

Center Frequency	Peaks Counted	$\frac{P/P_1}{f/f_1}$	$\frac{P/P_1/f/f_1}{P/P_1/f/f_1 \text{ max}}$
1.25	207	1	.64
3.75	965	1.56	1.00
7.5	1350	1.09	.70
12.5	2470	1.2	.77
19.0	2948	.938	.60
26.5	6169	1.41	.90
37	7561	1.23	.79
53.5	10952	1.24	.80
75.5	9923	.80	.51
106.5	22851	1.28	.82
150	27771	1.11	.71
206.5	13041	.38	.24
275.5	24736	.99	.63

If it is assumed that a single frequency is excited all the time (corresponding to a normalized value of 1.0), the other frequencies are seen to be excited in time ranging from 24% to 90% of the trip time. Only peaks greater than 0.1 g were used in these comparisons. The frequency assumed to occur continuously is near the natural frequency of the suspension system, as would be expected.

Tractor-Trailer (Renewed) - A study similar to the one described above was conducted on a

renewed tractor-trailer combination (4). Data obtained in these tests were to show the effects of rebuilding and reinforcing the trailer. In addition to monitoring accelerations, load cells were used to monitor input loads to the cargo. However, instrumentation problems rendered the load cell data unusable.

The measured data are summarized in Figs. 2 to 4. Fig. 2 summarizes all of the data measured in the vertical direction for the various locations on the cargo floor, for all of the road types and vehicle speeds. Weighting factors were employed to account for the probability of occurrence of the various road speeds and road type combinations. Fig. 3 summarizes the same data for the lateral direction and Fig. 4, the longitudinal direction. The effect of rebuilding a tractor is seen to be a significant reduction in the vibration levels at the high frequencies. This is to be expected, since any looseness in the system would be removed.

Because of the extent of data available for this particular vehicle, additional plots are presented to show the effect of various operating conditions. Fig. 5 shows the effect of vehicle speed, Fig. 6 the effect of load, and Fig. 7 the effect of location on the environment. Only the peak and rms values of the reported data are plotted. The effect of direction of measurement is shown in Fig. 8 by a plot of the 90% probability curves of Figs. 2, 3, and 4. The curves show that over most of the frequency range investigated: (1) higher speeds result in higher levels of accelerations, (2) an unloaded vehicle experiences higher levels of accelerations than a loaded vehicle, and (3) the aft location is less severe than the forward location in the vicinity of the fifth wheel. Further, the peak levels are approximately an order of magnitude larger than the rms value.

Flatbed Truck (2-1/2 ton) - Extensive measurements have been made of the vibration environment on a 2-1/2 ton flatbed truck (5). In this study, the data have been separated to show the vibration levels under what is considered normal operating conditions and those for abnormal conditions. The abnormal conditions included: (1) driving with two wheels on the shoulder of the road, (2) driving completely on the shoulder, (3) driving off the road in desert brush, (4) driving on the median of a 4-lane highway, and (5) driving on a dirt road. Summary results of this study are presented in Fig. 9 for the normal conditions. Comparisons indicated little difference between the normal and abnormal conditions. Fig. 9 reflects factors to account for the frequency of occurrence of the various conditions investigated. The specific weighting factors for normal operating conditions were as follows.

Factors applied to road types for deriving composite descriptions of environment:

Event	Factor
1. Backing up to dock	1
2. Crossing railroad tracks	8
3. Dip	2
4. Low level to high level	2
5. Overpass	1
6. Asphalt road at 50 mph	10
7. Access road	1.5
8. Four-lane highway	1.5
9. Construction zone	1
10. Blacktop at 60 mph	10

It was concluded from the study that the severest vibrations occurred in the vertical direction and resulted from driving over potholes and bumps. The location of the cargo on the truck bed has an effect on the severity of vertical inputs with cargo located over the rear wheels getting the roughest ride.

Rail Vehicles

Vibrations in railroad cars emanate from a variety of sources. Vertical vibrations result from the unevenness or roughness of the rail, discontinuities at the rail joints, flat spots on the wheels and wheel unbalance. Lateral vibrations are caused by the tapered wheel treads and the wheel flanges. (The purpose of the tapered wheel treads is to keep the car trucks centered between the rails while the flanges of the wheels limit the lateral excursion of the car trucks.) Longitudinal vibrations result from starts, stops, slack run-outs and run-ins. These latter effects result from the inherent slack in each coupler which can build up to large values for long trains. Characteristic frequencies associated with railcar vibrations are described in Refs. (6) and (7).

Flat Car - Extensive measurements of the vibration environment on a railroad flat car are reported in Ref. (8). Data are presented for measurements in the vertical direction, the lateral direction and the longitudinal direction. The data has been replotted to the same format as the previous data and are presented in Figs. 10, 11, and 12. Events included in the data are: train leaving switching yards, stopping, crossing intersecting tracks, climbing a hill, going downhill with braking, on level runs at 40 mph, crossing switches, crossing bridges, on rough track, on curves, and in tunnels. Weighting factors were used to account for the probability of occurrence of these events when developing the summarized data. The test car was part of three different train lengths varying in size from 65 to 120 cars.

The measurements indicate that there are two frequency bands in which the highest amplitudes occur, the 0-5 Hz and the 5-10 Hz bands. It is reported that the amplitude distributions in these bands showed little resemblance to vibration type distributions. Most of the peaks in these bands were a result of transient impulses rather than steady state vibration. Above 10 Hz, the vibration levels were below .72 g In

all the requency hands analyzed, the peaks in the vertical direction were highest. As a result of this study,it was concluded that the rail environment consists of low level random vibration with a number of repetitive transients superimposed in the low-frequency ranges.

A comparison of the frequency spectra for various operating conditions (4) is shown in Figs. 13 and 14. Fig. 13 shows the effect of speed on the vibration spectra. Fig. 14 shows the effect of direction of measurement for a particular event. Only the peak and rms values are plotted on these curves.

Aircraft

Vibrations in aircraft result from runway roughness, propulsion or power plant dynamics, unbalance in propellers or rotors, aerodynamic forces and acoustical pressure fluctuations. In addition, the surrounding air will also induce vibrations due to its turbulent nature. The air has vertical components of velocity which impart vertical accelerations to the aircraft.

Characteristic frequencies associated with the propeller-driven aircraft are the propeller blade passage frequencies.

Helicopter - The results of a recent study of the vibration environment on helicopters is presented in Ref. (9). The helicopter, an HH43B, has a pair of contrarotating rotors with blades 47 feet long and is powered by a turbo-jet engine. The events included in the study were: motor starts, rotor engagement, take-off, hover, climb, cruise 90 knots, straight flight and descent. A summary plot of this data is presented in Fig. 15. The curve includes measurements recorded at various locations for the various events. Weighting factors are applied to the data for particular events to account for the frequency of occurrence of the events. Some conclusions from this study were: (1) hovering produces the severest environment while rotor start and engagement produces the least, (2) the longitudinal direction produces the severest environment, and (3) straight or level cruise results in insignificant levels when compared to hover, climb and high speed events.

Turbojet - Statistical data describing the vibration environment on an NC-135, a version of the commercial 707 jet, is reported in Ref. (10). The severest environment was measured in the vertical direction and occurred during take-off. The data are presented in Fig. 16 in terms of the peak values and the probability of peaks being less than indicated levels. The data, however, only applies to one location on the floor of the aircraft.

Ships

Typical sources of vibration in ships include the propellers, the propeller shafting, the power plants, auxiliary machinery, and the hydrodynamic forces as the ship passes through the water. The hydrodynamic forces include those resulting from slamming, pounding and the wave-induced motion of the ship. Slamming is defined as the impacting of the ship with the water after the bow has left the water. Pounding is the impacting of the waves on the ship when all portions of the bottom are submerged. Wave-induced motion is the motion of the ship in response to the waves, excluding those resulting from slamming and pounding. A complete description of vibration sources in ships is given in Ref. (11).

A characteristic vibration frequency associated with ships is the blade passage frequency which results from the non-uniform pressure field acting on the hull as each propeller blade passes close to the hull.

As with other modes of transportation, proper design and maintenance reduces the severity of many of the sources of vibration. In addition, operational restrictions may be imposed to reduce the levels of vibration. For example, ships may be requested to reduce speed in rough water in order to prevent slamming, or ships may be routed around rough seas.

Much of the ship vibration studies have been conducted in quiet water on straight runs at various propeller speeds. Maneuvers and crashbacks (sudden reversal of direction) which generate higher levels of vibration than straight runs are also conducted.

In the past, the vibration levels for rough seas were established by using estimated magnification factors. The factors were based on experience and some scattered data and were applied to vibration levels measured in calm seas (Ref.(11)).

Dry Cargo Vessel - An extensive measurement program of the vibration environment on cargo vessels is reported in Ref. (12). Data on extreme values of load conditions to which cargo might be subjected is described. Seven accelerometers were installed at various locations aboard a 520-foot dry cargo ship operating in regular North Atlantic service. Data were recorded intermittently over a 15-month period.

The vibrations recorded aboard the ship included only the seaway-induced motions characterized as slamming, whipping and wave-induced acceleration. It is reported that the wave-induced frequencies ranged from 0.030 to 0.205 Hz, while slamming-induced transients having two basic components of 11.4 and 4.6 Hz. The whipping component of the ship induced by slamming occurred at 1.5 Hz.

During the test period, the wave-induced acceleration reached a maximum of 0.88 g (zero to peak) in the vertical direction at the bow. Slamming, or the impacting of the ship after it has left the water, produced higher frequency accelerations (approximately 10 Hz) in excess of 1.5 g's (zero to peak). Statistical analyses were only conducted on the wave-induced accelerations, since it is reported that sufficient data

were not recorded for slamming events. The results are presented in Fig. 17. The data are presented in terms of G_{rms} versus probability of occurrence. It can be seen that the bow vertical accelerations were most severe, followed closely by the transverse direction and the stern vertical direction. Fore and aft or longitudinal accelerations were least severe (approximately 40% of the bow vertical). The bow (vertical) was also most severe for slam. A technique for extrapolating the data to extreme values is also presented. Based upon the analysis, it is reported that the most probable maximum bow acceleration on the vessel, operating on the same route over a seven year span, would be 2.97 g's (peak to peak).

SHOCK

Shock is defined as a sudden and severe non-periodic excitation of an object or system. In most studies, it is defined as the motion of the cargo floor or platform on which the cargo or container is supported. Since there is no precise distinction between vibration and shock, the data in some instances has not been reported separately.

In this paper, shocks are described in terms of shock spectra when available. (A shock spectra is the response of a series of single degree-of-freedom systems to the excitation.) This is considered the most descriptive format for the complex transient inputs. It provides a convenient means for comparing a large amount of data describing very complex motions. It also gives information on the energy levels as a function of frequency of the shock excitation.

Truck - Shock inputs occurring during truck transportation include bumping into loading docks, crossing railroad tracks, cattle guards, and other transient road inputs.

Shock spectra for typical shock events encountered by a rebuilt tractor-trailer combination (4) are shown in Figs. 18 and 19. Fig. 18 is for the loaded tractor-trailer crossing railroad tracks at 40 mph. Fig. 19 is a spectra for the semi-trailer traversing a dip in the road at 40 mph.

Damping factors (C/C_c) used in computing the shock spectra generally range from zero to one. A commonly used ratio is .03 to .05 which is the damping in most structures. Zero damping provides an upper limit on the shock spectrum while .10 is characteristic of shock isolation systems.

Shock spectra for typical events encountered by a two and one-half ton flatbed truck (4) are shown in Figs. 20 and 21. Fig. 20 applies to the input resulting from crossing railroad tracks at a slow speed and at 45 mph. Fig. 21 is a shock spectra computed from longitudinal inputs resulting from the truck backing into a loading dock.

Shock spectra envelopes for an air ride suspension van are reported in Ref. (13) and are shown in Fig. 22. The curves envelope the maximum shock spectra in each direction for the various events encountered during a cross-country shipment.

Rail - Shocks to cargo in railroad cars result from: car switching or humping operations, stops, starts, slack take-up in the coupling systems, and transient inputs from the track.

Shock spectra for inputs resulting from slack run-ins and run-outs are shown in Fig. 23. (4) The curves envelope spectra for a number of events and are separated into longitudinal, vertical and lateral directions. Run-in and run-out shocks result from the inherent slack which exists in each coupler. While the slack is small for each coupler, the total slack for a long train is large. The accumulated slack produces a longitudinal whip action when the train moves up or down hills. These shocks are most severe for cars near the end of the train.

Shock spectra envelopes for inputs resulting from road crossings and switch crossings are shown in Fig. 24. The envelope curves have been separated to indicate the levels for the three directions (longitudinal, vertical and lateral).

The severest shock loading for railcars occurs during coupling or humping operation. The automatic feature of railcar couplers requires that they be impacted together to actuate the couplers. Due to uncontrollable factors (equipment and operators) affecting railcar accelerations during make-up of trains at a railroad yard, there is a wide variation in coupling speeds.

The shock levels resulting from coupling impacts are dependent primarily on the car weight, impact velocity, and the type of shock absorbing system (draft gear) on the coupler. A standard draft gear allows a travel of approximately four and one-half inches before bottoming. Cushioned underframes or cushioning draft gear have a travel of as much as 30 inches. Thus the car can be brought to a stop in a much longer time and therefore with lower deceleration.

Envelopes of shock spectra for common impact speeds of 2 to 5 mph are shown in Fig. 25. (4) Curves are presented for the longitudinal, vertical and lateral directions. Although 2 to 5 mph is a common coupling speed, a frequently used upper limit is 10 or 11 mph. This impact speed includes a high percentage (approximately 98%) of all impacts.

Air - Shock excitations occur in aircraft as a result of landing impacts, braking, and gust loading. Recent studies of the shocks encountered during landing operations with modern aircraft have shown that this event produces relatively low levels of shock when compared to other events. Extensive measurements of aircraft response to landing impacts have been made with the NASA velocity-acceleration-height (VGH)

recorder. The measurements are read directly from the records and reported in terms of peak acceleration. Spectral analyses are not performed. Typical results (14) showing the probability of exceeding given accelerations during landing impacts are presented in Fig. 26. The data shows that only once in 1000 landings did the normal acceleration reach 1.1 g's.

Extensive measurement programs of the gust loading of aircraft have also been conducted. However, as with the landing shocks, most of the data has been measured with the VGH recorder and has therefore been reported in terms of peak accelerations of the aircraft center of gravity. Typical data (14) showing the occurrence of gust accelerations per nautical mile are shown in Fig. 27 for a four-engine turbo-jet transport.

Ship - Shock loadings occurring on ships result from slammings and impacts with piers during docking operations. In general, both of these events are controlled to a large degree, resulting in very low shock levels. Data has not been reported describing the shocks encountered during docking. Data on ship slamming are generally included in the description of the vibration environment. Ref. (12), for example, describes a slam event as having a peak of 1.5 g's (zero to peak) with frequency components of 11.4 and 4.6 Hz.

DISCUSSION

Comprehensive descriptions of the transportation shock and vibration environment for typical transport vehicles are currently available. Data on the vibration environment defines the maximum acceleration as a function of frequency and also the probability that acceleration peaks are below specified levels. The data indicates that only occasionally do the acceleration peaks reach the maximum values. Comparisons of maximum peak values with root mean square values indicates an order of magnitude difference in some instances. Thus extrapolation from rms to peak value or the reverse can yield erroneous values when the commonly used factors of three or four (sigma) are used.

Shock data is available in terms of shock spectra which facilitates the comparisons of the very complex transient events. Fig. 28 compares the shock spectra for typical events on truck and railcar. The severest of the shock events is seen to be that which occurs during coupling events. The least severe shocks were those measured on an air ride suspension van.

The available data on shock and vibrations is generally applicable to transport vehicles which are well maintained. Thus the descriptions may not apply to systems which are poorly maintained and could be used in the shipment of general cargo. Further, the data is only applicable to cargo which is restrained or always in contact with the cargo floor. There is a total lack of data describing the shock and vibration environment encountered by unrestrained or loose cargo. Techniques are required to measure the shock and vibration environment on loose cargo and to translate the data to laboratory tests.

REFERENCES

1. Ostrem, F. E.; Libovicz, B. A.: A Survey of Environmental Conditions Incident to the Transportation of Materials. GARD Report 1512-1, Contract DOT-OS-00038, May, 1971.
2. Clements, E. W.: Measurement and Analysis of Acceleration Environments Generated by NRL Rough Road Simulator. Naval Research Laboratory, NRL Report 2097, Feb., 1970.
3. Foley, J. T.: The Environment Experienced by Cargo on a Flatbed Tractor-Trailer Combination. Sandia Corporation Research Report SC-RR-66-677, Dec., 1966.
4. Anon.: Data Package of 182 Documents from AEC/DOD Environmental Data Bank. Sandia Laboratory, Albuquerque, New Mexico, Feb., 1971.
5. Foley, J. T.: Normal and Abnormal Environments Experienced by Cargo on a Flatbed Truck. Sandia Laboratory Development Report SC-DR-67-3003, Feb., 1968.
6. Milenkovic, V.: Feasibility Study for a Wheel-Rail Dynamics Research Facility. General American Research Division, Dec., 1968, DB 182472.
7. Luebke, R. W.: Investigation of Boxcar Vibrations. DOT, Federal Railroad Administraction Report No. FRA-RT-70-26, Aug.,1970.
8. Gens, M. B.: The Rail Transport Environment. The Journal of Environmental Sciences, July/August, 1970, pp. 14-20.
9. Gens, M. B.: A Preliminary Observation of the Dynamic Environment of Helicopters. Institute of Environmental Sciences, 1968 Proceedings, pp. 423-432.
10. Harley, R. A.: Impromptu Vibration Data Acquisition with EL 1-31 Recorder. Institute of Environmental Sciences, 13th Annual Technical Meeting Proceedings, Vol. 1, April 10-12, 1967, pp. 83-93.
11. Buchmann, E.: Environmental Vibration on Naval Ships. Technical Note AVL-244-962, Naval Ship Research and Development Center, April, 1969.
12. Bailey, F. C.; Fritch, D. J.; Wise, N. S.: Acquisition and Analysis of Acceleration Data. Report SSC 159, Ship Structure Committee.
13. Schlue, J. W.; Phelps, W. D.: A New Look at Transportation Vibration Statistics. Bulletin 37, Part 7 (of 7 parts), Jan., 1968, The Shock and Vibration Bulletin.
14. Hunter, P. A.; Fetner, M. W.: An Analysis of VGH Data Collected from One Type of Four-Engine Turbojet Transport Airplane. NASA TN D-5601, Jan., 1970.

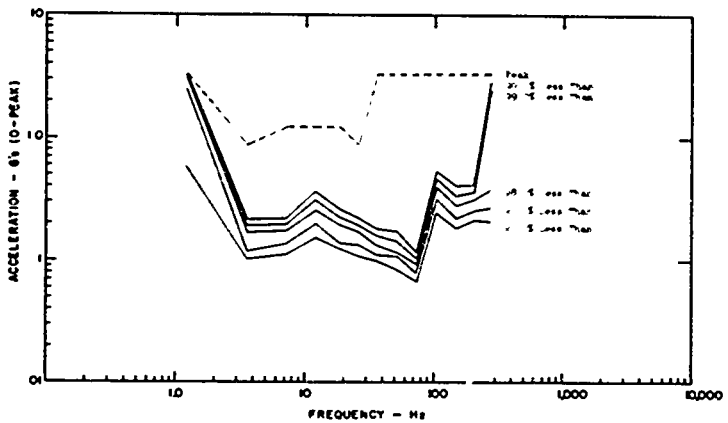

Fig. 1 - Frequency spectra, tractor-semitrailer, vertical direction

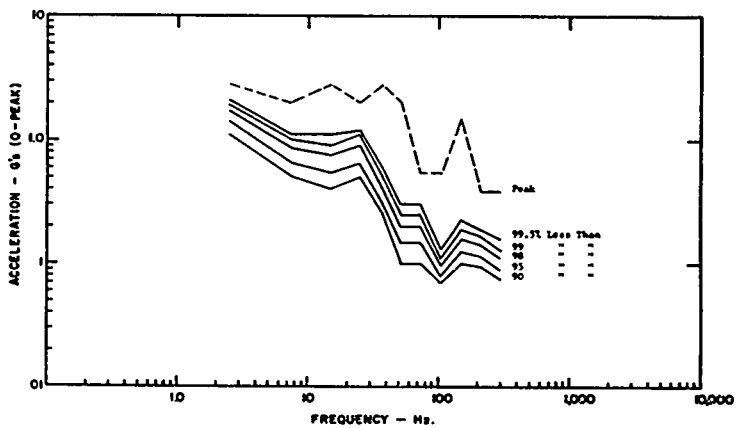

Fig. 2 - Frequency spectra, tractor-semitrailer (rebuilt), vertical direction

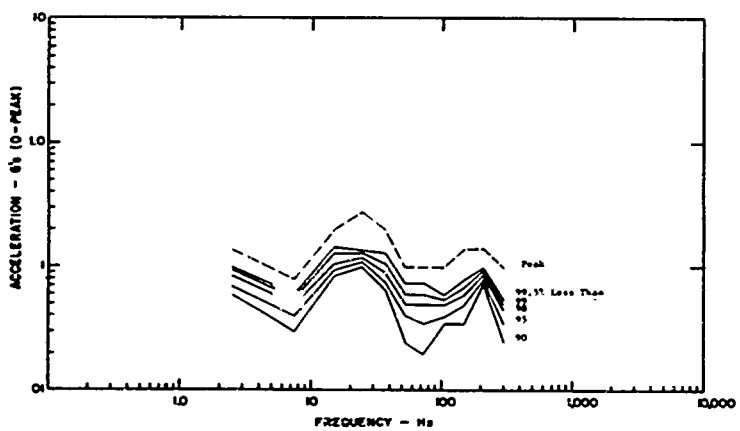

Fig. 3 - Frequency spectra, tractor-semitrailer (rebuilt), lateral direction

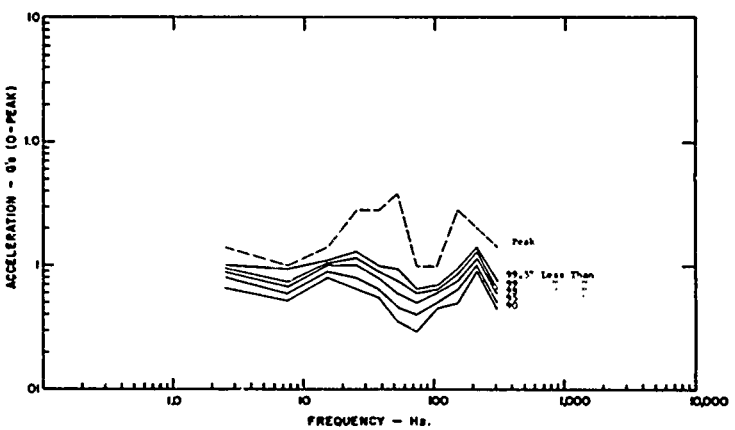

Fig. 4 - Frequency spectra, tractor-semitrailer (rebuilt), longitudinal direction

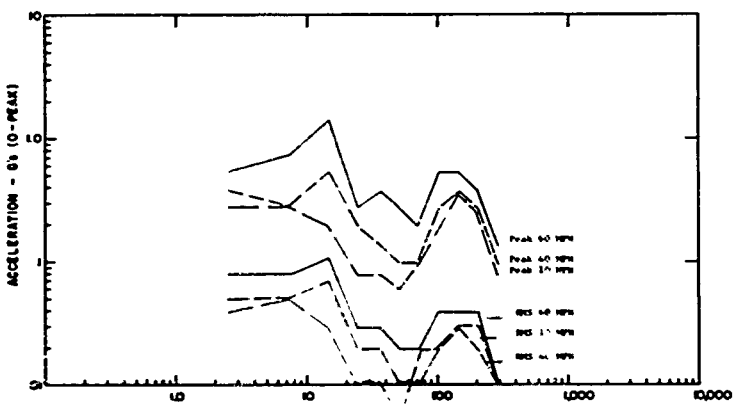

Fig. 5 - Frequency spectra, tractor-semitrailer (rebuilt), 10 mph, 40 mph and 60 mph

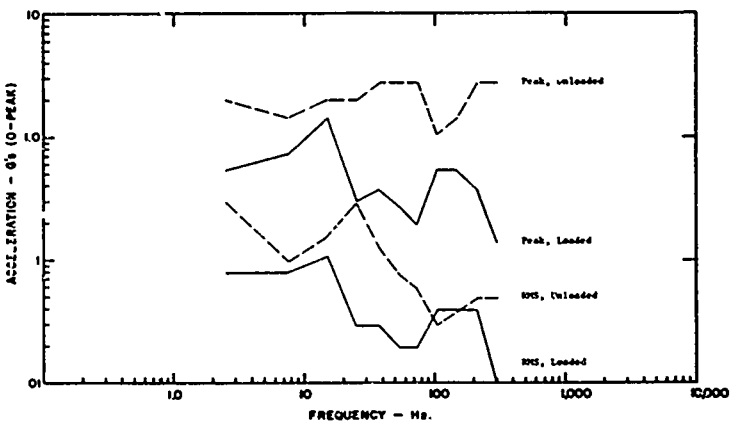

Fig. 6 - Frequency spectra, tractor-semitrailer (rebuilt), loaded and unloaded

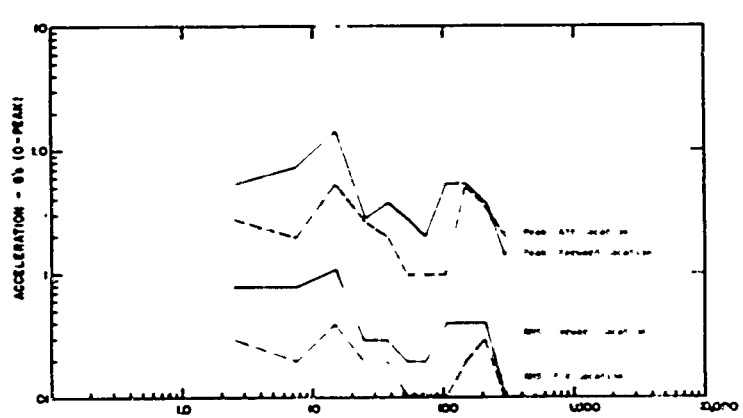

Fig. 7 - Frequency spectra, tractor-semitrailer (rebuilt), forward and aft locations

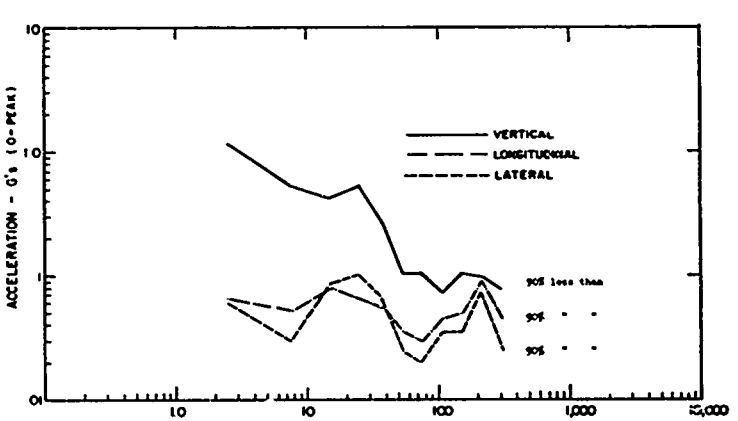

Fig. 8 - Frequency spectra, tractor-semitrailer (rebuilt), vertical, longitudinal, lateral

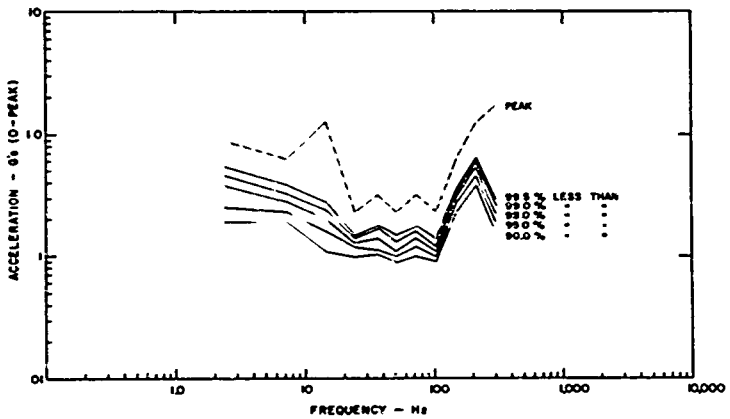

Fig. 9 - Frequency spectra, 2-1/2 ton flatbed truck, vertical direction

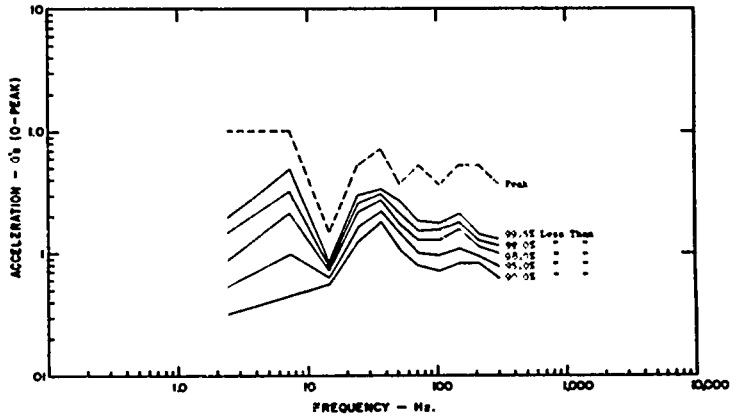

Fig. 10 - Frequency spectra, railroad, vertical direction

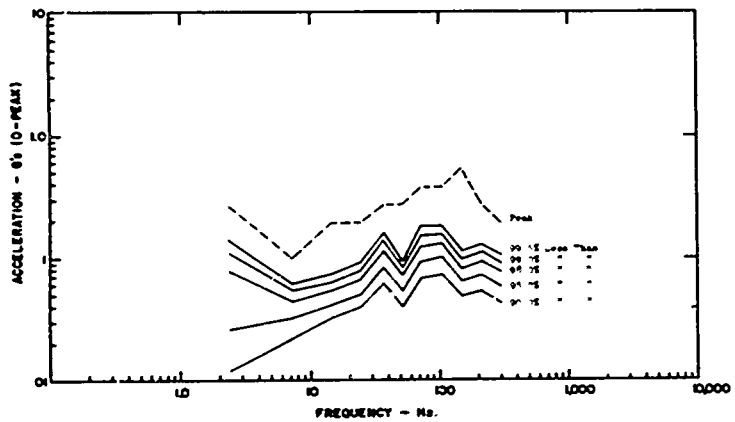

Fig. 11 - Frequency spectra, railroad, transverse direction

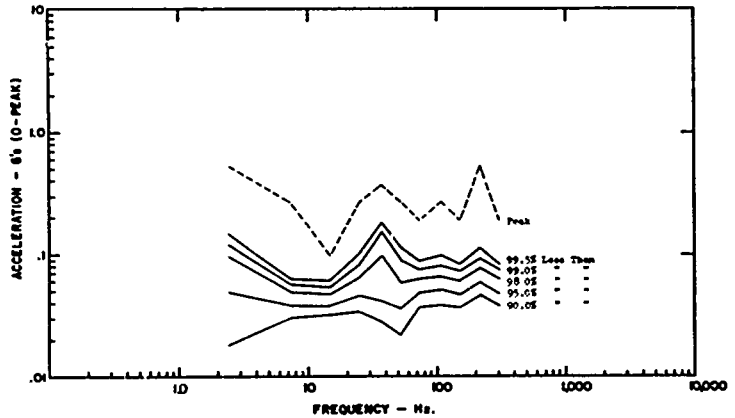

Fig. 12 - Frequency spectra, railroad, longitudinal direction

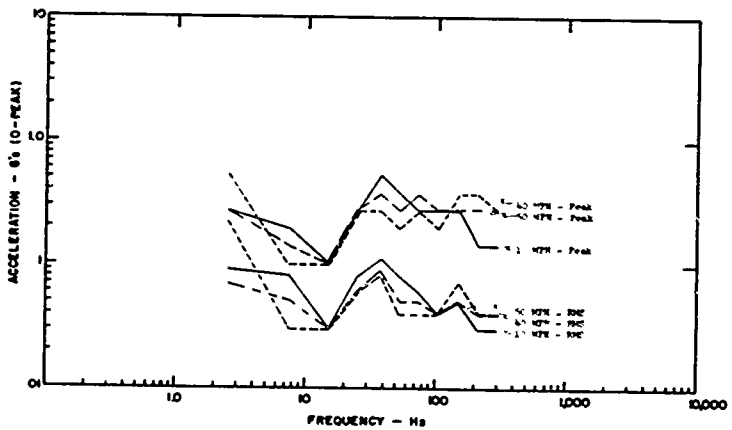

Fig. 13 - Frequency spectra, railroad flatcar, 10 mph, 40 mph, 50 mph

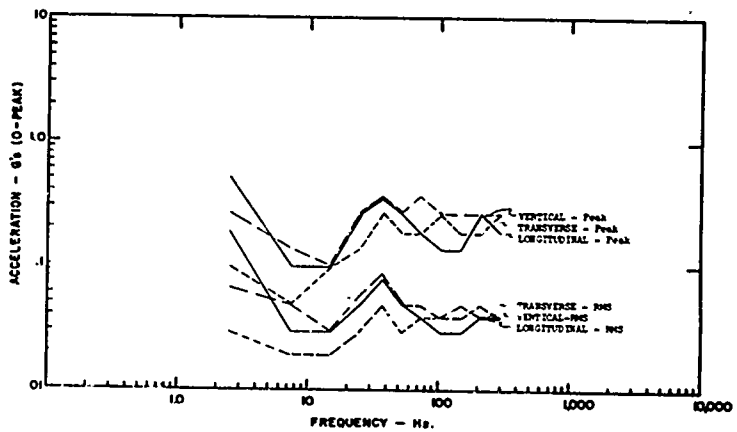

Fig. 14 - Frequency spectra, railroad flatcar, vertical, transverse, longitudinal

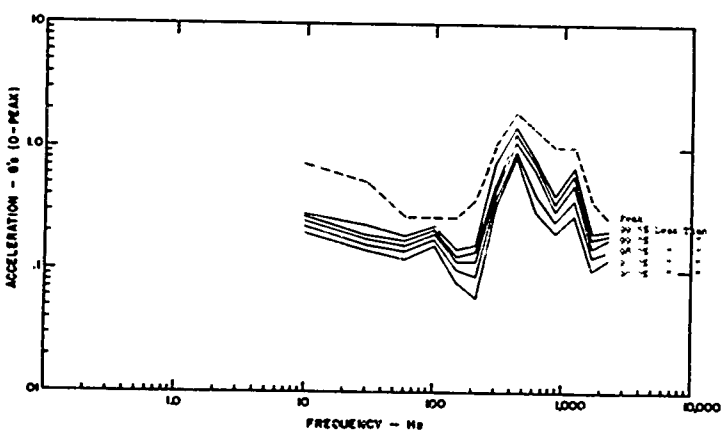

Fig. 15 - Frequency spectra, HH43-helicopter, all directions

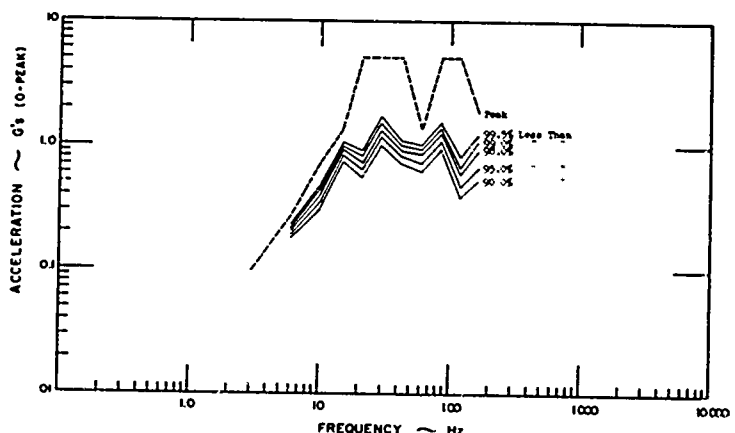

Fig. 15 - Frequency spectra, turbojet aircraft, vertical direction

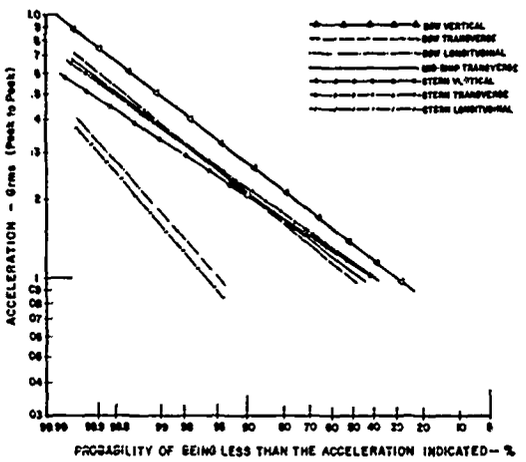

Fig. 17 - Ship-acceleration vs probability of occurrence

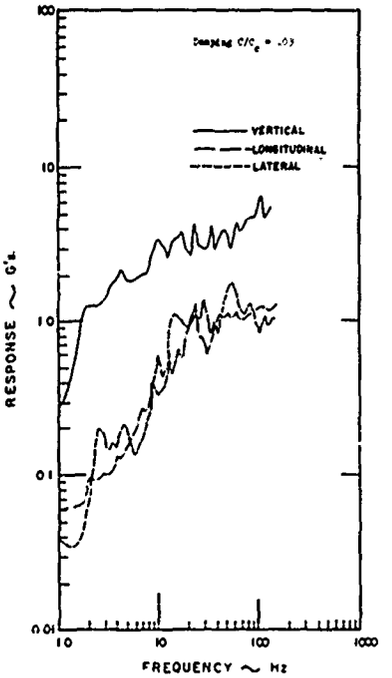

Fig. 18 - Shock spectra, tractor-semitrailer (rebuilt), crossing railroad tracks at 40 mph

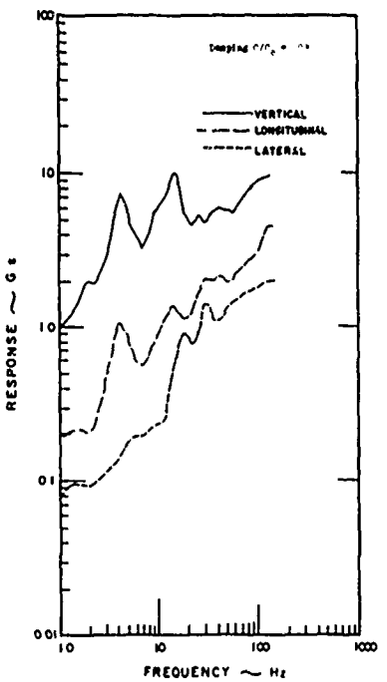

Fig. 19 - Shock spectra, tractor-semitrailer (rebuilt), dip at 40 mph

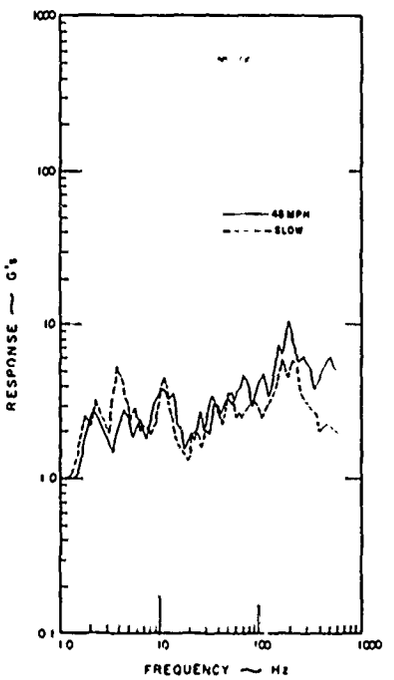

Fig. 20 - Shock spectra, 2-1/2 ton flatbed truck, railroad crossings

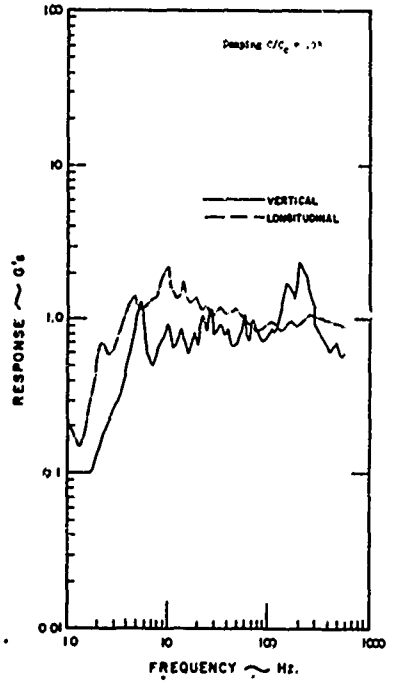

Fig. 21 - Shock spectra, 2-1/2 ton flatbed truck backing into loading dock

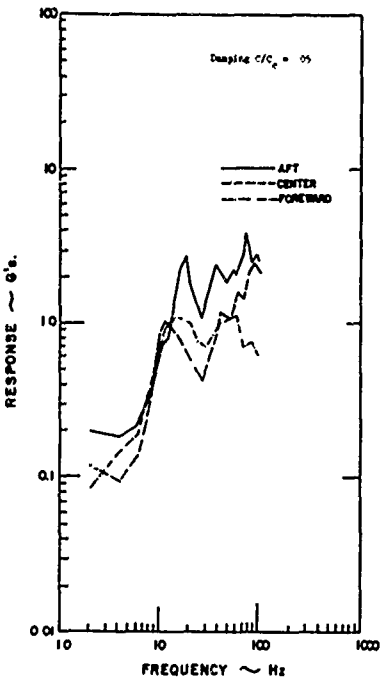

Fig. 22 - Shock spectra, tractor-trailer air-ride van

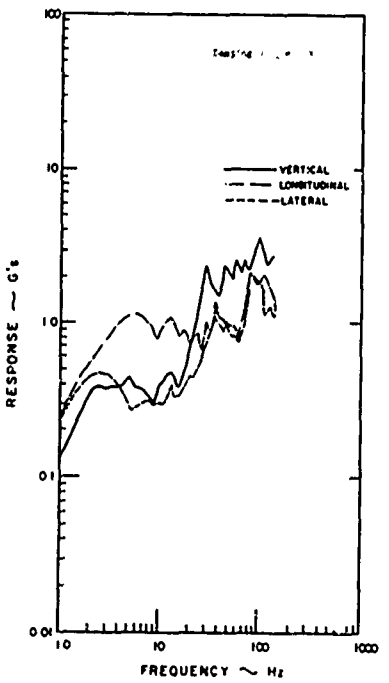

Fig. 23 - Shock spectra, railroad, slack runs ins/outs

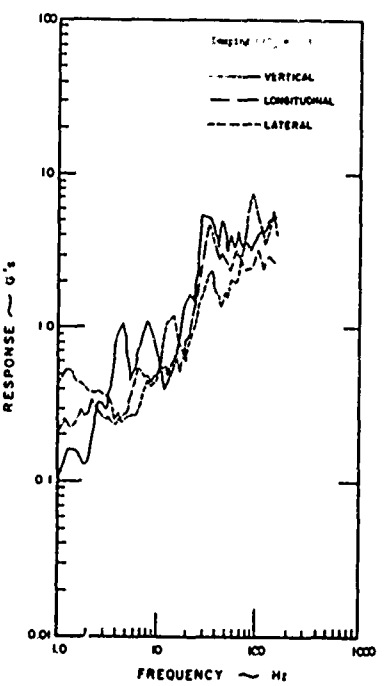

Fig. 24 - Shock spectra, railroad, road crossings, intersecting track, and switches

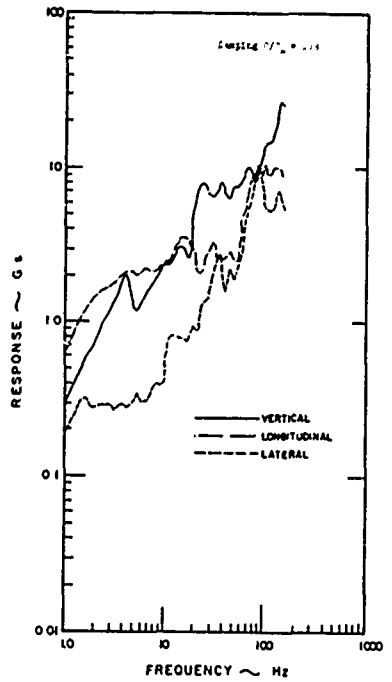

Fig. 25 - Shock spectra, railroad coupling (2-5 mph)

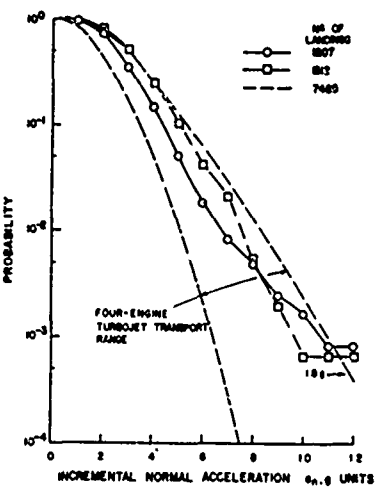

Fig. 26 - Landing-impact accelerations, turbojet aircraft

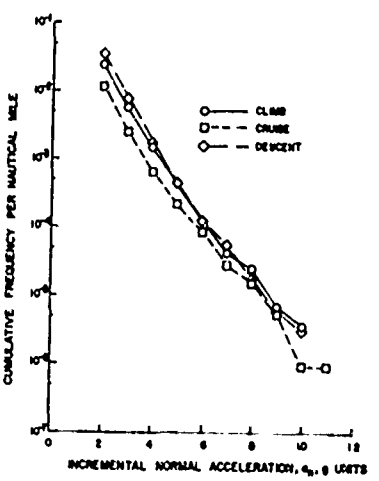

Fig. 27 - Gust accelerations, turbojet aircraft

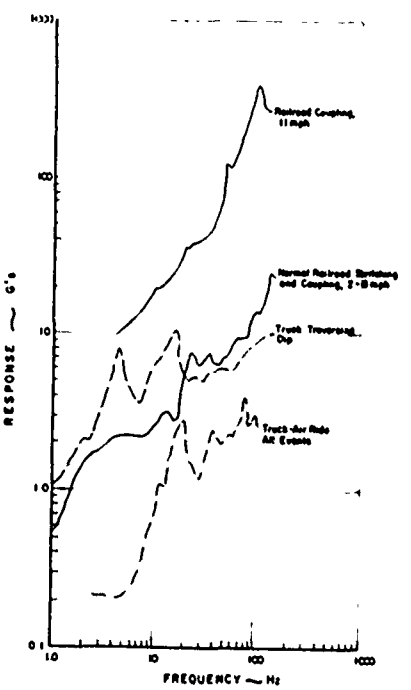

Fig. 28 - Summary of typical transportation shock events

DISCUSSION

Voice: What kind of instrumentation did you use to get this information?

Mr. Ostrem: This was a review, and we did not make any measurements. Most of the data has been developed by the Sandia Corporation. Maybe Mark Gens from Sandia would like to comment on the particular type of instrumentation that is used.

Mr. Gens: We will put you off until the next paper. The same instrumentation was involved.

Mr. Gaynes (Gaynes Testing Laboratories): First of all, you showed the rebuilt tractor. Were you able to get comparisons with a new tractor that had not been rebuilt?

Mr. Ostrem: Not on a new tractor; but the first slide presented data on a non-rebuilt tractor. The first one was just a typical tractor-trailer. The second was rebuilt.

Mr. Gaynes: What about freight cars? Is the difference in car age and rebuilt cars apparent in freight cars too?

Mr. Ostrem: Yes, this is one of the biggest problems. Most of the vehicles are carefully selected and this is the one drawback. It is not the information that would be applicable to general cargo where there is no option on the vehicle to be used.

Mr. Gaynes: Are you showing higher g forces at the higher frequency range as shown above about 10 cycles per second as compared to where we have been working in the past?

Mr. Ostrem: Yes, I think that is generally true.

Mr. Gaynes: In the past we have worked with much lower levels.

Mr. Ostrem: If you are talking about packaging, I think you are trying to point out that most of this is damped out before it reaches the package. I think this is one of the big problems. We do not have any information that would relate to the actual cargo. The response of so-called loose cargo is what we really need to know and we have no data on that.

Mr. Westine (Southwest Research Institute): When I looked at your curves for different velocities, I wondered if you could improve results and reduce the data to a single curve by non-dimensionalizing the accelerations. For example, you might multiply acceleration by a characteristic length and divide by the velocity squared. I notice that your axis numbers are nondimensional, in essence, and the curves are all similar in shape. It seems to me that you may be able to telescope all these different velocity curves into a single curve. Have you tried this?

Mr. Ostrem: No, I have not.

Mr. Clevenson (NASA Langley Research Center): First let me compliment you on a fine compilation of quite a bit of data. It is very interesting. I do have a question, however. The first half of your slides all started at 20 cycles-per-second. Does this imply that there are no data in the low frequency range down to half a cycle or so? I think most of us realize the low frequencies are also vitally important.

Mr. Ostrem: Yes, I think that is a good point. Some of the data did go down to about 2 Hertz. What we are really lacking is the low frequency, the so called rolling or rocking frequency information. Workers in the field are just starting to collect data in this area. The feeling is that this environment is doing a lot of damage, particularly for loose cargo. When cargo is stacked, many problems can occur due to this low frequency rocking phenomenon. No, I am not implying that there is no problem below 20 cycles. We are waiting for environmental investigators to generate information on the low frequency phenomena.

Mr. Monroe (Babcock & Wilcox): Do you have any data on barge shipments?

Mr. Ostrem: No, all I can do is refer you to the one study that was recorded in one of the Shock & Vibration Bulletins* and that was in the shipment of a Saturn rocket on a tote barge.

Mr. Deitrick (Hughes Aircraft Company): Why is not more work done in presenting this data in the form of PSD's. John Schlue of JPL, some years ago, put out the only work I have seen in this respect. By using peaks, you very

*R.W. Fruedell and K. E. Elliott, The Dynamic Environment of the S-IV Stage During Transportation, Shock and Vibration Bulletin 33, Part IV, p. 111, Naval Research Laboratory, Washington, D. C., 1964.

often wind up with a very conservative evaluation of the transportation environment.

Mr. Ostrem: I think the main reason is that most testing laboratories, at least for package evaluation, do not have the sophisticated random vibration equipment necessary for testing. They are trying to stick with some presentation relating to peak value and a sinusoidal frequency. Maybe, for very sophisticated cargo, one would go to other methods. I think some of the later papers will discuss that.

THE DYNAMIC ENVIRONMENT OF SELECTED MILITARY HELICOPTERS*

Mark B. Gens
Sandia Laboratories
Albuquerque, New Mexico 87115

The purpose of the study was to determine the dynamic input to cargo from the floor of the cargo space in the OH-6, UH-1, CH-46, and CH-47 helicopters. The instrumentation, test procedures, data reduction processes, and results are discussed. The vibration regime for helicopters is shown to consist of a base of Gaussian random excitation with superimposed decaying sinusoids which are associated with rotor activity.

INTRODUCTION

The increased use of helicopters for the transport of military supplies has caused interest in the dynamic input of this type of aircraft to cargo. Since the Environmental Criteria Group of Sandia Laboratories is charged with the task of supplying descriptions of the environmental levels which will be encountered during the life of AEC/DOD systems, it became essential that the dynamic environment of cargo during helicopter transport be a part of those descriptions. A literature search revealed little information on dynamic input measurements in the cargo space and that which was available was fragmentary because of specific areas of interest. In view of the Environmental Criteria Group's mission and the availability of instrumentation, it was decided to measure the environment and produce a spectrum of vibration in helicopter cargo compartments.

Since no firm data were available, the first step taken was to measure the dynamic input of an aircraft of convenience, even though not a likely cargo carrier, to attempt to define parameters for further work. This effort, reported elsewhere [1], suggested several areas of inquiry:

A. A specific effort should be made to measure low (0-10 Hz) frequency excitation.

B. The presence or absence of a series of decaying sinusoids needed to be investigated.

C. Data should be obtained during landing.

With these points in mind, a program was undertaken to define the dynamic environment of helicopter cargo spaces.

The helicopter differs from other aircraft in that it is supported by a rotary rather than a fixed wing. While airborne, the rotary motion tends to exert torque on the fuselage of the craft with the result that, failing correction, the fuselage has a tendency to rotate also. Two general methods have been employed to control this unwanted, if not dangerous, motion. One is to provide in the tail area a vertical propeller which exerts a countertorque equivalent to the force exerted by the rotor. The second control method is to provide countertorque by means of a contrarotating rotor. The latter has the advantage of providing lift and drive capability as well as rotary control. Helicopters employing each of these types of control needed to be considered.

THE HELICOPTERS

In addition to the plane used in the preliminary work (the HH43) two examples of each type were employed to derive data.

A. Contrarotating types:

1. CH46

2. CH47

*This work was supported by the U. S. Atomic Energy Commission.

B. Vertical propeller types:

1. OH6

2. UH1

The CH47, OH6, and UH1 were made available by the U. S. Army Aviation Board at Ft. Rucker, Alabama, while the CH46 was made available by the U. S. Marine Corps. at the Patuxent Naval Air Station, Maryland.

Both the CH46 and CH47 aircraft are primarily cargo-carriers. They are very similar in appearance, both built by the Vertol Division of Boeing Aircraft Company, both powered by two turboshaft engines. They are slightly different in size, the CH46 being 84 feet long and 16 feet high with 51 foot diameter rotors while the CH47 is 99 feet long, 19 feet high and has 60 foot rotors. The rotors are mounted fore and aft and rotate counter to each other. For the purposes of this work, the principal difference between them was that the CH47 has an isolated floor in the cargo compartment while the CH46 does not. The CH46 cruises at 110-120 knots while the faster CH47 cruises at 140 knots. The rotor speed of the latter is 230 rpm (3.83 rps).

The OH6 is primarily an observation plane but is adaptable to carriage of small cargo by removal of cabin seats. Manufactured by Hughes, it is 30 feet long and 8.5 feet high. The rotor is 26 feet in diameter. It has a cruise speed of 110-120 knots. Rotor speed is 465-514 rpm (7.75-8.57 rps). It is powered by a single turboshaft engine.

The UH1, built by the Bell Helicopter Co., is considered a utility aircraft. It may be used to carry up to seven passengers or approximately 300 pounds of cargo. It is 57 feet long, 14 feet high, and has a 48-foot rotor. Powered by a single turboshaft engine, it cruises 85-120 knots and has a rotor speed of 294 to 324 rpm (4.9-5.4 rps). (The specifications for all helicopters were taken from the respective pilot's manuals and Ref. [2].)

THE TEST PLAN

The test plan was developed partially as a result of the preliminary work and partially during conversations with the pilots. The standard data points which were established were:

A. Lift off

B. Low hover

C. Take-off

D. Low cruise

E. Climb

F. High cruise

G. Descent

H. Low flight

I. Turn

J. Hover

In addition to these, data points of opportunity, such as maximum power take-off, hover at three feet, at twenty-five feet, and clear air turbulence were sampled.

While helicopters are capable of direct take-off in a vertical direction, two factors tend to limit the frequency of such action. First, when operating from a standard airfield with its attendant traffic, the helicopter must move from its pad into the regular traffic pattern in order to take-off. Secondly, for aircraft with skids, this must be accomplished while out of contact with the ground. Often the wheeled helicopters do the same. Thus the sequence of events includes liftoff to a height of two to three feet, then moving to the edge of the runway and finally, on receipt of tower clearance, take-off which usually combines lift and forward motion. For these reasons, the test sequence shown was used.

INSTRUMENTATION

The instrumentation consisted of two clusters of accelerometers. One array was a triaxial set of piezoelectric accelerometers; the other a triaxial set of piezoresistive accelerometers. Each group was mounted on an aluminum block which in turn was mounted on the cargo floor at a structural member. With the exception of the CH47, the airframe structure supported the floor directly. On the CH47, a structural member of the isolated floor was chosen. The accelerometers were positioned to be normal to the major axes of the aircraft. (See Fig. 1.)

The two types of accelerometers were used to permit accurate measurement throughout the entire range of interest from DC to 2000 Hz. The piezoelectrics provided information on the higher frequencies while the piezoresistives were valuable for lower frequency response. The particular area of interest for the latter was below 10 Hz.

The recording equipment and power supply were located in the vicinity of the transducers. This provided a loading of approximately 200 pounds on the cargo floor. The recorder used was the ELI-31 developed by Sandia Laboratories [3]. It consists of a 14-channel tape recorder with the electronics necessary to provide

signal modulation and transducer calibration. The power supply is a 28 volt DC supplied by a NiCad battery. (See Fig. 2.)

The instrumentation was placed as nearly as possible in the same position in each type of aircraft. On the OH6, the equipment occupied most of the floor of the aft compartment with the seats removed. The floor of the aft compartments of the UH1 accommodated all of the apparatus with the seats in place. In both the CH46 and CH47 there was, of course, a surfeit of room.

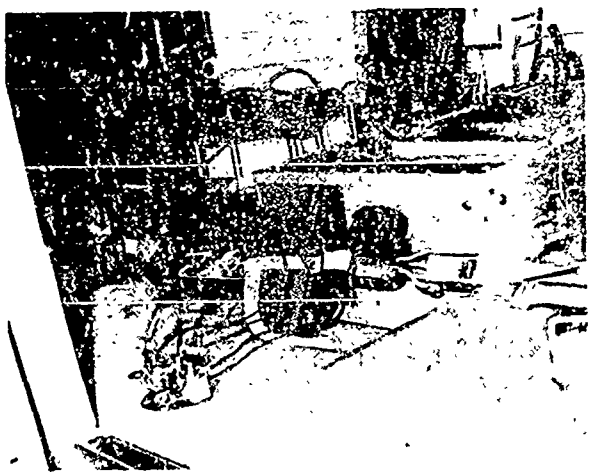

Fig. 1 - Typical Accelerometer Installation

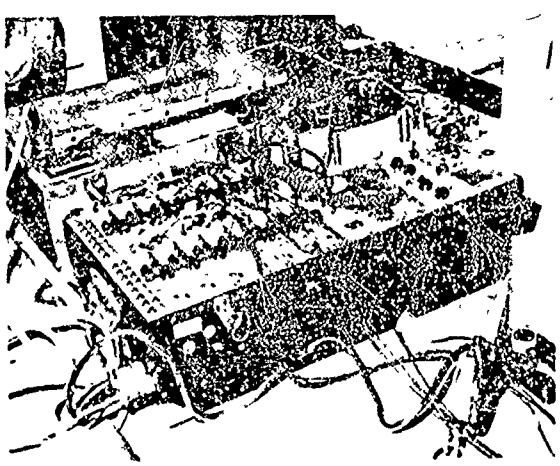

Fig. 2 - Fourteen Channel Recorder and Power Supply - Typical Installation

CONDUCT OF THE TEST

When possible, two operators accompanied each flight. One acted as a talker, communicating with the pilot and to a portable tape recorder. The other operated the test recorder and made a voice record on the test tape. This procedure permitted complete documentation. Calibrates were placed on the test tape prior to the flight. The pilot had a list of the desired events. He would inform the test engineers when he was about to execute a specific event and upon receiving assurance that the recorder was ready, would proceed with the maneuver.

The data were recorded in 20- to 30-second samples for two reasons: First, the magnetic tape on the recorder was limited to 7.5 minutes of record and, secondly, most aircraft events are of relatively short duration. For longer events, such as cruise, the dynamic excitation is essentially stationary, so samples are typical of the entire ride.

Upon completion of the flight on one helicopter, the equipment was installed in another until all had been sampled. The same instruments were used for each flight.

DATA REDUCTION

Data reduction was accomplished in the following steps:

A. Real-time analog oscilliograph record

B. Bandpass oscillograph record

C. VIBRAN analysis

D VAIL analysis

The analog oscillograph record was utilized to determine:

A. That the data had been recorded.

B. The portions of the data to receive further consideration.

Selected portions of the data were then subjected to the bandpass analysis technique, which provided further refinement of the portions to be reduced. In addition, it made it possible to begin to see the types of motion in the lower frequency ranges. We found, for instance, a very clear trace in the lowest frequency band of an excitation at about 0.3 Hz.

Sections of the record were selected for more detailed analysis. After careful examination, it was noted that the levels of excitation were generally higher for the CH46 and CH47 aircraft. It was decided to reduce samples of each event for these, but to select only a few events from the records of the UH1 and OH6

helicopters. These selected included low flight, climb, high cruise, and flight through clear turbulence. These records were reduced by program VIBRAN in three axes. The selected samples were from 5 to 10 seconds in length.

Program VIBRAN [3,4] produces an amplitude distribution table within frequency bands as shown in Fig. 3. This method permits a detailed look at the distribution of peaks by percent within a frequency band or within a record. An additional program VAIL [5], was employed to combine the VIBRAN records into a single record for each axis of each helicopter and, finally, into a single record per axis for all of the helicopters. Program VAIL operates by determining the number of peaks at each amplitude on each record, combining them, presenting the percentage of the total peaks at each level, and calculating the root mean square for each frequency band and overall for each resulting record. The report is in the same form as a VIBRAN record.

Further analysis, by frequency bands, was undertaken using the method proposed by Curtis [6]. He has shown the use of Rayleigh probability paper as a means of estimating whether a peak amplitude distribution is random or sinusoidal. Each frequency band in the summaries for each helicopter and for all helicopters was plotted to provide a curve which would indicate the characteristics of the vibration.

RESULTS

The vibration records for the two types of helicopters were sufficiently different in characteristics as to require separate discussion. In general, both showed the presence of decaying sinusoids, but in widely varying degree. The overall amplitudes of excitation in the single rotor aircraft were markedly lower than those in the dual rotor planes. The vertical axis generally had higher amplitudes in both types, but in at least one frequency band, the longitudinal axis predominated in each type.

Figure 4 is a representation of the 99 percent level of vibration for the single rotor helicopters. The 99 percent level was chosen for presentation because it not only is composed largely of steady state vibration, with few intermittents, but it tends to respond to the distribution within each frequency band more closely than do the peak values. The single rotor helicopters have low amplitudes in the lower frequencies. None of the amplitudes is much above 0.5 g until the frequency bands beginning with 250 Hz are reached. The greatest amplitudes are found between 500 Hz and 700 Hz, where there appears to be vigorous response in the longitudinal axis. The predominance of the longitudinal axis also appears between 180 Hz and 350 Hz as well as between 700 Hz and 1000 Hz. The transverse axis gains ascendency beyond 1000 Hz. In general, however, the vertical axis shows the highest peak amplitudes.

An analysis of peak distributions within each frequency band shows that 50 percent or more of the peaks lie below 0.14 g in the lower frequencies in the longitudinal and transverse axes. This condition obtains up to 120 Hz and again from 1000 Hz to 1900 Hz. It is true up to 240 Hz in the transverse axis. In the vertical axis, however, one must go to the 0.27 level before such a statement may be made. Even at that level, in three bands (0-20 Hz, 700-1000 Hz, and 1000-1400 Hz) the percentage of peaks at or below 0.27 g lies somewhat under 50 percent. The vertical axis shows an absolute peak at 1.9 g from 500 Hz to 1400 Hz; the longitudinal one of 2.7 g from 500 Hz to 700 hz. All of the transverse axis lies below these levels.

The presence of excitation caused by decaying sinusoids appear to be a characteristic of the helicopter environment. In the single rotor types, the distribution of peaks is largely Gaussian random, but at certain frequencies, particularly in the longitudinal and vertical axes, the character of the distribution is modified by the sinusoidal influence. Figure 5 is an illustration of this phenomenon. In the longitudinal axis, the sinusoidal presence appears between 120 Hz and 180 Hz and between 500 Hz and 1000 Hz. In the vertical axes, it is apparent below 20 Hz, between 40 Hz and 80 Hz, between 180 Hz and 240 Hz, and between 1400 Hz and 1900 Hz.

R100795-C1

CALIB RANGE 0 TO 1 1

HELICOPTER - CH 47
TEST MANEUVER-EVENT NO. 13 - FLIGHT ON DECK
AXIS- VERTICAL
INSTRUMENT TYPE - PIEZOELECTRIC
INSTRUMENT LOCATION - CARGO FLOOR

ACCELERATION
0 TO PEAK G

HELICOPTER VIBRATION RECORD - CH-47

PEAK DISTRIBUTION IN PER CENT

0 TO PEAK G												
10.000												
7.200												
5.200												
3.700												
2.700												
1.960				10.29								
1.400				17.28	.81	.17						
1.000		5.19	18.93	14.87	5.17	.26	.54				.07	
.720	3.30	25.18	17.28	24.87	16.55	4.13	6.29	1.51	.22		.16	.39
.520	31.87	28.89	14.40	21.89	22.93	16.77	18.71	9.69	4.57	.19	2.63	6.37
.370	15.38	16.30	8.64	17.30	23.79	30.97	25.72	25.15	18.75	2.89	12.63	24.15
.270	7.69	8.89	4.53	8.92	17.24	21.68	19.96	24.82	25.76	13.91	23.48	29.71
.190	23.08	8.89	4.53	6.76	6.72	15.10	14.75	20.11	22.37	29.88	25.81	22.11
.140	16.48	3.70	2.36	1.62	4.83	5.94	7.46	10.41	14.97	25.83	17.40	11.04
.100	2.20	2.22	1.65	1.89	1.72	3.87	5.13	6.81	10.44	20.66	14.14	5.50
.072		.74	.41	1.08	.86	1.29	1.44	1.51	2.92	6.64	3.75	.74
.052												
.037												
.027												
.019												
.014												
.010												
0.000												

FREQUENCY BAND=CPS	0 20	20 40	40 80	80 120	120 180	180 240	240 350	350 500	500 700	700 1000	1000 1400	1400 1900
RMS G	.29	.40	.73	.47	.37	.28	.28	.23	.20	.14	.18	.22
TOTAL PEAKS	91	135	243	370	580	775	1112	1527	2298	2667	4482	5672

Fig. 3 - Typical VIBRAN Record

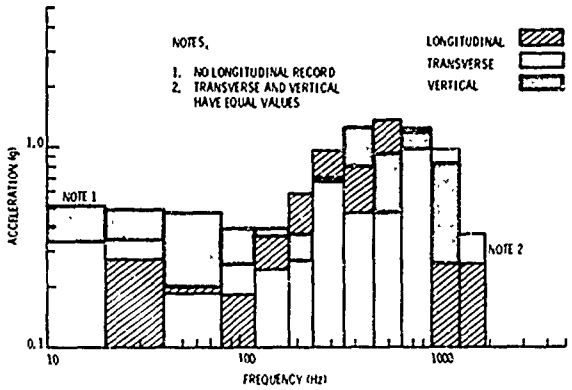

Fig. 4 - Helicopter Vibration - Single Rotor 99% Level

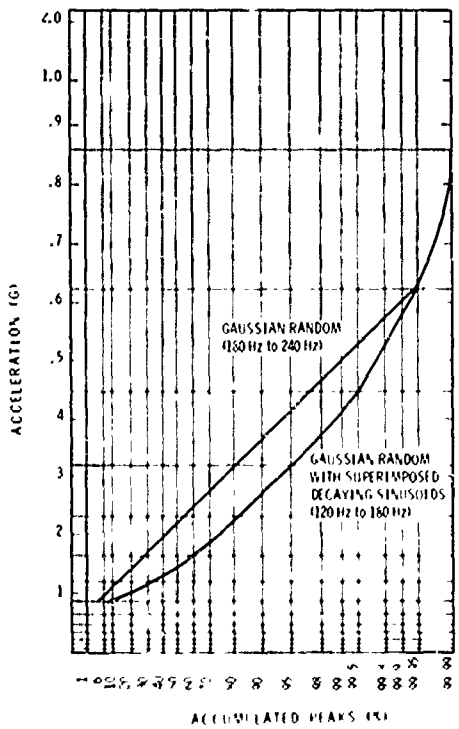

Fig. 5 - Typical Pure and Mixed Gaussian Random Peak Distributions

Figure 6 shows the 99 percent level of peak amplitudes for dual rotor helicopters. In this type, the lower frequencies show a much higher level of excitation. All of the frequency bands show values in excess of 1 g up to 500 Hz. The highest levels are found in the longitudinal and transverse axes between 350 Hz and 500 Hz. It is interesting to note that this is the only frequency band in which the vertical axis does not dominate. The high levels up to 120 Hz are contributed by the CH47, while those above that are representative of the CH46. An exception is the highest band (1400 Hz to 1900 Hz) which is CH47 data.

Peak distribution analysis reveals that 50 percent or more of the peaks are at or below 0.14 g in the longitudinal and transverse axes, except from 2.40 Hz to 700 Hz where the level rises to 0.52 g. In the vertical axis the 50 percent peak amplitude level is found at or below 0.37 g except in the 240 Hz to 350 Hz band where it rises to 0.52 g. The distributional shape is very similar in the two horizontal axes, but differs in the vertical. Absolute peaks are in the 350 Hz to 500 Hz band at 5.2 g for all axes.

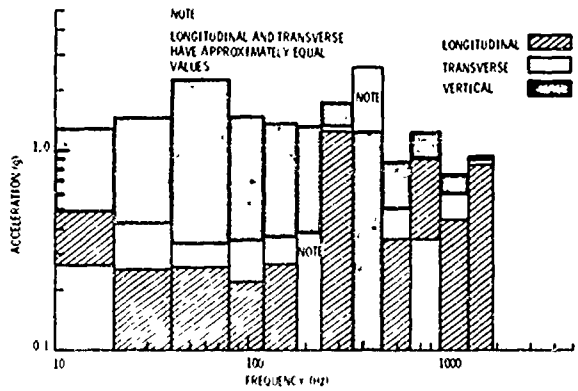

Fig. 6 - Helicopter Vibration - Dual Rotors 99% Levels

The presence of the decaying sinusoidal excitation is much more noticeable in the dual rotor type of helicopter. In contrast with the random vibration with superimposed decaying sinusoids discussed above, the dual rotor aircraft seems to have decaying sinusoids with superimposed Gaussian random characteristics . Figure 7 is an example. This trait is particularly evident in the vertical axis where it appears to some extent in each frequency band. In the longitudinal and transverse axes it is found only in the 240 Hz to 700 Hz and the 1400 Hz to 1900 Hz regions. Several other frequency bands exhibit traces of the decaying sinusoidal excitation, but are predominantly Gaussian random in nature.

It would appear on the basis of these data, in comparison with those of conventional aircraft, that the reason for the appearance of the decaying sinusoidal characteristic is the action of the rotors in the rotary wing vehicles. Additionally, it seems that the presence of two rotors intensifies the sinusoidal action to the extent that it predominates

in some frequencies and axes. While it is not the function of this study to determine causes, it might be conjectured that the sweeping of the rotor blade above the fuselage imparts a momentary additional lift. Another conjecture is that the entrance of the blade into the turbulent wash of the preceding one causes this action. At any rate, regardless of reason, the decaying sinusoid is a major component of the dynamic environment of the helicopter.

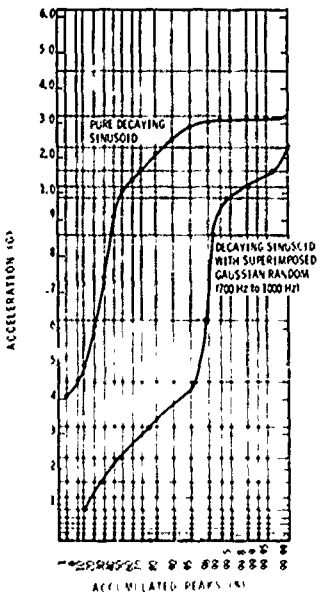

Fig. 7 - Typical Pure and Mixed Decaying Sinusoid Peak Distribution

Data on low frequency vibration were derived from the piezoresistive accelerometers. They were reduced in the same manner as that obtained from the piezoelectric transducers, but in narrower frequency bands. The bands of interest to this discussion are 0-5 Hz, 5-10 Hz, 10-20 Hz, and 30-45 Hz.

The bandpass oscillograph records were particularly valuable in considering the band of lowest frequency. They revealed the presence of very low frequency excitation on the order of 0.25 to 0.33 Hz. Figure 8 is a representation of the appearance of these data. The low frequency of these peaks permits very few of them during a sampling period of approximately 5 seconds. Indeed, the narrow band analysis of one record shown in Fig. 9 reveals that the peaks are discrete and that gaps exist between them. It is these discrete sinusoidal-like vibrations that are so noticeable to the passenger in the helicopter. Peak levels in the 0-5 Hz band were as high as 1.4 g in the vertical and transverse axes, but only 0.27 g in the longitudinal direction. Conversely, in the 5-10 Hz bands, the peak amplitudes were under 0.037 g in the vertical and transverse axes, but rose to 0.10 g in the longitudinal axes. Beyond 10 Hz the data becomes more regular and assumes a Gaussian random distribution. There is evidence of the influence of the decaying sinusoid here again. This effect is particularly evident in the vertical axis. Peak amplitude values range from 0.14 g to 0.19 g in the 10-20 Hz bands and from 0.072 g to 0.52 g in the 20-30 Hz frequency bands. The high values are in the vertical axis.

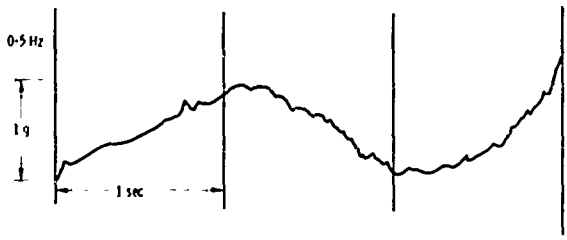

Fig. 8 - Stylized Low Frequency Bandpass Oscillograph Record

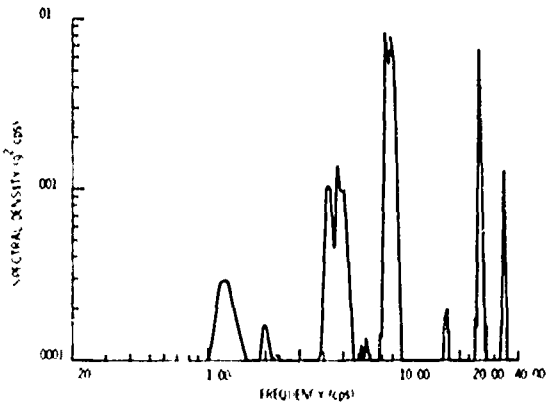

Fig. 9 - Narrow Band Analysis

SUMMARY AND CONCLUSIONS

This study consisted of the measurement of the dynamic environment of the cargo floor of two types of military helicopters. The single rotor type was represented by the OH6 and UH1 aircraft. The dual rotor type was represented by the CH46 and CH47 helicopters. Reduction of the data for the complete flights of the cargo carriers (dual rotor) and for selected events for the single rotor carriers was accomplished.

Analysis of these data revealed several aspects which appear to be unique to the helicopter environment. Among them are:

1. The presence of decaying sinusoids distributed in several frequencies. This type of excitation is often dominant in the dual rotor craft, but its presence in the single rotor environment causes a distortion of the otherwise randomly distributed vibration.

2. Discrete very low frequency excitation of moderate amplitudes are present.

3. Vibration amplitudes for the single rotor helicopters are lower (1.4 g maximum) than for the dual rotor types (2.9 g maximum).

4. The vertical axis generally has the greater amplitudes. In the higher frequencies, however, the longitudinal and transverse axes have amplitudes which approach those of the vertical.

While, in general, the dynamic inputs to cargo by the helicopters considered herein are not excessively high in relation to other modes of transport, the presence of relatively high amplitude, low frequency excitation is worthy of consideration during design of packages and tiedowns for helicopter transport.

BIBLIOGRAPHY

[1] M. B. Gens, "A Preliminary Observation of the Dynamic Environment of Helicopters," Proceedings, 14th Annual Technical Meeting, Institute of Environmental Sciences, April, 1968, St. Louis, Missouri.

[2] "U. S. Rotary-Wing Aircraft," Aviation Week and Space Technology, Vol. 94, No. 10, p. 76, March 8, 1971.

[3] J. T. Foley, "An Environmental Research Study," Proceedings, 13th Annual Technical Meeting, Institute of Environmental Sciences, pp. 363-373, April, 1967.

[4] J. T. Foley, "Preliminary Analysis of Data Obtained in the Joint Army/AEC/Sandia Test of Truck Transport Environment," Shock and Vibration Bulletin, No. 35, Part 5, The Shock and Vibration Center, U. S. Naval Research Laboratory, Washington, D. C., pp. 57-70, February, 1966.

[5] L. A. Faw, "Program VAIL, User's Manual," unpublished manuscript, Sandia Laboratories, Albuquerque, New Mexico, August, 1970.

[6] C. M. Harris and C. E. Crede, Eds. Shock and Vibration Handbook, Vol. 2, Chap. 22, McGraw-Hill, New York, 1961.

[7] M. B. Gens, "Dynamic Environment of Helicopters--Complete Data," SC-M-71-0604, Sandia Laboratories, Albuquerque, New Mexico, November, 1971. (To be published.)

DISCUSSION

Mr. Hughes (Naval Weapons Evaluation Facility): Did you try to correlate the frequency and the occurrences of the decaying sinusoid with the beat frequency of the rotors?

Mr. Gens: Yes, of course the rotor frequency lies somewhere between 4 and 8 Hertz which has to be multiplied by 4 because four blades are involved. We seem to find the harmonics rather than the basic frequency. The decaying sinusoid is not quite as prevalent at that frequency, but often at a multiple of it.

Mr. Hughes: But it does come from the rotor, does it not?

Mr. Gens: It appears to come from the rotors. We have not attempted to find the cause, but we guessed one of two things — either as the rotor passes over the fuselage it adds some additional lift, or perhaps it is encountering the wake of the preceding rotor which causes a perturbation of some type. Yes, we may be all wrong! Helicopter manufacturers can leap down my throat.

Mr. Earls (Wright-Patterson AFB): I understood you did your analysis on an octave basis and the peaks, for example, in the 500 and 700 Hertz range, were around 5 g's. What is the implication on specs for cargo? Should we test to 5 g's, or should it be done on an average basis? What about the peaks that you would have if you analyzed on a narrow band basis? What is the implication on specifications for cargo?

Mr. Gens: Expecting this question was one reason that I mentioned we are purists, and therefore, not very good at the testing angle. That is one reason we like to use a display like the VAIL VIBRAN display which I showed, or something like Mr. Ostrem showed. With these data presentations, the design and test people can use their judgement in choosing the level. Obviously a level of 5.2 g's peak would be extremely conservative when we are looking at a little over one g at the 99 per cent level. This is my thought about it. Is this the sort of answer you were looking for, sir? I hope I did not tell you anything, because I do not want to commit myself.

HIGHWAY SHOCK INDEX (U)

Robert Kennedy
U. S. Army Transportation Engineering Agency
Military Traffic Management and Terminal Service
Newport News, Virginia

The Army, Navy, Air Force, and Marine Corps have jointly sponsored and participated in the development of a Shock Index (SI) for highway transportation. A numerical SI, associated with a particular vehicle-load combination, can now be determined at a low cost by application of simple static field measurements. The SI provides classification for vehicle-load combination as regards probability of shocks transmitted to the cargo during highway shipments.

It has long been recognized that reasonably accurate estimates of shock transmitted to the cargo during highway transit can be made by a combination of experience and intuition. One experienced in conducting test runs and observing accelerometer readings can usually predict either a rough ride or a smooth ride for a particular highway vehicle with a known loading configuration. Basically, the four most important cues used either intentionally or accidentally by estimators are the capacity of the truck tractor, the relative amount of cargo, the usable suspension and tire deflections, and the load position. Other factors as trailer dynamic beam deflection, speed, and condition of the highway pavement contribute to cargo shocks, but are unimportant vehicle differences in shock attenuation. Several years back at the initiation of this work, it was decided to try to obtain physical measurements of static vehicle characteristics contribution to cargo shocks to facilitate more organized and reproducible shock estimation. The concept of shock index, then as now, is basically to measure static vehicle characteristics, run the measured vehicles over controlled courses, and mathematically fit the static measurements to the test shock measurements. The resulting formula for shock index is then tested with instrumented highway tests to determine the degree of accuracy of the empirically developed formula or performance prediction process. The results of these efforts to date have produced the following formula:

$$SI = \left[4.5\left(\frac{\text{max rated net wt}}{\text{max rated gross wt}}\right)\left(0.5 + \frac{4K_LK_S + K_L^2 - K_S^2}{4K_LK_S + 4K_S^2}\right) - 0.53\right]\left[\log \text{pct rated load} - 2.25\right] + \frac{(M+N)\,(P) + (S+T)\,(U)}{(F+G)\,(P) + (I+J)\,(U)} + 4.92$$

The maximum rated net weight is (A+B) - (C+D) and the maximum rated gross weight is (A+B). The symbols in the equation are defined as follows:

A - Combined front weight - rated load at any position.

B - Combined rear weight - rated load at same position as "A".

C - Combined front weight - no load.

D - Combined rear weight - no load.

K_L - Greatest combined suspension spring rate - front or rear.

K_S - Least combined suspension spring rate front or rear.

F - Combined front suspension deflection - rated load located forward.

G - Combined front tire deflection - rated load location forward.

I - Combined rear suspension deflection - rated load located rear.

J - Combined rear tire deflection - rated load located rear.

M - Combined front spring deflection - rated load at test position.

N - Combined front tire deflection - rated load at test position.

P - Combined front weight - rated load at test position.

S - Combined rear suspension deflection - rated load at test position.

T - Combined rear tire deflection - rated load at test position.

U - Combined rear weight - rated load at test position.

At first look the SI formula appears somewhere between awesome and gross. Further curve fitting should produce a more simple formula with accuracy consistent with data. The formula assigns numbers and coefficients to what is known about factors that determine truck-trailer ride performance. If a truck is loaded to near capacity, if the truck has a usable long-travel suspension, and if the load is positioned to work all springs, the best ride for the cargo will result. The other direction on any of the above factors will produce a rougher ride. The other end of the scale is a truck loaded with 10 percent or less capacity, with only a small portion of stiff suspension springs working, with high pressure tires, and with the load located directly over the rear axle. This arrangement produces the roughest ride and consequent high loss and damage to the cargo.

The most significant factor affecting the SI for a particular vehicle is the percent of rated load. Figure 1 is a plot showing how the shock index changes with percent rated load. It is apparent that most highway vehicles perform well as regard shock and vibration when loaded to near capacity. Most standard highway vehicles should range from SI 2.0 to SI 5.0 with changes in the weight of cargo. The SI should aid in communicating to those responsible for establishing the percent rated load in practice the great sensitivity of the relative weight on the cargo bed to the shocks transmitted to the cargo.

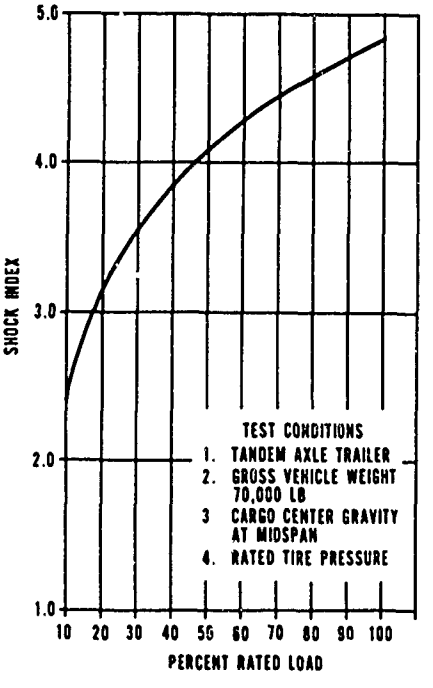

Fig. 1 - Vehicle performance for percent rated load

Highway vehicle mechanics have resulted in cumbersome and complicated practical applications. The essential elements as masses, springs, capacities, and load positions are quite understandable. The approach used to the problem has been to match up the understandable elements to the results sought. The factors in the formula have a mechanical basis. However, the goal was to obtain a formula of static measurements that works without too much concern for the theory involved. The formula is intended to give a shock index rating which would be similar to and as useful as octane ratings for gasoline or tire ratings for automotive tires.

In much of the work today the question "who needs it?" requires immediate and prompt attention. Traffic managers and shippers today rent or purchase highway equipment with the intent of providing minimum shocks and vibrations to the cargo. At present, the only criteria the traffic manager can use are the manufacturers' advertisements and the cost of the equipment. Other than for particular and fragile cargo, the traffic manager must choose transportation equipment ignorant as to its ride-cushioning ability. There is no documented correlation between the cost for rental of the equipment and the quality of the ride given to the cargo. For many years, automotive tires have been purchased by the consumer on the same basis of trust or ignorance. The only criteria available to the small consumer for purchase of gasoline have been the cost. Recent developments have made it possible for the consumer to purchase gasoline or tires based on a general empirical rating. This probably does little more than indicate comparative worth between the other items available; however, it is of great value to the consumer. Traffic management people have indicated a need for a factor as the shock index that will give them a comparative value between the various trucks available, especially for rental type transportation.

Designers also have a need for a quantity term shock index that will enable them to set goals for shock attenuation. Also, when a particularly good shock attenuating vehicle design has been achieved by highway vehicle design or development, a single factor term to describe this improvement is needed for proper promotion.

The third big need exists in communication in this area. Of the many tests and monitored instrumented movements, it has been difficult to communicate in general terms the relative merits of various highway systems. Shock and vibration people know the relative work by studying various curves, spectra, and tables. However, these data are indeed hard to communicate because of their great depth and the specialized knowledge required for understanding.

Not to belabor the gasoline analogy, but with an indicated octane rating for a gasoline, all from automotive engineer to hot-rod hobbyist benefit from the classification. Octane rating has done considerable to improve communications. The empirical, simplified approach has aided in pursuit of more precise, technological characteristics for gasoline performance. When one starts to investigate the need for a shock index, one finds out that just about everyone in the field of transportation has the need for a term that will roughly indicate the degree of shock and vibration severity to the cargo.

Briefly, the origin, generation, and development of the highway shock index came about over the last 4 years. The Army, Navy, Air Force, and Marine Corps entered into an interdepartmental agreement to pursue and sponsor this type of work jointly for all modes of transportation. The steering group, consisting of Mr. J. Pellant, Navy; Mr. H. Leonard, Air Force; Mr. T. Quast, Marine Corps; and Mr. R. Kennedy, Army, formulated the basic concepts for shock index during series of work sessions. General Testing, Incorporated, was awarded a contract to perform the necessary test runs and mathematically fit the data to the shock index equation. J. A. Johnson, Incorporated, was awarded a contract both to verify and determine the degree of accuracy and the range of applicability for the shock index formula.

It was realized early in the work that in order to obtain reasonable acceptance the entire scientific community need participate and approve, from concept to development to checkout. An advisory group was set up which comprised representatives from the National Bureau of Standards; National Academy of Sciences; Department of Transportation; Aerospace Industries, Incorporated; and NASA. This group has been instrumental in the development of the mathematical concepts, engineering concepts, and all scientific considerations.

The project proceeded generally in the following manner: mathematical equations for shock index were developed; sensitivity analyses were performed on the various equations to establish the number of pertinent variables. All of the work was set up to limit the shocks of interest to frequencies below 60 cycles per second; to a threshold of 1g, or 10 percent of the maximum rating, whichever is the greatest; and to the 95-percentile shock amplitude.

It is realized that many cargoes will respond to frequencies higher than 60 cycles per second; also that a threshold of 1g may not be adequate to cover shocks for extremely fragile cargo; and lastly, that eliminating the top 5-percent high shocks may be insufficient for

those cargoes that experience the damaging shocks that the formula ignores. The basic approach, however, was to loosen up the requirements as far as possible to see if the shock index still had a justifiable value. It turned out that even with the loose tolerances the shock index is of great value to the field today. Further work will be accomplished to make the shock index applicable for higher frequencies, lower threshold, and a higher range of extreme values.

A series of trucks covering as broad a range as possible for the trucks that are intended basically for transporting cargo were selected and static measurements made for each truck and load configuration. The trucks were then run over a standard short road course that had well-defined impediments or shock generators. A relationship between the 95-percentile maximum shock measured from the test runs and the shock index factor was developed. The shock index was set to rate from 1.0 for a very poor riding truck producing high shock to the cargo, to 5.0 for the best available truck. This range of numbers was selected to match the performance serviceability index which indicates general condition of highway pavements; this also runs from 1.0 for the worst, to 5.0 for the best.

After the formula was fitted to agree with the results of the shocks measured on the precalibrated road course, it was evaluated by separate contract over public roads using actual commercial equipment. The shock index validation test included trucks with SI ranging from approximately 2.0 to SI approximately 4.5. The amounts of load or cargo were varied, the load placement was varied, and various size trucks were used. During the validation contract all test runs were conducted at maximum legal speed and at one-third and two-thirds maximum legal highway speeds. Tests were also run over both flexible and rigid pavements. All work to date on the shock index has been entirely successful. The basic concepts checked out during the development phase, and the development work checked out during the verification phase. All the indications to date are that the general approach has considerable merit and that more factors should be brought into the shock index considerations to increase its range of applicability. Most of the test runs were made with the pavement indexes recorded for future correlation with the resulting shocks and vibrations.

The vehicle characteristics are altered for each test, and, in most tests, the characteristics are the extremes for rapid curve development. The most pressing need for progressing in this work is to establish mathematical and engineering relationships between the vehicle shock index and the pavement index.

This work was only performed because a need existed. It is planned to implement this shock index work by using the shock index concept and formula in operations. It is anticipated that traffic managers will specify shock indexes for particular cargoes that need better-than-average shock attenuation during highway movement. This use of the shock index will consider such factors as cost of packaging, price of the item, and military importance of the item. It is intended to start with the most important items first for specification of the shock index and broaden out to cover the majority of cargo within the next few years. Shock index as part of the specification for procured vehicles will be introduced during the planning stage. For evaluation of various vehicles that are still in the design and prototype stages, shock index will be calculated and used as a basis of worth. Manufacturers will be encouraged to use the shock index as part of their specifications where applicable.

The highway shock index is intended primarily for the transportation users, and it is predicted that in this area the shock index will find its greatest acceptance. Small users and consumers that do not have access to shock and vibration specialists or to an engineering department will have a guide that will indicate to some degree what they are getting in shock and vibration control for their money.

Mr. Schell (Shock and Vibration Information Center): Are you aware that there is another SI Index in the transportation field which is an index of shock severity? This is in the Department of Transportation Motor Vehicle Safety Standards. It is the time integral of a weighted acceleration. It is called the "Severity Index", and the symbol SI is used. It is an Index of shock severity on the human being or occupant of an automobile.

$$SI = \int a^n \, dt$$

Mr. Kennedy: We had a DOT representative on the advisory committee, and with the crowd you are talking about and the crowd we are talking about we do not think they are going to get mixed up, because most of our people are not going to be worried about the first integral or the second. They would not really know what it is.

Mr. Gaynes (Gaynes Testing Laboratories): Are you not getting involved slightly with a legal problem in relation to a gentlemen picking out a certain shock level truck and then finding out that he had bad damage? Is there a liability involved here?

Mr. Kennedy: I do not know about a liability — of course there are legal implications, but in our business there is a big legal department to handle those problems. You are correct, but this method will involve rate-making, and there will be interstate commerce problems, and we have lawyers that work on this sort of thing all the time.

Mr. Gaynes: But you are setting up a definite or finite number in relation to a shock level which, if it is exceeded, supposedly you could be held responsible.

Mr. Kennedy: As I mentioned, on household goods containers, we did almost the same thing. We had several thousand manufacturers to whom we sent a performance standard. Anybody that could equal or better the standard requirements would get preferred treatment by the traffic managers. We got a little rumble at first. But they are not being put out of business by such a requirement. Their services are simply not selected, so they quickly come up to the standard requirements. As a matter of fact, the truck manufacturers want to know what their snock index is, because if it is low, they will go about raising it. It does not take much work on a truck to improve its springs and damping to the point that it has a good Shock Index.

Mr. Bacile (Martin Marietta): I guess I need to be led by the hand. Let us assume I have some cargo that I want shipped. Let us also assume that I have already defined the fragility envelope for this cargo. I want to ship it from here to there. How do I tie in this fragility envelope to the shock index? How do I use this protective tool?

Mr. Kennedy: The traffic manager would specify, he tells the shipping company that he wants a truck with a shock index of 4.5 or better for this particular cargo.

Mr. Bacile: How do I get from the fragility envelope to the shock index?

Mr. Kennedy: If you refer to a sophisticated missile component or something like that, shock index would not come into play at all. But if you mean troop support cargo such as rations, small ammunition, and that sort of thing, we have quite a record of experience in shipping such items. As shippers, we at least know the things that break easily and those that never break. We know the things that are expensive and those that are not expensive. We know the things that are well packaged and those that are not. Traffic managers know all these facts. The only thing he does not know is which truck is good and which is bad. If he has fragile, expensive cargo, poorly packaged, he will ask for a good truck. You have to pay more to get a highly rated truck, one with a high Shock Index. Most of our very fragile items, such as warheads, are closely studied to determine accurate shock and vibration fragility levels. If we put them on a light truck, the accelerations could be a factor of three to five times higher than they would get on a heavy truck. We are trying to get away from this kind of thing because we who have the technical ability do not get an opportunity to order trucks. We have to instruct the traffic manager, the transportation officers and that type of personnel so that they can order a truck. That is why the Shock Index was developed.

DEVELOPMENT OF A ROUGH ROAD SIMULATOR AND SPECIFICATION FOR TESTING OF EQUIPMENT TRANSPORTED IN WHEELED VEHICLES

Harold M. Forkois and Edward W. Clements
Naval Research Laboratory
Washington, D.C.

A Rough-Road Simulator machine has been constructed and placed in successful operation. The simulator employs rotating drums with detachable road profiles, or bumps, which are interfaced with a wheeled vehicle to provide a random shock and vibration environment. This machine was the experimental device employed to simulate field conditions in the laboratory for the acquisition of shock and vibration data. The analysis of acceleration records of the response of the wheeled vehicle platform, both unloaded and with incremental loads, provided a description of the simulated environment, or what alternatively may be described as a calibration of the performance of the rough-road simulator machine. A proposed draft of a Wheeled-Vehicle Rough-Road Transportation Test Specification is presented, which is related to the use of this machine.

INTRODUCTION

A definite need has existed for many years for the development of an adequate and realistic method for laboratory shock and vibration testing of Navy and Marine Corps electronic equipment and missiles transported in conventional wheeled vehicles. Current specifications for ground equipment require separate and distinct vibration and shock tests using conventional testing machines which do not satisfy adequately the requirements of this ordinary but complex environment [1-2]. It is agreed, generally, that the most sophisticated method of simulating this shock-excited environment within a laboratory building would be to employ an appropriate number of hydraulic actuators which would be programmed to provide the required six-degree-of-freedom motions to a suitable structure or platform. The cost of such complex test facilities for general use is considered prohibitive when compared with a substantial investment decrease effected by utilization of a recently constructed type of testing machine which formed the basis for the development of the proposed test specification. This machine has been described previously in recent publications under the descriptive title "Rough Road Simulator for Wheeled Vehicles," prior to publication of the experimental results [3-6]. These results together with the proposed specification appear in Ref. [7-8].

DESCRIPTION OF THE ROUGH ROAD SIMULATOR

This machine consists of a truck, trailer, or other similar vehicle, which has its rear wheels supported by steel drums onto which suitable bumps can be attached (Fig. 1). The upper surfaces of the drums are at floor level, and all associated equipment is mounted in a pit with a depth of 5 ft below floor level. The pit is covered with steel gratings to maintain floor continuity. The steel drums, which have a diameter of 33-1/2 in., are driven by V-belt drives powered by two hydraulic motors. At 1500 psi operating pressure the maximum average speed of the drums is 380 rpm corresponding to hydraulic motor speeds of 1265 rpm, estimated horsepower of 28.5 per motor, and speedometer reading of approximately 38 mph for a 2-1/2-ton 6 × 6 military truck. The speed controls of each set of drums on each side are independently adjustable. Enough slippage occurs in the belt drive between the fore and aft drums so that a random and variable phase relation exists between them. The vehicle is constrained laterally by one large turnbuckle hooked to the frame of the truck at the center location of the rear spring, and longitudinally by a hook arrangement attached to the front bumper. Adjustable steel brackets, bolted to rails anchored in the concrete floor, provide the necessary end restraints. When a smaller

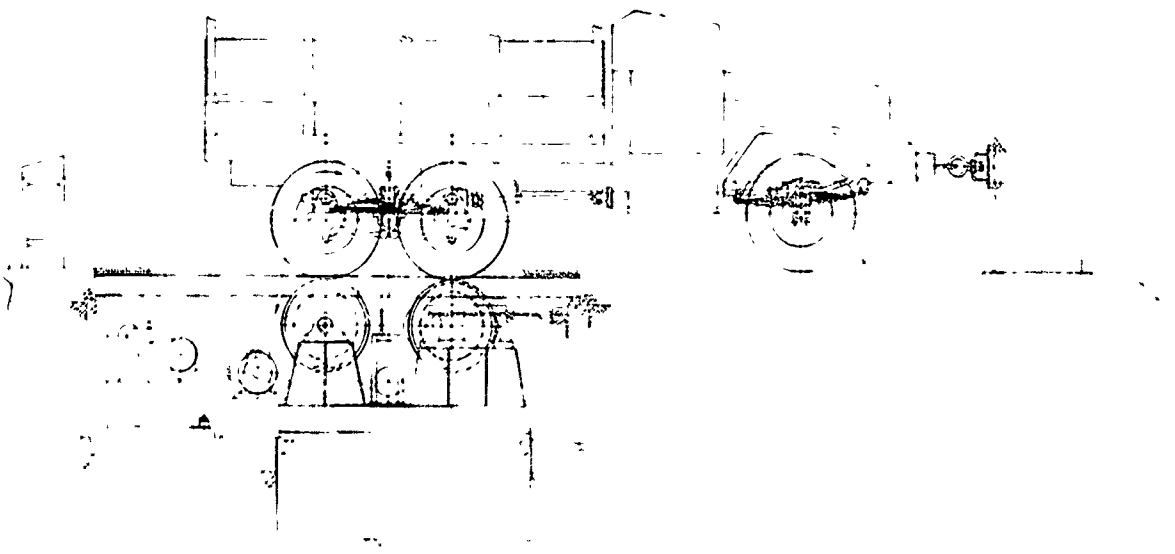

Fig. 1 - Rough-road simulator for wheeled vehicles (general arrangement)

vehicle is utilized, such as a jeep, its rear wheels are located on top of the forward drums, and manual disengagement of the clutches provided on the shafts of the aft drums renders them inoperative, excitation to the vehicle then being provided by the front drums only. The forward pair of drums are adjustable in the longitudinal direction to accommodate vehicles of different wheel bases. The same lateral and longitudinal restraint arrangement as described for the truck is utilized. Heavy vehicles can be driven by the simulator at speeds up to 40 mph. Greater speeds are possible for powered vehicles if the engines are used to boost the driving power of the hydraulic motors. Figure 2 is an overall view of the installation.

Ground Shock Isolation

To mitigate ground shock effects, the steel drum-foundation brackets are bolted to a separate reinforced concrete block which rests on the soil directly. The block is approximately 10 × 8 ft on its base and 3 ft deep, extending below the bottom of the pit floor level. It weighs about 20 tons. A 1-in. thick premolded joint filler separates this foundation from the concrete floor of the pit. In addition, resilient pads are interposed between the bearing pedestal and pedestal brackets. The resilience of these pads under dynamic loading causes relative motions between the drum shaft pulleys. Because of these relative motions, the V-belt tension varies and when the tension decreases slipping of the belts on the pulleys occurs which, in turn, causes the phase changes in bump excitation. Building disturbances have been small even though the simulator is in close proximity to wall and column footings.

Description of Hydraulic Drive

Figure 3 is a schematic drawing of the elements utilized in the drive and control system. A 100-hp constant speed electric motor drives two constant-volume fluid pumps which, in turn, energize the two fluid motors. Speed control is achieved by the "on-off" operation of two pilot-operated relief valves (one for each fluid motor), with maximum pressure adjustment of 2000 psi. The actuating pilot valves are solenoid operated, and in turn the solenoids are actuated by the "on-off" operation of two independent centrifugal switches located on the control panel. The centrifugal switches are driven by two independent flexible cables attached to the motor pulleys. Two tachometer generators, driven by the rear drums, provide signals for two panel meters for rpm speed indication of the drums. Also, two panel gages indicate instantaneous pressures in each drive system. Accumulators, pressurized to 500 psi initially, are provided to smooth out the speed control. Speed regulation is in the order of 5-10 percent depending on the operating speed and vehicle loading.

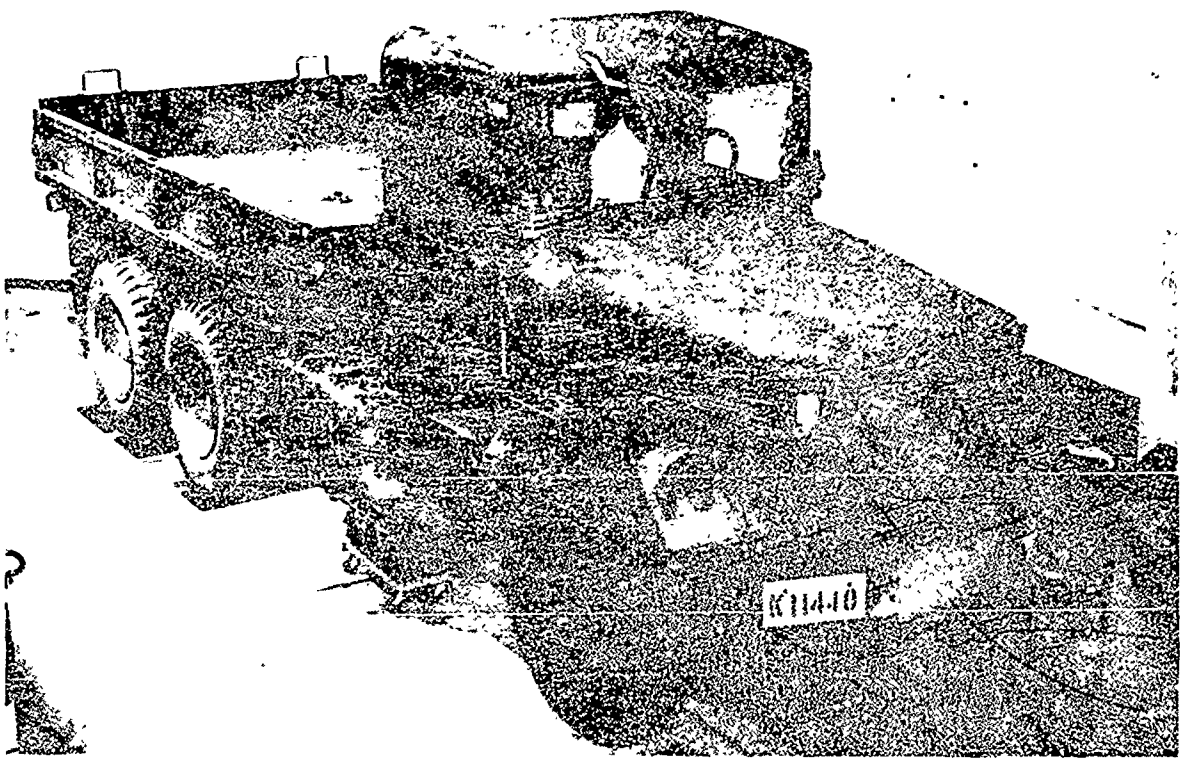

Fig. 2 - Overall view of simulator installation

Bump Profiles for Drums

The shock excitation for the proposed specification simulator machine was generated by equipping each of the four drums with two bumps with maximum eccentricities of 3/4 in. and 1-1/2 in. They are spaced 180 degrees apart on the drums. The contacting surfaces of the bumps are circular in form, and for the chord length used, are nearly the same shape as a half sinusoid. One bump has an external radius of 10-3/4 in. and a chord length of 12 in. The other has an external radius of 8-5/32 in. and a chord length of 12 in. The bumps are aluminum castings made of alloy 356-T6.

Three other road profiles were provided. These profiles are similar to three vehicle courses located at the Munson Test Area, Aberdeen Proving Ground, Md. and are identified as the Six-Inch Washboard Course, Radial Washboard Course, and Three-Inch Variable Washboard Course [9]. The use of these profiles on the drums poses a practical difficulty because of the high starting torque required to rotate the drums. It is rather difficult to achieve a smooth controlled motion with these other profiles even though the power train of the truck is used to supplement the hydraulic motors. The use of these road profiles was not considered feasible especially with the small diameter drums provided.

WHEELED-VEHICLE SHOCK ENVIRONMENT

In determining the accelerations transmitted to equipment items transported in a wheeled vehicle, there are three separate phenomena which must be considered [10]. The first is the forced vibration of the vehicle body on its springs usually associated with low speed (5-15 mph). This phenomenon corresponds to a forced low frequency vibration with displacement amplitudes dependent on the spacing and heights of the road irregularities and on the speed of the vehicle. The input acceleration levels are substantially below 1 g. The second phenomenon is associated with the higher speeds

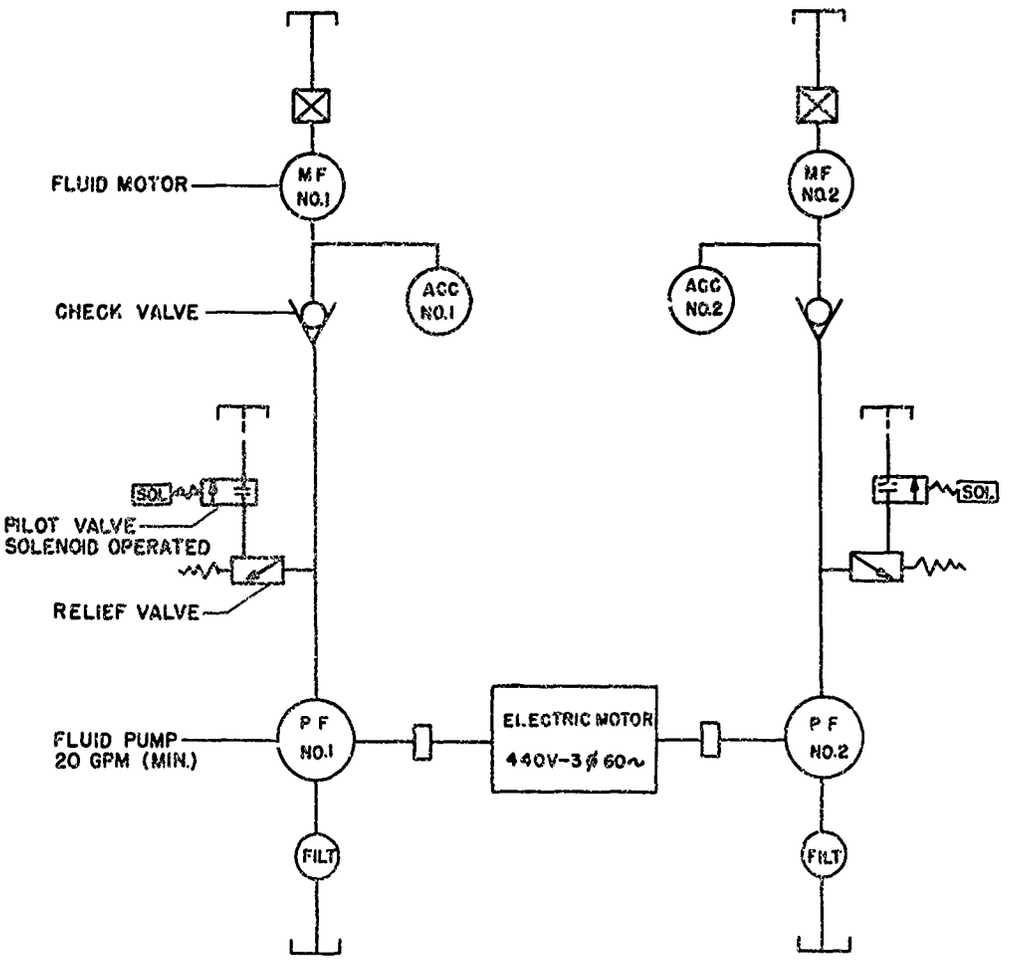

Fig. 3 - Schematic drawing of hydraulic control system

(15-40 mph) over the same irregularities as for the first phenomenon and results in a severe wheel bounce producing a random vibration. The third phenomenon occurs when a single road discontinuity of large magnitude is traversed at sufficient speed, causing the body of the vehicle to strike the rubber pads (snubbers) on the axles. During the time the axle pad and the body are in contact, the suspension system is changed by the effective removal of the main springs from the system, thus giving the body of the vehicle a large acceleration or deceleration. This impact can produce a medium-level shock pulse in excess of 10 g maximum for a duration of several milliseconds.

Statistical Data

Figure 4 presents data from tests on nine trucks constituting 1848 test miles. The acceleration data were taken in the cargo spaces of the vehicles operating over rough roads at speeds which caused discomfort to the driver. Some of the high-g level points were recorded on body appendages and not in cargo spaces. The frequency and amplitude distribution indicates the complexity and randomness of the motions involved. The values of the constant "g" levels presented by the sloping straight lines leads to the conclusion that the data does not include incidents of "hard" spring bottoming. The predominant frequencies of vibration occur in the ranges of 2-5 Hz, 7-15 Hz, and 60-200 Hz. These frequency ranges are the natural frequencies respectively of the main springs, the tires, and the body structures. It is noted that the average acceleration amplitude is constant at about 0.5 g with most points being contained under a line representing 3 g amplitude. As would be expected, the low frequencies up to 5 Hz are associated with large

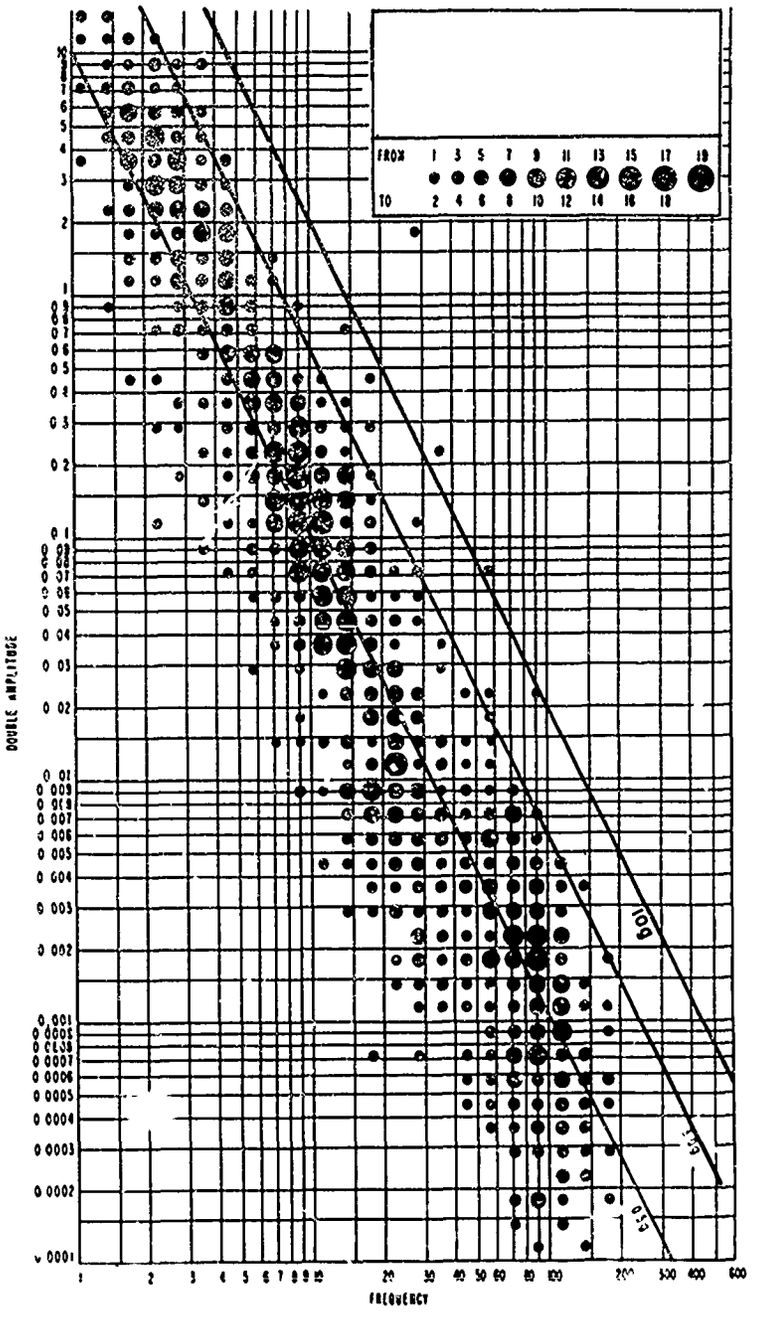

Fig. 4 - Vibration data for truck transportation. The number of data points in adjacent equal squares is represented by centrally located spots whose point value is indicated in the inset. (Source, USAF Air Material Command, circa 1951.)

displacement amplitudes of 1-10 in., and the higher frequencies of 50-200 Hz are associated with small displacement amplitudes generally less than 0.01 in. The intermediate range of frequencies 5-50 Hz have displacement amplitudes in the range of 0.01-1.00 in. Since predominant frequencies are absent in the range of 15-60 Hz, the optimum natural frequencies for equipment shock isolators is in the range of 25-35 Hz for conventional wheeled vehicles.

Typical Records

A typical reproduction of acceleration records (taken originally on magnetic tape) for a location at the center of the cargo platform of an unloaded 2-1/2 ton 6 × 6 military truck, for the three mutually perpendicular directions (vertical, longitudinal, and transverse), is shown in Fig. 5. The corresponding truck speed is 20 mph. The acceleration signals have been

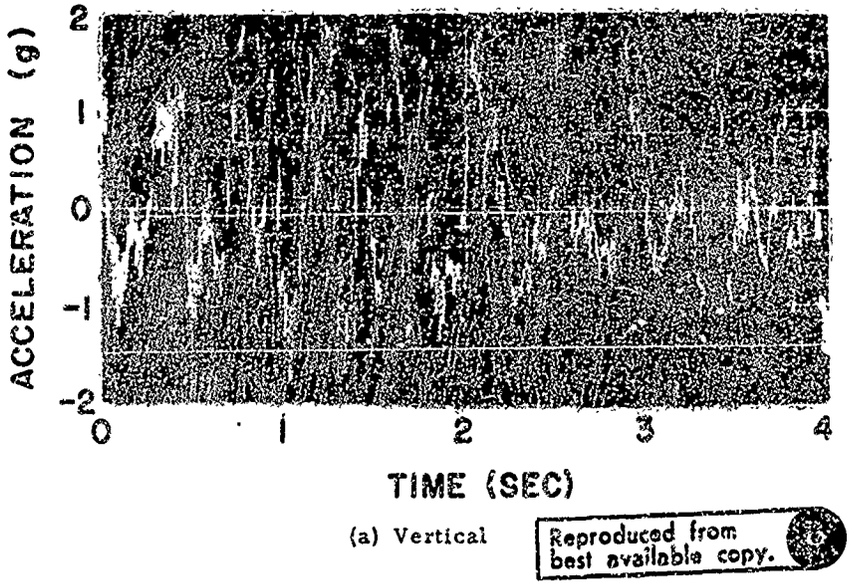

(a) Vertical

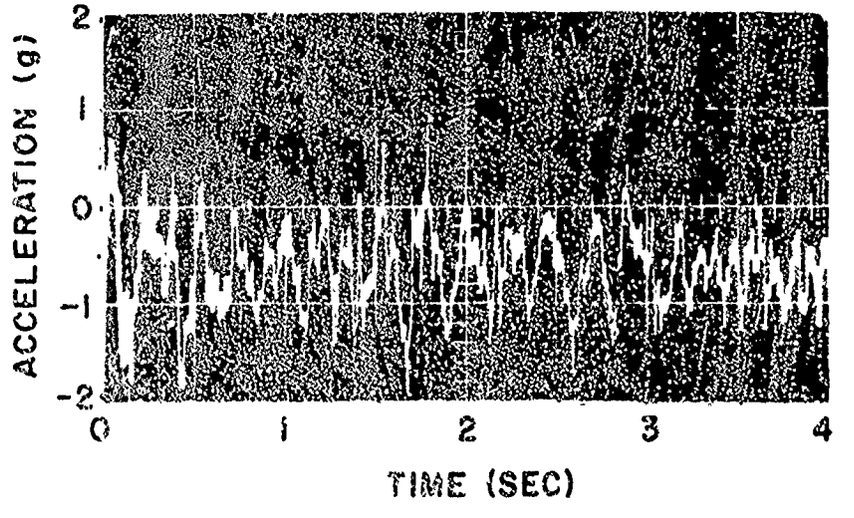

(b) Transverse

Fig. 5 - Acceleration-time signatures of the principal components of input acceleration at the center of the cargo platform of an unloaded 2-1/2 ton, 6 × 6 military truck, recorded at a speed of 20 mph

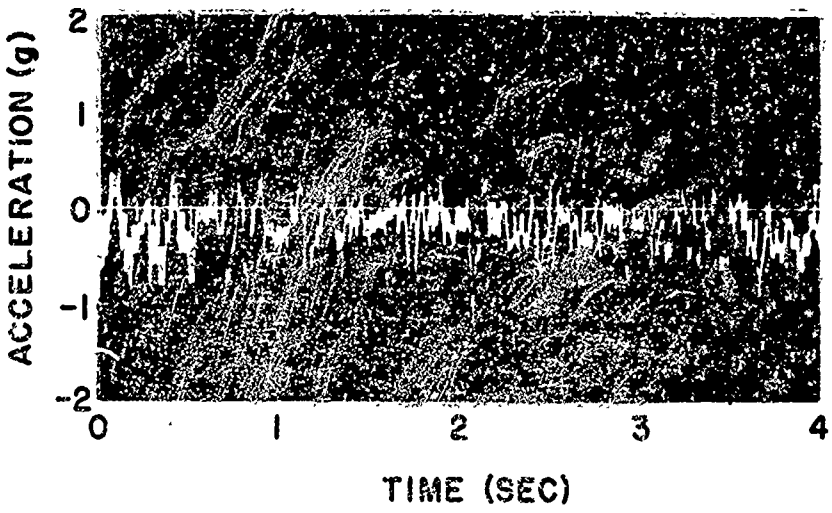

(c) Longitudinal

Fig. 5 - Acceleration-time signatures of the principal components of input acceleration at the center of the cargo platform of an unloaded 2-1/2 ton, 6 × 6 military truck, recorded at a speed of 20 mph--Continued

passed through a 50 Hz low-pass filter, and clipped by the recording system at ± 2 g. The dc offset is due to slight unbalance in the recording system, and should be disregarded.

Even though the excitations of each of the driven wheels are relatively periodic, the initial states of the truck at the times of transit over the bumps are always different. This causes more randomness in the magnitude of the excitation than might be expected. Thus little periodicity is noticeable in the truck motions. Of course, dominant frequencies exist which are caused by particular modes of vibration of the truck structure.

Procedure for Measurement and Analysis of Rough Road Simulator Output Motions

The test vehicle was an M35 6 × 6 truck carrying dead weight loads of 0, 2316 and 4522 lb. With each load, triaxial acceleration measurements were made at each of twelve selected locations of the cargo space at speeds of 5, 10, 15, 20, 25, 30, and 35 mph. The locations were arranged in a matrix of four rows and three columns: Row 1 midway between the front of the cargo space and the forward rear axle, Row 2 over the forward rear axle, Row 3 midway between the rear axles and Row 4 midway between the after rear axle and the tail-gate. Column 1 was chosen midway between the left edge of the cargo space and the left main frame member, Column 2 at the center line of the cargo space and Column 3 over the right main frame member. This arrangement provided a reasonably complete sampling of the varied structural details of the cargo space (Fig. 6).

The accelerometer signals were low-pass filtered and recorded on magnetic tape. For analysis, the rms acceleration levels were read off during playback and selected recordings were transcribed onto loops for extracting power spectral density and amplitude distribution. The latter analyses were performed with the loop recirculating at eight times original speed to reduce the processing time and translate the signal's component frequencies to a more convenient range.

Instrumentation Characteristics

The accelerometers used were piezoelectric units with a natural frequency of 12 kHz and a linear range of 0.001 to 20 g. They were connected to wide-band charge amplifiers, the frequency response of the combination being essentially flat from 0.05 to 4800 Hz. The outputs from the charge amplifiers were low-pass filtered at 2500 Hz and recorded in high-density FM mode at 7.5 ips. Each was recorded on two tape channels, at high gain having nominal dynamic range of 0.03 to 10 g and at low gain with dynamic range 0.06 to 20 g. The lower limit

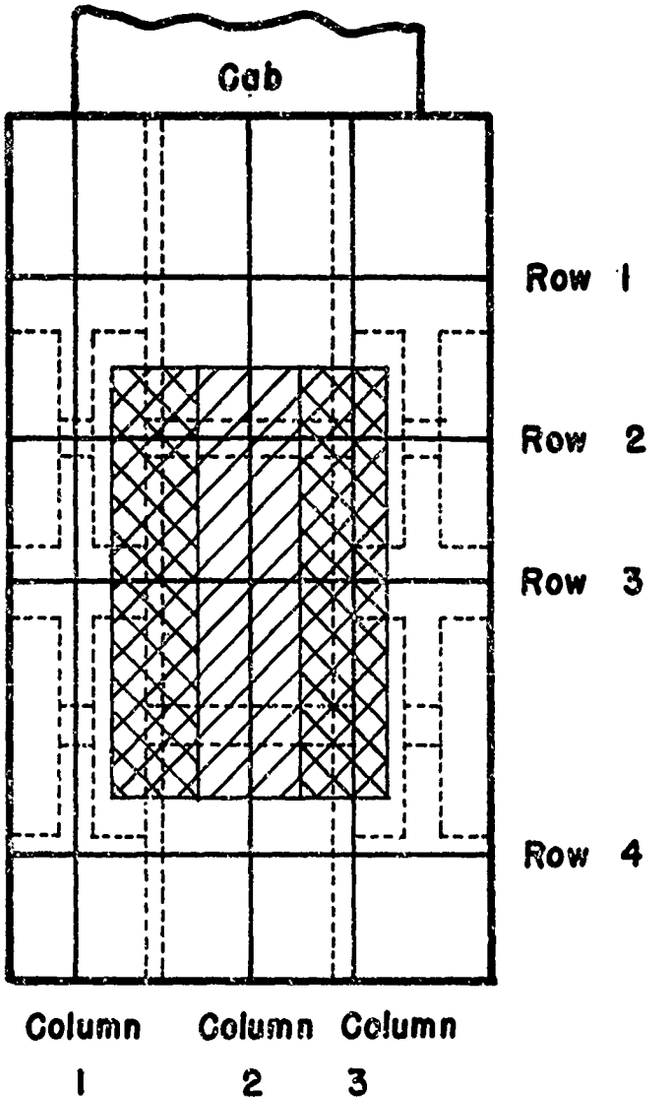

Fig. 6 - Arrangement of measurement locations on the truck

in each case corresponds to the rms noise level of the recorder.

The rms acceleration levels were monitored directly from the master tapes at normal speed with a true rms voltmeter. The selected recordings transcribed onto tape loops were played back at 60 ips and contained a (real time) forty second sample of the recorded signal. The amplitude distribution of each of these signal samples was measured with a cumulative distribution function analyzer, and at the same time the power spectral density function was plotted by a swept-frequency heterodyne wave analyzer. Even with the factor of eight speedup the time required for a spectral analysis was long, so the frequency range covered was restricted to 2 to 300 Hz (real time). The analysis filter bandwidths employed (in real time equivalents) were 0.25 Hz from 2 to 12.5 Hz, 1.25 Hz from 12.5 to 62.5 Hz and 6.25 Hz from 62.5 to 300 Hz. For a completely random signal the worst case error estimate would be ± 25% at the 80% confidence level. The instrumentation setups are outlined in the block diagrams of Figs. 7 and 8.

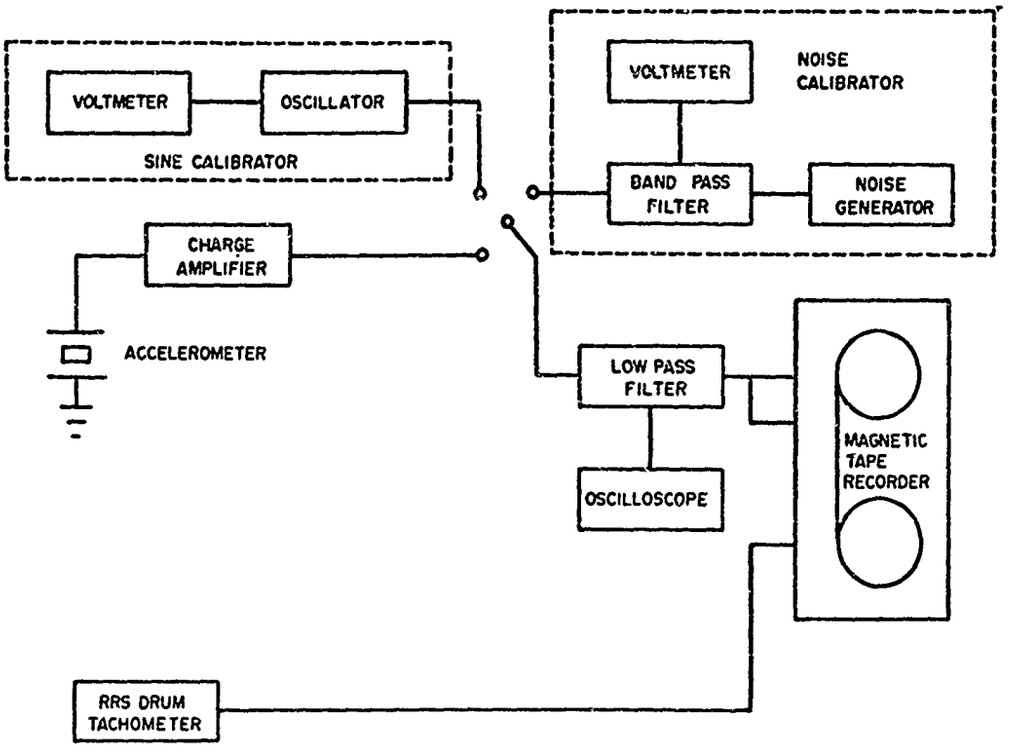

Fig. 7 - Block diagram of measurement system. The acceleration channel shown in one of three, the drum speed channel one of two. Acceleration channel calibrations were inserted behind the charge amplifiers, the charge-to-voltage transfer coefficient of the charge amplifiers being check independently.

RESULTS

Figure 9 displays the rms accelerations at each speed for each of the three load conditions averaged over the ensemble of measurement positions; the bar labelled L shows the average rms longitudinal component, T the average rms transverse component, V the average rms vertical component, and R the rms resultants of the individual L, T, V sets averaged over the ensemble of measurement positions. Figure 10 summarizes the rms resultants at each position averaged over all speeds for each of the three load conditions. The bars are plotted in roughly the geometrical relationship of the actual measurement locations, and their heights represent the rms accelerations (in g) whose values are indicated at the tops of the bars. The average values for each row and each column are indicated by vertical lines at the ends of the row and column markers. Figure 11 shows a typical group of spectral density plots obtained for platform position row 2 column 3, for zero-lb load and speed of 20 mph.

Figures 12 and 13 are photographs showing the steel-weight arrangements for the nominal 2300-lb and 4500-lb truck loads. These loading assemblies were bolted to the transverse channels supported by the truck's main frame members.

Determination of Severity Level of Random Vibration Inputs

The basic data which formed a guide for the selection of the eccentricities of the circular contoured bumps described in a previous paragraph, was taken from Fig. 4 which showed that practically all g levels were contained under a line representing a 3-g peak amplitude for the frequency range 1-200 Hz. An estimated average acceleration amplitude is shown at approximately 0.5 g. Referring to Fig. 9, the maximum vertical rms acceleration is indicated about 1.4 g at 10 mph for the zero-lb load condition. It was assumed that this average value of 1.4 g rms at 10 mph for the empty or light

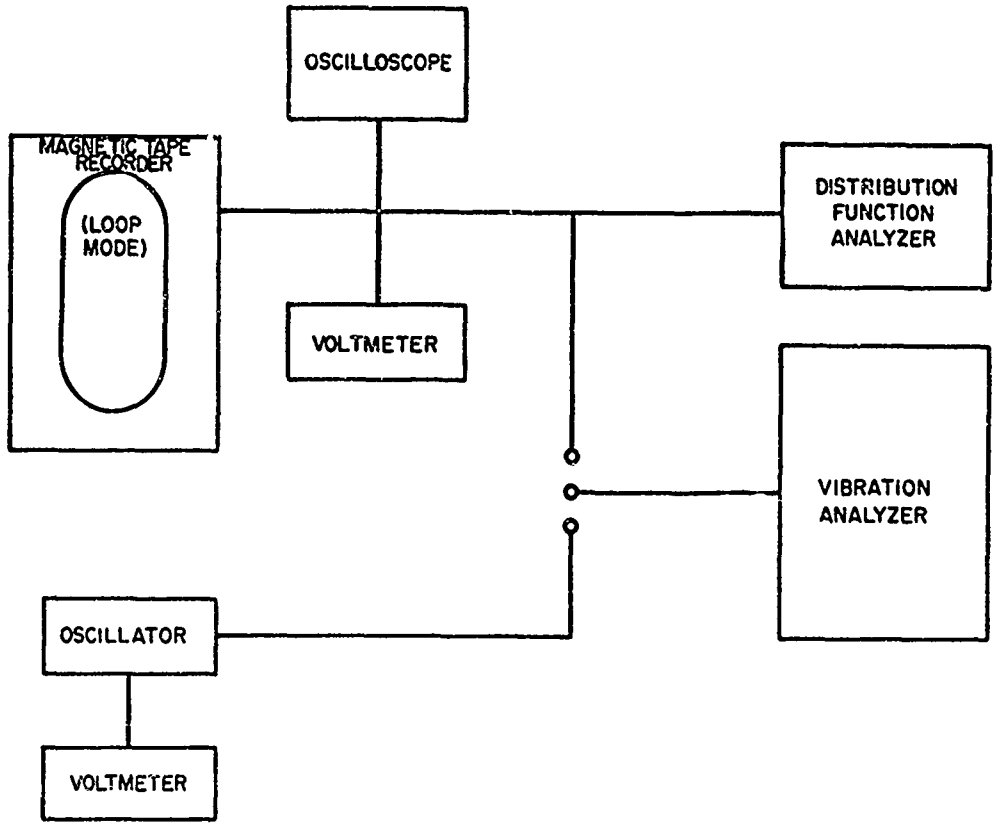

Fig. 8 - Block diagram of analysis system

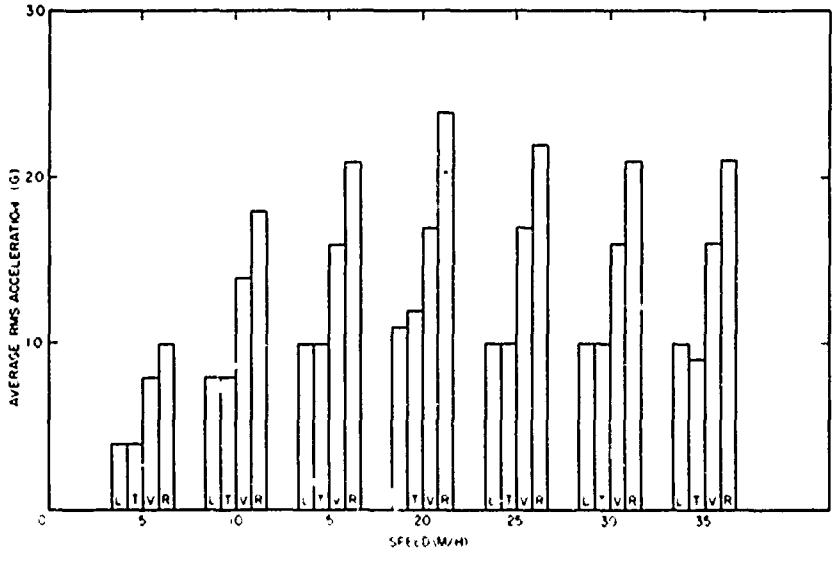

(a) Zero-lb load

Fig. 9 - Average rms accelerations of all the measurement locations

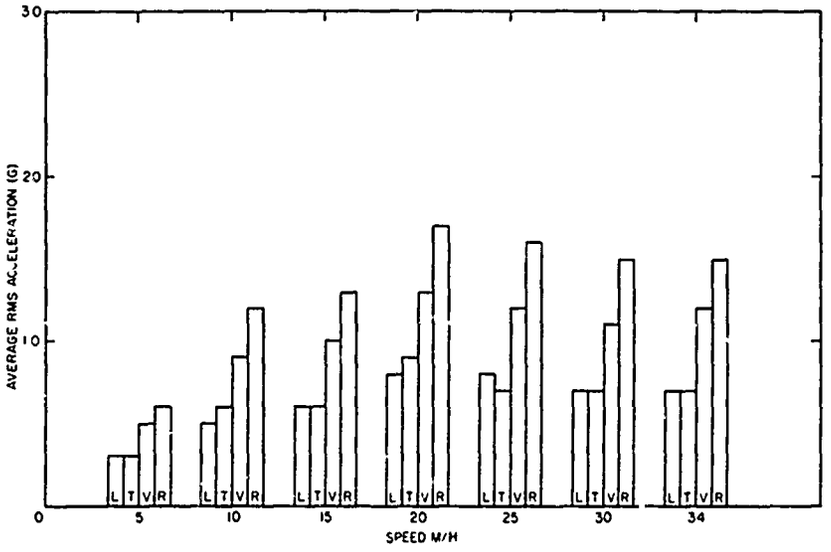

(b) 2300-lb load

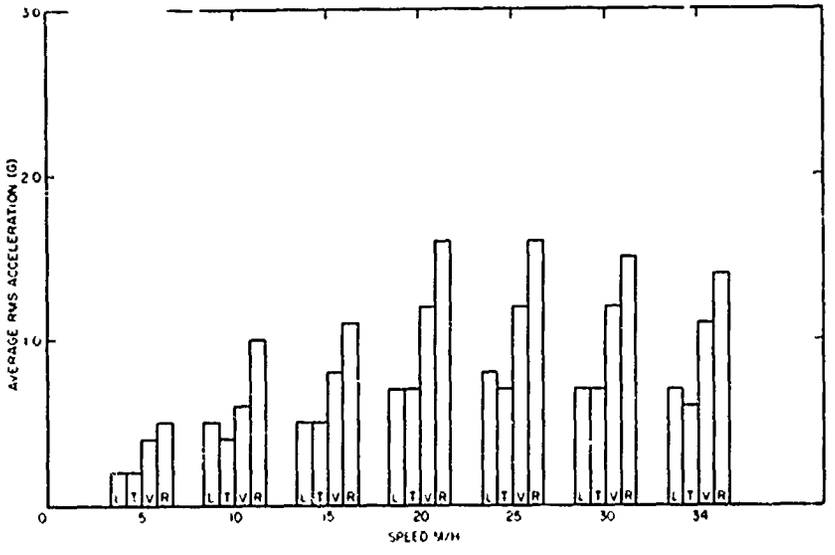

(c) 4500-lb load

Fig. 9 - Average rms accelerations of all the measurement locations--Continued

load condition represented the approximate maximum severity level tolerated by the drivers of the nine trucks for the tests which produced the data presented in Fig. 4. Also, it has been shown that in a random process 99 percent of the peak values will be below a value of 3 times the rms value. Accordingly the 1.4 g rms value translates to a peak value of 4. 2 g. This peak value is considered acceptable from a fiduciary viewpoint, where the maximum level may be arbitrarily set at 3 g as suggested by Fig. 4. The zero or light-load condition represented by Fig. 9(a) and 10(a) in terms of g rms, represents the most severe condition since additional loading suppresses the high-frequency vibration components generated by the truck platform panels. This is demonstrated by comparisons with Fig. 9(b) and 9(c), and with Fig. 10(b) and

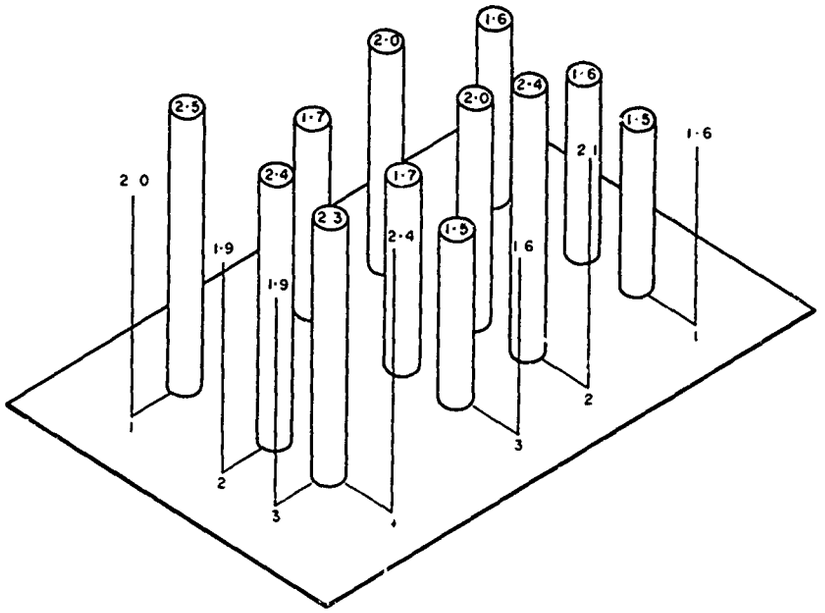

(a) Zero-lb load

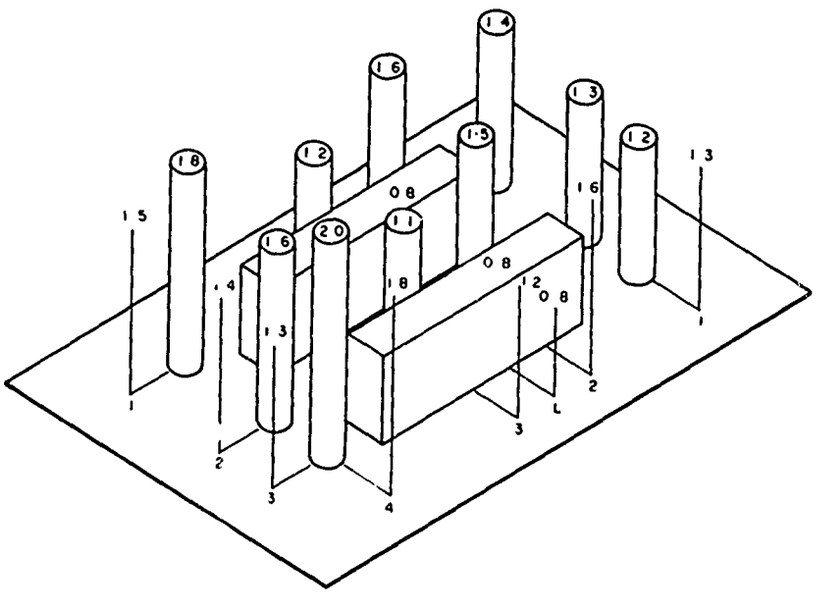

(b) 2300-lb load

Fig. 10 - Average rms resultants of each position for all speeds. Bars are placed at the approximate measurement locations and their heights represent the rms accelerations (in g) whose values are indicated at the top of the bars. Vertical lines indicate average rms values for each row and column.

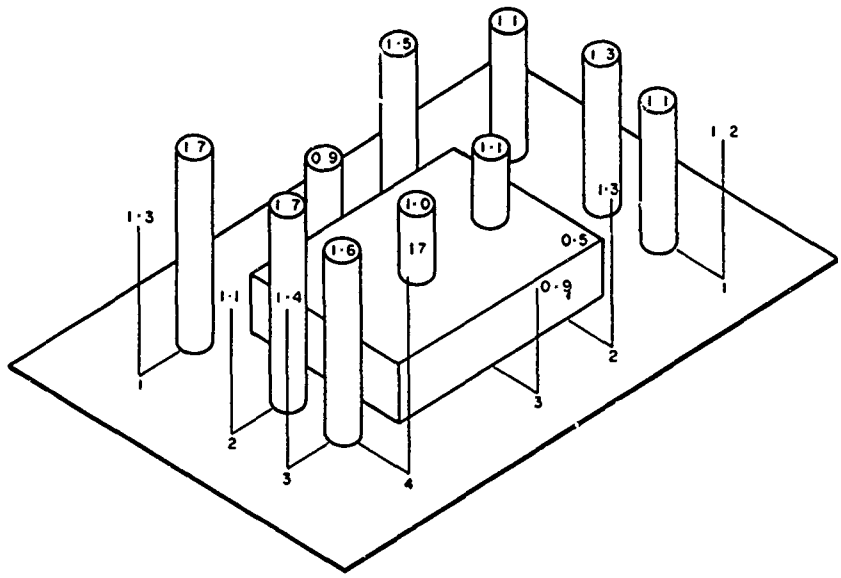

(c) 4500-lb load

Fig. 10 - Average rms resultants of each position for all speeds. Bars are placed at the approximate measurement locations and their heights represent the rms accelerations (in g) whose values are indicated at the top of the bars. Vertical lines indicate average rms values for each row and column--Continued.

10(c). It should be noted that the structural stiffening effect of the steel-weight loads bolted to the floor panels reduces the resulting g-rms responses considerably on the weight loads themselves. For the 2300-lb load as shown for position LL (on left load), Fig. 10(b), the acceleration level is 0.8 g rms. For the 4500-lb load a value of 0.5 g rms is indicated at the corner of the load assembly near location 2-3, Fig. 10(c).

It can be inferred, therefore, that the data analysis supports the conclusion that the bumps used on the simulator drums, in the development of this proposed specification, generate adequately a random vibration corresponding to the upper level of severity demonstrated to occur in the field.

DETERMINATION OF DURATION OF TESTING PROCEDURE

The duration of testing for the proposed specification is based on experience with the application of other specifications. Military Standard MIL-STD-167 (Ships), "Mechanical Vibrations of Shipboard Equipment," was adopted as a principal guide in this determination because of the long-term equipment developmental program conducted by the Naval Research Laboratory under its requirements, and one of its predecessors, BUSHIPS Specification 40T9.

Since 1947 Shock and Vibration, Test and Evaluation Programs at the Naval Research Laboratory have been conducted on a developmental rather than "go-no-go" basis. For most of the damages occurring during the tests, modifications were made which precluded the same failure. Consequently, as testing progressed difficulties were gradually worked out of a design. If indicated modifications were major, or the equipment was shown to be generally unsatisfactory for test requirements, it was returned to the manufacturer for the changes.

In Fig. 14 the number of vibration damages to 120 equipments tested under this developmental program according to BUSHIPS Specification 40T9, is plotted for the three principal directions of vibration [11]. Fifty of the units were shock-mounted and seventy were not shock-mounted. Both medium and lightweight, electronic and nonelectronic equipments were included in the results, and only those equipments which satisfactorily completed the tests were considered in compiling data.

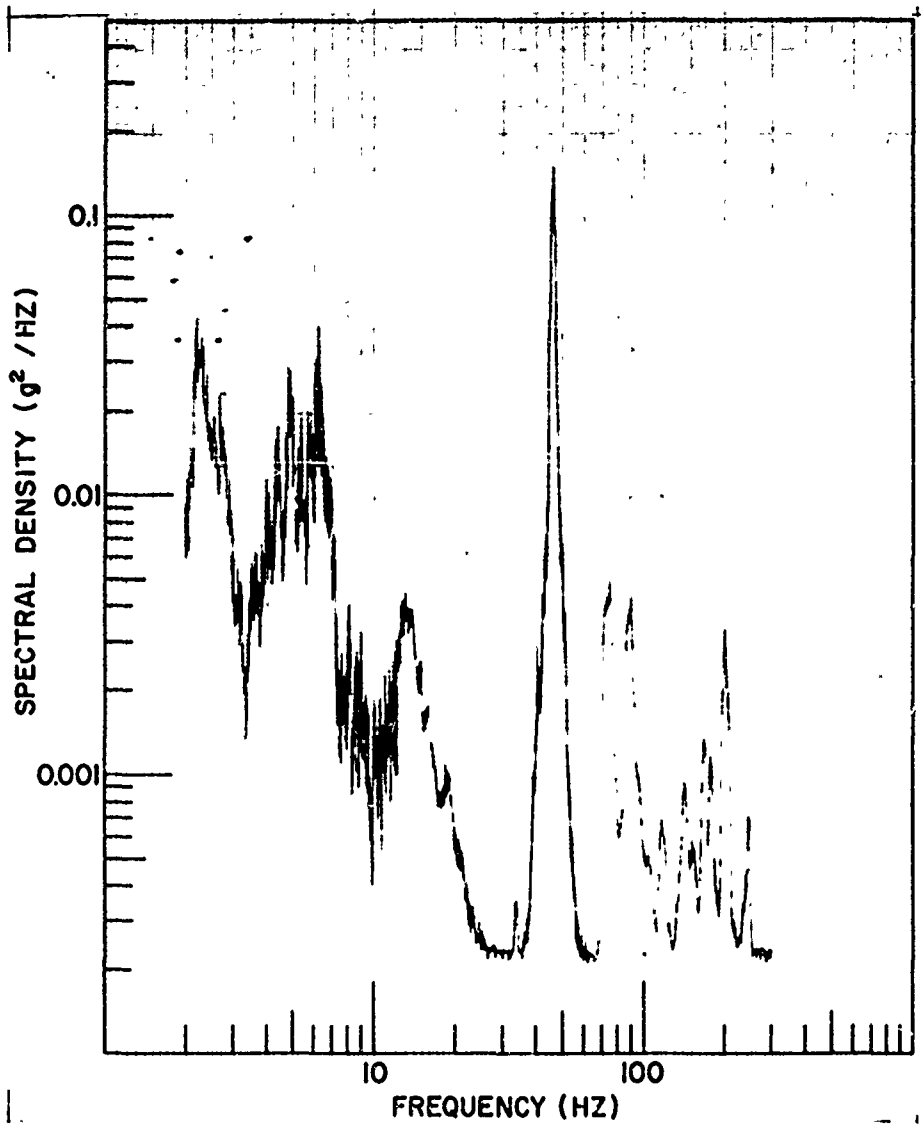

(a) Vertical

Fig. 11 - Typical group of spectral density plots obtained for platform position row 2 column 3, for zero-lb and speed of 20 mph

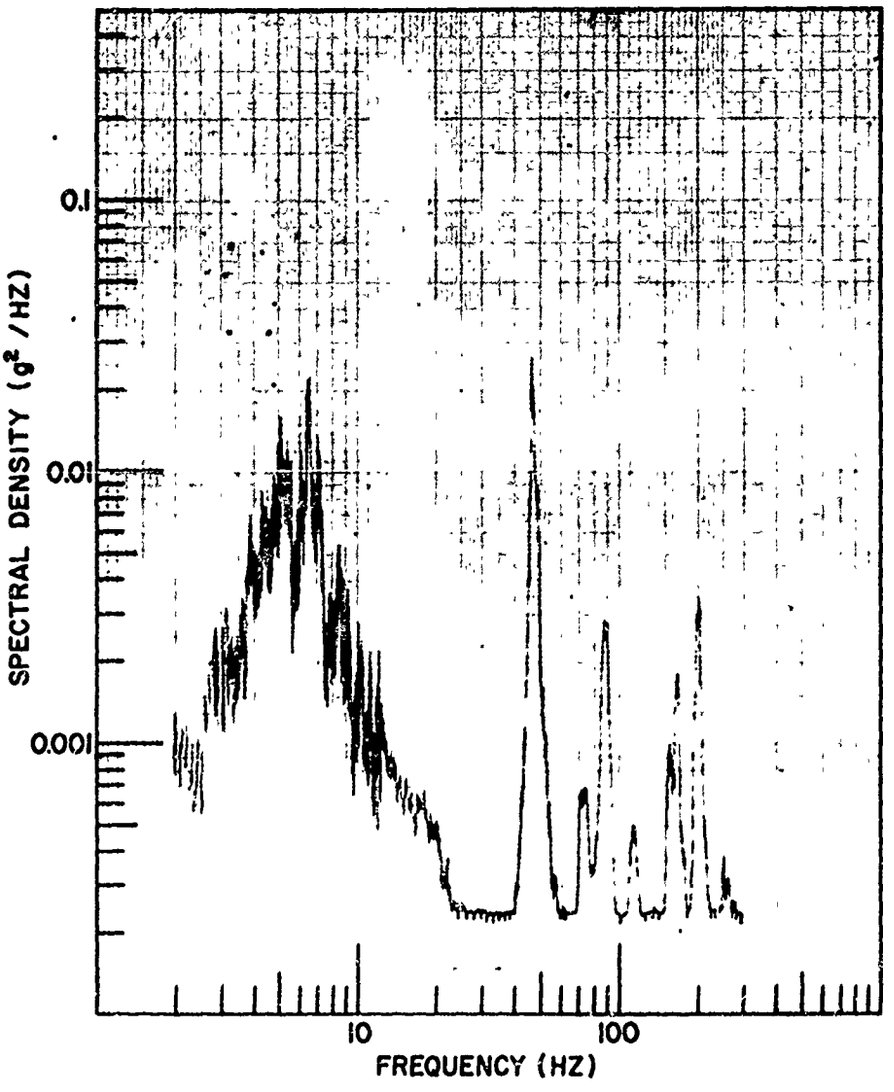

(b) Transverse

Fig 11 - Typical group of spectral density plots obtained for platform position row 2 column 3, for zero-lb and speed of 20 mph--Continued

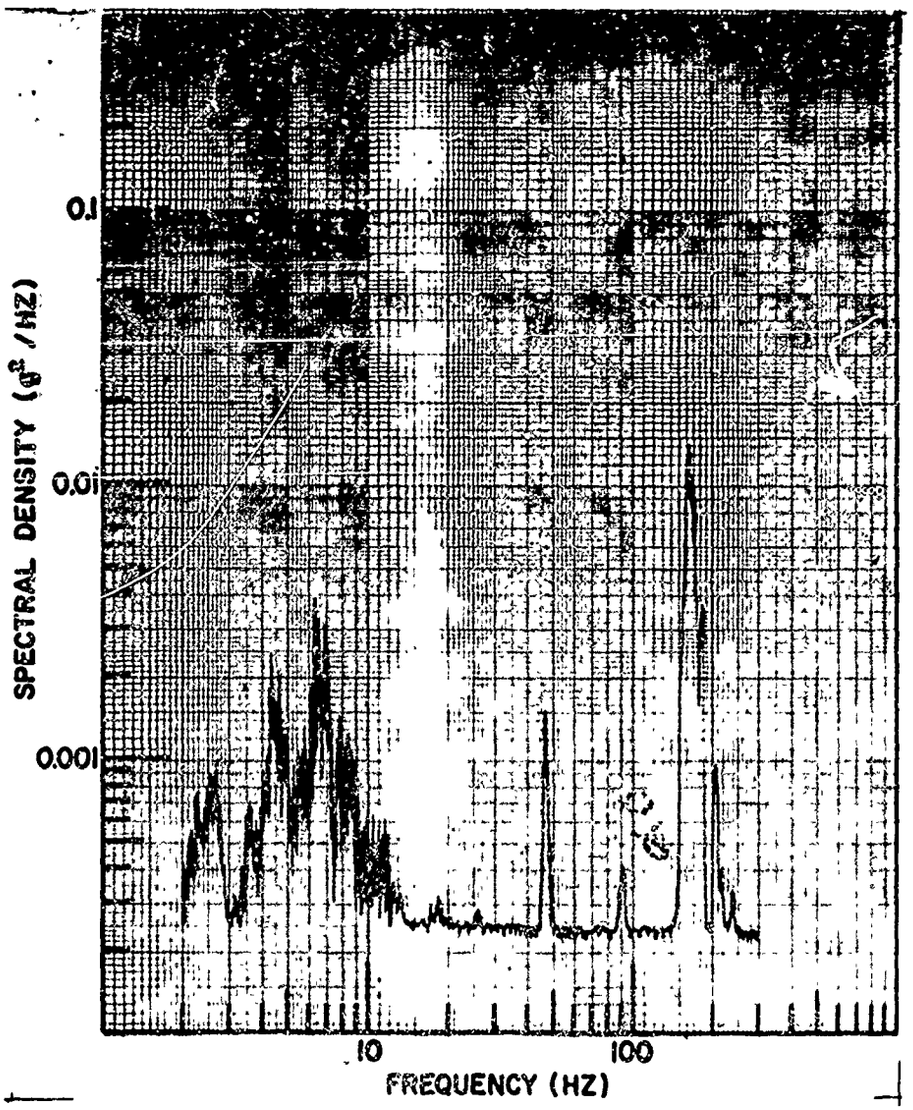

(c) Longitudinal

Fig. 11 - Typical group of spectral density plots obtained for platform position row 2 column 3, for zero-lb and speed of 20 mph--Continued

Fig. 12 - Steel-weight arrangement for the nominal 4300-lb truck load

Vibrations in the directions corresponding to the lowest horizontal resonant frequency and in the vertical direction are seen to be of approximately equal severity. Low resonant frequencies of the rocking modes of vibration were the chief cause of damages in the first direction, whereas low individual chassis resonances probably the great number for the latter. Only the first mode of vibration in each direction was excited by the frequency requirements of the testing specifications. The few damages occurring in the last half-hour test period in each direction indicated that the duration of the endurance test, 2-hr in each direction, was adequate to determine with a high degree of confidence whether or not an equipment displayed good dynamic characteristics.

Since the rough-road simulator produces vibration simultaneously in three directions it was concluded that the total testing time should be limited to about one-third of the total time required for testing in three mutually perpendicular directions consecutively, in accordance with the procedures of MIL-STD-167 (SHIPS), which is 13 hr and 15 min or 4 hr and 25 min in each direction up to 33 Hz maximum. The total maximum testing time required by the proposed specification is 3 hr and 48 min, of which 2 hr is designated as the endurance portion.

SUMMARY

1. A proposed draft of a Wheeled-Vehicle Rough-Road Transportation Test Specification is presented as Appendix A herewith.

2. The specification is related to the use of a specific machine designated by the descriptive

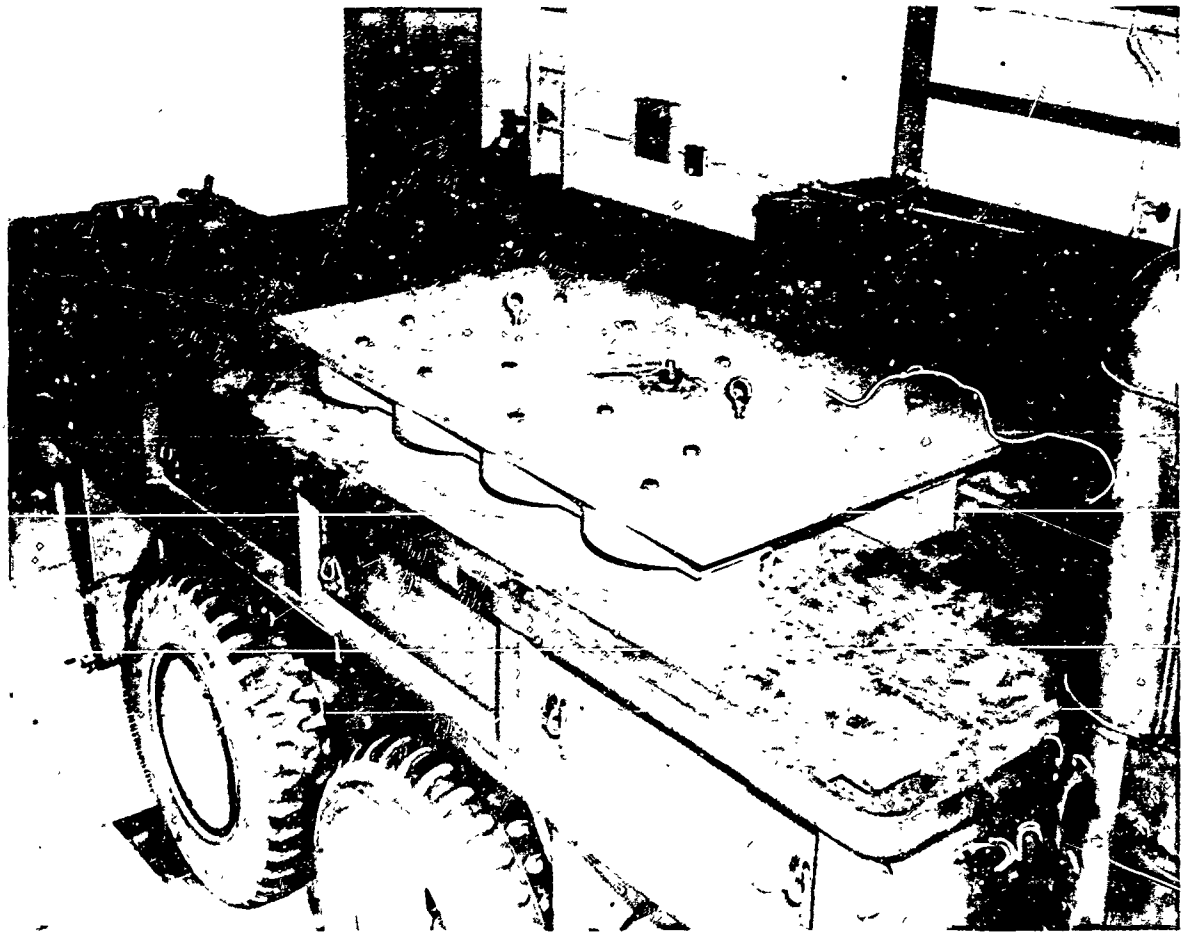

Fig. 13 - Steel-weight arrangement for the nominal 4500-lb truck load

title of "Rough-Road Simulator for Wheeled Vehicles."

3. This machine has been placed in successful operation and provides a practical and economical laboratory device for the simulation of the shock and vibration environment encountered by equipment transported in wheeled vehicles.

4. Representative samples of spectral density plots (g^2 per Hz) for three different loadings and several speed combinations for a 2-1/2-ton, 6 × 6 open body truck were obtained to illustrate the statistical analysis of the responses.

5. Advantages accruing by use of this machine and specification are enumerated in the following subparagraphs.

a. Since this machine produces transport-like motion simultaneously in three directions, only one test-mounting set-up is normally required versus two or three mounting set-ups incurred in vibration testing with conventional vibration machines.

b. The simulator input of simultaneous random vibration in three directions is a reasonably accurate duplication of the wheeled-vehicle transportation environment and results in reducing the test duration to one-third of that required when conventional vibration testing machines are used.

c. The impedance coupling frequencies for varying weight loads imposed on the test vehicle are duplicated precisely without manipulation for a given road profile.

REFERENCES

1. U.S. Military Standard, Environmental Test Methods, MIL-STD-810B 15 June 1967, METHOD 514, METHOD 516.

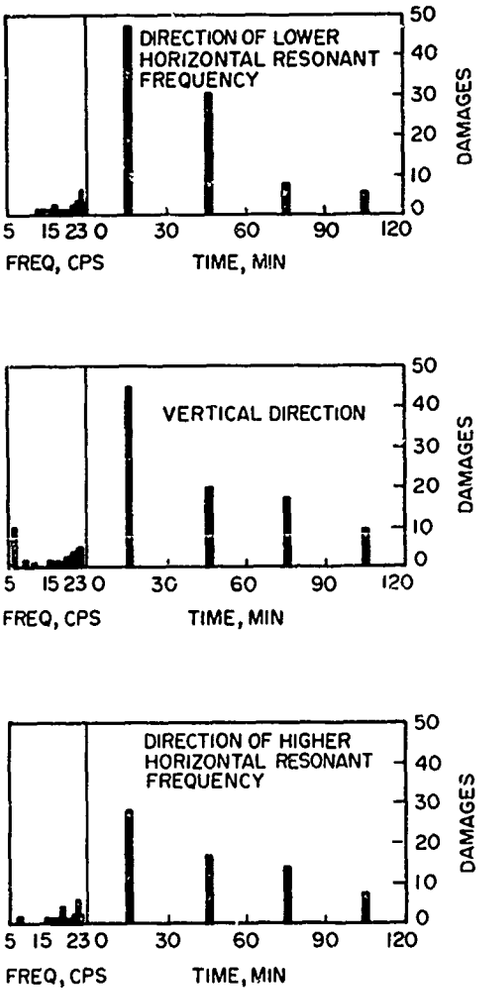

Fig. 14 - Vibration damages to equipments tested according to Bureau of Ships. Specification 40T9.

2. U.S. Military Standard, Test Methods for Electronic and Electrical Component Parts, MIL-STD-810B Notice 2, 27 May 1965 METHOD 201A, METHOD 202B, METHOD 205C, METHOD 213

3. H.M. Forkois, Report of NRL Progress, January 1963, pp. 14-17

4. H.M. Forkois, "Rough Road Simulator for Wheeled Vehicles," SAE Journal 71, No. 6, June 1963

5. H.M. Forkois, "Rough Road Simulator for Wheeled Vehicles," Naval Engineers Journal, December 1963

6. E.W. Clements, "Analysis of NRL Rough Road Simulator Outputs," Report of NRL Progress, July 1967

7. H.M. Forkois, "Development of a Rough-Road Simulator and Specification for Testing of Equipment Transported in Wheeled Vehicles," NRL Memorandum Report No. 2100

8. E.W. Clements, "Measurement and Analysis of Acceleration Environments — Measurement and Analysis of Acceleration Environments Generated by NRL Rough Road Simulator," NRL Memorandum Report No. 2097

9. "Standard Load Vibration Test on the Munson Test Area," Automotive Division Publication, Aberdeen Proving Ground, Maryland, December 1959

10. Shock and Vibration Bulletin No. 6, U.S. Naval Research Laboratory Report S-3200, November 1947

11. K.E. Woodward and H.M. Forkois, "Designing for Resistance to Shock and Vibration," Electrical Manufacturing, July and August 1954

Appendix A

A PROPOSED DRAFT OF A WHEELED-VEHICLE ROUGH-ROAD TRANSPORTATION TEST SPECIFICATION

1. Scope

1.1 The purpose of this specification is to establish tests which can be used to determine whether or not an equipment or assembly is sufficiently rugged to withstand vibration environments when transported in trucks, or other wheeled vehicles, incident to traversing rough roads and cross-country terrain.

1.2 Test procedures are given which provide a simulation of the general vibration environment occurring in wheeled vehicles in traversing these worst-case surfaces.

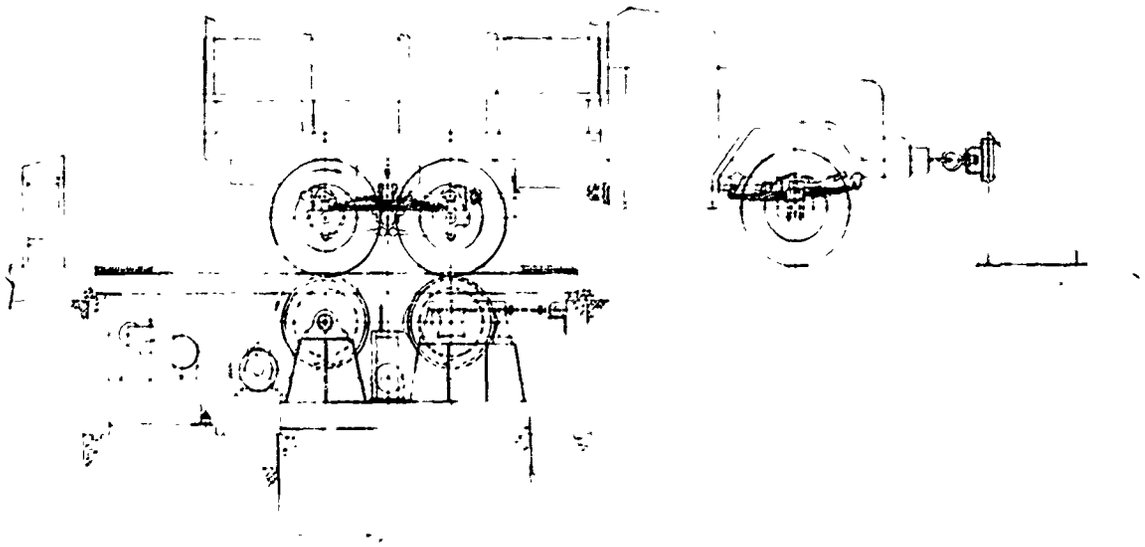

Fig. A1 - Rough-road simulator for wheeled vehicles (general arrangement)

2. Rough-Road Simulator or Test Machine

2.1 General Description. The simulator consists of a test-machine vehicle which is placed with its wheels on the drum wheels of the test machine (Fig. A1). The surfaces of the drum wheels are provided with a suitable contour by bolting bumps to their surfaces. The test machine vehicle is constrained from moving appreciable distances fore and aft and sideways. As the drums are rotated, shock excitation is applied to the vehicle. The equivalent road speed is equal to the surface velocity of the drum wheels.

2.2 Test-Machine Vehicle. The test machine vehicle may be any one of several types. If the item to be tested is to be transported, or installed, in a particular vehicle type, then a test-machine vehicle similar to this type may be used. If no preference of vehicle is indicated then the test-machine vehicle shall be a 2-1/2-ton 6 × 6 open body truck. Other test-machine vehicles may be jeeps, trailers, or special carriers.

2.3 Maintenance of Test-Machine Vehicle. The test-machine vehicle shall be maintained in proper operating condition. The tires shall be inflated to recommended values before each test. If the vehicle is equipped with shock absorbers their effectiveness shall be subject to weekly inspections. The chassis shall be lubricated as specified in the maintenance manual, at least once a month, or after each 50 hr of machine operation.

2.4 The test-machine vehicle shall have no other loads except those of the items or assemblies under test and such auxiliary equipment as may be necessary for the performance of the test.

2.5 Bumps or Drum-Wheel Profiles. Unless otherwise specified the drum-wheel profiles shall consist of two bumps of different eccentricities per drum. They shall be placed 180 degrees apart and they shall be shaped as shown in Fig. A2.

3. Methods of Performance of Tests

3.1 Location and Mounting of Test Item in the Test Machine Vehicle. The test item shall be secured to the test machine vehicle in a manner which would simulate normal practice. If several different methods of securing the test item are probable, and they involve different orientations of the test item, then it may be required that the test be performed for each of the several orientations. The test item shall be secured at a location immediately above the rear wheels of the test vehicle and as near the right or left hand side of the vehicle as is practical.

3.2 Unsecured Test Items. If the test item is unsecured then the forward part of the cargo

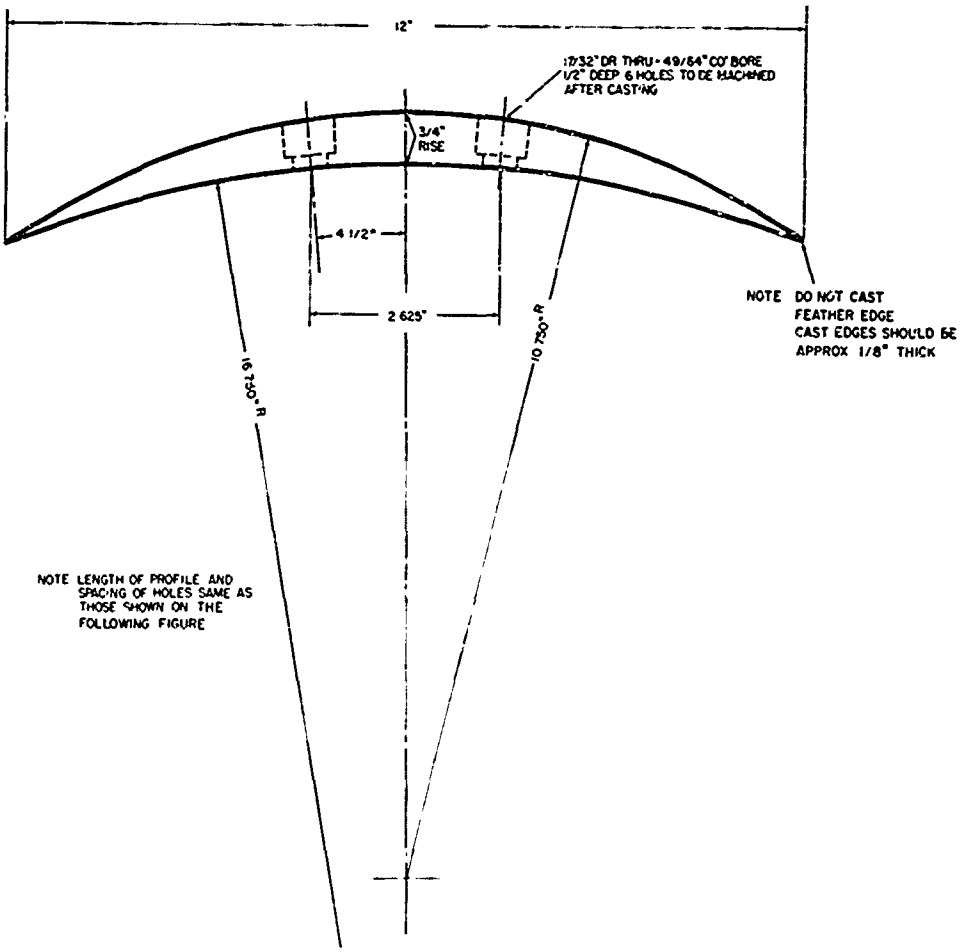

(a) 3/4-in. eccentricity

Fig. A2 - Details of bump contours

space shall be fenced off so that the test item will be contained in the rear part of the cargo space. If the size of the test item permits, the fence should divide the cargo space into two approximately equal parts.

3.3 Exploratory Test. The first part of the test is to provide an opportunity for short time observation of the responses of the test item at any equivalent road speed. The test machine shall operate so that the drum-wheel peripheral speed corresponds to an integral number of miles per hour from 5 mph up to some maximum value appropriate for the vehicle. The maximum value shall be 35 mph unless otherwise specified. The time of test shall be 3 minutes at each average integral value of speed.

3.4 Endurance Test. The endurance test shall consist of a minimum of 15 min at each speed that is a multiple of 5 mph, up to the maximum value. In addition there shall be a 15-min test at a speed which is deemed by the test engineer to be most damaging to the test item or assembly. In no case shall the endurance test be less than 2-hr duration.

4. Criterion for Acceptable Performance of Test Items

4.1 Equipment Subjected to Infrequent Transportation Environment. Unless otherwise specified, a test item in this category will be considered to have acceptably passed the rough-road transportation test if after the test there is not evidence of major structural damage and the equipment can be put into proper operating condition with but minor adjustments.

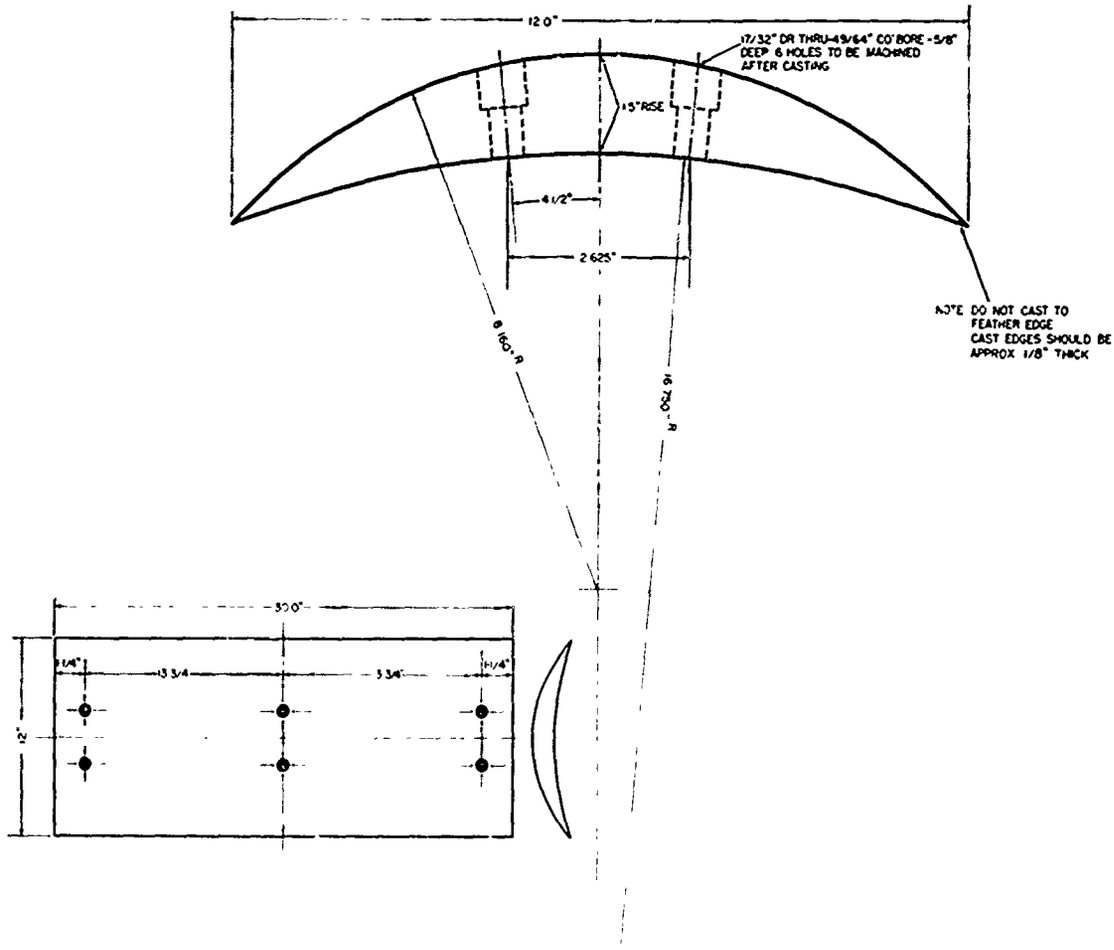

(b) 1-1/2-in. eccentricity

Fig. A2 - Details of bump contours--Continued

4.2 Equipment Mounted in Vehicles and Portable Equipment. No significant damage shall be acceptable for equipment that is subjected frequently to transportation environments. Equipment that is required to operate during transportation shall be in an operating condition during the test, and if not so required, it shall be specified that the equipment be capable of restoration to normal operation with no unusual delay after the completion of the test. Acceptable down-time should be stated in the equipment specification.

5. Nature of the Transportation Environment

Because of the complex nature of a test machine vehicle, and the random nature of the vibrations generated, it should not be expected that tests on different test vehicles of the same type will be identical, even though the equipments carried and their methods of attachment are the same. However, if the rms values of the vibrations derived under these conditions with instrumentation having a prescribed bandwidth, deviates appreciably more than 10 percent from each other, there may be reason to suspect damage or wear to parts of the suspension system of the vehicle, namely springs and shock absorbers. Improper inflation of the tires or brake drag may be other causative factors for large deviations. In some cases, design changes in the suspension systems of more recent vehicle models may cause substantial variations in the rms vibration values.

LABORATORY CONTROL OF DYNAMIC VEHICLE TESTING (U)

James W. Grant
U. S. Army Tank-Automotive Command
Warren, Michigan 48090

In order to study vehicle suspension and frame dynamics under controlled and reproducible laboratory conditions, TACOM's road simulator or "shaker test" was developed. A road simulator is a laboratory test device which imparts dynamic forces simulating road inputs, on a complex vehicle. It is the purpose of this study to develop vertical position control signals for the road simulator so that good correlation between laboratory test and field results is obtained. As a result of this study, the design engineer has a more exact vehicle model than he has had and the test engineer has a laboratory simulation which has been verified for vertical dynamic inputs. The combined effect of these two engineering tools will serve to produce a better prototype vehicle which in turn will eliminate many of the initial field test failures which plague new vehicles.

INTRODUCTION

The road simulator concept of laboratory vehicle testing came into existence to facilitate studies of frame and suspension dynamics. Prior to the road simulator, frame and suspension components were divorced from the vehicle for laboratory evaluation. In most cases, the control or excitation signal for the test was some well defined mathematical function whose correspondence validity to actual field excitation is questionable. Testing then progressed to a point where recorded field signals and shaped random noise were used to control component tests.

Since there is interaction between the component being tested and the vehicle to which it is mounted, it became apparent that a road simulator which would test the total vehicle system in the laboratory would yield useful results. The early road simulators provided vertical inputs of low amplitude to each wheel of a passenger car. The inputs were accomplished using four electro-hydraulic linear actuators with pedestals on which the tires rested.

Laboratory testing of off-road vehicles offered a new challenge. Due to the large wheel deflections, the vehicle must be restrained from falling off the road simulator. In order to facilitate restraining the vehicle and also to allow the addition of longitudinal excitation forces, the wheels were removed and the spindles attached to the actuator through a multiple degree of freedom assembly. The restraints were attached from vehicle to ground so that their effect on the dynamic motion of the sprung mass was minimal.

The present state of the art includes vehicles in the 5-ton payload class with up to six vertical and four horizontal linear actuators. Currently being constructed at the U. S. Army Tank-Automotive Command (TACOM) is a road simulator for 1/4-ton class vehicles which has four vertical actuators with position control, four horizontal actuators with load control and four rotary hydraulic pumps to be used as absorption dynamometers with torque control. This simulator, fully operational, will test the total vehicle system under controlled laboratory conditions.

The analog position or force signals which control the electro-hydraulic actuators must produce motions or forces in the vehicle which can be correlated with those which were recorded during field tests. This paper will present in detail three different techniques by which valid position control signals may be obtained from recorded field data or from surveyed terrain elevations.

CONTROL SIGNAL GENERATION TECHNIQUES

The analog signal which controls the electro-hydraulic actuators of the road simulator may be proportional to either position or force. The vertical road input actuators are position controlled and the fore and aft horizontal road input actuators are load controlled. The most readily obtained field data which can be transformed into vertical wheel spindle displacements are vertical accelerations of the wheel spindles. Terrain profile data can also be transformed into vertical wheel spindle displacement if accurate vehicle and tire models are on hand.

Double Integration

The acceleration signal which is to be double integrated is the vertical acceleration of the wheel spindle. The vertical accelerations of each wheel are recorded simultaneously so that the control signals generated from these accelerations will have the proper phase relationship. The acceleration signals thus recorded are a function of the suspension geometry, the suspension parameters, the tire characteristics and the terrain profile. Changes in any of the above vehicle characteristics would require that a new test course traverse be made. For the following analysis, assume that an accurate recorded acceleration signal is available.

The integral of well defined mathematical functions can be found in any calculus text. Mathematically, the integral of a continuous random variable such as vertical wheel acceleration is also well defined. In fact, the double integral of acceleration which results in displacement is also well defined. The physical implementation of double integration, however, is not well defined.

It is a well known fact that a stable perfect double integrator which has the transfer function $G_1(S) = 1/S^2$ is not physically realizable. The task, then, is to develop a stable transfer function, the frequency response of which approaches the double integrator in the desired frequency band of .5 to 50Hz. This band is within the response limits of most road simulators and also includes the frequencies of interest for suspension dynamics studies. The transfer function chosen to double integrate the recorded acceleration signal to produce the position control signal for the road simulator is $G_2(S) = \frac{KS^2}{(S+4)^4}$

As can be seen in Figure 1, the frequency response curve for $G_2(S)$ when K = 1 asymptotically approaches perfect double integration beyond .636 Hz. The important characteristic of $G_2(S)$ is that the low frequency components of the input signal are suppressed. These low frequency components, especially zero frequency of D.C. offset, are the prime contributors to unstable double integration. This fact is quite clear in Figure 1. As frequency approaches zero, $G_1(S)$ approaches infinity and $G_2(S)$ approaches zero. The low frequency accuracy of $G_2(S)$ can be theoretically improved by shifting the intersection of its asymptotes to the left. This can be accomplished by decreasing the constant 4 in the denominator to 3, for example. However, as this constant approaches zero, $G_2(S)$ approaches $G_1(S)$. Another way to increase low frequency accuracy is to increase K. Increasing K, however, raises the whole response curve and the higher frequency accuracy decreases. Stability is also reduced as K is increased. Either method requires trial and error to determine which K or which denominator gives acceptable response in the desired frequency range.

Figure 2 shows the result of playing a field-recorded acceleration signal into $G_2(S)$ with K = 1. The acceleration signal was recorded at the front wheel spindle of an M656 5-ton 8x8 cargo truck as it traversed the Aberdeen Proving Ground Belgian Block Course at an average speed of 15 miles per hour. The displacement signal peak to peak magnitude of .2 feet (Figure 2) was observed during the recording of the acceleration tape.

The accuracy of the approximate double integration depends, of course, upon the transfer function used to perform this operation. The

correlation between the field recorded vertical acceleration of the wheel and the laboratory recorded vertical acceleration of the wheel can be computed to numerically determine the accuracy of the double integration.

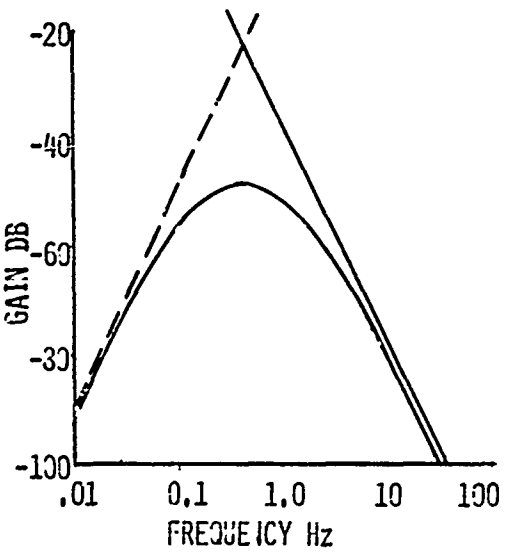

FIGURE 1 BODE PLOTS FOR $1/S^2$ AND $S^2/(S+4)^4$

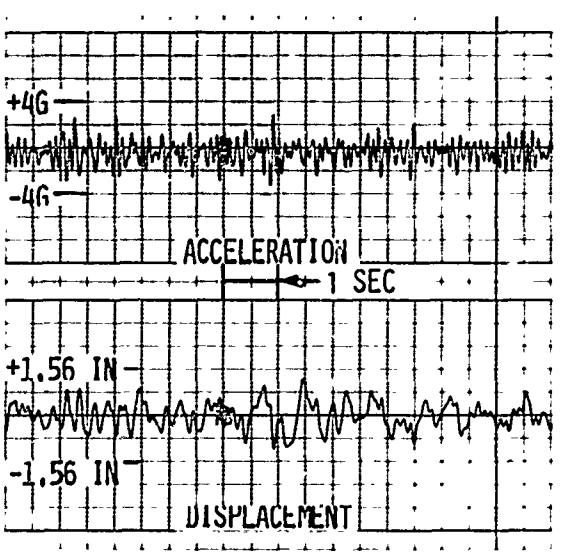

FIGURE 2 ACCELERATION AND RESULTING DISPLACEMENT-TIME TRACES FOR $G_2(S)$

Filtered Noise

The idea of playing random noise, which has a flat power spectrum, through a shaping filter to control a laboratory road simulator has been suggested previously (references 1 and 2).

In order to apply this control technique, the vertical wheel spindle acceleration must be recorded on magnetic tape during field runs. From this data, a shaping filter for random noise is desired such that the filter output is a displacement signal statistically equivalent to the recorded acceleration signal.

Let the filter to be defined be a linear time invariant function so that conventional methods of analysis may be used. The total system is:

$$y(t) = h(t) \times n(t) \qquad (1)$$

Where--

$n(t)$ is the random noise input
$h(t)$ is the filter
$y(t)$ is the output displacement

Using the convolution integral and the fourier transform, as described in reference 3, page 182, the following relationship is obtained from equation (1):

$$S_{dd}(f) = |H(j2\pi f)|^2 \; S_{nn}(f) \qquad (2)$$

Where--

$S_{dd}(f)$ is the power spectral density (PSD) of the desired displacement control signal.

$S_{nn}(f)$ is the PSD of random noise. This is a constant and will be defined to be unity.

$H(j2\pi f)$ is the frequency response function for the shaping filter.

The relationship between displacement and acceleration PSD's is defined to be:

$$S_{dd}(f) = \frac{1}{(2\pi f)^4} \cdot S_{aa}(f) \qquad (3)$$

Substituting $S_{dd}(f)$ in equation (3) gives:

$$S_{aa}(f) = (2\pi f)^4 \; |H(j2\pi f)|^2 \; S_{nn}(f) \qquad (4)$$

Since $S_{nn}(f) = 1$ by previous definition:

$$H(j2\pi f) = \frac{1}{(2\pi f)^2} \cdot \sqrt{S_{aa}(f)} \qquad (5)$$

Equation (5) will now be used to obtain from field data the frequency response for the desired filter.

Figure 3 is a PSD curve of the vertical front wheel acceleration of an M656 5-ton 8x8 cargo truck. The acceleration signal was recorded during field tests at Aberdeen Proving Ground at an average vehicle speed of 14.2 miles per hour. The test courses were the Belgian Block Course, Three-Inch Spaced Bump Course, Two-to-Four-Inch Radial Washboard Course, Imbedded Rock Course and Two-Inch Washboard Ccurse. Substituting the values for $S_{aa}(f)$ from Figure 3 into equation (5) results in the desired frequency response curve shown in Figure 4. The desired curve was approximated using an ESIAC algebraic computer by the following transfer function where $j2\pi f$ is replaced by the Laplace Operator S:

$$H(S) = \frac{15.123\,(S^2 + 86.4S + 202S)}{(S^2 + 10.5S + 122S)\,(S^2 + 5S + 25)} \qquad (6)$$

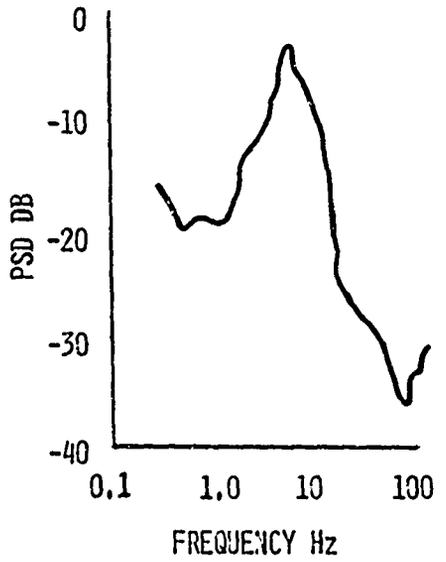

FIGURE 3 PSD OF FIELD RECORDED VERTICAL WHEEL ACCELERATION

The actual frequency response curve for equation (6) is the dashed curve in Figure 4. Figure 5 is the output of the filter with a random noise input.

Since PSD is an approximate measurement and the actual filter response function is an approximation of the desired filter response function the accuracy of this technique depends upon the accuracy of the approximations. This technique is validated using statistical measurement techniques such as histograms, cross correlation and probability density functions.

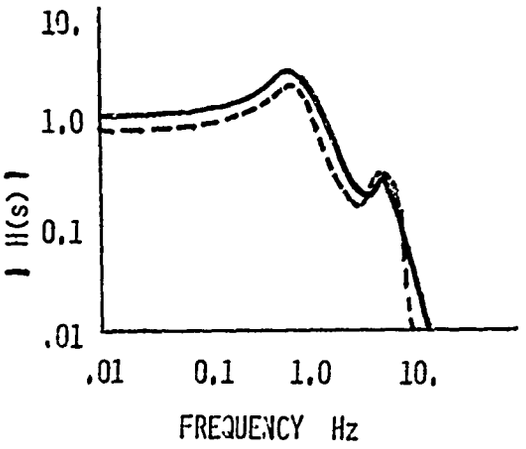

FIGURE 4 FREQUENCY RESPONSE CURVES FOR DESIRED AND ACTUAL FILTERS

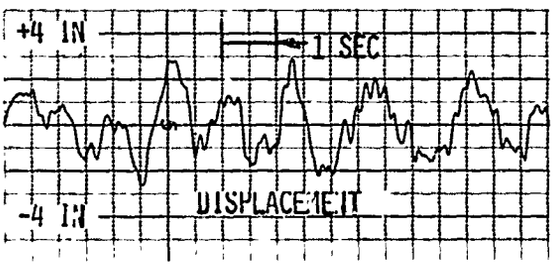

FIGURE 5 POSITION CONTROL SIGNAL - SHAPED RANDOM NOISE

Terrain Profile

The two previous methods of control signal generation required that vehicle dependent acceleration signal at the wheel spindle be recorded during test course traverse. In other words, new instrumented test runs must be made for each different vehicle configuration. Consider now the possibility of using surveyed terrain profiles to control the road simulator system where the excitation is through the wheel spindle as previously stated.

Surveyed terrain elevation data are readily available, in reference 4, for example. The major problem to be solved then is the transfer function from terrain to the wheel spindle. This transfer function represents not only the tire assembly dynamics but is

also a function of the suspension dynamics and the sprung mass. It is concluded then that a mathematical model of the total vehicle system is required. This model would be programmed on an analog or hybrid computer and run in parallel with the road simulator to provide the wheel spindle position control signal. The block diagram of this system is shown in Figure 6.

FIGURE 6 SYSTEM BLOCK DIAGRAM

The system in Figure 6 assumes an accurate model of both the tire and the vehicle. The tire is a complex non-linear system which is discussed thoroughly in reference 5. A tire model can be made so complex that it is unwieldy or it can be simplified to a second order mass-spring-damper system. The latter case with a realistic non-linear spring and point follower, Figure 7, may give satisfactory results for the vertical control of a road simulator.

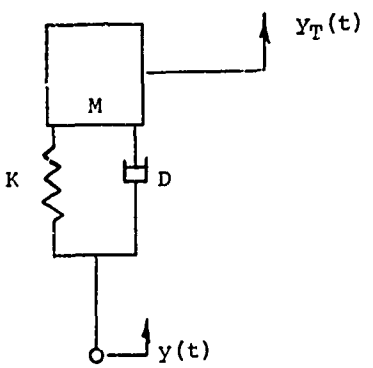

FIGURE 7 SIMPLE TIRE MODEL

Where--

M is the unsprung mass
K is the spring rate
D is the damping coefficient
y(t) is the terrain profile
$y_T(t)$ is the wheel displacement

NOTE that the velocity profile, y(t), of the terrain is also required. The digitized terrain profile is digitally differentiated to obtain y(t).

Obtaining an accurate mathematical model of the vehicle dynamics is facilitated by the availability of the road simulator. The differential equations of motion for the vehicle are obtained using any of the conventional techniques such as Lagrangian or Newtonian mechanics. The equations are then programmed on an analog or hybrid computer. The computer model and the road simulator are excited at the wheel spindles with identical signals and the responses are compared. The response is a combination of sprung mass output signals, which could include, for example, pitch, bounce and roll displacements. The parameters of the computer model are adjusted either manually or automatically such that the error between comparison signals is minimized. Reference 6 presents a continuous parameter tracking technique which could be extended to attain the automatic parameter adjustment.

Once the accurate model is obtained, its parameters may be easily adjusted to maximize some index of performance such as driver comfort. The sensitivity of any performance parameter to changes in each of the physical vehicle parameters can be measured. This type of study tells the design engineer a range of acceptable values for each physical parameter. The physical parameters include spring rates, damping coefficients, center of gravity location, wheel base, etc.

The above described technique is an ambitious undertaking currently being implemented at TACOM. Extensive computer analysis is required, but the resulting vehicle model will give the design engineer a new tool with which to improve vehicle performance.

SUMMARY

Three methods for obtaining the road simulator control signal (the input at the wheel spindle of the test vehicle) have been presented.

The double integration of field recorded vertical wheel spindle acceleration and the filtered random noise both require field data acquired by a vehicle similar to the test vehicle. These two methods are well suited to long term durability studies.

The third method requires and facilitates the development of an accurate mathematical model of the vehicle. The selected terrain profile is played into the computerized vehicle model and the wheel displacement signals from the model are then used to control the road simulator.

The mathematical model resulting from this technique may now be adjusted to produce improved ride quality. From this study, new hardware may be developed to improve the vehicle's ride quality.

The first two techniques have been used at TACOM to control simulators. The third technique is currently being implemented; we expect to be using it by November, 1971.

REFERENCES

1. Van Deusen B.D., et al, "Experimental Verification of Surface Vehicle Dynamics", NASA CR-1399, National Aeronautics and Space Administration, Washington, D.C., September, 1969.

2. Van Deusen, B.D., "A Statistical Technique for the Dynamic Analysis of Vehicles Traversing Rough Yielding and Non-Yielding Surfaces", NASA CR-659, National Aeronautics and Space Administration, Washington, D.C., March, 1967.

3. Davenport, W.B., Jr., and Root, W.L., "An Introduction to the Theory of Random Signals and Noise", McGraw-Hill Book Co., Inc., New York, N.Y., 1958.

4. Heal, S., and Cicillini, C., "Micro Terrain Profiles", RRC-9, U.S. Army Tank-Automotive Center, Warren, Michigan, 14 August 1964.

5. Schuring, D., and Belsdorf, M.R., "Analysis and Simulation of Dynamical Vehicle-Terrain Interaction", Cornell Aeronautical Laboratory, Inc., Cornell University, Buffalo, N.Y., May, 1969.

6. Jackson, G.A., and Grant, J.W., "Linear Suspension System Parameter Identification", SAE 710227, Automotive Engineering Congress, Detroit, Michigan, January, 1971.

IMPACT VULNERABILITY OF TANK CAR HEADS

Jen C. Shang and John E. Everett
General American Research Division
General American Transportation Corporation
Niles, Illinois

An Impact Vulnerability study of tank car heads was undertaken by means of semi-analytical evaluation of head failures through careful observation of indentations and punctures which were produced in a series of full-scale tests. The parameters which would influence the vulnerability of tank car heads were identified. Simple formulas which could be used to determine the permanent indentation and the impact force were developed in conjunction with a theoretical analysis of influential dimensionless parameters and an application of Hertz' force-indentation law to collision problems. Finally, the tank car head failure criteria were established.

INTRODUCTION

In the past several years, a number of railroad derailments resulted in catastrophic failure of tank cars, either in the form of indentation or puncture, which caused the evacuation of cities, personal deaths and injuries, and property losses totalling millions of dollars. Although defects and improper maintenance on railroads are the major causes cited by government safety experts for derailment which have soared 105% in seven years, a method of solution must be sought to protect tank cars to reduce the frequency of head punctures in accidents, especially for tank cars transporting hazardous materials.

A number of tank-car heads are either indented or even punctured by couplers, side sill, end sill or other flying objects during derailments. Application of a shield, bumper or other possible protective structure to the lower part of tank car heads appears to be one feasible approach to reducing the number of incidents involving release of the product.

The first step, protecting tank car heads from puncture damage, is to determine the impact vulnerability of tank car heads. However, so far, no direct observations or instrumentations of head failure phenomena have been made in any accidents. Furthermore, it was also realized that it would be extremely difficult or impossible to launch a full-scale analytical investigation on this subject within a short period of time. Consequently, the study has to be simple and yet not sacrifice its accuracy in predicting the failure behavior due to a collision of a projectile and a tank head. Hence, the investigation reported herein was undertaken by means of semi-analytical evaluation of head failures through careful observation of indentations or punctures which were produced in a series of full-scale tests conducted in the laboratory.

The parameters which would influence the vulnerability of tank car heads were identified as follows:

(1) head properties: thickness, geometry, material
(2) commodity: outage, internal pressure, weight
(3) impact characteristics: force and duration, impact velocity, impact location, and orientation
(4) tank car design and attachment construction details
(5) characteristics of draft gear - coupler assembly
(6) insulation: material, thickness

Simple formulas which could be employed to determine the permanent indentation and the coupler impact force were developed in conjunction with a theoretical analysis of influential dimensionless parameters, and an application of Hertz' force-indentation law to collision problems. Finally, the impact failure mechanism was identified and the tank car head failure criteria were defined.

Despite the fact that a limited number of old cars were tested, which had been subjected to fatigue and corrosive environments, the analysis deduced from the tests yielded results which correlated with failure data within engineering accuracy. The results of this study indicate that (1) filled non-pressurized tank cars are less susceptible to puncture than pressurized cars, (2) empty cars are more vulnerable to puncture than liquid filled tank and (3) tank heads when struck near the knuckle radius are more susceptible to puncture than when struck at the center of the head, and (4) the primary mode of failure was attributed to the plug formation due to the shear force exerted on the coupler impact impression.

Correlation of such failure analysis can be used as a guide to develop rational criteria for designing tank car head protective devices in the future.

TANK CAR DESIGN REVIEW

The formulation of additional design criteria in order to significantly reduce head puncturing must take into account the various designs and types of tank cars in service. These are:

Pressure Car - A tank car whose tank is designed and fabricated under the provisions of Paragraph 179.100 of the DOT Regulations. These cars are characterized by tanks whose designs are primarily governed by internal pressure loads. Tank wall thicknesses are therefore greater than in non-pressure car tanks, typically being between 9/16" and 15/16". Design, fabrication and inspection requirements for these tanks are also more stringent.

Non-Pressure Car - A tank car whose tank is designed and fabricated under the provisions of Paragraph 179.200 of the DOT Regulations. These tanks are required to handle a small amount of internal pressure, up to 35, 45, and 75 psig in various cases. Normally, the tank wall thickness required to handle these low pressures is below that which is required to handle the mechanical loads of rail transportation; hence, such tanks are built thicker than required for the pressure load only. Typically, non-pressure tank car tanks have wall thicknesses between 7/16" and 1/2".

Underframe Car - A tank car built with a center sill running continuously from end to end. The tank is attached to this "underframe" by a center "anchor" for longitudinal support, and is held down by steel bands on cradles over each truck for vertical support. The cradles provide no longitudinal support other than that produced by friction. In this construction, steady train loads are transmitted directly through the underframe, and longitudinal dynamic loads causing the tank to accelerate or decelerate are transmitted through the anchor.

Underframeless Car or Car Without Continuous Center Sill - A tank car built with end "stub" sills only. The stub sills are similar to an underframe in cross section, but merge into the tank at a point inboard of each truck. There is no center anchor. Longitudinal support is achieved by welding the tank solid to the cradles. In this construction both steady and dynamic longitudinal train loads pass through one stub sill, through the tank, and then through the other sill. Special design requirements are specified by the AAR Committee on Tank Cars for this construction to provide for the safe transmittal of loads by the tank.

Insulated Cars - A tank car that has a layer of insulation around the tank shell and heads. The insulation is covered with a metal jacket, usually 1/8" in thickness and is flashed with metal around all openings for weather-tightness.

HEAD FAILURE ANALYSIS AND CORRELATION WITH FAILURE DATA

It is realized that it would be extremely difficult or even rather impossible to launch a full-scale analytical investigation on this subject within a short period of time. Consequently, the study must be simple and yet not sacrifice its accuracy in predicting the failure behavior due to a collision of a projectile and a tank head. The study can be commenced by identifying the problem areas related to the tank head failures.

Problem areas related to the development of design criteria involve (1) general physical characteristics of head failures, (2) mechanics considerations, and (3) the objectives to be accomplished in this task.

The dissipation of the initial kinetic energy of a flying projectile (coupler, sills, etc.) during impacting a tank-car head produces various effects, their nature depending on the physical characteristics of colliding bodies (such as rigidity, mass, material) and the magnitude of the relative velocity. However, there are essentially two fundamental failure mechanisms into which the failure behavior of damaged tank head can be classified. They are: (1) indentation and (2) puncture.

Indentation may be defined as the deformation created by a force which exists in the contacting surface of colliding bodies without producing penetration of the striking object into the head. This action involves either the relative mass ratio, the relative stiffness (rigidity) and the relative velocity of colliding bodies.

On the other hand puncture implies the complete piercing of tank head by the projectile. The complicated mechanism encountered in this process has not yet been completely explained or examined, even though a considerable amount of damage data has been collected over the past years.

For the case of tank-car heads, it can be reasonably predicted that an indentation will be produced by a projectile, such as coupler, under a low or intermediate impact velocity. This is because the head with a thickness often less

than 1 inch is considerably more flexible than a massive coupler head. In addition, the tank head is made of ductile material (steel) such that the initial impact energy would be primarily converted into elastic energy stored in the unyielded zone of the head and plastic deformation of the head shell creating an indentation (crater), with smaller amounts accounting for elastic waves, the rebound of the striking object, friction and heat.

Moreover, for the case of pressurized tank cars, it is understood that the internal pressure tends to stiffen the head shell to resist the impacting force. However, internal pressure, unfortunately, simultaneously reduces the flexibility to cushion the impact.

It becomes obvious that different methods of approach should be taken to determine the influencing parameters involved in the foregoing failure mechanisms, indentation of puncture. However, the general laws of conservation of momentum, energy or other laws of mechanics should hold for both cases.

In the analytical investigation of the failure phenomena, the laws of conservation of momentum and energy must be satisfied.

For the case of perfect elastic impact, there must be no loss in the energy of the system. Thus, the following conditions must be satisfied:

$$m_1 v_1 + m_2 v_2 = m_1 v_1' + m_2 v_2'$$

$$\frac{1}{2} m_1 (v_1^2 - v_1'^2) = \frac{1}{2} m_2 (v_2^2 - v_2'^2)$$

in which m_1, m_2 = mass of colliding bodies

v_1, v_2 = velocity of colliding bodies prior to impact

v_1', v_2' = rebound velocity of colliding bodies after impact.

As for the case of plastic impact, two collided bodies will move with a common velocity after impact. This common velocity can be easily obtained from the momentum consideration, that is

$$v' = \frac{m_1 v_1 + m_2 v_2}{m_1 + m_2}$$

Subsequently from the energy consideration, the energy dissipated during the impact process or converted to other form of energy, can be evaluated by

$$E = \frac{m_1 m_2}{2(m_1 + m_1)} (v_1 - v_2)^2$$

Under actual conditions, one would expect some deviation from perfect elastic impact; there always will be some loss in energy of the system during collision. Thus for the case of semi-elastic impact, the momentum and energy considerations will give

$$m_1 v_1 + m_2 v_2 = m_1 v_1' + m_2 v_2'$$

and $v' - v_2' = e (v_1 - v_2)$

where e = coefficient of restitution.

When e = 1, the above equations coincide with those of elastic impact, whereas for e = 0, it will give formulas for the plastic impact.

For empty tank cars, the failure of the tank head appears to be described by the plastic impact. However, for pressurized cars, more careful consideration should be given to determine in which mode the tank head had failed, either plastic or semi-elastic mode.

In addition, the momentum-impulse relationship gives

$$m(v - v') = \int_0^T F(t)\, dt$$

where T = impulse duration
v = initial velocity of mass m at t = 0
v' = mass velocity at t = T

Thus, the total change in momentum of a mass, m, during a finite interval of time, T, is equal to the impulse of the acting force, F, on the mass, m, during the same period.

From the work-energy consideration, one also obtains the following relation

$$\frac{1}{2} m (v^2 - v'^2) = \int_{x_o}^{x} F(x)\, dx + E'$$

where x_o = initial position of the force application
x = final position of the force application
and E' = energy loss involved in the simultaneous action of elastic and plastic deformation of head, crack formation, spalling, elastic and plastic wave propagation, friction and heating, strain-rate effects and perhaps even shattering of the striker.

This research program is designed to develop a "shield", "bumper", or other possible protective structure which can be applied to the heads of existing and new tank cars in order to significantly reduce the head damage resulting from derailments. The technical data to be developed in this investigation are:

(1) The approximate magnitude of probable tank head failure force by reviewing the characteristics of tank car head failures;
(2) The criteria which would govern the design of tank car head protective structure.

The study is planned for three major phases of effort in order to achieve the program goals as identified in the previous section. The

effort will be specifically focused on finding answers to the following questions:

(1) How can tank head damage, indentation or puncture be predicted as a result of a projectile striking a tank head, if the initial velocities and the masses of both colliding cars, the head geometry, the head material and the commodity condition are known?

(2) How can the maximum impacting force developed during the impact be estimated from the direct observation of head damage?

(3) How can the impact failure criteria be established, if some analytical tools such as those obtained in steps (1) and (2) are available?

Even though a number of studies, such as those reported by Goldsmith, Ref. (1), Fugelso, Ref. (2), and Cristescu, Ref. (3), are available in the field of mechanics of impact and penetration, no problem similar to the case of tank head collision was investigated in these references.

Realizing the difficulty of formulating the problem entirely on an analytical basis, a method of semi-theoretical procedure will be sought. The procedure is comprised of a theoretical analysis of influential dimensionless parameters upon the test data which will be obtained in a short series of tests that will, under laboratory-controlled conditions, somewhat duplicate various types of head failure on current tank car designs. The tests will also permit the measurement of head damage (indentation of puncture) and the force that produces head damage.

A theoretical evaluation of test data with an application of the dimensionless analysis in terms of various important parameters will yield results from which other tank head failures and required impacting force can be estimated.

A series of full-scale tests was designed and conducted by the Engineering Department of the Tank Car Division of General American Transportation Corporation at the Sharon Plant. The test data obtained are tabulated and presented in the report by Everett, Ref. (4), from which Table 1 was extracted. The test data were then forwarded to the General American Research Division of General American Transportation Corporation for theoretical evaluation.

One of the objectives to be accomplished in this task is to develop a procedure which would approximately describe the relation between the impact force and the corresponding indentation produced by collision of couplers and tank heads.

During the past decade, increasing attention has been focused on the problems attendant to the collision of a projectile on a target. Consequently, numerous impact problems have been studied and solutions for various impact conditions were found by many investigators.

One method which is worth mentioning is the application of the Hertz force-indentation law to predict the force developed during a collision of two deformable bodies.

Some questions have been raised concerning the validity of the theory under dynamic conditions, since the Hertz theory is based on the quasi-static contact. Nevertheless, the Hertz theory has been applied in the impact studies, particularly for the case of low-to-moderate velocity impacts (up to 300 fps). Hertz, Ref. (5), extended his solution of two spheres in contact to impacting bodies in 1882 and Tsai, Ref. (6) has proven the validity of the Hertzian impact theory through an analysis of Rayleigh surface waves in an impacted glass block.

Davis, Ref. (7) also indicated that for the case of impact of elastic bodies at moderate velocities, the problem of elastic contact and elastic impact are in essence identical. Tsai and Kolsky, Ref. (8), found that the quasi-static treatment approximates very closely the stress in dynamic impacts. Roman, Ref. (9), applied the Hertz theory to the investigation of the coefficient of restitution and found that for moderate thicknesses of plate (0.138" - 1"), the theoretical calculated and experimentally observed values agreed well.

Finally, Yang concluded in his studies, Ref. (10,11), that the combined application of the dynamic field equation of solids and together with Hertz' law, to the impact problem of plates and shells, yielded a reasonable result. His results confirmed the validity of using the Hertz law in the problem of impact and also supported the conclusion that the application of Hertz' law could be extended to the contact of visco-elastic bodies.

In the Hertz theory, the force-indentation relationship is given by

$$F = \alpha (d)^{1.5}$$

where F = contact force
d = indentation
α = constant

The constant α depends on the geometrical and physical properties of tank head, and the magnitude of internal pressure. It will be determined experimentally.

The collision of two bodies may involve a variety of processes whose existence and relative importance depend almost exclusively on the shapes, the physical characteristics of the objects, environmental condition, and, most important, on the relative impact velocity. The relevant mechanical behavior of the materials is ordinarily classified as being elastic, plastic, viscous, or a combination of these; a quantitative description of these properties is formulated as a relation between stresses and

strains and, in the case of time-dependent effects, their respective rates.

Impact is differentiated from rapid loading in which the forces acting at the contact point are created and removed in a very short time interval. The rapid loading generates stress waves that subsequently propagate throughout the entire system. In addition to the generation of stress waves, the collision produces a relative indentation at the area of contact.

It is generally true for low velocity impacts that the energy transmitted by wave propagation is small compared to the initial kinetic energy and is thus usually neglected relative to the energy consumed in the local indentation. Furthermore, the process is often treated as isothermal for the sake of simplicity, so that temperature and other thermodynamic effects need not be considered.

A major objective of the investigation is to identify the modes of failure which would be created by a striking coupler on a tank head. To supply the proper background, a short summary of possible mechanisms for plate perforation process is presented.

The perforation of plates involves the simultaneous action of crack formation, spalling, elastic and plastic deformation and wave propagation, friction, heating and even shattering of the striker. The plate may fail in a variety of ways among which are: 1) plug formation, 2) petal formation or dishing, 3) ductile hole enlargement and 4) fragmentation. They are illustrated in Figure 1. Physically, plate failure appears to occur by a combination of these various patterns, with one of the mechanisms predominating.

Plugs are more likely to be found in the case of hard plates of moderate thickness or in the case of projectiles with sharp edge contours. Investigations of the mechanism of plug formation indicate that the plug failure mode is produced by plastic deformation along a surface of maximum shear.

Petal formation (or dishing) occurs where thin plates are struck by a projectile at low velocity. The shape of the displaced plate is often assumed to be similar to that obtained under quasi-static conditions, and an energy solution for a rigid plastic target material can be employed. The energy components considered should include the elastic, and plastic works performed in the displacement of the head, the acceleration of the particles in the deformed part of the plate, the kinetic energy of the entire system and the heat produced by friction. The analysis usually is based on the hole opening process with assumptions that the striker will neither disintegrate nor plastically deform. In addition, the elastic vibration and the wave effects are also neglected. The ductile type of failure is the kind most commonly observed in thick plates. The perforation is accomplished by radial expansion of the plate material as the projectile passes through. Fracturing, such as scabbing, that can be attributed to interaction between transient disturbances generated by the projectile may also be present.

Numerous theoretical and empirical formulae have been developed in attempts to predict the perforating ability of a projectile. However, the behavior of the perforating mechanism is so complex, and involves so many influential factors that none of these formulae are completely satisfactory.

Since no attempt will be made to conduct a complete theoretical investigation on the subject of tank head failure, experimental evidence will be introduced to assist in identifying the mechanism under which the tank head may fail.

Figure 2 shows the impression made by the striking coupler on a tank head in Test No. 1 at 4.3 mph speed. There are clear indications that excessive shear deformations were produced (as shown by arrows) at the impressed areas which correspond to the upper edge corners of the striking coupler when the head was struck near the center of the head. The degree of shear deformation would be increased as the striking speed increases. Eventually, the tank head would be sheared at more severe impacts. Figure 3 shows a typical shear failure when a tank head was struck at a speed of 15.7 mph.

In addition to the striking velocity, the vulnerability of tank heads increases with increasing internal pressure. As shown in Figure 4, internal pressure offers considerable resistance to the overall deformation of the tank head. Consequently, the force applied would produce a deformation which would be highly localized around the area of force application. As a result of deformation concentration characteristics in the area of force application, the tank head would fail with less overall tank head deformation and at a lower energy level as compared with the case of non-pressurized tank heads. It should be noted that such localized deformation characteristics will become more severe as the internal pressure increases.

A typical failure example of pressurized tank head is demonstrated in Test No. 14. In Test No. 14, a tank head was completely punctured when the tank head was pressurized to 40 psi at 16 mph speed. As observed in Figure 5, the primary failure was attributed to the plug formation resulting from the great magnitude of shear force which was applied at the top edge of the coupler knuckle impact impression. The secondary failure which took place at the lower edge was due to the dishing and this portion of the tank head failed in tension.

Based on the primary mode of failure by the maximum shear developed around the contour of the impressed area, the magnitude of the

maximum force which the tank head can sustain will be estimated.

For the case of knuckle impacts, the deformation characteristics would be substantially different from the case of central impact of tank heads. Generally the knuckle area is reinforced by a reinforcing plate. In addition, the transition weldment is attached between the tank head and the stub sill. This entire attachment detail provides a considerable restraint in the knuckle region against deformation. Thus, the tank head would be torn at the transition weldment area where an excessive shearing force would be developed. Such phenomenon can be easily appreciated by observing Figures 6 and 7. Figure 8 shows the failure mechanisms when the tank head is struck at the knuckle area. It indicates that the primary failure of the tank head is in shear developed at the tank head attachment area and the secondary failure of the tank head is in tension by dishing the area above the knuckle.

In sharp contrast with the case of internal pressure, the liquid content in tank cars could serve as an impact cushion medium to absorb a portion of the impact energy. However, an exact evaluation of the contribution made by the contained liquid to the overall strength of the tank head would require an extensive investigation of the interface behavior of the tank head and the liquid. Thus, for the time being, a simplified method of analysis would be sought. Instead of seeking a solution by means of shell theory, the solution for circular plates subjected to a concentrated load will be employed for the first approximation. Taking the first five-term approximation, the maximum stress is given by

$$\tau = 1.81 \frac{F}{Rh}$$

where F = total applied load
R = tank radius
h = head thickness

The failure criterion would be established on the basis of the ultimate shear strength of tank head. That is to say, if $\tau \geq \tau_u$, the failure of tank heads would be expected, where τ_u is the ultimate shear strength of tank head material.

Results of the study are summarized as follows:

(1) Impulse-Momentum Relation

$$m_1 (v_1 - v_1') = \int_0^T F \, dt$$

where m_1 = mass of striking car
T = impulse duration
v_1 = initial impact velocity
v_1' = velocity of striking car at $t = T$

(2) Permanent Indentation Estimation

$$d = 5 \times 10^{-9} \left(\frac{D}{h}\right)^2 \left(\frac{w_2}{w_1}\right)^{\frac{1}{4}} \left(\frac{w_1}{g} v_1\right) e^{-0.018 \frac{P_i}{P_o}}$$

where d = estimated permanent indentation (in.)
D = diameter of tank head (in.)
h = thickness of tank head (in.)
w_1 = weight of striking car (lbs.)
w_2 = weight of struck car (lbs.)
v_1 = striking velocity (in./sec.)
g = 386 in./sec.^{2}
P_i = internal pressure (psi)
P_o = 15 psi

(3) Maximum Impact Force Estimation

$$F = 35 \times 10^6 (d)^{1.5} \left(\frac{h}{D}\right)^3 \left(\frac{P_i + P_o}{P_o}\right)^{0.6}$$

where F = estimated maximum impact force (kips)
d = permanent indentation (in.)
D, h, P_i and P_o = as defined in the previous formula for computing d

(4) Failure Criteria

For central impacting

$$\tau = \frac{F}{ChL} \geq \tau_u$$

For knuckle impacting

$$\tau = \frac{1.81F}{RhC} \geq \tau_u$$

where F = total impact force (kips)
C = constant which depends on the environmental condition inside the tank, taken as unity for full tanks and 0.5 for empty tanks, respectively
τ_u = ultimate shear strength of tank head material (ksi)
h = head thickness (in.)
L = perimeter of impressed area (in.)

Despite the fact that a limited number of old cars were tested, which had been subjected to fatigue and corrosive environments while they were in service for a great number of years, the analysis deduced from the test yields results which correlate well with experimental failure data.

Table 2 presents the impulse-momentum relationship for the striking car. The total impulse was evaluated by measuring the area confined by the force-time curve. The momentum change was

calculated from the mass and the changing in the measured velocity of the striking car. As observed in Table 2, the correlation of the impulse with the momentum change is very satisfactory within engineering accuracy.

Table 3 shows the comparison between the estimated permanent indentation with that measured in the tests, whereas in Table 4, the results on the maximum impact forces and the criteria under which the tank heads would fail were tabulated.

As can be seen in Tables 3 and 4, the analytical results and results obtained in the test agree well, with the exception of a few cases in which some unmeasurable factors such as fatigue and corrosion might have played an important role. It also can be concluded that the assumption of plug failure due to shear as the primary mechanism appears to be correct. With only two tests conducted for the case of empty tanks, no decisive conclusion can be drawn with regard to the impact resistance of the head when tanks are empty. However, there is an indication that tanks can only resist half of the impact force when empty as compared with the case when the tank is filled with liquid. In general, the maximum impact force to which tank knuckle heads can be subjected is approximately 500 kips for liquid-filled tanks and 250 kips for empty tanks, respectively. For the case of central impact, the ratio of approximately 1.6 can be multiplied to the maximum endurable impact force estimated for the case of knuckle impact. The maximum impact force which tank heads can sustain decreases with increasing internal pressure by the amount of $\left(\frac{P_o}{P_i + P_o}\right)^{0.6}$ The results are presented in Table 5.

As for the final and important note, it appears that the maximum force developed during impact would literally independent of the tank geometry when the indentation formula is substituted into the impact force equation. This is misleading for the following reason.

Fifteen out of seventeen tanks tested were equipped with the head plate of 7/16 inch in thickness. Moreover, the geometry of tanks tested ranges from 78"ø x 1/2" tk. to 88"ø x 7/16" tk. Subsequently, with such narrow variation in the geometric parameter designated by D/h, the influence of the tank geometry would become irrelevant. Since tank car construction allows more freedom for altering the thickness than the diameter, a large range in the plate thickness is recommended for the future experiments.

In addition, these formulas should be considered engineering approximations since the exponents applied to all the influential paramaters included in the indentation and force formulas contain only two significant digits.

In conclusion, the results of this study indicate that (1) filled non-pressurized tank cars are less susceptible to puncture than pressurized cars (2) empty cars are more vulnerable to puncture than a liquid filled tank, (3) tank heads when struck near the knuckle radius are more susceptible to puncture than when struck at the center of the head, and (4) the primary mode of failure was attributed to a plug formation due to the shear force exerted on the coupler impact impression.

REFERENCES

1. Goldsmith, W., "Impact, The Theory and Physical Behavior of Colliding Solids," Edward Arnold, London, 1960.

2. Fugelso, L.E., "Mechanics of Penetration," Vol. II, GARD Report No. MR1127, December, 1962.

3. Cristescu, N., "Dynamic Plasticity," North-Holland Publishing Co., Amsterdam, 1967.

4. Everett, J., "Impact Tests on Full Scale Tank Cars," RPI-AAR Report No. 27053, January, 1971.

5. Hertz, H., "Ueber die Beruhrung fester elastischer Korper," Journal fur die reine und angewandte Mathematik, Vol. 29, 1882.

6. Tsai, Y.M., "Surface Waves Produced by Hertzian Impact," NSF-GP-2010/5, Nov., 1966.

7. Davis, R.M., "The Determination of Static and Dynamic Yield Stresses Using Steel Ball," Proc. Royal Society, London, Vol. 197, pp. 416-432, 1949.

8. Tsai, Y.M. and Kolsky, H., "A Study of the Fractures Produced in Glass Blocks by Impact," J. Mech. Phys. Solids, Fol. 15, pp. 263-278, 1967.

9. Raman, C.V., "On Some Applications of Hertz' Theory of Impact," Physics Review, Vol. 15, pp. 277-284, 1920.

10. Yang, C.S.J., "Application of the Hertz Contact Law to Problems of Impact in Plates," NOLTR 69-152, U.S. Naval Ordnance Laboratory, September, 1969.

11. Yang, C.S.J., "A Study of Hertzian Impact on Glass and Aluminum Hemispherical Shells with Mitigator," NOLTR 70-11, U.S. Naval Ordnance Laboratory, September, 1969.

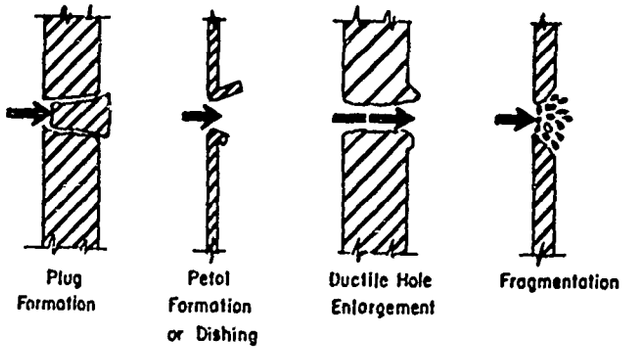

Figure 1, POSSIBLE MECHANISMS FOR PLATE PERFORATION

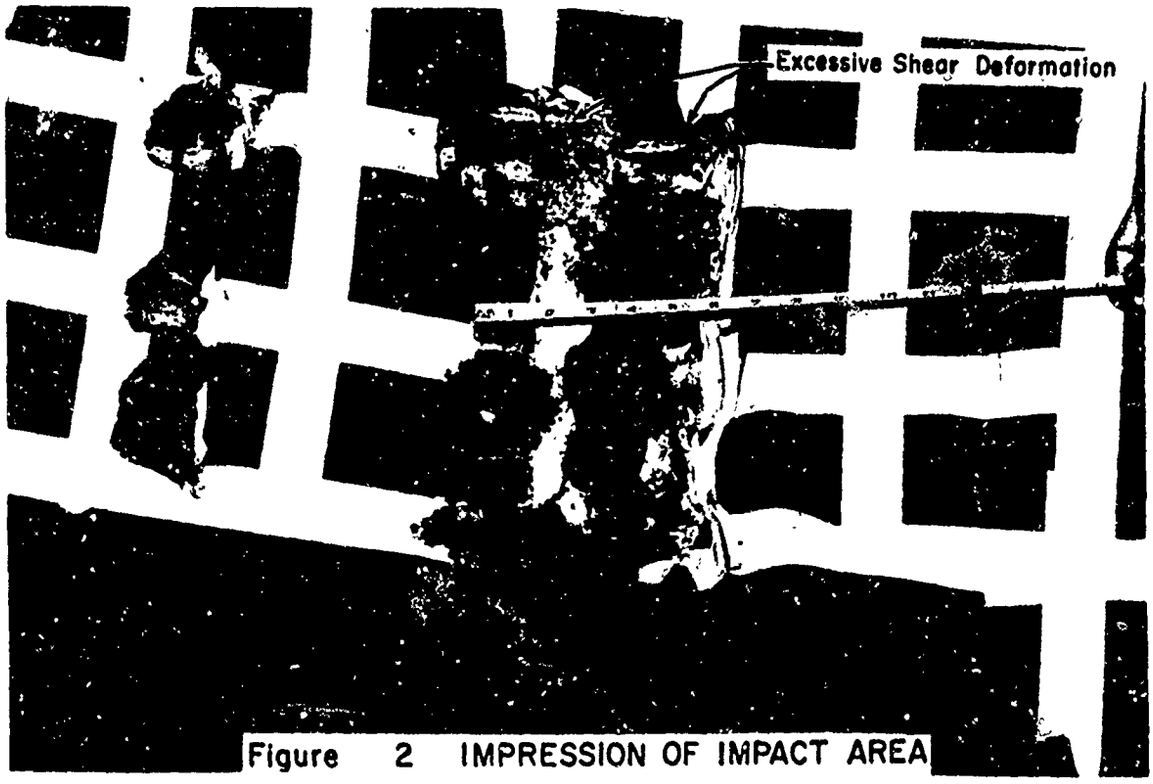

Figure 2 IMPRESSION OF IMPACT AREA

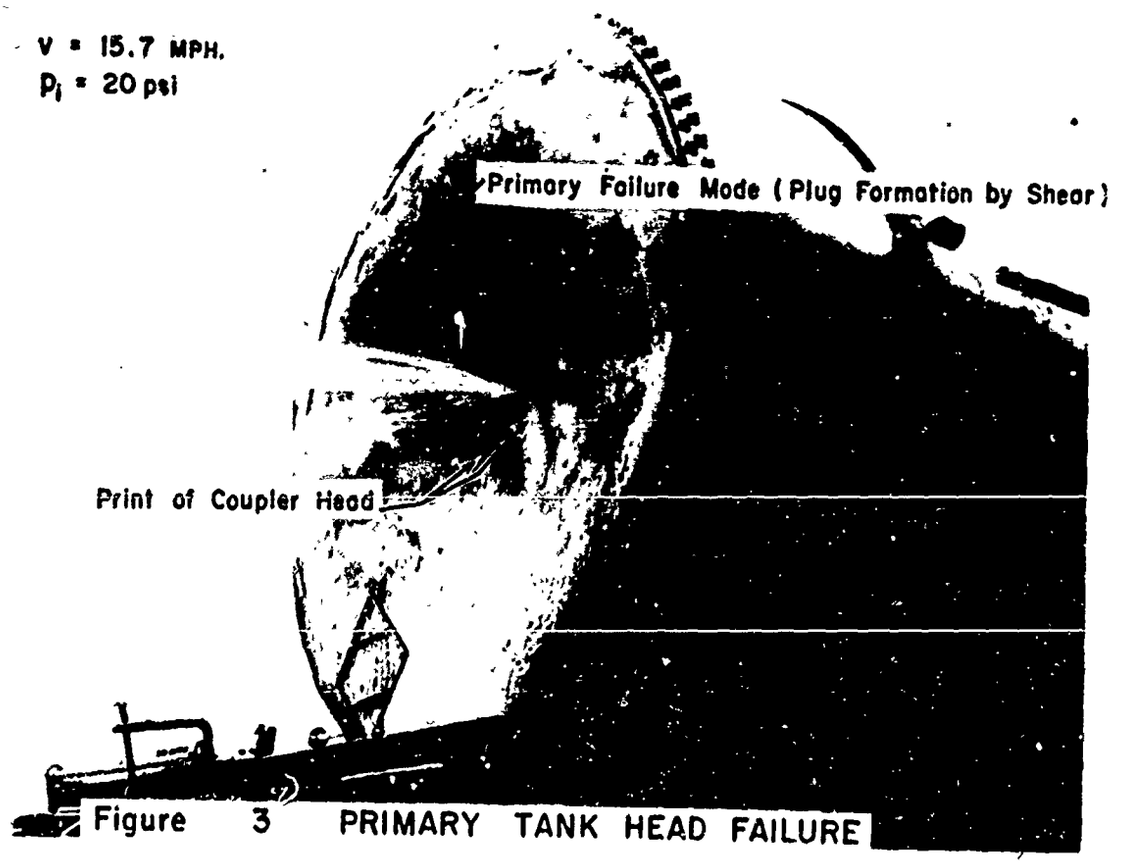

Figure 3 PRIMARY TANK HEAD FAILURE

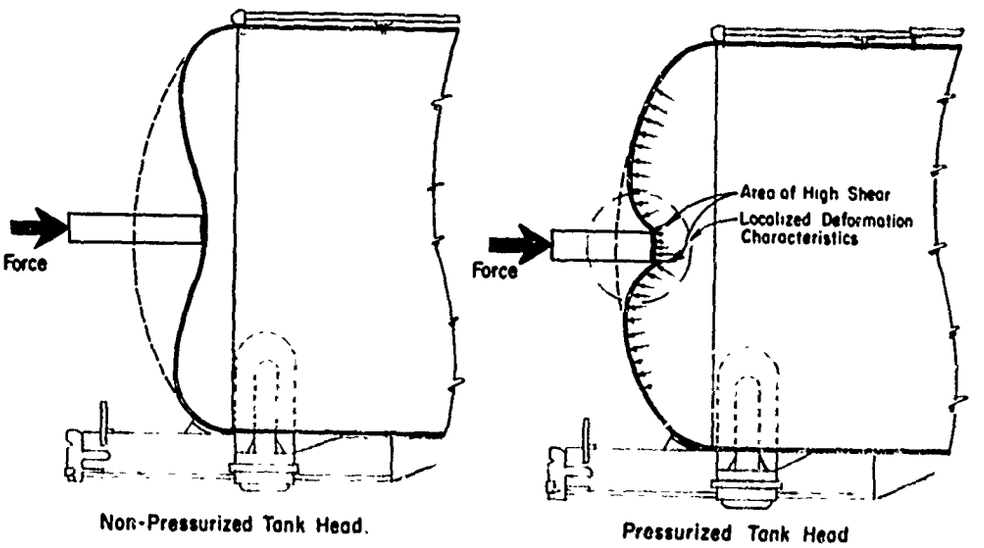

Figure 4. SCHEMATIC VIEWS OF TANK HEAD DEFORMATIONS

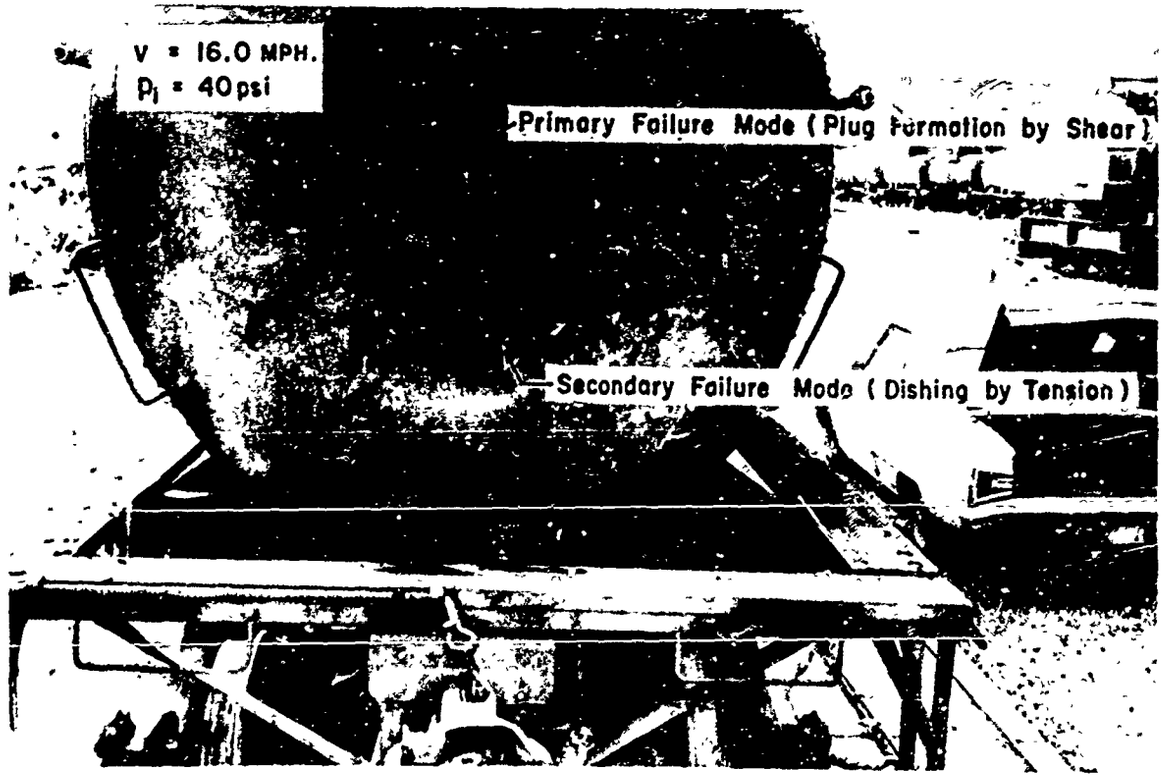

Figure 5 TANK HEAD IMPACT FAILURE (Complete Puncture)

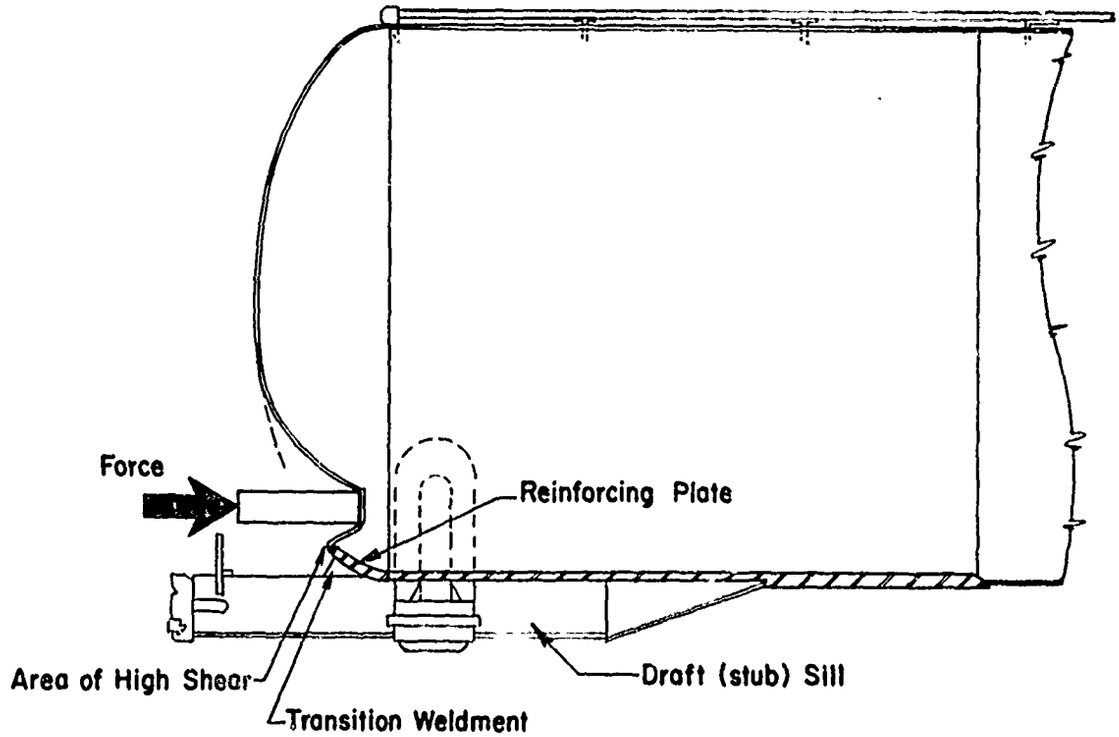

Figure 6, SCHEMATIC VIEW OF KNUCKLE DEFORMATION

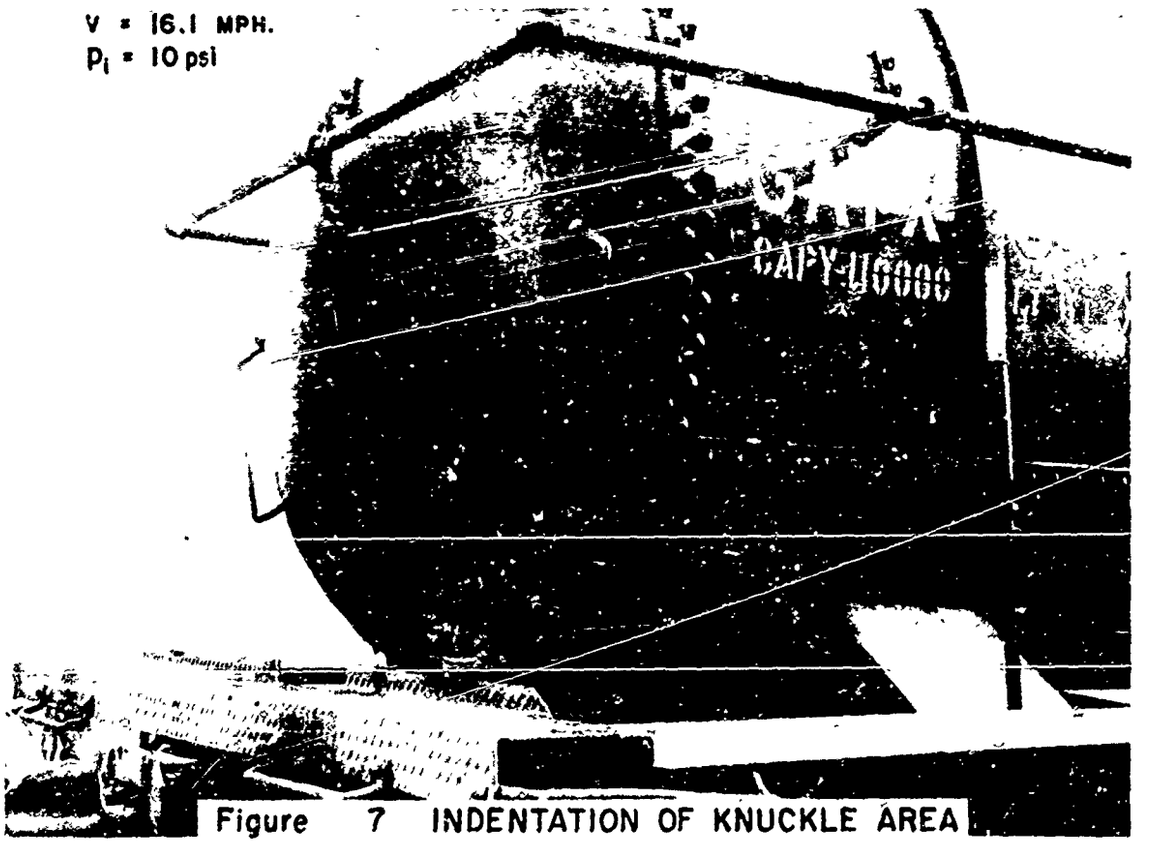

Figure 7 INDENTATION OF KNUCKLE AREA

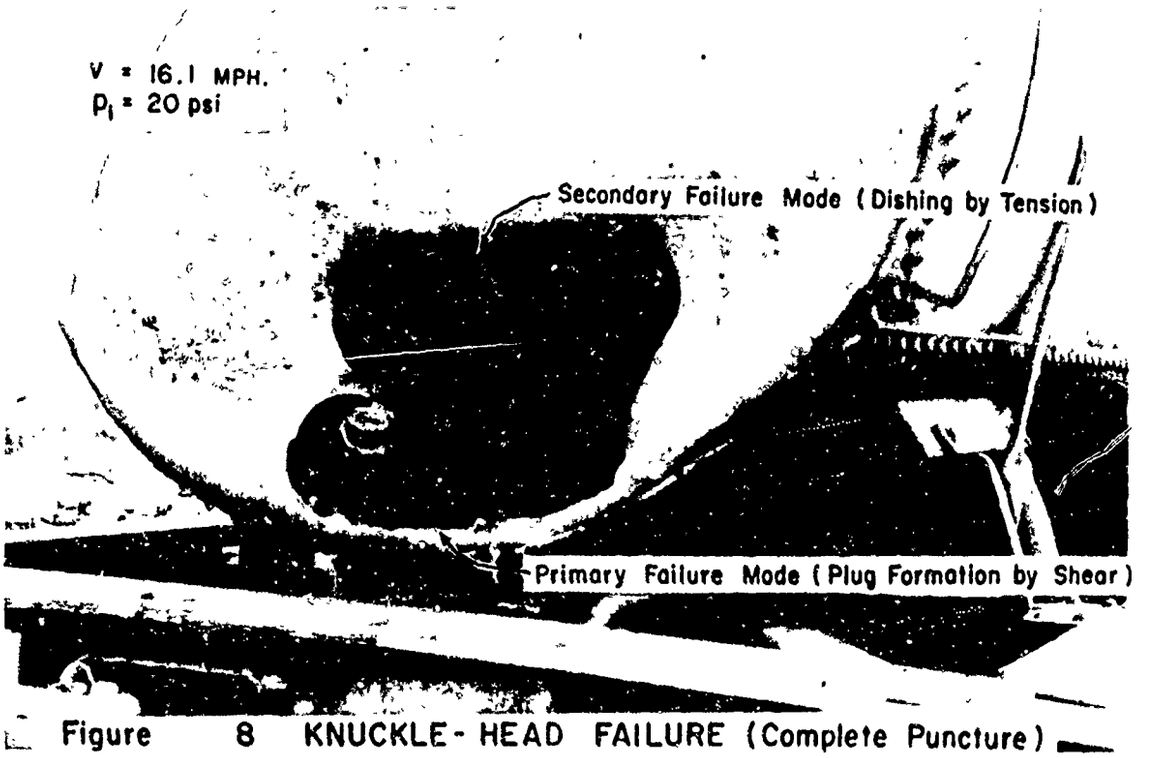

Figure 8 KNUCKLE-HEAD FAILURE (Complete Puncture)

TABLE 1

FULL SIZE HEAD IMPACT TEST RESULTS SUMMARY

Impact No.	Impact Speed (mph)	Outage (%)	Internal Pressure (psi)	Striking Car Wt. (lbs)	Struck Car Wt. (lbs)	Head Size (in.)	Impact Location	Head Damage	
								Permanent Indentation (in.)	Failure
1	4.3	2	0	128,900	96,500	78 x 1/2	Center	30 x 2-3/4	
4	7.2	2	0	"	107,300	80 x 7/16	"	40 x 6-1/2	
6	10.2	2	0	"	128,900	88 x 7/16	"	60 x 11-1/4	
8	8.7	2	20	"	128,200	88 x 7/16	"	48 x 8-1/4	
10	11.0	2	40	"	108,400	80 x 7/16	"	42 x 7-1/2	
12	14.0	2	40	"	107,500	83 x 7/16	"	36 x 8	
14	16.0	2	40	"	130,000	88 x 7/16	"	*	Puncture
15	14.9	2	20	"	128,800	88 x 7/16	"	60 x 16	
16	15.0	2	20	"	127,000	88 x 7/16	"	60 x 14-1/2	
17	15.7	2	30	"	127,400	88 x 7/16	"	60 x 14-1/2	Shear
18	15.7	2	20	"	107,600	83 x 7/16	"	66 x 15-1/2	Shear
19	16.0	2	0	"	107,300	80 x 7/16	"	72 x 16	
20	8.5	100	0	"	40,900	83 x 7/16	"	51 x 9	
22	16.0	2	0	"	96,600	78 x 1/2	Knuckle	40 x 12	
23	16.1	2	20	"	108,400	80 x 7/16	"	*	Puncture
24	16.1	2	10	"	128,300	88 x 7/16	"	*	Shear+
25	16.1	100	0	"	48,000	88 x 7/16	"	*	Puncture

* No data.

+ Threshold puncture.

TABLE 2

IMPULSE - MOMENTUM RELATION

Test No.	Total Impulse (kip-sec)	Change in Momentum (kip-sec)
1	6.52	7.45
4	11.95	15.90
6	16.60	15.20
8	19.48	18.75
10	24.38	22.40
12	16.60	*
14	12.02	27.02
15	42.90	41.70
19	44.28	41.80

* No data available.

TABLE 3

PERMANENT INDENTATION

Test No.	Outage (%)	Internal Pressure Pi (psi)	Head Damage			
			Permanent Indentation, d (in.)		Maximum Indentation Recorded (in.)	Failure
			Calculated	Measured		
1	2	0	2.84	2.75	4.35	
4	2	0	6.35	6.50	5.0	
6	2	0	11.60	11.25	13.0	
8	2	20	9.65	8.25	9.5	
10	2	40	8.04	7.50	12.8	
12	2	40	10.53	8.00	*	
14	2	40	13.00	*	19.4	Puncture
15	2	20	16.00	16.00	18.6	
16	2	20	16.67	14.25	*	
17	2	30	16.70	14.25	*	Shear
18	2	20	14.35	15.50	*	Shear
19	2	0	15.75	16.00	*	
20	100	0	7.05	9.00	*	
22	2	0	10.70	12.00	*	
23	2	20	14.25	*	*	Puncture
24	2	10	16.00	*	*	Shear +
25	100	0	14.90	*	*	Puncture

*No data.

+ Threshold puncture.

TABLE 4

MAXIMUM IMPACT FORCE AND FAILURE CRITERIA

Test No.	Outage (%)	Internal Pressure Pi (psi)	Maximum Impact Force, F (kips)			Failure Criteria		
			Calculated			Shear Stress (ksi)		
			Based on d Estimated	Based on d Measured	Measured	Theoretical	Minimum Ultimate	Failure Mode
1	2	0	44	42	55	2.9	38.5	Dent
4	2	0	100	103	89	7.6	38.5	Dent
6	2	0	169	158	141	12.9	38.5	Dent
8	2	20	210	165	201	16.1	38.5	Dent
10	2	40	288	256	283	22.0	38.5	Dent
12	2	40	381	255	454	29.0	38.5	Dent
14	2	40	525	*	469	40.1	38.5	Puncture
15	2	20	448	448	490	34.3	38.5	Dent
16	2	20	477	368	475	36.5	38.5	Dent
17	2	30	560	467	469	42.9	38.5	Dent
18	2	20	496	510	446	38.0	38.5	Dent
19	2	0	361	368	410	27.6	38.5	Dent
20	100 Empty	0	103	139	118	15.8**	38.5	Dent
22	2	0	324	384	391	40.1	38.5	Dent
23	2	20	496	*	414	51.4	38.5	Puncture
24	2	10	446	*	365	41.9	38.5	Shear+
25	100 Empty	0	241	*	258	45.0**	38.5	Puncture

* No data.

** C = 0.5 for empty tanks; otherwise, C = 1.0.

+ Threshold puncture.

TABLE 5

FAILURE FORCE AND FAILURE MODES

Test	Estimated Failure Force (kips)	Maximum Measured Force (kips)	Failure Mode
1	800	55	Dent
4	800	89	Dent
6	800	141	Dent
8	481	201	Dent
10	366	283	Dent
12	366	454	Dent
14	366	429	Puncture
15	481	360	Dent
16	481	375	Dent
17	414	465	Shear
18	481	462	Shear
19	800	416	Dent
20	400	118	Dent
22	507	321	Dent
23	391	314	Puncture
24	367	365	Shear *
25	256	258	Puncture

* Threshold puncture.

DISCUSSION

Mr. Baker (Southwest Research Institute): I want to compliment you on an excellent presentation. I wondered, in looking at these movies, if you were familiar with some work done at Stanford Research Institute some years ago on the problem of penetration of containment shells for reactors if a control rod were to be thrown out. They ran a number of penetration tests with long rod-like objects thrown against steel plates and a group of formulas was developed. You might be able to correlate Stanford's results with whether or not penetrations occur in your study.

A STUDY OF IMPACT TEST EFFECTS UPON FOAMED PLASTIC CONTAINERS

Don McDaniel
Ground Equipment and Materials Directorate
Directorate for Research, Development, Engineering
and Missile Systems Laboratory
US Army Missile Command
Redstone Arsenal, Alabama 35809

and

Richard M. Wyskida
Industrial and Systems Engineering Department
The University of Alabama in Huntsville
Huntsville, Alabama 35807

Various types of foamed thermoplastic materials are utilized as cushioning systems in military containers. The primary aspects of cushioning design theory currently being utilized by container designers to predict the response of packaged items when subjected to free-fall drop tests are discussed. The test results of all readily available military container designs utilizing foamed plastic cushioning systems are analyzed to determine the statistical significance of the various factors affecting container response. The analysis of the factors involved is then compared with cushioning theory. The superimposed dynamic cushioning curve technique is then presented as an improved method for presenting the cushioning properties of foamed plastic materials.

INTRODUCTION

A container designed for military use, such as for shipping missiles and missile components, is required to perform its basic functions throughout its operating life. Current military policy, based on the need for worldwide deployment, dictates that containers are to be capable of withstanding the rigors of a logistic pattern geared to worldwide distribution. Consequently, the container and its contents, in combination, must withstand all environments and modes of transportation, in addition to the hazards peculiar to the handling of material in transit.

An extensive literature search was conducted of the qualification test programs performed by the military on missile containers that utilize foamed plastic cushioning. Data from those test programs that had sufficient documentation were then utilized as the basis to determine which factors influenced the response of the packaged item. Based upon these findings, the dynamic cushioning curve technique currently being utilized for response prediction of military containers was investigated to determine if response predictions for foamed plastic containers were adequate.

STATE OF THE ART

One of the most important considerations in the design of military shipping containers is the selection of the materials that are utilized in the container [1]. The internal packing materials, frequently called cushioning systems, are designed to protect the contents of the containers from severe shocks induced when the container is dropped. One of the most promising types of materials currently being utilized for cushioning systems is foamed plastics, frequently called cellular plastics. These are among the most exciting new materials that have emerged from the chemical laboratories during the past 10 years. This versatile family of materials is now being used for insulating, filtering,

cushioning, floating, and a multitude of uses that is continually growing.

Foamed plastics are particularly attractive for use as low-cost, easily fabricated cushioning systems in shipping containers. Lightweight plastic foams are being used in conjunction with, and replacing, many of the standard packaging materials, because they have unique characteristics and properties, are easily fabricated, and are economic when compared to the rising costs of wood, paper, rubber, and metal products.

To date, foamed plastics have been incorporated into military container designs on a limited basis. One limiting factor is the difficulty the container designer has in predicting the response of the materials when subjected to the extreme environmental conditions encountered under military deployment. These conditions are simulated by extensive environmental testing programs. Of particular concern in container designs that utilize foamed plastics are impact tests conducted at the temperature extremes. The thermoplastic nature of the foamed plastic materials induces a temperature sensitivity that can cause variations in the container response during these tests.

In order to fully utilize foamed plastics for military containers, container designers require sufficient information to accurately predict response variations. Current practice is to provide the container designer with cushioning data for each type and thickness of cushioning material. These data are provided in the form of dynamic cushioning curves. For any particular container design program, the designer is generally given a maximum allowable fragility level which the packaged item is permitted to experience when packaged in its container. Also, the particular organization involved will have an established testing policy defining appropriate impact tests, which generally is given as a number of free-fall drops to be performed at certain prescribed heights and temperatures. These parameters form the basis for the design of the shock mitigation characteristics and the selection of one of the various cushioning schemes available for the container. If foamed plastic cushioning is to be utilized, the designer will then generally structure his cushioning system using dynamic cushioning curves for particular materials.

Dynamic cushioning curves are generated for a particular type and thickness of cushion by performing drop tests using standard weighted specimens that are dropped onto the cushion. The static stress is determined by:

$$S_s = \frac{W}{A},$$

where S_s is the static stress (psi), W is the specimen weight, and A is the footprint of specimen in the cushion (in.^{2}). A different curve is required for each drop height, thickness, and type of material. The curves are a good indication of the protection to be expected for a particular cushion scheme. Fig. 1 illustrates a series of dynamic test curves for various thicknesses of 2.5-pound density polystyrene foam [2].

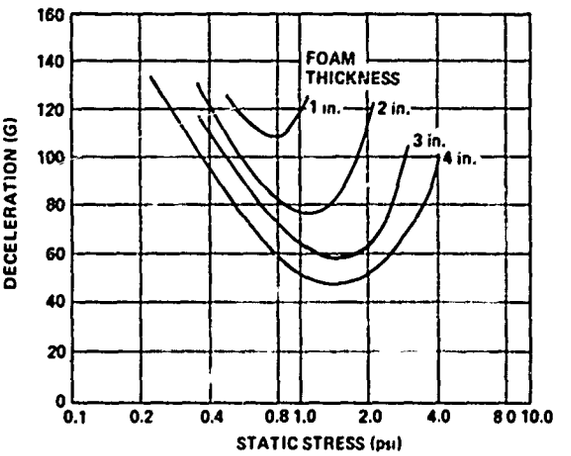

Fig. 1 - Dynamic cushioning curve for polystyrene foam (30-in. drop height, 70°F temperature, 2.5 lb/ft^3 density)

FOAMED PLASTICS FOR MILITARY PACKAGING

Foamed plastics comprise a versatile new family of lightweight materials which are made in a variety of processes remotely resembling the making of bread. These synthetic materials are polymers which have been expanded in volume by a gas so that they have a uniformly cellular structure which can look like an extremely fine honeycomb or a mass of very tiny ping-pong balls fused together. The cells of some foamed plastics are large enough to be seen; cells in others are so fine that a microscope is needed. These materials come in a variety of consistencies ranging from that of raw cotton to hardwood. Flexible, semi-rigid, and rigid foams are available in densities

of about 0.1 to 80 lb/ft^3.

Three types of foamed plastics, namely, polystyrene, polyurethane, and polyethylene, have been utilized in packaging applications in the military. The most widely accepted foamed plastic material utilized for packaging is expanded polystyrene. This unique material is manufactured in the form of small translucent beads or granules containing an expanding agent. The particles are free flowing, and when expanded by the application of heat they produce an opaque foam which has little or no odor and is nontoxic. Expandable polystyrene materials offer many properties desirable in a packaging material, i.e., lightweight, high strength-to-weight ratio, low moisture absorption, and good insulating properties.

Expandable polystyrene materials are processed in a number of different ways for use in packaging; however, the most common method is steam chest molding. The beads or granules are normally "prefoamed," by application of heat or steam, to the desired density prior to molding. The hydrocarbon foaming agent within the individual granules causes the softened material to expand into discrete multicellular foam spheres or pellets. In the molding operation, these prefoamed particles are confined in a retaining mold, then subjected to steam and pressure, causing them to expand further and knit together to form a unicellular homogeneous plastic foam article. The unlimited variety of shapes and sizes that can be molded and the low cost of processing are benefits of interest to the molder and ultimate consumer of this packaging material. Steam-chest-molded expandable polystyrene has excellent impact and shock absorbing properties.

Polyurethane foam materials have attracted considerable interest for industrial, military, and commercial packaging applications. These materials have extremely versatile properties, and formulations can be varied from extremely rigid to very flexible, within a wide range of densities. Polyurethane foams are of two basic types, polyester and polyether materials. Polyester-based urethanes were the first to be developed, but due to relatively high cost are not being utilized extensively for packaging. Polyether-based foams, most frequently used in packaging, are made by reacting toluene diisocyanate with polyglycol materials in a simple mixing operation.

The greatest technical advance made in recent years has been the development of what is known as the "one-shot" system, in which the blowing agent, the polyol, the catalyst, and the emulsifier are all preblended and the isocyanate is added at the last minute. When this technique is coupled with a still more recent development in which the ingredients are "frothed" prior to dispensing, producers can achieve greater uniformity of foam densities, lower temperatures and pressures, and better flow characteristics, and can develop thinner skins; thus, less costly jigs and dies can be utilized.

Polyurethane foam is frequently utilized as a cushioning material in packaging because of its extremely resilient properties. These materials are frequently supplied in large buns or slab stock which can be easily cut or shaped into the required shapes. Also a foam-in-place technique can be used for packaging small items. Here the item is positioned in the exterior container, and the polyurethane foam is introduced in a one-shot liquid form into the cavity between the item and the container exterior wall and allowed to "foam up" and capture the item.

The third foamed plastic, polyethylene foam, is manufactured in slab form, most commonly at a density of approximately 2.0 lb/ft^3, which is expanded about 30 times from the solid state of polyethylene. It is a cellular, lightweight material with each cell closed off from its neighbor. Polyethylene foam is a tough, resilient material having good flexibility characteristics.

Polyethylene foam can be fabricated with conventional hand tools or power tools such as band saws and routers. Due to its flexible nature, polyethylene foam is most easily fabricated by tools or equipment with blades or bits having a slicing type action. Polyethylene foams can also be fabricated by electrically heated resistance wires. It may also be thermally shaped by the use of contoured molds equipped for both heating and cooling.

Polyethylene foam provides high energy absorbing characteristics for insert packaging applications. Its springback rate is slow enough so that the energy absorbed during a sudden shock is not released with equal rapidity; rebound occurs at a relatively slow rate. Due to its relatively predictable properties, it is one of the most frequently utilized packaging materials in military applications.

DATA COLLECTION

In order to establish a meaningful appraisal of cushioning design theory to foamed plastic containers, a substantial investigation was requi-

red. Many military organizations are involved in the design, development, and testing of containers; and they were solicited for data on the drop testing of containers that utilized foamed plastic cushioning. Also, a comprehensive literature search was performed by the Defense Documentation Center, Alexandria, Virginia, on any container drop tests conducted within the last 15 years. Every program of drop testing of a container that utilized foamed plastic cushioning materials was reviewed.

It became quite apparent at the outset that hundreds of container drop test programs would not provide usable data. The primary difficulty was that there was no quantitative measure of container response, such as the G-levels experienced by the packaged items. Many drop test programs were conducted only at ambient temperatures, and many were one-shot tests with no repetition or duplication within the test. It was also determined that some container designs were qualified for issue into the field with no testing at all.

The results of the investigation provided 15 candidate containers using foamed plastic cushioning that had undergone adequately documented drop testing. Three of the containers were designed by the Navy for Sparrow, Brighteye, and SUBROC. Six of the containers are Army designs for the missiles and spare parts for the Chaparral, Redeye, and Shillelagh systems. The remaining five containers were designed by container manufacturers for use by the military in missile systems applications.

The basic drop test data for each container are tabulated in Table 1. The bases for the data are the accelerometer measurements of G-levels experienced by the packaged item when subjected to the type of drop indicated. Also, the tabulated G-levels are those taken from the accelerometer whose axis is oriented parallel to the drop axis. These are usually the maximum G-level readings.

Three factors vary throughout the data, any one of which could have affected the G-level response. The temperature and the attitude of the drop both varied within the tests. Also, the type of cushioning material varied from one type of container to the next. In the analysis the requirement is to assess these three main factors: temperature, type of material, and stress levels (a function of attitude of drop), to determine which of these factors influenced the response of the packaged item when subjected to the drop tests.

DATA ANALYSIS AND SYNTHESIS

The drop test data for each container experiment tabulated in Table 1 were analyzed to determine the effect of the factors involved. The test programs conducted by the various organizations in their development programs were not uniform. However, the tests contained three main treatment effects that can be analyzed: the effect due to change of temperature, the effect due to change of stress level, and the effect due to different types of materials used in the cushioning.

A factorial design was utilized to analyze the data, and the interactions were included in the analysis. A factorial design requires that each treatment be applied at every level of every other treatment [3]. Fortunately, the drop test programs were conducted so that in each test each type of drop was conducted at each temperature.

In the drop test program, for any particular container, the fixed factors in the experiment would be the weight of the container and its contents, and the drop height. The variable factors were of different magnitudes in some of the container tests but all experiments included the following:

Temperature (T_i)	i from -65° to 160°F
Kind of drop (D_j)	j corresponds to bottom, top, end, 45 deg, etc.

A mathematical equation can be written that defines one observation value which is expressed in G-levels. This observation value can be equated to all the variable factors that have an effect on the G-levels and is given as

$$X_{ijk} = T_i + D_j + TD_{ij} + \epsilon_{ijk}$$

where X_{ijk} is an observation value made with T at level i, D at level j, and a random error term at level k; ϵ is the error term introduced during the repetition of the experiment; and TD_{ij} is an interaction between T and D that affects the G-levels. From this mathematical equation, four null hypotheses can be postulated.

(1) Temperature factor: Changes in temperature can have an effect on the G-levels. It is also important to note that temperature is a quantitative factor (the levels of the factor can be expressed in numerical terms) and can have

TABLE 1

G-Level Response of Packaged Item When Subjected to the Type of Drop Indicated at the Temperature Indicated

Container Name	Temperature (°F)	Type of Drop													
		Bottom			Top			Nose			Breech			45 deg	
		1	2	3	1	2	3	1	2	3	1	2	3	1	2
Sparrow G&C	70	30	30		37	36		55	41		92	64		72	41
	-50	46	46		68	68		59	66		82	75		50	68
Brighteye	160	95.8	92.2					23.2	21.1		46.0	38.8		35.6	33.2
	70	101.0	99.6					35.0	34.0		22.4	18.5		38.5	25.6
	-65	99.9	95.2					31.8	27.4		21.2	18.8		36.5	31.1
SUBROC	0	20	24	22	20	24	22	24	26	27	24	22	25		
	75	21	24	24	22	25	26	28	28	27	24	26	27		
Redeye Monopak	160	140	150		140	220		250	160		300	160		90	220
	-65	275	500		170	220		160	190		225	550		130	260
Chaparral Target Detector	160	29.1	32.0		24.1	24.3		24.5	31.3						
	70	24.0	29.4		24.5	24.0		18.4	20.4						
	-65	36.3	33.3		34.8	36.3		25.9	37.9						
Chaparral Warhead	160	18.4	19.4		26.2	27.1		21.6	22.5						
	70	19.4	16.6		25.0	25.0		26.2	27.1						
	-65	32.8	33.3		31.0	33.8		27.8	19.2						
Chaparral Guidance	160	18.7	22.8		14.5	16.1		18.1	19.9					16.3	15.2
	70	23.4	25.4		16.1	21.3		19.9	21.3					19.1	22.9
	-65	26.6	31.2		18.4	30.1		38.6	41.1					17.5	20.7
Shillelagh Crate-Rite	70	34.8	44.0		36.8	37.6		30.8	32.0		28.4	32.2			
	-65	12.3	11.6		12.4	16.8		32.0	31.6		36.8	35.6			
	160	17.2	16.4		23.2	20.0		31.6	35.2		27.6	41.2			
Shillelagh Halliburton	-65	99	84		10.8	111		52	53		39	51		10	29
	70	15	18		22	21		19	22		14	35		20	21
	160	21	18		18	18		16	22		15	50		14	17
Redeye Production	155	60	100		125	90		90	120					154	140
	70	90	110		130	130		100	130					180	180
	-65	50	50		130	80		130	110					175	133
Shillelagh R&D	155	59	68		24	28		40	56		61	63			
	70	43	44		40	40		42	47		39	37			
	-65	50	34		41	46		39	48		63	64			
Redeye R&D	-65	121	191		210	246		99	65					70	47
	70	71	164		130	193		72	99					59	58
	160	169	110		197	201		96	103					148	87
Shillelagh Skydyne	70	40	38		25	40		60	60		20	40		20	90
	-65	66	59		74	66		55	49		30	88		63	46
	160	36	50		26	26		26	32		16	105		15	34
Shillelagh Molded Fiberglas	70	33	35		35	30		31	33		17	24		42	34
	-65	43	48		38	46		43	40		40	53		33	21
	160	40	32		37	42		52	35		29	50		26	36
Shillelagh Steel Drum	70	25	25		25	17		13	19		11	9		12	17
	-65	36	48		97	60		79	73		36	36		60	60
	160	44	41		41	46		65	43		26	46		26	56

a significant linear component.

Hypothesis 1. Temperature does not affect recorded G-levels significantly.

Hypothesis 2. Temperature does not affect recorded G-levels linearly in a significant manner.

(2) Kind of drop factor: The attitude of the container at impact can have an effect on the G-levels.

Hypothesis 3. The kind of drop performed does not have a significant effect on recorded G-levels.

(3) Interactions: The interaction between kind of drop D and temperature T can have an effect on the G-levels.

Hypothesis 4. The (T) x (D) interaction does not have a significant effect on recorded G-levels.

The four null hypotheses were tested by an F-test at 90-percent significance for each experiment; the results are tabulated in Table 2. In each instance marked with "No," the null hypothesis stating that the treatment in question has no effect was not rejected as a valid conclusion. Those marked with "Rej" signify that the null hypothesis was rejected.

The null hypothesis regarding type of drop was rejected in all but four of the container tests. This indicated that considerable importance is attached to the type of drop, which is consistent with the emphasis that is placed on this factor as the abscissa of dynamic cushioning curves.

The analysis of the individual container experiments provided information on the effects of stress levels and temperature on container response. In order to provide information on the effect of different types of materials used as cushioning, an additional analysis is required.

The type of material used in a container cushioning system was fixed within the container prior to the drop tests discussed earlier. Therefore, the individual analysis did not include effects of different types of cushioning material since no significant variation existed in any one experiment. However, when the 15 separate container designs were considered as a group, considerable variation existed in the type of material utilized. Included in the group were container designs that utilized the three main types of foamed plastics used in packaging: polyethylene, polystyrene, and polyurethane foams. A technique is required for grouping all the drop tests in order to analyze the type of material effect.

Certain limitations regarding the grouping of the individual drop test data should be recognized at the outset. The drop tests were conducted by a variety of organizations that undoubtedly used different types of test equipment and response monitoring techniques. The procedures have become relatively straightforward as a result of extensive testing of this type by the many testing laboratories over the last few years. However, certain subtle differences do exist, and these differences are confounded in G-level response values that will be operated upon. It is reasonable, however, to assume that these subtle differences are an order of magnitude less than the effects generated by the major variables in the experiment such as the type of material.

The data from the 15 individual container tests were separated according to the type of cushioning and stress level to provide the data of Table 3 with each observation expressed in terms of G-level response of the packaged items. Sufficient data existed to provide two G-level readings for each level of each factor. These were considered as replications for analysis purposes.

A factorial design can be used to analyze these data since each treatment, in this case, temperature, type of material, and stress level, was applied at every level of every other treatment. The factorial design was selected for this analysis approach because there are four possible interaction effects, and these interactions between the various treatments could be most significant and should be separated for analysis.

The variables in the experiment included:

Temperature (T_i)	i from -65° to 160°F
Stress levels (D_j)	j from 1 to 5
Type of material (M_l)	l is polyurethane, polyethylene, or polystyrene foam.

The mathematical equation that depicts one observation of the experiment and includes all the variable factors involved would be:

$$X_{ijkl} = T_i + D_j + M_l + TD_{ij} + TM_{il} + DM_{jl} + TDM_{ijl} + \epsilon_{ijlk}$$

TABLE 2

Summary of Drop Test Experiments

Name	Size of Container (in.)	Packaged Item Weight (lb)	Drop Height (in.)	Temperature (°F)			Drop Attitudes	Reps	Size of Factorial Experiment	Main Treatment of Experiment				
				Low	Amb	High				(T)	(D)	(T x D)	T_{Linear}	Type Cushioning (Foam)
Sparrow	86 x 14 x 14	135	24	-50	70	-	5	2	2 x 5	Rej	Rej	No	-	PU
Brighteye	68 x 12 x 13	142	30	-65	70	160	3	2	3 x 3	No	Rej	No	No	PS
SUBROC	23 x 23 x 16	12	30	0	70	-	4	3	2 x 4	Rej	Rej	No	-	PE
Monopak	60 x 15 x 13	30	30	-65	-	160	5	2	2 x 5	Rej	No	No	-	PU
Chaparral	15 dia x 22	10	30	-65	70	160	3	2	3 x 3	Rej	No	No	Rej	PS
Chaparral Warhead	18 dia x 28	25	30	-65	70	160	3	2	3 x 3	Rej	Rej	Rej	Rej	PE
Chaparral G&C	22 dia x 35	31	30	-65	70	160	4	2	3 x 4	Rej	Rej	Rej	Rej	PE
Shillelagh Crate Rite	13 x 13 x 52	60	30	-65	70	160	4	2	3 x 4	Rej	Rej	Rej	Rej	PE
Shillelagh Halliburton	56 x 15 x 13	60	30	-65	70	160	5	2	3 x 5	Rej	Rej	Rej	Rej	PU
Redeye Unipak Production	56 x 10 x 15	30	30	-65	70	160	4	2	3 x 4	Rej	Rej	No	No	PS
Shillelagh R&D	56.25 x 17 x 17	60	30	-65	70	155	4	2	3 x 4	Rej	Rej	Rej	Rej	PE
Redeye R&D	56 x 10 x 15	30	30	-65	70	160	4	2	3 x 4	Rej	Rej	No	No	PS
Shillelagh Skydyne	47 x 12 x 12	60	30	-65	70	160	5	2	3 x 5	No	No	No	No	PU
Shillelagh Molded Fiberglas	50 x 13 x 13	60	30	-65	70	160	5	2	3 x 5	Rej	No	No	No	PS
Shillelagh Steel Drum	50 x 13 r 14	60	30	-65	70	160	5	2	3 x 5	Rej	Rej	No	Rej	PE

NOTE: Rej = reject the hypothesis of no effect.
No = cannot reject the hypothesis of no effect.
PS = Polystyrene.
PU = Polyurethane.
PE = Polyethylene.

TABLE 3

Combined Analysis Data Matrix

		Stress Levels (psi)	Polyurethane Foam		Polystyrene Foam		Polyethylene Foam		
			Replication 1	Replication 2	Replication 1	Replication 2	Replication 1	Replication 2	Average
Low Temperature	1	0-0.2	62.2	82.1	50.6	42.1	37.9	25.9	50.1
	2	0.2-0.4	66.4	73.7	38.3	71.6	75.5	31.5	59.1
	3	0.4-0.6	39.1	51.4	99.9	75.6	36.3	24.8	54.5
	4	0.6-0.8	55.3	49.5	42.9	39.6	39.0	48.2	45.8
	5	0.8 up	68.6	73.0	21.2	48.9	35.6	63.1	51.7
		av	58.3	65.9	50.1	55.5	44.8	38.7	52.2
Ambient Temperature	1	0-0.2	50.1	16.5	75.0	40.2	28.4	20.4	38.4
	2	0.2-0.4	40.2	25.8	85.0	32.2	16.8	42.2	40.3
	3	0.4-0.6	14.0	35.6	71.8	99.6	29.4	26.6	46.1
	4	0.6-0.8	40.0	30.0	31.0	33.0	26.1	42.2	33.7
	5	0.8 up	34.5	48.8	22.4	48.6	22.8	68.7	40.3
		av	35.7	31.3	57.0	50.3	24.7	40.0	39.8
High Temperature	1	0-0.2	21.1	28.4	26.2	39.6	24.5	44.2	30.7
	2	0.2-0.4	26.3	35.7	99.0	39.6	54.0	62.7	52.9
	3	0.4-0.6	14.8	30.2	75.8	92.2	29.1	23.9	44.1
	4	0.6-0.8	26.3	32.6	31.9	34.6	40.0	56.0	40.2
	5	0.8 up	30.0	40.7	23.2	37.2	19.7	27.8	29.7
		av	23.7	33.5	55.2	48.6	33.4	42.7	39.5

NOTE: Tabulated values are G-level readings.

where X_{ijlk} is one observation made with T at level i, D at level j, and M at level l; ϵ is the error term introduced during repetition at level k; TD_{ij} is interaction effect due to the interaction of T and D, etc; and TDM_{ijl} is an interaction of the three factors T at level i, D at level j, and M at level l (referred to as a third-order interaction).

Eight null hypotheses were postulated for this experiment, and F-tests were made at the 90-percent significance level to determine whether or not to reject the hypotheses.

The hypotheses to be tested were as follows:

Hypothesis 1. Temperature does not affect recorded G-levels significantly.

Hypothesis 2. Temperature does not affect recorded G-levels linearly in a significant manner.

Hypothesis 3. The variations in static stress levels, as associated with type of drop, do not affect recorded G-levels significantly.

Hypothesis 4. The type of cushioning material does not affect recorded G-levels significantly.

Hypothesis 5. The temperature-stress interaction does not have a significant effect on recorded G-levels.

Hypothesis 6. The temperature-material interaction does not have a significant effect on recorded G-levels.

Hypothesis 7. The stress-material interaction does not have a significant effect on recorded G-levels.

Hypothesis 8. The third-order interaction (stress-material-temperature) does not have a significant effect on recorded G-levels.

Table 4 shows that the null hypotheses regarding the type of material effect and the material-temperature and material-stress level effects could be rejected. Further, the mean square values indicate that temperature and material effects and the material-stress interaction effect have more impact on recorded G-levels than the effect due to variations in stress.

The hypothesis regarding the third-order interaction could not be rejected. An interaction that involves three factors such as this one is frequently incorporated into the error term. It occurs as a separate entry here to maintain as much definition as possible in the error term, but its mean square value was the smallest and could have been incorporated into the error term with very little consequence, as can be seen in Table 4.

TABLE 4
Combined Data Analysis
ANOVA

Source	Degrees of Freedom	Sum of Squares	Mean Square	90% Significance F-Test
Material (M)	2	5,669.8	2,834.9	Significant
Stress (D)	4	3,065.8	766.4	Significant
Temperature (T)	2	3,399.9	1,699.9	Significant
(M) x (D)	8	15,769.7	1,971.2	Significant
(M) x (T)	4	3,657.8	914.4	Significant
(D) x (T)	8	1,441.0	180.5	Not Significant
(M) x (D) x (T)	16	1,618.2	101.1	Not Significant
T_{Linear}	(1)	—	2,686.7	Significant
Error	45	11,545.6	256.6	
TOTAL	89	46,171.2		

SUPERIMPOSED DYNAMIC CUSHIONING CURVE

The analysis of the available data shows that changes in temperature that were introduced in the drop test programs to simulate world-wide extreme conditions have a significant effect on the response of the packaged item. In the analysis of individual drop tests, all but two of the 15 container test programs had a significant temperature effect.

Temperature effects are not considered in the dynamic cushioning curve technique that is currently utilized for presenting information on cushioning materials. The requirement is a technique that provides for temperature effects.

The superimposed dynamic cushioning curve technique provides information on the

effect of temperature on the response of containers that utilize foamed plastic cushioning systems. The dynamic cushioning curve technique provides information on the response of a packaged item for one certain set of conditions: thickness, type of cushioning material, and drop height. This same technique can be extended to the superimposed dynamic cushioning curve technique, whereby the dynamic cushioning curves that are generated at the military temperature extremes (-65° and 160°F) are superimposed on the ambient temperature curve for any one set of conditions; one such curve that the authors constructed (Fig. 2) was derived from information provided by the manufacturer of polyethylene foam, the Dow Chemical Company [4]. Fortunately, Dow provided container designers with separate dynamic cushioning curves for polyethylene foam at -65° and 155°F as well as at ambient temperature for a 30-inch drop height.

In Fig. 2 the temperature effects are seen as a relocation of the curves. In this instance the optimum point on the curve shifts horizontally to the right as the temperature varies from 155° to 70° to -65°F. This demonstrates that increased static stress is required to compress the cushion to its optimum when the material stiffens as it gets colder.

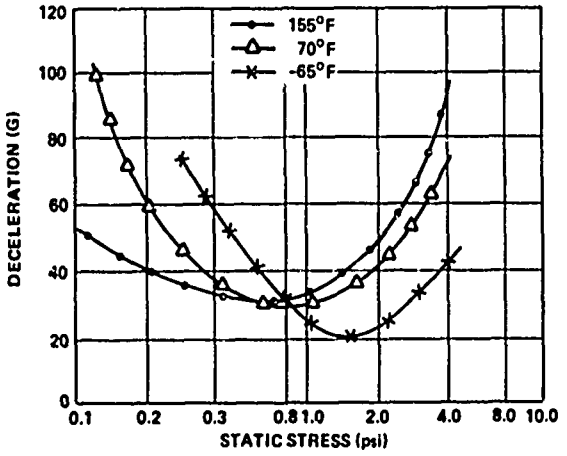

Fig. 2 - Superimposed dynamic cushioning curve for a 2-inch thickness of polyethylene foam (2 lb/ft^3 density; -65°, 70°, and 155°F temperature; 30-inch drop height)

Application of superimposed dynamic cushioning curves provides the container designer with a tool for prediction of the response of a container design under the extreme temperature conditions. A particular static stress condition can be selected for the particular package design in the same manner as with the standard dynamic cushioning curve. This selected static stress condition can then be projected onto the temperature curves and the results correlated. For example, if the design conditions required a 30-inch drop height and polyethylene foam were being considered in 2-inch thickness, then Fig. 2 would be appropriate. By using the 70°F curve, a static stress of 0.4 psi might be selected to provide 40 Gs of protection to the packaged item. However, when 0.4 psi is projected on the -65°F curve, the 40-G requirement is exceeded. The 0.4 psi would then be discarded, another static stress would be selected for consideration, and the correlation would be repeated until a suitable response is obtained.

CONCLUSIONS AND RECOMMENDATIONS

The analysis shows that the effect of changes in temperature introduced into the drop test program of containers, to simulate worldwide extreme conditions, was significant. Temperature effects were significant in the majority of all individual container tests, and polyurethane foam containers were extremely sensitive to low temperature.

The dynamic cushioning curve technique does not provide information on the effects of temperature. However, present cushioning theory can be extended to provide the superimposed dynamic cushioning curves, which do present temperature effects. Fig. 2 demonstrates this technique of constructing superimposed cushioning curves for polyethylene foam at temperature extremes.

Besides temperature effects, the other two main effects that were analyzed were the effect of changes in the type of material and the stress levels within the cushioning. Polystyrene and polyethylene show the same shaped curves, with polyethylene giving consistently lower G-levels. It can be stated that generally the main effect due to the type of material is discernible using dynamic cushioning curves since the curves are segregated by the type of material. However, the additional information on temperature effects that is given in the superimposed curves is required to assess the material-temperature interaction effects.

The stress level effects were shown to be significant in the analysis also. The dynamic

cushioning curves and the superimposed dynamic cushioning curve use the stress level as the abscissa for the curves which provides complete information on this effect.

The superimposed dynamic cushioning curve is recommended for adoption as the technique for presenting information on cushioning materials. This extended technique can be utilized by manufacturers to present information on cushioning materials, while government agencies can employ the technique in evaluating cushioning materials.

REFERENCES

1. K. Brown, Package Design Engineering, John Wiley & Sons, Inc., New York, April 1959.

2. Dylite Expandable Polystyrene—Principles of Packaging Design, Koppers Co., Plastics Division, Pittsburgh, Pennsylvania, January 1969.

3. Charles R. Hicks, Fundamental Concepts in the Design of Experiments, Holt Rinehart Winston, New York, 1964.

4. Packaging with Ethafoam, Dow Chemical Co., Plastics Department, Midland, Michigan, 1966.

DISCUSSION

Mr. Yang (University of Maryland): I thought it was a very interesting paper. I have two comments to make. My first comment is that I would like to speak up for both Navy and Air Force because I have consulted with both, and in the area of these energy absorbers, both the Navy and Air Force have done a lot of work in getting properties and doing a lot of tests. As a matter of fact, there are a lot of reports in this area. As a result of consultation with the Navy and Air Force, I myself have five or six papers in the area — especially these three materials. One of the papers was referenced by Professor Shang in a previous paper which was presented two years ago at the Shock and Vibration Symposium. The material was polyurethane, and also there are many other papers which do what you have mentioned in your paper. I would be very happy to go over some of these papers if you are interested.

Mr. McDaniel: I am familiar with them. What is being done is primarily on a bulk cushion in a drop test environment, testing an individual cushion of a particular thickness as opposed to a container with an item in it. Is that true?

Mr. Yang: Yes, the researches to which I was referring are on a more basic level rather than on particular cases. They would study densities and thicknesses of each material at various temperatures and strain rates. These are basic research studies, but I do not know about tests of a particular container.

Mr. McDaniel: That was the point of this study. Really, fundamental to the container design, is how that item behaves in the container, and we can take this information that is available on the elementary level and apply it. There is a lot of variability in how a particular container responds when you configure the material and test as opposed to just testing, for example, raw sheet material.

Mr. Yang: That is true. However, I do think that, from this basic research, you can get a lot of ideas which can be used. My second comment is that I think this temperature effect is excellent that you were looking at. Also, I think another thing you should take into account is also the rate. I do not know what rate you are dealing with, but that is another thing you should look into.

Mr. McDaniel: The viscoelastic property of a urethane foam does present a rate problem. However, in a container that rate is married into the test. You do not really have to address each individual item if you test the basic configuration.

Mr. Schell (Naval Research Laboratory): I was very much interested in the results on your peak g, static stress curves for various temperatures, where the optimum actually is better for low temperatures than for higher temperatures. I noticed that, for low static stresses, the cushion behaved as one would expect, that is, it would stiffen up and give higher

g's. For the larger static stresses you got just the opposite effect. Have you made any conjectures as to why this happened? Is there a possibility that you are getting material breakdown at the higher static stresses due to embrittlement or something of this nature?

Mr. McDaniel: I do not really know. Maybe Mr. Yang would like to answer that. All I know is how these containers behave. It would be good if we had this type of information available to us as designers, but we do not.

Mr. Langhaar (duPont Company): What maximum thickness of foam did you test, and did you discover any method of extrapolating the results to very large thickness, for example, 24 inches?

Mr. McDaniel: I think the thickest material we looked at was in one of the Redeye polystyrene versions which is about 8 or 9 inches. Again, once you select a static stress, and once you select your material, these are frozen into the design of the container, and there is really no opportunity to change these things. You can change nicely on sheet material and generate a curve, but once you have built it into a container you are stuck with it, so to speak. Then is when you must have made the right choice on the basis of this type of information. No, we had no opportunity to change anything. We changed drop attitudes and that is about it.

Mr. Westine (Southwest Research Institute): From the theoretical point of view, when you correlate with acceleration and so forth, this means you are in the quasi-static load realm. That is, the durations of loading are very long relative to the response time associated with the structure dropped. Throughout all these presentations we saw the acceleration being put forth. But if the durations of loading are short relative to response times, quite frankly, acceleration does not matter. Velocity, not acceleration, becomes important. It puts you in what we call the impulsive loading realm. You can also be in a knuckle which gives you both acceleration and velocity as the significant initial conditions. So, in a certain sense you should be talking about what these period-ratios or these time-ratios are like. When you say, for example, "I make the null hypothesis that temperature is not significant. I test and find it to be false, therefore, temperature is significant." That does not necessarily follow. It may be there is something else that you are ignoring and not treating as a variable. I do not say that it is not, because in making that statement, it does not really test it to the contrary, does it? From a philosophical point of view, perhaps because one of the dimensions in the space such as velocity of impact is not being included. Perhaps your times relative to response times are such that it should be included. You might be overlooking an important variable. As an illustration, perhaps what you are showing as a two-dimensional space should be a three-dimensional volume. We do not seem to be talking in terms of these variables. They are certainly present, and you can show theoretically that these realms exist. The other reaction I had is that you are always putting accelerations up in g's. Gravity has nothing to do with it.

Mr. McDaniel: Well, that is the real world right now. The way we are approached as a container designer is: "Given a missile system with a particular fragility level, design on a particular basis to provide the necessary protection." So, that is what we live with, and whether we can ever get our missile people to talk to us in other terms is something for the future. I think you are right.

Mr. Gertel (Kinetic Systems): I gathered that the drop height, the curves of acceleration and static stress were for a particular container configuration instead of the sheet material type of data which you normally find.

Mr. McDaniel: The superimposed dynamic cushioning curve that we showed last was on sheet material. I got the information from a manufacturer and compiled it the way it was presented. It does not perform exactly that way in a container, but it comes close.

Mr. Gertel: That was the question I had whether you noticed any particular difference between the curves for sheet material, and the material as actually used in containers.

Mr. McDaniel: Yes, significant at times.

Voice: Was there any pattern?

Mr. McDaniel: No, there was complete variability in what I found. You can not really use sheet material data and extrapolate directly, but it is a good guide. It is the best we have right now, and I think this type of information would make it better.

Mr. Leonardi (Picatinny Arsenal): One of the reasons you can not do this, is that you have to include parameters such as the degree of confinement which you have in a container and the air escapement function which is always present.

The response level, which you have mentioned, is another parameter. What you are doing is something we also are trying to do. We are trying to measure the overall effect of the structure, and sometimes this is the simplest way out. In the final analysis it gives you an answer — some quantitative value with which to work.

Mr. McDaniel: That is right. When you take sheet-material data and apply it directly, the unknowns you mentioned give results that are not predictable from the data used. Just by cutting a piece of foam material into smaller pieces, you change the response because of the viscoelastic properties of air flowing through the materials. Once you build a container, you are stuck with a particular design, and you will be testing on that basis.

Mr. Gaynes (Gaynes Testing Laboratories): Others of us have done work in this area, and we have found variables introduced by the test method. For example, where accelerometers are mounted can make a difference. The amount of cushioning above your product also makes a difference. that is the relationship of the top cushion to the bottom cushion. Also a question— was that 30 inches of free-fall as compared to a vacuum, or was that strictly a 30 inch free-fall height the way you measure it?

Mr. McDaniel: Well, the standard military documents present the free-fall drop test in terms of height as a function of the weight of the item or sometimes the weight and size or shape of the item. It is a free-fall drop in air. It is just an anticipated stevedore operation type of thing.

Mr. Gaynes: The only reason I bring that up is because, normally, in conducting free fall tests, the surface upon which you drop is a very important factor in relation to the resulting g force.

Mr. McDaniel: That is right. These tests are defined as a drop on a steel plate or on a concrete immobile surface.

DEVELOPMENT OF A PRODUCT PROTECTION SYSTEM

Dennis E Young
IBM General Systems Division
Rochester, Minnesota 55901

and

Stephen R Pierce
Michigan State University
East Lansing, Michigan 48823

A workable method for development of a product protection system, based on hardware and established procedure, is presented. The date and techniques used in product design determine the inherent strengths and fragilities of a product. These characteristics are determined by fragility assessment. Coincidentally, a continuing program statistically quantifies the non-use environment through which the product must pass. This data, along with knowledge of packaging methods and material characteristics, are combined to engineer the package. Once engineered, the package and product are tested by dynamic simulation of the non-use environment. The packaging program described indicates that the method maximizes the packaging engineer's chances of submitting the ideal economic and protective package the first time.

INTRODUCTION

Since the birth of American industry, goods in transit from the manufacturer to the consumer have been exposed to damage. From these early beginnings, the problem of damaged goods has grown along with the nation's industrial performance until today these damage costs amount to billions of dollars.* Coincidentally, experts have realized the need for solving the problem. Among those attacking the problem are professionals in packaging, transportation, materials handling, and associated fields of materials science, dynamics, testing of various types, communications, and education. The thrust of this work has been to minimize functional degradation to goods which are subjected to hostile, non-use environments. This paper presents a case study of one approach to a solution that seems promising.

At the IBM Rochester, Minnesota, facility we have a move on to "reconceptualize" the information and action flow necessary to solve a possible exposure to goods damage in transit. The preliminary result was a simple flowchart of the major elements in development of a product protection system, as shown in Fig. 1.

* Estimate based on Office of Policy Review of the US Department of Transportation.

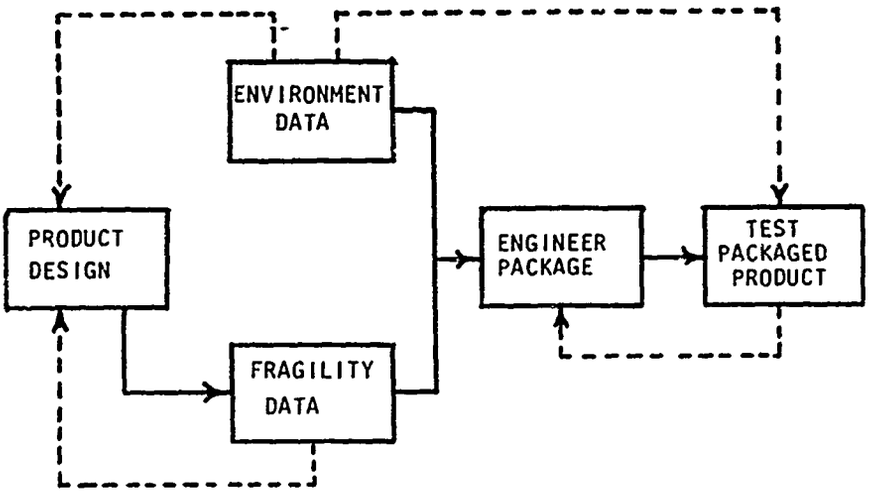

Fig. 1 - Product Protection System Development

ELEMENTS OF THE CONCEPT

Product Design

Elements of the mechanical design of any product determine the inherent strengths and fragilities of that product. The more rugged the initial product, the less exotic and expensive the package required. Attention to design concepts at this stage can reap economic benefits when the product is later exposed to transit shock and vibration.

Fragility Data

Within the constraints of a given mechanical design, it becomes necessary to assess the fragility of the product. Fragility may be simply defined as the level of dynamic input required to cause minimal non-functionality in a product. Recent literature has emphasized a method to determine shock fragility specifications based on parameters of deceleration and total change in velocity [1-3]. The result of this empirical analysis is called a damage boundary. Vibration fragility is specified by the natural frequencies of the product, with emphasis on the lowest primary resonance [4,5].

Environment Data

In response to a need, continuing efforts have accounted for wide availability of data on the transit environment [6-9]. The forms of data reduction and presentation vary considerably. While general data is available, specific techniques for application to product protection problems are conspicuous by their absence. In general, packaging engineers are not highly trained in dynamics, and thus the requirement is for a straightforward set of environmental data that relates well to empirical fragility data. A further constraint is that the environmental quantification be relatively easy to perform by the engineer. Having this ability, the persons responsible for the protection system can assign priorities to applicable modes of transportation.

User generation of data has some disadvantages also. Among them is the relatively small quantity of data that one organization can effectively accumulate. Data used for this type of application is a set of graphs of either deceleration or change in velocity treated statistically.

Engineer Package

The information on fragility and environment is combined with material data and knowledge of packaging methods and processes to engineer the product protection system or package. Graphic data on cushion performance is widely available. Some additional types of information necessary for designing the package are only now under development, and so must be generated by the user either for each application or under a continuing program of material evaluation. Some of the most useful forms of this data are given in Table 1.

TABLE 1
Packaging Material Performance Data [10-15]

Data Type	X-axis Parameter	Y-axis Parameter
1	Percent creep	Time
2	Static stress	Response deceleratior
3	Static stress	Natural frequency
4	$\frac{\text{Forcing frequency}}{\text{Natural frequency}}$	Transmissibility
5	Strain	Stress

Test Package Product

Once a prototype of the proposed design has been built, the product and its package are subjected to a series of tests to assess the ability of the package to protect the product during transit. This testing is an environmental simulation, with three basic types of inputs: vibration, horizontal shock inputs, and vertical shock inputs.

Feedback

Throughout the development procedure there is feedback to insure the proper application of data. If the stage of product development allows, results of environment and early fragility tests are given to the product designer. By identifying critical areas of the product, it is often possible to effectively trade off package design versus product modification to the best economic advantage. A change to the product early in development can increase its ability to withstand the non-use environment between manufacture and ultimate use, without affecting its use environment performance, and at minimal cost.

Environmental information sets the levels for transit simulation testing of the packaged product [16]. Results of this testing are fed back into the package engineering cycle for possible improvement of the package design.

Thus, the application of the concept shown in Fig. 1 allows an orderly and logical progression of data and action resulting in the development of an economic product protection system.

PACKAGING CONCEPT APPLICATIONS

The Product

The product to be packaged is a keyboard subassembly used in the IBM 129 card data recorder. The unit is manufactured at Rochester, Minnesota, and then shipped to the IBM Toronto, Canada, facility for installation in the host machine. Volume of shipment is significant relative to products of this type. The unit (Fig. 2) weighs approximately 14 lb. It sets in the host machine with the lower mechanical portion beneath the table top. Construction is a combination of plastic and metal, with the major components mounted on a relatively rigid frame suspended from the cover structure by screws. Cabling for connection to the host machine exits from the rear of the keyboard. Unit cost is relatively high, thus no damage/packaging cost trade offs are allowed.

The units are shipped by general commodity carrier truck from Rochester to Toronto, and are handled at least five times.

Product Testing

Shock Fragility

One of the critical preliminary determinations--prior to shock fragility testing--is to establish a damage criteria for the product. The damage criteria decision was simplified because of a standard Quality Engineering test performed prior to shipment.

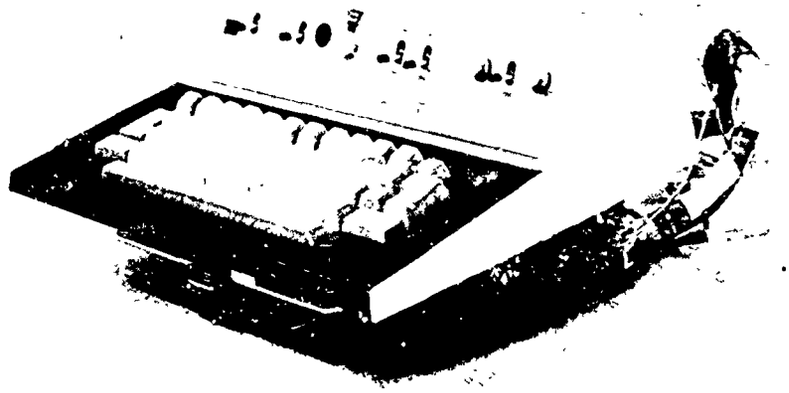

Fig. 2 - IBM 129 card data recorder keyboard

The unit is mounted on a keyboard test adapter (KTA) connected to an IBM 1130 computing system. A stored test program is then run. During the test, all functions are tested for proper operation. The total test time is only minutes, making the repeated dropping and testing required for shock fragility determination practical. The environmental data, discussed in detail below, indicates that the principle danger of damage exists in the vertical direction. Since units are shipped in multiples of 36 (to make use of a standard outer container) the potential for damaging horizontal shock or tipovers appears slight. Environmental data bore out the opinion that cushion design, if required, would apply only to the vertical orientation. This was confirmed later in the environmental simulation phase.

Testing for shock fragility is an equipment-dependent type operation. Although literature suggests several alternate methods, the testing for this application was done on the shock machine* shown in Fig. 3. The machine, which can handle 1500-lb. specimens, has horizontal dimensions of 60 by 60 in. An open top allows a package height limited only by stability. The device incorporates a lifting system to raise the shock table to a preset drop height level. The lifting mechanism is then lowered away and the table dropped on programming devices. For shock fragility testing, pneumatic programmers charged with nitrogen gas are used.

The rise time of the pulse is controlled by changable elastomer pads on the bottom of the table; the stiffer the pad, the faster the rise time of the pulse. When the decelerating table force equals the combined pressure of the gas in the six programmers, the programmers begin to stroke at a constant deceleration rate, then rebound at the same constant rate until the pressure is again equal to the force. The rebound then continues at a rate determined by the elastomer. The resultant pulse is a trapezoid wave shape (acceleration vs time). Wave shapes affect the results of testing significantly, and thus the trapezoidal wave is preferred, since it is the closest practical approach to the ideal rectangular wave [2].

* Model 6060 MKII, manufactured by MTS Systems Corporation, Minneapolis, Minnesota.

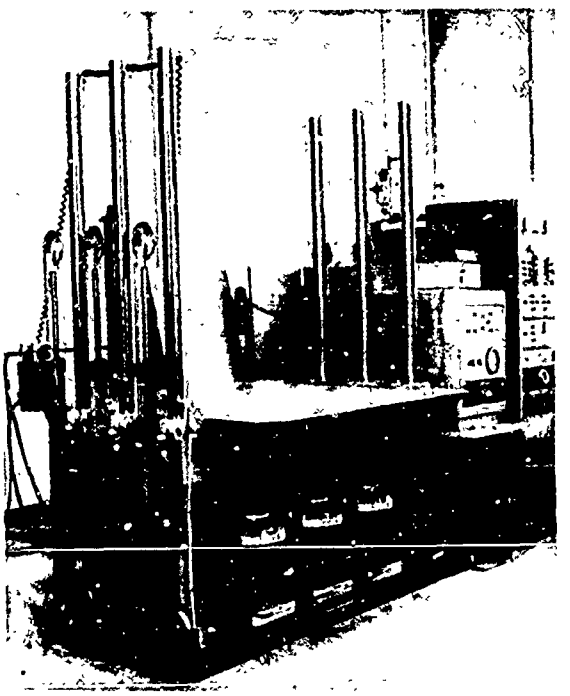

Fig. 3 - MTS shock machine

One of the problems associated with this type of testing is that most products are sensitive to the manner in which the shock pulse is applied. Therefore, the method of fixturing becomes important, as it must represent the intended method of supporting the product within the package. In the keyboard application, the product was supported by the outer edge of the cover, with the lower frame free of contact with the fixture. The keyboard was then held firmly in the fixture to avoid rebound. The shock fragility test cycle was then started.

The first series of tests determined the deceleration or g force side of the damage boundary. The first test was a 9g pulse, from a 7-in. drop height, with total change in velocity of 120 in./sec. Total change in velocity is calculated as follows:

$$\Delta V_t = V_i \ (1+c_r)$$

or

$$\Delta V_t = V_i + V_r$$

where

V_t = total change in velocity,

V_i = impact velocity,

c_r = system coefficient of restitution ($0.0 \leq c_r \leq 1.0$), and

V_r = rebound velocity.

The first impact was not damaging. Two consecutive runs were made on the testing system without deviation.

By increasing the pressure in the pneumatic programmers, the g force level was gradually increased with each successive test. On test No. 7, no damage was seen at 36 g input. On test No. 8, the metal plate between the frame and the cover bent in two places, displacing the keys downward and making the unit inoperative. The g side of the damage boundary had been tentatively established at between 36 and 45 g. To establish the change in velocity side, the programmer pressure was increased so that the g fragility would be exceeded on each drop. The first drop of the second series was 85 g and 78 in./sec. change in velocity, with no damage. The second drop was 93 in./sec. with no damage, but the third drop, at 102 in./sec., caused the same type of damage as occurred in drop No. 8. Since the first series was done at a change in velocity level that would place the point of the damage boundary established on the knee, or curved portion of the curve, the g side was rerun, this time with sufficient drop height to make the point established on the asymtopic portion of the damage boundary. Thus the g side was more clearly defined as 35 g. The damage boundary for the vertical direction of the 129 keyboard was available, and graphed as seen in Fig. 4. For most applications, the more conservative graph, showing a square corner, has proven easier to interpret and use, while maintaining the ability to establish the curved or knee portion if the need arises.

Vibration Fragility

Since the determination of product resonance was important only considering the primary cushion as the springing member, these tests were performed with the keyboard mounted in a prototype holding tray, similar to the fixture used for shock fragility

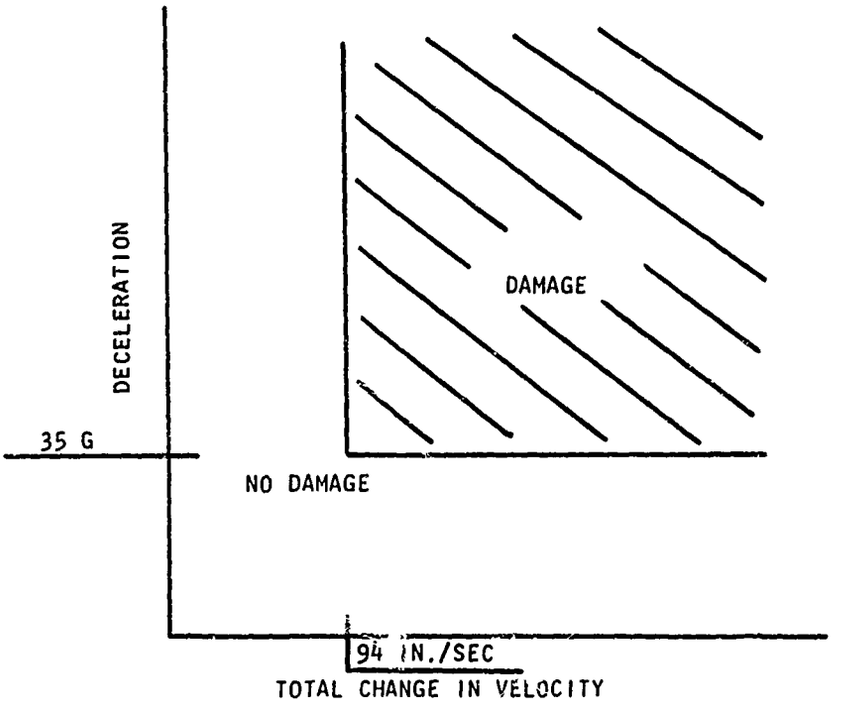

Fig. 4 - 129 keyboard vertical damage boundary

testing. The unit was mounted to an electrodynamic vibrator with a 500 lb. vector force rating. The frequency swept from 10 to 200 Hz. Audio noise was noted at the 25 Hz and at the 75 Hz levels. Use of slower sweeps and stroboscopic techniques identified the lowest primary resonance at 26 Hz, at which point the entire structure hanging beneath the covers resonated. Testing was at approximately 0.029 in. displacement, or 1 g, zero to peak.

Environment Testing

Our continuing environmental quantification program is based on the Transportation Environment Measuring and Recording System (TEMARS*). TEMARS, as shown in Fig. 5, is a portable, battery powered system that records shock inputs experienced in the transit environment. Recordings are made on a 7-track magnetic tape, in NRZI mode, to provide compatibility with electronic data processing equipment. Data recorded is peak measured g force and duration at a preset threshold. Thresholding minimizes recording of low level, relatively useless data. For the trips used in this program, 20 g full scale and 10% of full scale threshold values were selected. The makers of TEMARS also provide a standard software computer program to print out recorded data. This standard program was modified to provide output data punched in cards for further processing. These cards are the raw data processed through an IBM 1130 computing system by user-written programs to further reduce the data to graphic form. The raw data is also converted from g-force data to change-in-velocity data, and again treated graphically. Fig. 6 shows the general data processing flow, Figs. 7 and 8 the graphic end result.

* Manufactured by Endevco Corporation, Pasadena, California.

The graphic data is also available to the user through a television-like graphic display unit, where the user specifies information about the TEMARS trip of interest, and the computer selects and displays the appropriate information on the screen. Data used for this application was from trips along a different, shorter route, but representing the intended environment. While data so collected is a small sample of the total environment population, it is assumed that the data falls in the middle of some undefined normal distribution of values, that is, that both higher and lower inputs do occur with some frequency. We further assumed that the continuing program will make available ever increasing amounts of data that will add significantly to the confidence level of the information.

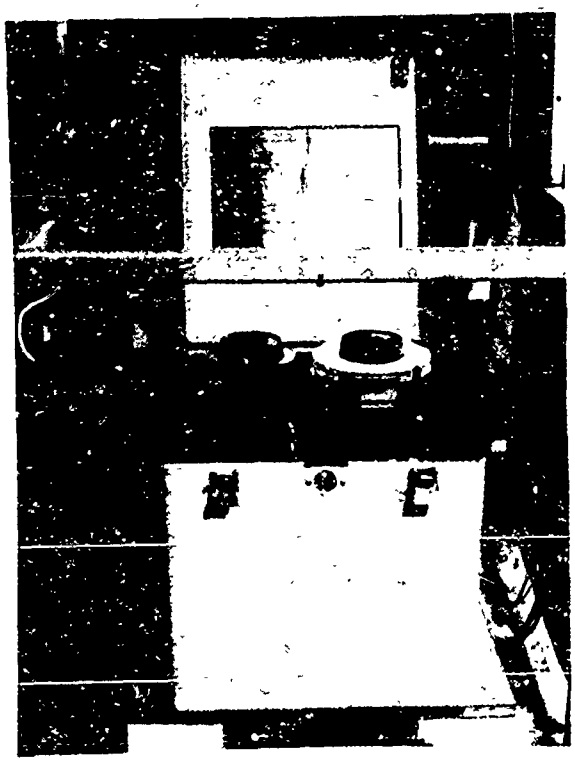

Fig. 5 - Environment sampling device

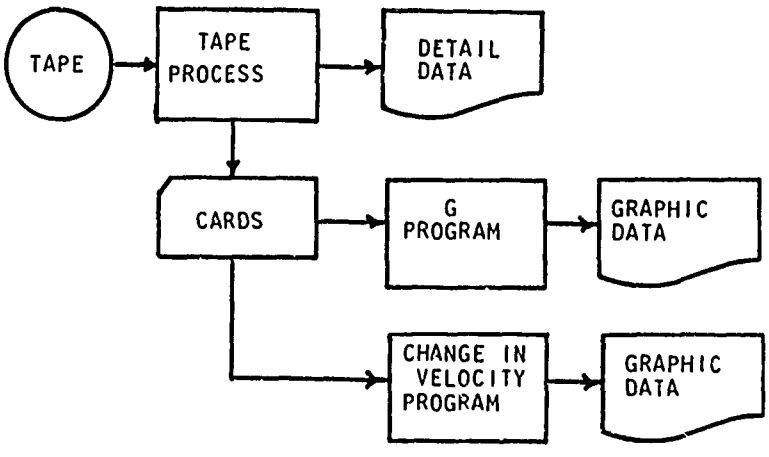

Fig. 6 - Environment data reduction flowchart

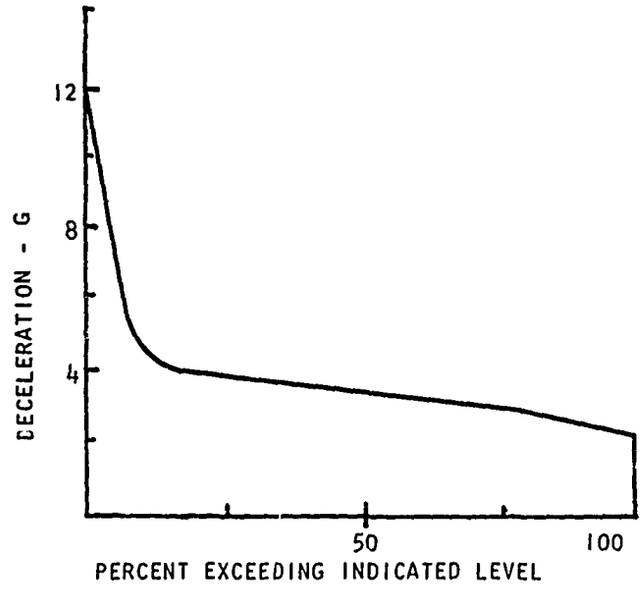

Fig. 7 -Example g-force environment data

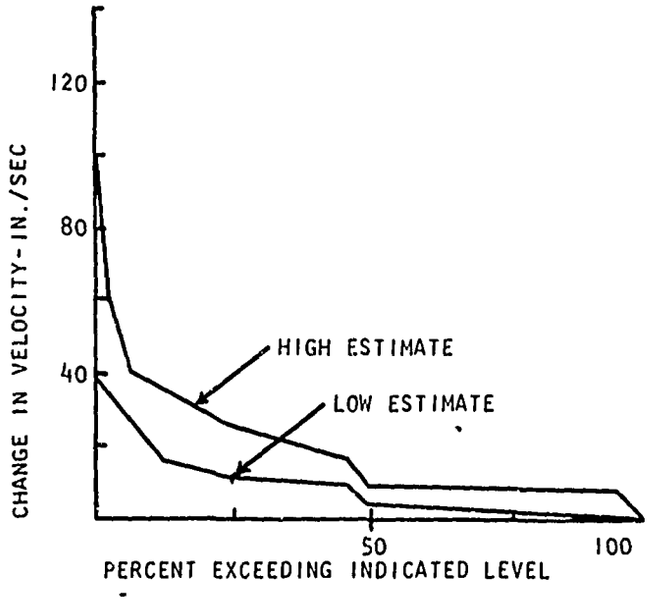

Fig. 8 - Example change-in-velocity environment data

Packaging Engineering Process

Examination of the environmental data available and the fragility curve convinced us that cushioning was required to protect the product from the most severe inputs expected. Amplification of g level inputs were anticipated, thus damaging levels could be expected. Enough change in velocity to cause damage was seen in several cases. We estimated that the concurrent g force and change in velocity was sufficient to cause damage. Further, we noted that damage costs to one bulk load of units was sufficient to pay for a month's supply of the proposed packaging. Design drop height was based on available

environment data. Maximum changes in velocity were seen as possibly occurring with 0.0 coefficient of restitution, therefore design drop height becomes a function of only the impact velocity. This is a most severe case. Calculations were as follows:

$$H_d = \frac{V_i^2}{2g}$$

where H_d = design drop height,

V_i = impact velocity, and

g = gravitational constant

g = 386.1 in./sec.

Using an apparent maximum impact velocity of 100 in./sec., a design drop height of 13 in. was assigned. For a gross bulk weight of about 600 lb., this is slightly less than some recommendations [14,16].

Little information is available on static stress versus deceleration data (type 2 from Fig. 2) on the 12-in. drop height [15]. The 18-in. data shows that several cushions give the desired performance.

Two optional approaches were identified for trial. One, a molded urethane foam end cap, was later dropped because of difficulty in adjusting for nonsymmetrical weight distribution and because of cost. The other initial approach was to use polyether urethane foam cushions under the unit holding tray. Weight distribution of the unit is 40% front and 60% rear. The size cushions underneath the front and rear were adjusted accordingly. Based on a type 2 curve, we decided to use 0.2 psi as the static loading. This point falls on the left side of the lowest portion of the curve. The unit and holder weigh 15 lb., so the cushion sizes for front and rear were calculated as follows:

$$A_r = 0.6M/S_s$$

$$A_f = 0.4M/S_s$$

where A_r and A_f = cushion areas for rear and front, respectively,

0.6 and 0.4 = weight distribution factors,

M = total unit weight, and

S_s = desired static stress.

The next problem was to assess the compatibility of the proposed cushion system with the vibration fragility of the unit. The standard recommendation is to use a cushion with a natural frequency that will provide 60% reduction, or attenuation of the g level at product resonance. As a guideline, this often occurs when the natural frequency of the cushion system is one-half of the natural frequency of the product. In this case, the product resonated at 26 Hz, so the targeted cushion frequency was 13 Hz. No data is yet available for the natural frequency versus static stress performance of ether urethane. Data is available, however, on the stress-strain relationship of this material [10], so the system's natural frequency was estimated as follows:

$$f_n = \frac{1}{2\pi}\sqrt{\frac{g}{x_s}} \quad (1)$$

f_n = 13.9 to 15.5 Hz for static deflections of (x_s) 0.05 to 0.04

where

f_n = system natural frequency, and

g = gravitational constant

g = 386.1 in./sec.

Another method of estimating static deflection provided similar results. In a preliminary test, a free fall drop of 8 in. gave an experienced force reading of approximately 20 g. Deflection of the system under dynamic load is calculated as:

$$x_t = \frac{2H}{G-2}$$

where

x_t = total dynamic deflection,

H = drop height, and

G = experienced g.

By this analysis, total dynamic deflection is 0.89 in. Static deflection is then given by

$$x_s = \frac{x_t}{G}$$

$$x_s = 0.045 \text{ in.}$$

By applying Eq (1), natural frequency again falls between 14 and 15 Hz. A frequency sweep across this area on the electrodynamic vibrator showed that because of the lack of total rigidity in the keyboard holding tray, the system did not resonate cleanly. However, the point at which the system seemed to begin to resonate was between 13 and 14 Hz, thus confirming that range as the critical one. This is somewhat higher than the ideal mentioned above. If transmissability performance data were available, it would be possible to evaluate this increase. From other data [15], it appears that, at worst, the natural frequencies identified would transmit input forces at a ratio of 1 to 1. While this is less favorable than the recommendation, we decided to try this method and test the system in the vibration mode during environment simulation.

A prototype set of packaging for the individual keyboard was completed and preliminary tests were run to determine the feasiblity of the design. After some minor dimensional adjustments, the basic design was approved as shown in Fig. 9. Samples were secured for further testing. Since it was necessary to ship multiple keyboard units, a method was devised to permit each individual tray and keyboard to act separately on its cushions, while receiving outer protection from a larger, multiple unit package. The outer package is a standard double cover tube on a pallet. The tube and caps are made of corrugated fibreboard, with inside dimensions of 40 by 48 by 36 in. high. The cubage was then divided into four layers of nine units each, each unit having its own "hatch".

Environmental Simulation

Based on available equipment and data, the following three-part environmental simulation was specified.

- Vibration Testing

  --Unit level vibration

  --Sweep from 10 to 200 Hz at nominal 0.5 g input at a sweep rate of approximately 1 octave/min

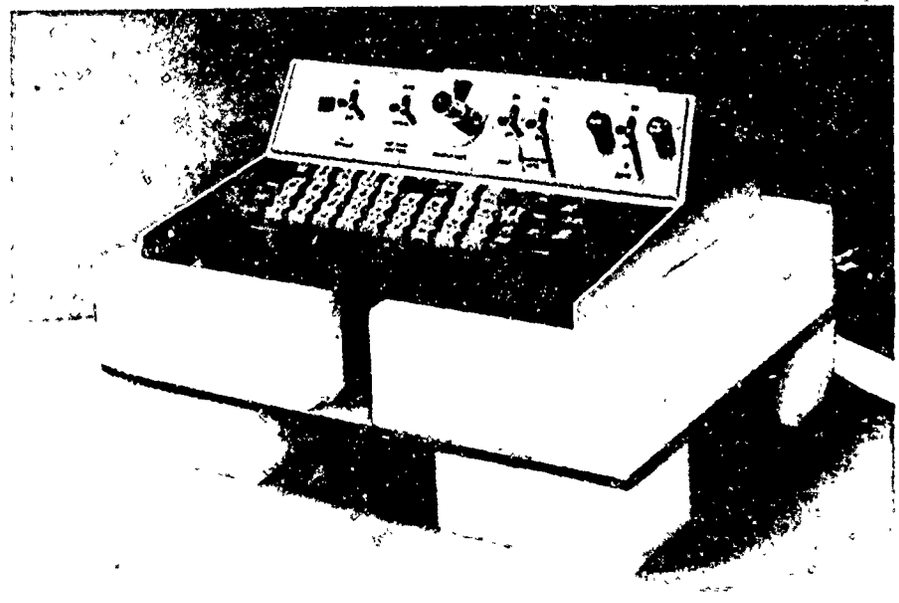

Fig. 9 - 129 keyboard and its protection element

--Multiple unit vibration: circular synchronous vibration for 60 min at 3.0 Hz

- Horizontal Shock Inputs

--Two impacts each face of the multi-unit package at 35 in./sec. impact velocity

- Vertical Shock Inputs on Step Velocity Programmers

--20 Inputs at 30 in./sec. impact velocity

--2 Inputs at 100 in./sec. impact velocity

Since there was no damage to the units, the package was deemed sufficient to ship the product through the handling/transit environment.

SUMMARY

The process detailed in this paper is a case study of an attempt to apply existing information and methodology to the problems of product protection. Since this method was adopted, none of the several thousand 129 keyboards have been damaged in transit. The current cost of the packaging material and labor for this unit is significantly less than 1% of the value of the unit. Several alternate methods of packaging have been suggested and investigated, with no evidence that adequate protection can be offered at less cost. The packaging program described in this paper is an indication that the method minimizes cut-and-try engineering, and maximizes the packaging engineer's chances of submitting the ideal economic and protective package the first time.

Some gaps remain in the theory and application of product protection system development. Even more severe gaps exist in the material data area. The situation in both of these areas will improve as the demand for more information increases. When data is made available to the packaging community, as generated by material users, manufacturers and independent sources, the rate of improvement should increase.

As knowledge and experience increase, other improved methods will replace Product Protection System Development. It is through this process of change and improvement that scientific protective packaging will come of age.

REFERENCES

1. F. C. Bresk and A. Abate, "Cost Savings Through Reduced Product Fragility and Optimized Package Design," presented at AMA National Packaging Conference, Chicago, May 1971.

2. R. E. Newton, "Fragility Assessment Theory and Test Procedure", Sponsored by Monterey Research Laboratories, Monterey, Calif., 1968.

3. M. Kornhauser, "Prediction and Evaluation of Sensitivity to Transient Accelerations", J. Applied Mech., Vol. 21, No. 4, Dec. 1954.

4. 5 Step Packaging Development. MTS Systems Corp., Minneapolis, Minn. 1971.

5. R. E. Newton, "Package Vibration Testing," prepared for MTS Systems Corp., Minneapolis, Minn. 1971.

6. F. E. Ostrem and M. L. Rumerman, "Shock and Vibration Environment Criteria," Contract NAS 8-11451 Final Report 1262, General American Transportation, Research Division, Sept. 1965.

7. Ibid., Report 1262-2, April 1967.

8. F. E. Ostrem, "Survey of Cargo-Handling Shock and Vibration Environment," Shock and Vibration Bulletin 37, Part 7, Jan. 1968.

9. R. W. Luebke, "Investigation of Boxcar Vibrations," Contract DOT-FR-9-0038, Report No. FRA-RT-70-26, Aug. 1970.

10. R. K. Stern, "Package Cushioning Design," MIL-HDBK-304, prepared for Department of Defense, Washington, D. C., Nov. 25, 1964.

11. H. C. Blake III, "Creep Properties of Selected Cushioning Materials," School of Packaging, Michigan State University, East Lansing, Mich. Nov. 15, 1964.

12. H. C. Blake III, "24-in. Drop Height Peak Deceleration-Static Stress Curves for Selected Cushioning Materials," School of Packaging, Michigan State University, East Lansing, Mich., Nov. 1, 1964.

13. H. C. Blake III, "Peak Deceleration-Static Stress Curves for Selected Cushioning Materials," School of Packaging, Michigan State University, East Lansing, Mich., July 10, 1964.

14. Packaging With Ethafoam, Form No. 171-458-10M-1266, Dow Chemical Company, Plastics Department, Midland, Mich. 1966.

15. P. E. Franklin and M. T. Hatae, Shock and Vibration Handbook, C. M. Harris and C. E. Crede, editors, pp. 41-1 through 41-45, McGraw-Hill, New York, 1961.

16. A. T. Mickel, IBM. Armonk, N. Y., correspondence.

MOTION OF FREELY SUSPENDED LOADS DUE TO HORIZONTAL SHIP MOTION IN RANDOM HEAD SEAS

H. S. Zwibel
Naval Civil Engineering Laboratory
Port Hueneme, California

The theory is developed for the swinging motion induced in a wire suspended load due to the horizontal motion of a ship. An explicit formula is obtained for the significant amplitude of horizontal load motion when the ship is exposed to random head seas. Numerical results are presented for two typical cargo ships in a sea state three. It is found that very large motions are suffered by the load. For critical line lengths, resonance effects magnify the ship motion by several orders of magnitude. In addition, numerical solutions are also obtained for the pendulation due to simple harmonic motion of the support while the load is being raised or lowered. The peak displacements are considerably less in this case, however, they are still undesirably large.

INTRODUCTION

Loading and off-loading from ship-to-ship (or ship-to-pier) is a requirement for the Expeditionary Logistics Facility (ELF). In a wave environment the ships are subjected to forces that generate translational and rotational accelerations. The horizontal motions due to surge and pitch from bow-on waves in a sea state 3 have been shown to be quite small [1] (fractions of feet for the significant surge amplitude for ocean-going vessels). The influence of these small motions on a wire suspended load may not, however, be negligible. It is the aim of this investigation to determine the motion of such wire suspended loads induced by horizontal ship motion.

In the next section the constant line length, random motion problem is solved. This is followed by an analysis of the pendulation while raising and lowering the load assuming simple harmonic motion of the support.

FIXED LINE LENGTH

In this section the steady-state pendulation induced by random seas and constant line length is presented.

Theory

The horizontal motion of the ship is transferred to the load by means of the lateral vibrations of the lifting line. These vibrations are due to the motion of the line attachment point which is assumed to be rigidly connected to the ship. In order to make the problem tractable the following assumptions are made:

(a) the line is a fixed length
(b) the line is flexible and uniform
(c) the load is considered to be a point mass
(d) the mass of the load is much greater than the mass of the line
(e) the deviation from equilibrium is small

The coordinate system used to describe the dynamics is presented in Figure 1. The horizontal position from equilibrium of the support is denoted by X_s and, as far as the line vibration is concerned, is a given function of time. The horizontal displacement from rest of a piece of line at position z below the support at time t is $\eta(z,t)$. The mass m, which is a distance L below the support, therefore translates through a horizontal displacement of $\eta(L,t)$.

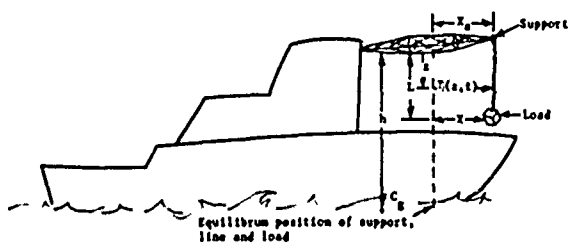

Figure 1. Coordinate system.

The dynamics of this system are described by the one-dimensional wave equation for $\eta(z,t)$ for the line and F = ma for the mass. The equations,* including boundary conditions are given below:

$$\frac{\partial^2 \eta(z,t)}{\partial z^2} = \frac{1}{c^2}\frac{\partial^2 \eta(z,t)}{\partial t^2} \tag{1}$$

$$\eta(0,t) = X_s(t) \tag{2}$$

$$m\frac{\partial^2 \eta(L,t)}{\partial t^2} = -mg\left.\frac{\partial \eta(z,t)}{\partial z}\right|_{z=L} - \frac{1}{2}\rho C_D A \frac{\partial \eta(L,t)}{\partial t}\left|\frac{\partial \eta(L,t)}{\partial t}\right| \tag{3}$$

The first equation is the wave equation for the line. The velocity of propagation (c) for transverse vibrations is $\sqrt{T/\mu}$, where T is the tension in the line, and μ is the mass per unit length of the line. It is assumed that $m >> \mu L$, hence T = mg (g is the gravitational acceleration), therefore

$$c^2 = \frac{mg}{\mu} \tag{4}$$

The second equation imposes the horizontal motion of the ship, $X_s(t)$, on the upper end of the line. The third equation is F = ma for the load of mass m. Since $\eta(L,t)$ is the displacement of the mass, it appears as a boundary condition for the motion of the line. The first term on the right hand side of equation (3) is the horizontal force exerted on the mass due to tension in the line. The second term on the right is the damping force on the mass due to its motion through the air. ρ is the density of air; C_D is the drag coefficient; A is the cross-sectional area of the load; $\partial\eta/\partial t\ (L,t)$ is the horizontal velocity of the load. It should be noted that this term is non-linear. The non-linearity presents several complications. First, it means that the equations must be solved numerically. Second, the linear methods of random analysis are not applicable. In order to avoid these difficulties, this term is linearized. The method of equal energy dissipation is used [2]. It is assumed that the driving function is harmonic in time, i. e., $X_s(t) = \bar{X}_s \cos \omega t$. If the damping is sufficiently small, the system will predominately respond harmonically with frequency ω. The linearized damping force is given by

$$F_{LD} = -\gamma \frac{\partial \eta(L,t)}{\partial t} \tag{5}$$

where

$$\gamma = \frac{4}{3\pi}\rho A C_D \omega X_o \tag{6}$$

X_o is an unknown constant and equals the amplitude of the motion. More will be said about this later. At this point of the discussion, it is sufficient to regard γ as a constant.

*Equation symbols are defined where they first appear and in the notation listing at the end of the text.

Substitution of the linear drag term for the non-linear term in equation (3) gives

$$m\frac{\partial^2 \eta(L,t)}{\partial t^2} = -mg\left.\frac{\partial \eta(z,t)}{\partial z}\right|_{z=L} - \gamma\frac{\partial \eta(L,t)}{\partial t} \tag{7}$$

The steady state response of the system for a harmonic motion of the support is readily obtained. Let the displacement of the support be given by

$$X_s(t) = Re\left[\bar{X}_s(\omega)\, e^{-i\omega t}\right] \tag{8}$$

$\bar{X}_s(\omega)$ is the complex amplitude of the support at frequency ω and Re [ ] means the real part of the bracketed expression. Then the $\eta(z,t)$ that satisfies equations (1), (2), and (7) is

$$\eta(z,t) = Re\left\{\left[kmg\cos k(L-z) - (m\omega^2 + i\gamma\omega)\sin k(L-z)\right]\left[kmg\cos kL - (m\omega^2 + i\gamma\omega)\sin kL\right]^{-1} X_s(\omega)\, e^{-i\omega t}\right\} \tag{9}$$

where

$$k = \sqrt{\frac{\mu}{mg}}\,\omega \tag{10}$$

Of prime interest in this study is the displacement response amplitude operator of the load. This is given by the complex amplitude of the load divided by the amplitude of the forcing function.

Denoting this complex response operator by $R(\omega)$, equation (9) (for z = L) gives

$$R(\omega) = \frac{kmg}{kmg\cos kL - (m\omega^2 + i\gamma\omega)\sin kL} \tag{11}$$

For practical situations, equation (11) can be simplifed somewhat. For frequencies of interest and the fact that $m >> \mu L$, it follows that $kL << 1$. It is then possible to let $\cos kL \sim 1$ and $\sin(kL) = kL$. Introducting this into equation (11) yields

$$R(\omega) = \left[1 - \left(\frac{\omega}{\omega_o}\right)^2 - \frac{i\gamma\omega L}{mg}\right]^{-1} \tag{12}$$

where

$$\omega_o = \sqrt{\frac{g}{L}} \tag{13}$$

From $R(\omega)$ one is able to determine the statistics of the load motion when the ship is exposed to a random sea. Before doing this, however, it is worthwhile pointing out several things. First, the amplitude has a peak at $\omega = \omega_o$. This is understood by observing that the resonant frequency of a simple pendulum of length L is equal to $\sqrt{g/L}$ (which is ω_o). The line-mass system therefore acts like a pendulum due to the large $m/\mu L$ ratio and the low

frequencies considered. Second, the magnitude at resonance is equal to $(\gamma\omega_0 L/mg)^{-1}$ and the width is equal to 1/2 $(\omega_0^2\gamma L/mg)$. This is shown in Figure 2. For practical situations $\gamma\omega_0^2 L/(2mg) \ll \omega_0$, so that the response amplitude operator is a sharply peaked function. This property will be used in the following development.

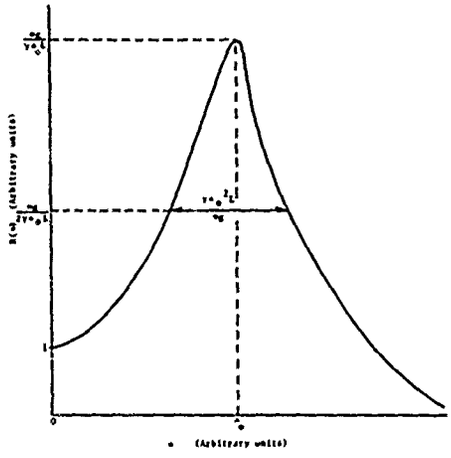

Figure 2. Example of resonance.

It is now assumed that the ship is exposed to random process with a known power spectral density function, $S(\omega)$. The horizontal motion of the ship (assuming linear ship theory) is then also a stationary Gaussian random process with power spectral density function, $S_s(\omega)$ given by

$$S_s(\omega) = |X_s(\omega;h)|^2 S(\omega) \tag{14}$$

$X_s(\omega;h)$ is the ship's horizontal complex response amplitude operator at a height h above the center of gravity of the ship.

In terms of $S_s(\omega)$, the power spectral density function for the load is given by

$$S_L(\omega) = |R(\omega)|^2 S_s(\omega) \tag{15}$$

This assumes that the motion of the load is linear. Even though the drag term was linearized, the solution at this stage is still not linear due to the fact that γ depends on the amplitude of the motion for the various frequencies.

One way to surmount this difficulty is to replace γ by some average value. Let $\bar{\gamma}$ be this average value; it will be chosen in a logical fashion after some further development.

The relevant statistical quantities are obtained from the area under the power spectral density curve, e. g., if E denotes this area, then the significant swing amplitude, $X_{1/3}$, which is the average of the largest one-third amplitudes is [3]

$$X_{1/3} = 2\sqrt{E} \tag{16}$$

E is given by

$$E = \int_0^\infty S_L(\omega)\,d\omega \tag{17}$$

which, from Equations (14, 15) becomes

$$E = \int_0^\infty |R(\omega)|^2 |X_s(\omega;h)|^2 S(\omega)\,d\omega \tag{18}$$

$|R(\omega)|^2$ is calculated from Equation (12); which when inserted into Equation (17) gives

$$E = \int_0^\infty \frac{|X_s(\omega;h)|^2 S(\omega)\,d\omega}{\left[1-\left(\frac{\omega}{\omega_1}\right)^2\right]^2 + \left(\frac{\bar{\gamma}\omega L}{mg}\right)^2} \tag{19}$$

Due to the extreme narrowness of $R(\omega)$ compared to the other functions in integrand great simplifications are possible. To see this more clearly let $\nu = (\omega - \omega_0)/\omega_0$. E then becomes

$$E = \omega_0 \int_{-1}^{\infty} \frac{|X_s[\omega_0(1+\nu);h]|^2 S[\omega_0(1+\nu)]\,d\nu}{\left[2\nu\left(1+\frac{\nu}{2}\right)\right]^2 + \left[\frac{\bar{\gamma}\omega_0(1+\nu)L}{mg}\right]^2} \tag{20}$$

The denominator becomes very small for $\nu = 0$, and rapidly increases for non-zero ν. The width of this resonance is $\bar{\gamma}/(2m\omega_0)$ and is much less than 1. Compared to this narrow resonance, the integrand is a slowly varying function about $\nu = 0$ and can with little error be taken outside the integral. Equation (2) then becomes

$$E = \omega_0 |X_s(\omega_0;h)|^2 S(\omega_0) \int_{-1}^{\infty} \frac{d\nu}{4\nu^2\left(1+\frac{\nu}{2}\right)^2 + \left[\frac{\bar{\gamma}\omega_0(1+\nu)L}{mg}\right]^2} \tag{21}$$

Furthermore, since the main contribution arises for $\nu \ll 1$, ν can be ignored when compared to 1. In addition, the lower limit can be extended to $-\infty$. With these simplifications E becomes

$$E = \omega_0 |X_s(\omega_0;h)|^2 S(\omega_0) \int_{-\infty}^{\infty} \frac{d\nu}{4\nu^2 + \left(\frac{\bar{\gamma}\omega_0 L}{mg}\right)^2} \tag{22}$$

which, at last, is integrable. The final result is

$$E = \frac{\pi}{2}\frac{mg}{\bar{\gamma}L}|X_s(\omega_0;h)|^2 S(\omega_0) \tag{23}$$

Using this expression for E, (and Equation (16)) the significant swing amplitude of the load is

$$X_{1/3} = \left[\frac{2\pi mg}{FL} S(\omega_e)\right]^{1/2} \Big/ X_s(\omega_e; h) \Big| \quad (24)$$

Everyting is well defined in Equation (24) with the exception of $\bar{\gamma}$, which is some average value of γ, and must now be determined. γ from Equation (6) is equal to

$$\gamma = \frac{4}{3\pi} \rho A C_D \omega_e X_0$$

and involves the amplitude of the motion. It is reasonable to let

$$\bar{\gamma} = \frac{4}{3\pi} \rho A C_D \omega_e \bar{X}_0 \quad (25)$$

where $\bar{X}_0$ is an "average" amplitude.

The problem now is to select $\bar{X}_0$. Recall that $\bar{X}_0$ is, in some sense, a representative amplitude. As with all such vaguely defined quantities there are a variety of possible and equally logical choices. For example, several possibilities are:

(1) Let $\bar{X}_0$ equal the significant swing amplitude (i. e., $\bar{X}_0 = X_{1/3}$).

(2) Let $\bar{X}_0$ equal the most probable swing amplitude (i. e., $\bar{X}_0 = 0.626\ X_{1/3}$).

(3) Let $\bar{X}_0$ equal the average swing amplitude (i. e., $\bar{X}_0 = 0.5\ X_{1/3}$).

Its clear that the list could be expanded. For all reasonable choices it would appear, however, that

$$\bar{X}_0 = \alpha X_{1/3} \quad (26)$$

where α is some constant between one-half and one. Since "the" choice for α is unknown, the general form will be kept intact. In this way the sensitivity of $\bar{X}_0$ on the results can be evaluated.

When Equation (26) is inserted into Equation (24) (via Equation (25)) the resulting expression can be solved for $X_{1/3}$; the result of this manipulation is

$$X_{1/3} = \left[\frac{3\pi^2 m}{2\rho A C_D \alpha}\right]^{1/3} \Big| X_s(\omega_e, h) \Big|^{2/3} \left[\omega_e S(\omega_e)\right]^{1/3} \quad (27)$$

The solution is written as the product of these factors, each one of which represents a separate aspect of the problem. These are discussed below.

The first factor contains the parameters that pertain to the viscous drag force and the physical characteristics of the load. These parameters are independent of the off-loading ship and the ambient sea state. Notice that the dependence on α is quite mild. A change in α by a factor of two (the reasonable range for α) changes $X_{1/3}$ by a factor of only 1.26. The maximum spread in $X_{1/3}$ due to a 100% variation in α is therefore only 26%.

The inner bracketed expression contains the response operator for the horizontal motion of the line support. It depends on the dynamic response of the ship to regular waves with frequency $\omega_0 = \sqrt{g/L}$. If the surge and pitch complex response operators for the ship are given by $X_s(\omega_0)$, $\Theta_{s*}(\omega_0)$ respectively; then, $X_s(\omega_0; h)$ is given by*

$$X_s(\omega_e; h) = X_s(\omega_0) + h\, \Theta_s^*(\omega_e) \quad (28)$$

where it will be recalled, h is the vertical distance from the line support to the ships center of gravity.

These response operators can be determined either by experiment of by mathematical analysis. The analysis approach is taken in the report. The standard strip theory method was utilized to develop the NCEL computer code RELMO (RElative MOtion). A complete presentation of RELMO is given in reference 1. RELMO calculates the heave, surge and pitch response of the ship. The added mass and damping coefficients are calculated using subroutine ADMAB [4] and is based on Grim's [5] method.

The last bracketed expression in Equation (27) contains the Power Spectral Density Function for the sea. At the present time the most widely used spectrum is due to Pierson and Moskowitz [2]. This is given by

$$S(\omega_e) = 8.1 \times 10^{-3} g^2 \omega_e^{-5} \exp\left[\frac{-33.56}{(H_{1/3}\omega_e^2)^2}\right] \quad (29)$$

where $H_{1/3}$ is the significant wave height for the sea (e.g., in a sea state 3, $H_{1/3}$ is between three and one-half and five feet). In terms of L, the last bracket in Equation (27) becomes

$$\left[\omega_e S(\omega_e)\right]^{1/3} = .201\, L^{2/3} \exp\left[-0.0108\left(\frac{L}{H_{1/3}}\right)^2\right] \quad (30)$$

This factor is a function of L and is shown in Figure 3 for several values of $H_{1/3}$. The function rises from zero (at L = 0) to peak at L $\approx$ 5.56 $H_{1/3}$ and then falls to zero for large L. For sea state 3, L is obtained by replacing the last bracket in Equation (27) by Equation (30)

$$X_{1/3} = 0.201 \left(\frac{3\pi^2 m}{\pi \rho A C_D \alpha}\right)^{1/3} \Big| X_s(\omega_e, h) \Big|^{2/3} \quad (31)$$
$$L^{2/3} \exp\left[0.0108\left(\frac{L}{H_{1/3}}\right)^2\right]$$

It is also of interest to determine the significant accelerations. These are readily obtained due to the fact that the acceleration response amplitude operator is simply ω^2 times the displacement response amplitude operator. Let $\ddot{X}_{1/3}$ be acceleration significant amplitude; then one has

$$\ddot{X}_{1/3} = \left(\frac{3\pi^2 m}{2\rho A C_D \alpha}\right)^{1/3} \Big| X_s(\omega_e; h) \Big|^{2/3} \quad (32)$$
$$2.033 \exp\left[\frac{-0.0108 L^2}{H_{1/3}^2}\right]$$

*The pitch angle is positive for bow down.

This expression is similar to $X_{1/3}$; a plot of the last bracketed expression for several values of $H_{1/3}$ is shown in Figure 4.

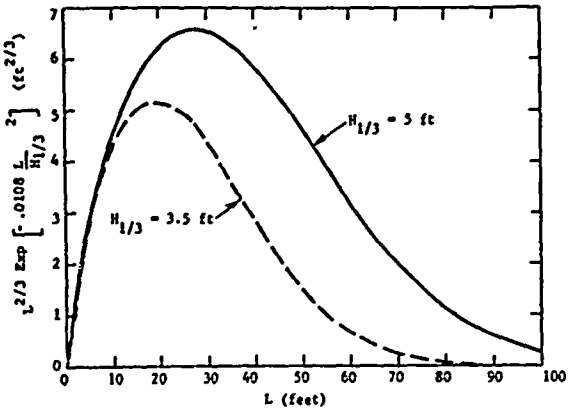

Figure 3. Sea spectrum contribution of $X_{1/3}$.

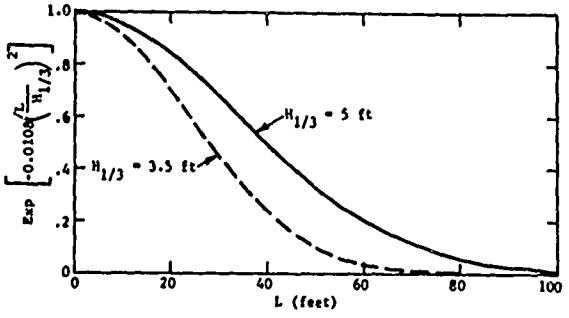

Figure 4. Sea spectrum contribution of $\ddot{X}_{1/3}$.

RESULTS

Due to the large number of parameters involved (e. g., the mass and cross-sectional area of the container, type of ship, height of support, etc.) a certain amount of specialization is required. For convenience, Equation (31) is repeated below

$$X_{1/3} = 0.201\left(\frac{3\pi^2 m}{\rho A C_D \alpha}\right)^{1/3} \left|X_5(\omega_e;h)\right|^{2/3} L^{2/3} \exp\left[-0.01 C_D \alpha \left(\frac{L}{H_{1/3}}\right)^2\right]$$

Several of these quantities can be assigned a constant value. First consider the damping contributions. The density of air as sea level and at a temperature of 60°F is taken as representative; according to Bretschneider [6] this value of ρ is 2.4×10^{-3} slugs/ft^3. From the same reference the drag coefficient C_D is 2.03. The parameter α, as noted, is somewhere between 0.5 and 1.0. In the interest of conservatism α is chosen to be 0.5.

The containers are considered to be 8'x8'x 20' and have a load capacity of 20 tons. Again, in order to be conservative, the cross-sectional area, A is taken to be 64 ft^2 and the mass, m, is 20 tons/g.

For convenience, the assigned parametric values are listed below:

$\rho = 2.4 \times 10^{-3}$ slugs/ft^3

$C_D = 2.03$

$\alpha = 0.5$

m = 20 tons/g

A = 64 ft^2

Denoting $X_{1/3}$ and $\ddot{X}_{1/3}$ for this parametric choice with an asterick, the expression for $X_{1/3}$ and $\ddot{X}_{1/3}$ are

$$X^*_{1/3} = 9.9\times10^{-7}\left|X_5(\omega_e;h)\right|^{2/3} L^{2/3} \exp\left[\frac{-0.01 C_D \alpha L^2}{H^2_{1/3}}\right] \quad (33)$$

$$\ddot{X}^*_{1/3} = 3.11\left|X_5(\omega_e;h)\right|^{2/3} \exp\left[\frac{-0.01 C_D \alpha L^2}{H^2_{1/3}}\right] \quad (34)$$

In Equation (33) L must have units of feet. The units for $X_{1/3}$ and $\ddot{X}_{1/3}$ are respectively ft and g (32.2 ft/sec^2). $X_{1/3}$ and $\ddot{X}_{1/3}$ for other choices of these parameters can be obtained from $X^*_{1/3}$ and $\ddot{X}_{1/3}$ from the following expressions:

$$\begin{bmatrix} X_{1/3} \\ \ddot{X}_{1/3} \end{bmatrix} = \left(\frac{mg}{20 \text{ tons}}\right)^{1/3}\left(\frac{2.4\times10^{-3} \text{ slugs/ft}^3}{\rho}\right)^{1/3} \left(\frac{64 \text{ ft}^2}{A}\right)^{1/3}\left(\frac{1.0}{C_D \alpha}\right)^{1/3} \begin{bmatrix} X^*_{1/3} \\ \ddot{X}^*_{1/3} \end{bmatrix} \quad (35)$$

The two ships selected for study are a C8 and a C4 and are fairly representative of the cargo ships to be encountered. Their characteristics are given in the table below:

	Displacement (LT) (fully loaded)	Length (ft)	Beam (ft)	Draft (ft)
C8	44,428	772	100	34
C4	22, 630	564	76	32

X_s $(\sqrt{g/L};h)$ for these ships are plotted in Figures 5-6. Each ship exhibits a pronounced resonance; the C4 at a frequency such that $\sqrt{g/L}$ corresponds to a line length of 41 feet and the C8 to a line length of 53 feet. The motion at resonance is still quite small; for the C4 and C8 it is respectively 0.17 and 0.11 feet for a one foot wave.

$X^*_{1/3}$ and $\dot{X}^*_{1/3}$ for a sea state 3 ($H_{1/3}$ = 3.5 ft and $H_{1/3}$ = 5.0 ft) as a function of line length, L, are presented in Figures 7-10. The general features exhibited by $X^*_{1/3}$ are not surprising. The sea spectrum falls off rapidly for both large and small L and consequently so does $X^*_{1/3}$. These are peaks in $X^*_{1/3}$ due to the resonance exhibited by X_s and the peak in the sea spectrum. The extreme responses are presented in Table 2.

Table 2. Extreme Significant Amplitude $X^*_{1/3}$

$H_{1/3}$ ft	h (ft)	C4			C8		
		Max $X^*_{1/3}$ (ft)	L at Max (ft)	$(X_s)_{1/3}$	Max $X^*_{1/3}$ (ft)	L at Max (ft)	$(X_s)_{1/3}$
3.5	0.0	3.6	38	.019	3.1	26	.017
	20.0	6.2	37	.034	3.2	28	.019
	40.0	8.3	36	.050	3.4	29	.023
5.0	0.0	8.6	40	.056	5.3	47	.036
	20.0	12.2	40	.096	7.8	47	.051
	40.0	15.7	40	.14	10.3	47	.072

There is one significant fact, namely, the magnitude of $X^*_{1/3}$. In order to understand the effect, the amplitudes must be compared with the significant amplitudes for the horizontal motion of the support, $(X_s)_{1/3}$, given respectively in columns 5 and 8 of Table 2. The support displacement is a fraction of a foot, whereas the load swings through many feet. This large amplification (a factor of 100 or more) is due to the sharpness of the resonance. As is evident, such systems are quite efficient at extracting whatever energy is available at their resonant frequency.

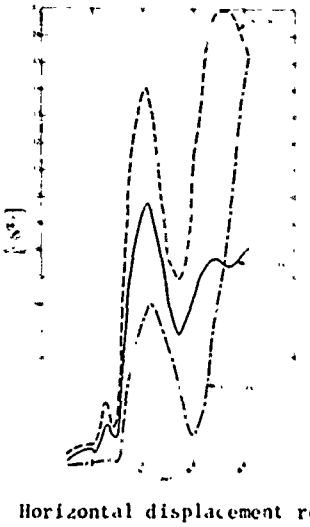

Figure 5. Horizontal displacement response operator for a C4.

The curves for $\ddot{X}^*_{1/3}$ are shown in Figures 11-14. The extremes in the significant amplitudes for the acceleration are given in Table 3. Fairly large horizontal accelerations are evident. For example, at a 0.4 g horizontal acceleration (which is a reasonable upper limit) a horizontal force of 8 tons is acting on the load.* The implication is that forces of this magnitude would be required to restrain the horizontal oscillation.

Table 3. Extreme Significant Acceleration, $\ddot{X}^*_{1/3}$

$H_{1/3}$ (ft)	h (ft)	C4		C8	
		Max $\ddot{X}^*_{1/3}$ g	L at Max (ft)	Max $\ddot{X}^*_{1/3}$ g	L at Max (ft)
3.5	0	.12	37	.115	22
	20	.18	36	.125	22
	40	.24	35	.130	22
5.0	0	.22	40	.15	26
	20	.32	38	.18	49
	40	.43	36	.25	50

*The force F is obtained from F = ma. In this problem m = 20 tons/g and a = 0.4g, therefore ma = 20 tons/g × 0.4g = 8 tons.

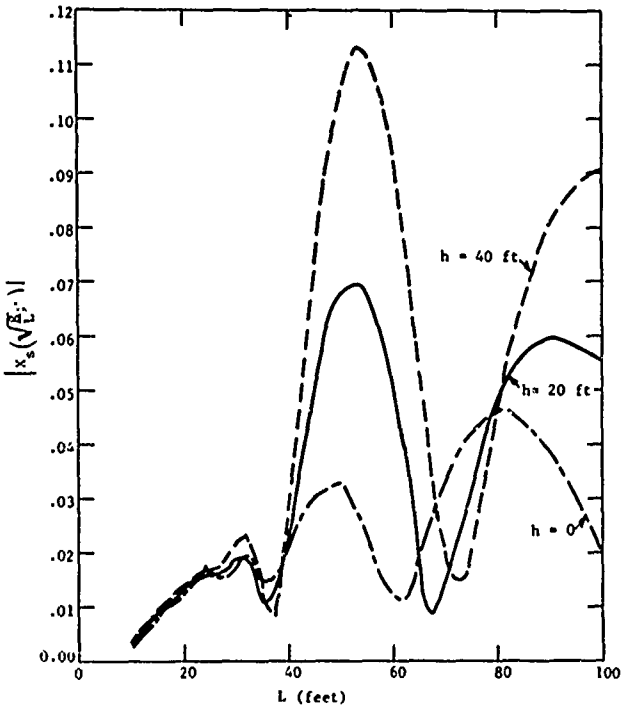

Figure 6. Horizontal displacement response operator for a C8.

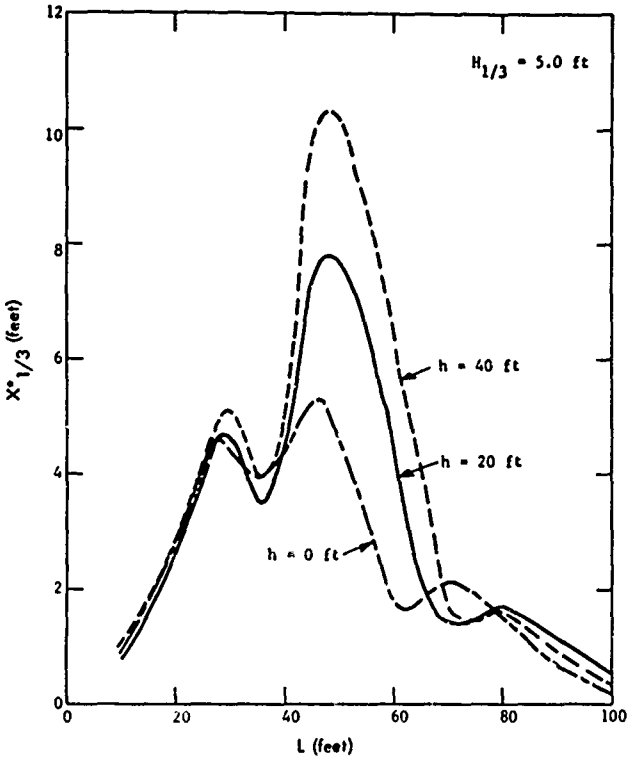

Figure 8. Significant load amplitude for C8.

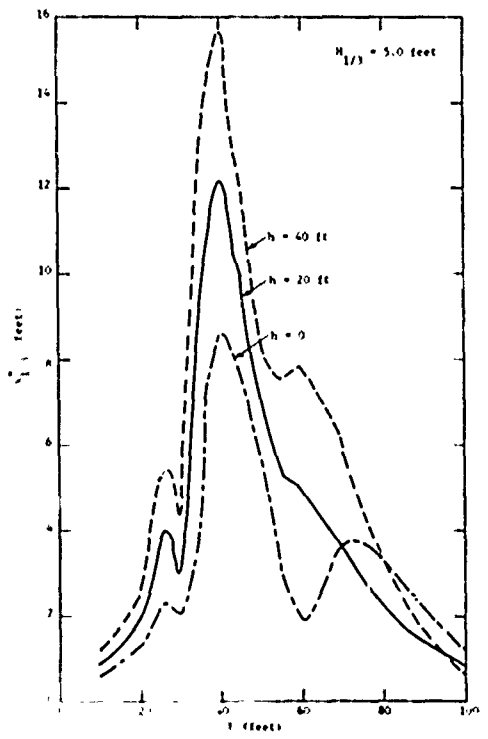

Figure 7. Significant load amplitude for C4.

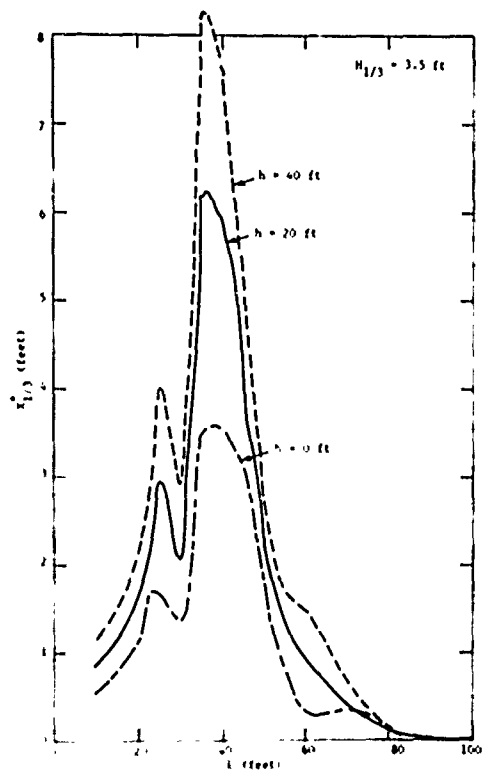

Figure 9. Significant load amplitude for C4.

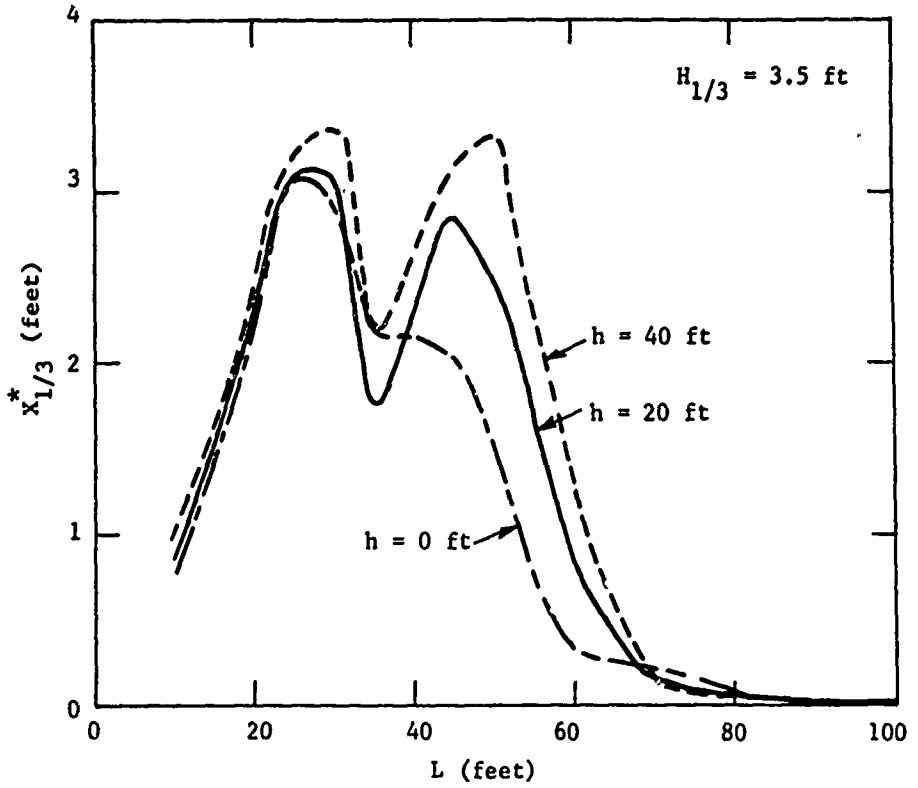

Figure 10. Significant load amplitude for C8.

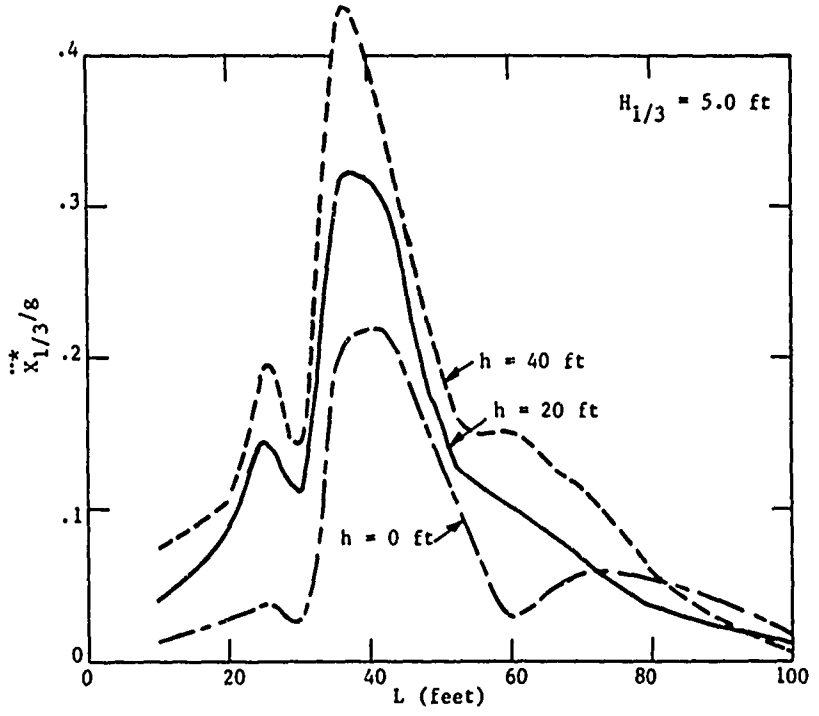

Figure 11. Significant load acceleration for C4.

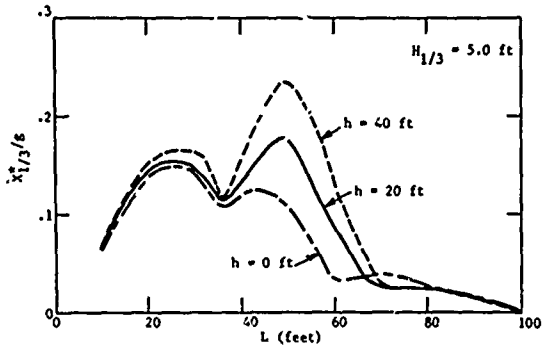

Figure 12. Significant load acceleration for C8.

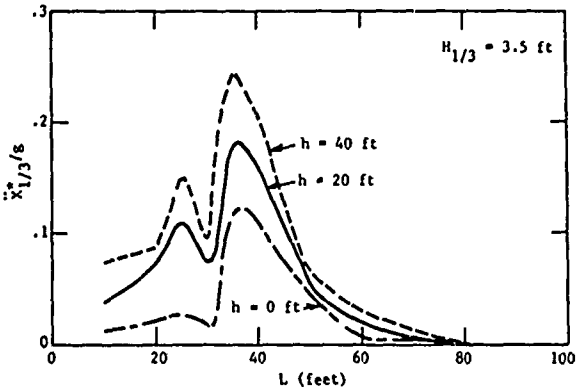

Figure 13. Significant load acceleration for C4.

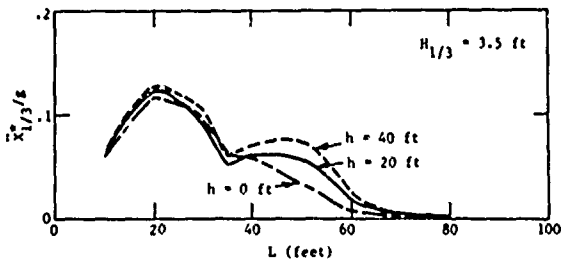

Figure 14. Significant load acceleration for C8.

TIME DEPENDENT LINE LENGTH

It's clear from the foregoing analysis that steady-state response for a constant line length yields extremely large pendular motion. In this section the pendulation while raising and lowering of the load is considered.

The differential equation describing the motion is given below:

$$\ddot{\theta}(t) = \frac{-2\dot{L}(t)\dot{\theta}(t)}{L(t)} - \frac{g \sin\theta(t)}{L(t)} - \frac{\ddot{X}_s(t)\cos\theta(t)}{L(t)} \quad (36)$$

where

$\theta(t)$ = pendulation angle from vertical
$X_s(t)$ = horizontal motion of the support
$\ddot{X}_s(t)$ = the horizontal acceleration of the support
$L(t)$ = length of the line
$\dot{L}(t)$ = the time derivative of the line length the pendulum angle with respect to the vertical

Rather than take the support motion to be random, it is assumed that $X_s(t) = X_o \sin \omega t$. The line length is to vary linearly with time as follows: $L(t) = Lo + vt$ where v is the line speed and Lo is the initial length of the line. The equation to be solved is

$$\ddot{\theta}(t) = \frac{-2v\dot{\theta}(t)}{Lo + vt} - \frac{g \sin\theta(t)}{Lo + vt} + \omega^2 X_o \sin\omega t \cos\theta(t)\,(Lo + vt)^{-1} \quad (37)$$

Analytical solutions are not available, however, numerical solutions are readily obtained. The numerical procedure is based on Hamming's modified predictor-corrector method for systems of first-order, initial-value differential equations. [7] This method is forth-order and utilizes an error criteria whereby the time increment is adjusted to meet prescribed accuracy. Details are given in reference [7].

Example Problem

By way of illustration, the problem of a floating crane raising a load from a stationary platform is presented. It is assumed that the load is to be raised 30 feet; the original line length is 100 feet, hence the line is shortened from 100 feet to 70 feet.

Since the purpose of this problem is to demonstrate pendulation under conditions of varying line length, the actual motion of the boom has been arbitrarily assigned an amplitude of .1 feet. Results for a line speed of 90 feet/minute are shown in Figure 15 for three different periods of excitation. These results can be partially understood by observing that the initial line length (100 feet) has a resonant period of 11.1 sec and 9.2 sec for the final length (70 feet). One would, therefore, expect the response to be larger for the 10 second motion than for the 3 sec or 7 sec excitation.

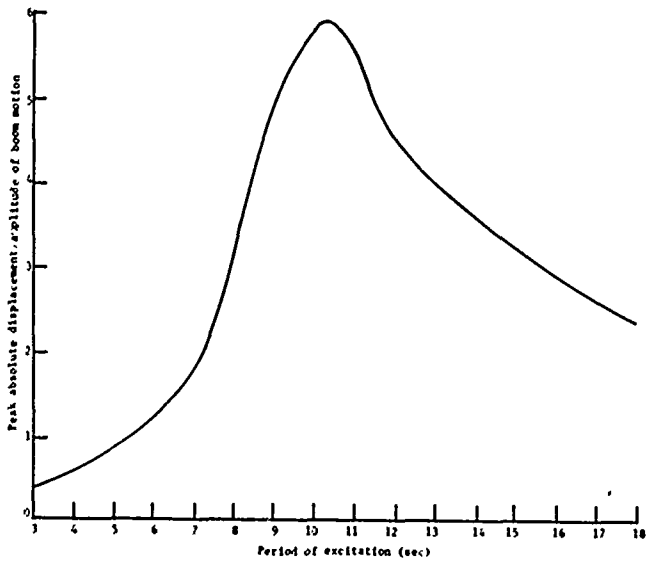

Figure 15. Pendulation time histories while raising load from 100 ft to 70 ft.

This is brought out more clearly in Figure 16. The largest response per unit amplitude excitation is plotted versus the excitation period. The peak response occurs for an excitation period of about 10 seconds. The shape of this "resonance" curve is not symmetrical due to the fact that only the first twenty seconds of the motion is considered. The longer period excitations reach their peak somewhat later and hence do not exhibit their largest response. It should be noted that the boom motion is amplified by a factor of six for the ten second period excitation.

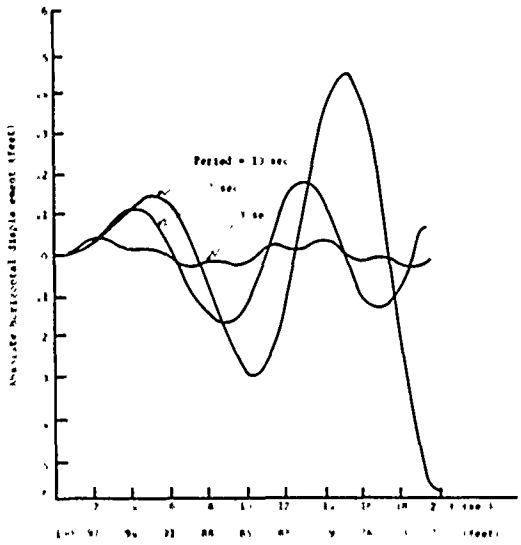

Figure 16. Peak response versus period of excitation.

FINDINGS AND CONCLUSIONS

A theory was developed to determine the steady state horizontal response of a wire suspended load due to the horizontal motion of the ship in a random sea. Based on this theory, calculations were performed for two types of ships (a C8 and a C4) in sea state 3. It was found that the motion induced in a wire-suspended load due to horizontal motion of a ship is very large. The significant amplitudes for the horizontal movement of the load (5 to 10 feet typically) are 100 or more times larger than the horizontal significant amplitudes for the ship.

The pendulation is much less violent when one considers time varying line lengths, however, the motion is still excessive. This study indicates that anti-pendulation devices will be required inorder to transfer cargo in regular waves. A calculation is currently underway to extend the analysis to random waves, however, this will not completely eliminate the need for anti-pendulation devices due to the fact that regular waves (i. e., swell) will also be encountered.

REFERENCES

[1] D.A. Davis and H.S. Zwibel, "The Relative Motion Between Ships in Random Head Seas," NCEL Technical Note N-1183, September 1971.

[2] M. St. Denis, Floating Hulls Subject to Wave Action, pp. 12-72. McGraw-Hill, New York, 1969.

[3] W. Frank and N. Salvensen, "The Frank Close-Fit Ship-Motion Program," NSRDC Rept. 3289, June 1970.

[4] L. Vassilopulos, "The Anayltical Prediction of Ship Performance in Random Seas," MIT Rept. No. 64-2, February 1964.

[5] O. Grim, A Method for a More Precise Computation of Heaving and Pitching Motions Both in Smooth Water and in Waves, pp.483-518. Office of Naval Research, Washington, D. C., 1962.

[6] C. L. Bretschneider, Overwater Wind and Wave Forces, pp. 12-2 to 12-24, McGraw-Hill, 1969.

[7] System/360 Scientific Subroutine Package (360A-CM-03X) Version III, pp. 337-342.

LIST OF SYMBOLS

a	Acceleration
A	Cross sectional area of load (ft^2)
c	Phase speed of transverse wave in wire
C_D	Drag coefficient

E	Area under power spectral density curve
F_{LD}	Linearized drag force
g	Acceleration of gravity (32.2 ft/sec^2)
h	Height of support above ship's center of gravity (ft)
k	Wave number for transverse waves in wire
L	Length of wire (ft)
$R(\omega)$	Load horizontal displacement amplitude operator
$S(\omega)$	Power spectral density of sea
$S_{L(\omega)}$	Power spectral density of load
$S_{s(\omega)}$	Power spectral density of support
t	Time (sec)
T	Tension in line (lbs)
$x(t)$	Horizontal displacement of load
$X_s(t)$	Horizontal displacement of support
X_o	Amplitude of load motion
$\bar{X}_o$	Average amplitude
X_s	Amplitude of support motion
$X_s(\omega;h)$	Horizontal displacement response operator for support
$X_s(\omega)$	Surge displacement operator
$X_{1/3}$	Significant amplitude of load displacement (ft)
$\ddot{X}_{1/3}$	Significant amplitude of load acceleration (ft/sec)
$X^*_{1/3}$	Significant amplitude of load displacement for selected set of parameters (ft)
$\ddot{X}^*_{1/3}$	Significant amplitude of load acceleration for selected set of parameters (g)
$(X_s)_{1/3}$	Significant amplitude for load support (ft)
z	Vertical coordinate
α	Dimensionless constant
γ	Linearized drag parameter
$\bar{\gamma}$	Average linearized drag parameter
$\eta(z,t)$	Displacement of line at position z at time t (ft)
$\Theta(\omega)$	Pitch response operator for ship
$\theta(t)$	Pendulation angle from the vertical
μ	Mass per unit length of line (slugs/ft)
ν	Dimensionless frequency variable
ρ	Mass density of air (slugs/ft)
ω	Frequency of waves (rad/sec)
ω_o	Resonant frequency of load (rad/sec)